2014-04-30

Relating forearm muscle electrical activity to finger forces

Jennifer Keating
Worcester Polytechnic Institute

RELATING FOREARM MUSCLE ELECTRICAL ACTIVITY TO FINGER FORCES

by

Jennifer Keating

A Thesis

Submitted to the Faculty

of the

WORCESTER POLYTECHNIC INSTITUTE

in partial fulfillment of the requirements for the

Degree of Master of Science

in

Electrical and Computer Engineering

May 2014

APPROVED:

_____

Professor Edward A. Clancy, Major Advisor

_____

Professor Gregory S. Fischer, Committee Member

_____

Professor Donald R. Brown, Committee Member

Abstract

The electromyogram (EMG) signal is desired to be used as a control signal for applications such as multifunction prostheses, wheelchair navigation, gait generation, grasping control, virtual keyboards, and gesture-based interfaces [25]. Several research studies have attempted to relate the electromyogram (EMG) activity of the forearm muscles to the mechanical activity of the wrist, hand and/or fingers [41], [42], [43]. A primary interest is for EMG control of powered upper-limb prostheses and rehabilitation orthotics. Existing commercial EMG-controlled devices are limited to rudimentary control capabilities of either discrete states (e.g. hand close/open), or one degree of freedom proportional control [4], [36]. Classification schemes for discriminating between hand/wrist functions and individual finger movements have demonstrated accuracy up to 95% [38], [39], [29]. These methods may provide for increased amputee function, though continuous control of movement is not generally achieved.

This thesis considered proportional control via EMG-based estimation of finger forces with the goal of identifying whether multiple degrees of freedom of proportional control information are available from the surface EMG of the forearm. Electromyogram (EMG) activity from the extensor and flexor muscles of the forearm was sensed with bipolar surface electrodes and related to the force produced at the four fingertips during constant-posture, slowly force-varying contractions from 20 healthy subjects. The contractions ranged between 30% maximum voluntary contractions (MVC) extension and 30% MVC flexion. EMG amplitude sampling rate, least squares regularization, linear vs. nonlinear models and number of electrodes used in the system identification were studied.

Results are supportive that multiple degrees of freedom of proportional control information are available from the surface EMG of the forearm, at least in healthy subjects. An EMG amplitude sampling frequency of 4.096 Hz was found to produce models which allowed for good EMG amplitude estimates. Least squares regularization with a pseudo-inverse tolerance of 0.055 resulted in significant improvement in modeling results, with an average error of 4.69% MVC–6.59% MVC (maximum voluntary contraction). Increasing polynomial order did not significantly improve modeling results. Results from smaller electrode arrays remained fairly good with as few as six electrodes, with the average %MVC error ranging from 5.13%–7.01% across the four fingers. This study also identified challenges in the current experimental study design and subsequent system identification when EMG-force modeling is performed with four fingers simultaneously. Methods to compensate for these issues have been proposed in this thesis.

Acknowledgements

First and foremost I would like to thank my advisor, Professor Ted Clancy. I am incredibly grateful that you afforded me the opportunity to research with you in your lab and to learn from you. I am honored to have had the chance to contribute to the meaningful work of the Laboratory for Sensory and Physiologic Signal Processing.

Thank you to my committee, Professors Gregory Fischer and D. Richard Brown III, for your advice and feedback on this thesis. I am hopeful that this work will go on to contribute meaningfully to the development of the robotic exomusculature glove in the Automation and Interventional Medicine Laboratory.

Thank you to Professor Joseph Petruccelli for your advice regarding the statistical evaluation methods used in this thesis.

Thank you to my research partner, Berj Bardizbanian, for your hard work, support and friendship over the past year.

Thank you to all of our study subjects without whom this research would not have been possible.

Brett, thank you for being my rock, as only a rock could have withstood the last 2.5 years.

Mom, Dad and Kim, thanks for your constant encouragement and the grace with which you handled my crazy schedule.

To my friend Ali Hause – you are a superhero. Thanks for embracing your inner nerd and tirelessly supporting my work.

To my friends Brie Rawson, Alex Margiott, and Bengi Aygün thank you for your friendship, guidance and support.

To my friend and mentor, Dr. Ken Flaton, thanks for always challenging me and expecting nothing less than the best. I owe a large part of my development as an engineer and person over the past few years to your expectations and guidance.

Thank you to Grove Instruments, Inc. for supporting my educational goals and helping me to grow as an engineer over the past four years.

Finally, thanks to the WPI Electrical and Computer Engineering department professors and administrative staff for all that you have contributed to my studies over the years.

Table of Contents

Table of Figures

Table of Tables

Table of Equations

1 Introduction

The primary muscles used to flex and extend the fingers reside within the forearm. Hence, many upper limb amputees retain control of these muscles, even though they are no longer attached to the fingers. These muscles can still contract, producing electrical activity (electromyogram or EMG) that can be sensed at the surface of the skin. There is emerging evidence that the electrical activity of these remnant muscles can be used to control detailed movement of novel hand prostheses [1]. Existing commercial hand prostheses are mostly limited to one function – opening and closing. The ability to control multiple functions of multiple fingers at one time is strongly desired by amputees. The EMG of the remnant forearm muscles provides a possible manner to achieve this control.

Similarly, people who experience a stroke can lose some of their ability to move their fingers, hand, and wrist. We are developing a powered orthotic device that is worn as an exoskeleton over the arm [2]. One of its prime functions is to assist a weakened hand in various movement and gripping tasks. Our target population for this orthotic is stroke patients who retain some partial voluntary finger movement. In that case, the forearm muscles again produce EMG when the fingers are flexed or extended. Our goal is to sense the EMG activity and use it to command the powered orthotic to assist in the patient's movement or gripping task. The device could also be used as a rehabilitation aid.

For both of these application goals, we are measuring the forearm EMG and relating it to the forces produced in the fingers, hand, and wrist. Hence, this experiment will record EMG from several conventional electrodes placed around the circumference of the forearm and relate that electrical activity to the forces produced in the fingers, hand, and wrist. This work is completed on healthy, intact subjects, but can be extended to amputee and stroke populations in the future. We anticipate scientific advances in EMG-to-force processing that are applicable to both applications.

1.1 Project Motivation

When muscles contract, they emit an electrical signal that can be detected by electrodes placed on the surface of the skin. If electromyogram (EMG) signals from the forearm can be sufficiently detected and processed to form high performing proportional relationships with hand/wrist forces, these models could benefit at least two applications: the control of prosthetic hands/wrists and the control of orthoses used for stroke rehabilitation.

Nearly two million people in the United States are living with limb loss [3], with partial hand amputation being the most prevalent. As much as 70% of all upper limb amputations are distal to the elbow [4]. Many upper limb amputees can still control their remnant forearm muscles, producing muscular contractions and therefore electrical activity. Preliminary work by Liu et al. [1] showed promising results that electrical activity in the forearm may be used to estimate forces applied at the fingertips.

In most clinical applications, EMG signals are acquired using bipolar electrodes oriented parallel to muscle fibers [5]. The magnitude and slope of these signals (among other possible features) is then used as a control signal for the prosthesis. However, commercially available myoelectric prostheses provide extremely limited functionality to amputees, offering either discrete state recognition (open/close hand) or one degree of freedom of control and requiring multiple independent EMG control sites. This functionality is a limitation for daily activities, and the ability to control individual fingers is strongly desired by amputees.

Stroke affects 795,000 people annually in the United States [6] with approximately 80% of stroke survivors suffering from weakened limbs/hands [2]. Repetitive task practice, a therapy in which typical tasks (e.g. drinking from a glass) are broken down to smaller parts which patients complete repeatedly, has been shown to improve motor function for both subacute and chronic stroke patients [7], [8]. Repetitive task practice is especially effective when used in conjunction with robotic technologies [9], [10], [11], [12]. This kind of therapy typically occurs in clinical settings, but the desire is for it to take place in the home [2].

The WPI AIM lab is developing a soft exoskeleton glove that can be used for rehabilitation and assistive grasping for those suffering from stroke or with physical disabilities [2]. This glove will support forearm-EMG controlled active assistance, active resistance, and preprogrammed motions.

The relationship between surface EMG and torque has been studied extensively in the elbow (e.g., E.A. Clancy), but little has been done to examine the relationship between the surface EMG and forces generated at the fingertips [13], [14], [2]. The promising results obtained by Liu et al. [1] in combination with the need for more dexterous hand/wrist prosthetics and orthoses are the driving forces behind this research. We aimed to develop EMG signal processing methods for the hand/wrist that increase the functionality of these devices.

1.2 Thesis Contribution

This research focused on developing signal processing methods that increased the functionality of prostheses worn by amputees, as well as rehabilitation orthoses worn by stroke victims during rehabilitation. In each case, this thesis investigated the relationship between forearm electrical activity and forces exerted by the fingertips.

To achieve this relationship, flexor and extensor EMG signals from the forearm were collected on 20 healthy subjects during constant-posture slowly force varying contractions. Subjects had no known neuromuscular deficits of their right hand, arm, or shoulder. Contraction trials ranged between 30% maximum voluntary contraction (MVC) flexion and 30% MVC extension, and EMG signals were acquired using 12 bipolar surface EMG electrode amplifiers mounted circumferentially around the forearm. Force was collected using a 100 pound load cell in contact with the fingertips. A model was developed to relate EMG amplitude to forces in the fingertips and model performance was compared across all 20 subjects.

Deliverables of this thesis include:

- A large (N=20 dataset (EMG and force recordings) in the forearm/fingers to facilitate the development of signal processing methods for increased dexterity in prosthetics and orthotics, comprised of:
    - Slowly force-varying contractions of each of four fingers.
    - Force-varying contractions of each of four fingers (1 Hz bandwidth).
    - A dataset for classification of various hand grips/wrist contractions.
    - Additional data related to contraction of multiple fingers at the same time.
- A model used to relate forearm extension/flexion EMG amplitudes during slowly force varying contractions to forces in the fingertips.
- Characterization of model performance vs. the number of electrodes used.
    - Specifically, identification of the best electrodes sets per subject for electrode sets of sizes 6-12.

2 Background

This chapter provides general background information relevant to the contribution this thesis makes to the field. The electromyogram (EMG) signal is detailed from its origin to its recording and signal processing techniques. It begins with a brief discussion of electrical activity in the muscles and the EMG signal. An overview of the methods of signal processing and the subsequent uses of EMG signals, especially in the control of prosthetics and assistive rehabilitation devices, is provided.

2.1 Origin of the EMG Signal

Body movement is a result of muscle contraction [15]. As shown in Figure 1, the type of contraction depends on the muscle tension (force exerted on an object) and load (opposing force exerted on muscle by an object). In an *isotonic* contraction, the (fixed) muscle tension overcomes the load and muscle shortening occurs (e.g., lifting a suitcase). In an *isometric* contraction, tension is developed but a load is not moved (e.g. pushing against a wall). During this kind of contraction the maximum tension for the muscle in use can be reached, but the muscle only shortens slightly from applying tension to tendons and ligaments.

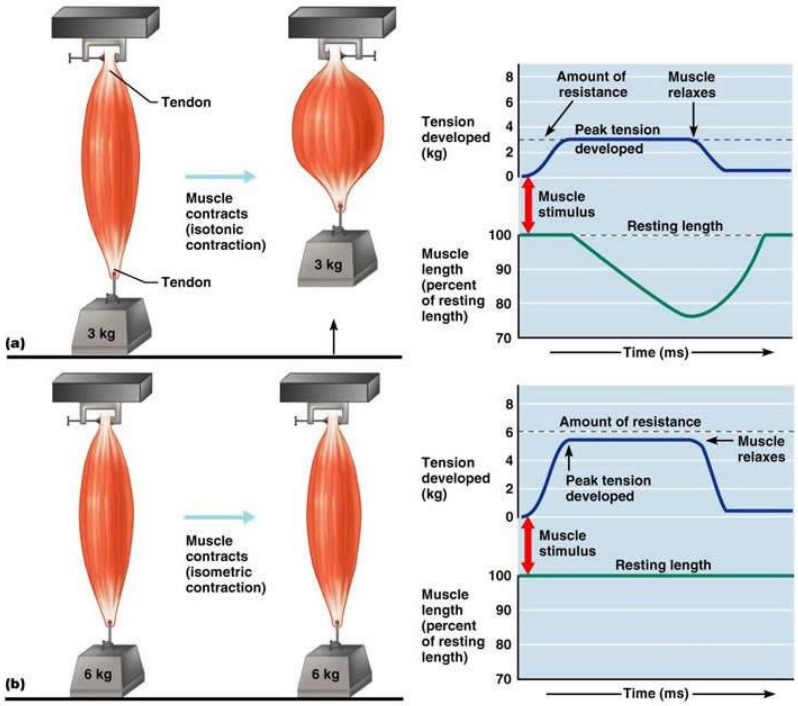

Figure 1: Illustration of isotonic and isometric contractions [15].

For the development of prosthetics and assistive orthoses, voluntary movements such as grasping an object are of concern. Skeletal muscles are the only muscles in the body that can be controlled voluntarily. They do so with varying force and different periods of time, both of which are defined by the function of the *motor unit*.

Motor units are composed of muscle fibers (elongated muscular cells) and a motor neuron. When stimulated, a motor neuron produces an electrical impulse that transmits down the length of its axon causing all muscle fibers innervated by the neuron to contract. This stimulation results in the depolarization of each muscle fiber, which disseminates in both directions along the fibers [16]. This action potential, due to ion movement, generates an electromagnetic field around the muscle fibers – referred to as a motor unit action potential (MUAP).

Motor units can be composed of between four and several hundred muscle fibers, for the purposes of fine (e.g. eye movements) and coarse (e.g. weight bearing muscles) control, respectively [15]. Since muscle fibers in a motor unit are randomly distributed across a muscle, the stimulation of one motor unit causes a weak contraction of the whole muscle

[15], [16]. The depolarization of individual muscle fibers overlaps in time. Thus, any one MUAP is a spatial-temporal superposition of individual action potentials from each muscle fiber, as depicted in Figure 2 [16].

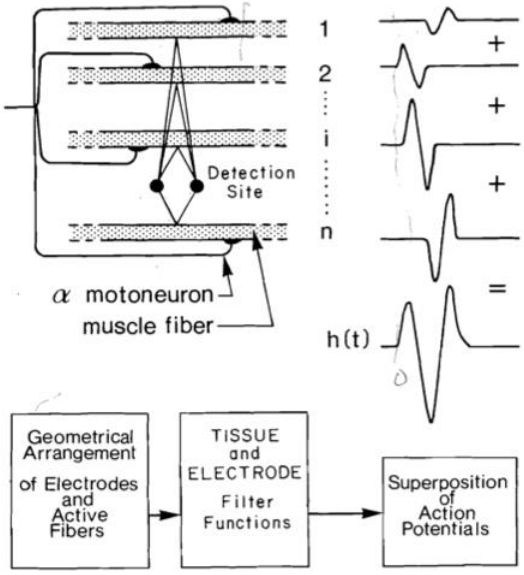

Figure 2: Schematic representation of generation of motor unit action potential (MUAP) [16].

Any portion of a muscle may contain muscle fibers belonging to 20-50 motor units [16]. During a muscle contraction, multiple motor units are repeatedly stimulated [15]. These stimulations typically occur asynchronously to facilitate smooth movements and delay muscle fatigue. This excitation pattern results in a sequence of MUAPs called a motor unit action potential train (MUAPT) [16].

The sum of overlapping MUAPTs and the way in which the motor units discharge results in the surface EMG signal resembling a zero-mean random stochastic process with a standard deviation proportional to the number of active motor units and their rate of activation [1]. Merlo et al. [17] modeled the surface EMG signal as:

$$s(t) = \sum_j MUAPT_j(t) + n(t) = \sum_j \sum_i k_j f\left(\frac{t - \theta_{ij}}{\alpha_j}\right) + n(t)$$

Equation 1: Model of surface EMG signal by Merlo et al. [17]

where k_j is an amplitude factor for the *j*th motor unit, *f()* is the shape of the action potential discharge, θ_{ij} is the time at which the MUAP occurs, α_j is a scaling factor, and *n(t)* is additive noise [17].

The sEMG signal is dependent on the level and duration of contraction, the state of the contraction (static or dynamic), fatigue, and sweat from the skin. The maximum level that a skeletal muscle can contract to is referred to as maximum voluntary contraction (MVC), and contraction levels are typically referred to by the percentage of MVC that they represent. Studies have found that the distribution of the EMG signal is more sharply peaked near zero than a Gaussian distribution, and that at low contraction levels, the signal is more likely to be best modeled as a zero mean LaPlacian process [18].

2.2 Extracting the EMG Signal

The EMG signal is an easy signal to collect, but a difficult one to interpret and understand. Analysis of the EMG signal may provide us with the ability to understand force generation in the muscles and the way in which muscles produce movement, but our ability to extract this information correctly depends upon proper signal acquisition methods. A common EMG signal extraction process is therefore composed of three important stages: signal capturing, signal conditioning, and signal processing. Figure 3 shows these stages.

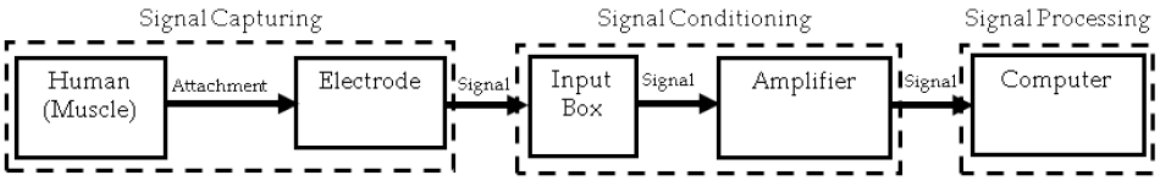

Figure 3: EMG signal extraction process [19].

2.2.1 Signal Capturing

Since muscle contraction results in electrical activity near the skin's surface, it is possible to place sensors, called electrodes, onto the skin to detect the electrical activity. The area that an electrode is in direct contact with is referred to as the detection surface [16]. Physiological data recorded by a surface electrode is called a surface EMG (sEMG). As shown in Figure 4, the sEMG signal is the summation of all MUAPTs from all active motor units detected by an electrode.

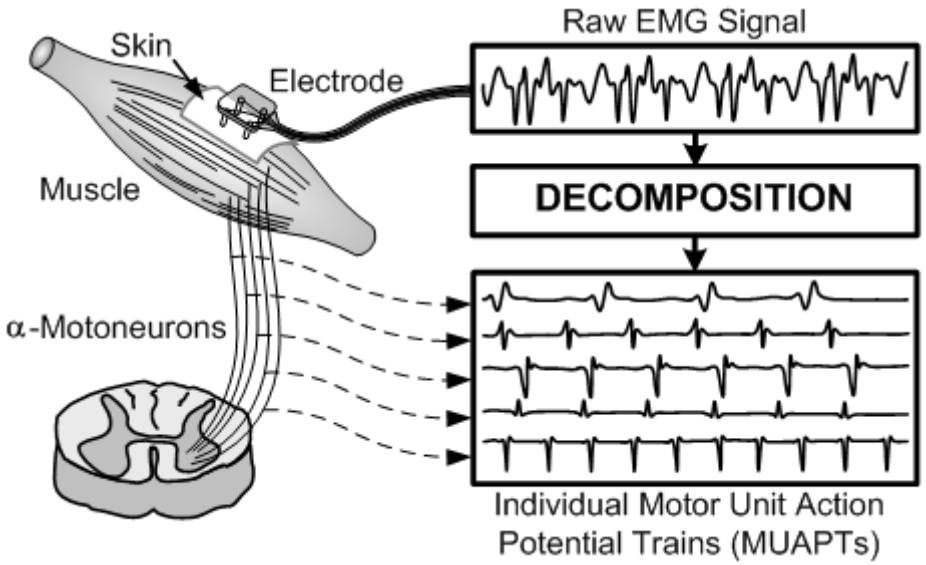

Figure 4: Diagram of method of detecting EMG signals and their decomposition into MUAPTs [20].

As the force output of a muscle increases, so does the number of active motor units. Since multiple motor units are active during a muscle contraction, signals belonging to multiple motor units are detected by a single electrode simultaneously. The shape and amplitude of the MUAP depends on the orientation of the muscle fibers with respect to the electrode (among other factors). During a MUAPT, the MUAP waveform remains constant if there are no changes between electrode positioning and muscle fibers, electrode properties, and no significant biochemical changes in the muscle tissue.

The Surface Electromyography for the Non-Invasive Assessment of Muscles (SENIAM) project was initiated to solve problems preventing a useful exchange of data in the area of sEMG research, and to establish standards that allow for European cooperation in this area of research [21]. One of its primary objectives was to develop recommendations on sensors and sensor placement procedures. Authors identified 352 electrode location descriptions in 144 papers in which

sEMG was utilized. Most descriptions were found to be generic and indicated muscle belly (the thicker middle region of the muscle), motor point (where the axon contacts a muscle fiber), or midpoint of the muscle as the location of choice; these locations often coincide with innervation zones which have effects on sEMG signal features such as frequency characteristics [5].

Factors that influence the stability of EMG recordings include the presence of motor units/muscle tendons, the presence of other active muscles nearby [22], the distance between the active muscle fiber and detection site [16], filtering properties of the electrode, and the location of innervation zones in relation to the recording electrodes [5]. It is recommended that bipolar electrodes be positioned parallel to muscle fibers with a minimum spacing of 20 mm between centers of electrode poles [21]. This placement is small enough to avoid most crosstalk, but large enough to allow selection from a pool of motor units [5].

While sEMG sensors have traditionally been placed on top of the muscle belly over the motor endplate zone due to the ease with which large signals can be obtained, it has been found that the sEMG pattern in this region is not stable or reproducible [22]. It is therefore recommended that sensors be placed halfway between the most distal motor endplate zone and distal tendon, and that the geometrical distance of the electrode from other muscles be maximized (i.e. place electrodes at the muscle surface away from the edge of the muscle) [23], [22]. These recommendations have been reconfirmed by research conducted on the effect of electrode size and orientation on the sensitivity of myoelectric pattern recognition systems in which electrodes oriented parallel to muscle fibers significantly outperformed perpendicular ones [5]. A reference electrode (or ground electrode) should be placed on neutral tissue (e.g. over a bony structure) to provide a common reference for the electrode amplifiers [24].

Finally, special care must be taken when using surface electrodes, as it is possible for them to lose contact with skin and therefore distort the recorded signal [16]. High electrode-skin impedance can reduce signal amplitude and distort EMG waveforms [18]. It is recommended that there is continuous pressure on applied surface electrodes and that a saline gel or paste is used between the electrode and skin for increased conductivity [16]. Also important is skin preparation itself – which includes cleaning with alcohol and lightly exfoliating the area on which the electrode amplifiers will be placed [18].

2.2.2 Signal Conditioning

Most sEMG-based research utilizes more than one surface electrode placed on one or more muscles to characterize the physiological movement of concern (e.g. torque about a joint). The signals from these electrodes are fed to the *Signal Conditioner* block shown in Figure 3.

While electrode-amplifiers (*Signal Capture block* in Figure 3*)* are designed to reduce electrode-skin impedance, signal conditioning may be necessary to further improve the quality of the recorded EMG signal. Signal conditioning methods include filtering for the reduction of motion artifact/offset potentials, attenuation of noise outside of the physiological range (e.g. power line interference), and amplification of the EMG signal such that the signal is represented on the same scale as the parameters of the data acquisition system (e.g. ±5 V).

Electrode motion artifact can arise from either the deformation of the skin under surface mounted electrodes, or the mechanical disturbance of the electrode charge layer. The power density of motion artifact is known to be below 20 Hz; thus, a high pass filter can be used to improve signal quality. Such filters can have a corner frequency anywhere between 10 and 20 Hz, but should not be any higher to avoid loss of EMG signal power. Filtering techniques for motion artifact include 8^{th} order Chebychev high pass filters, and adaptive filtering based on orthogonal Meyer wavelets [18].

Electronics within an EMG acquisition system are designed to reduce power line interference via differential amplification, equipment shielding, and short electrode leads. Careful skin preparation can additionally attenuate power

line interference; however the inability to perfectly match skin impedance makes it possible for common mode signal to be transformed into the recorded EMG signal. In North America the offending frequencies are at 60 Hz and its harmonics. Narrow fixed notch filters centered at the fundamental frequency (and its harmonics) are often used to remove this noise offline. It is important to note that when this procedure is performed, the portion of the EMG signal occurring at these frequencies is also removed – altering the signal. Therefore, the bandwidth of the notches should be as narrow as possible (e.g. 0.25 Hz).

2.2.3 Signal Processing

The EMG signal is desired to be used as a control signal for applications such as multifunction prostheses, wheelchairs, gait generation, grasping control, virtual keyboards, and gesture-based interfaces [25]. The raw EMG signal, due to its random nature, cannot be used directly as a control signal. Rather, small portions of the EMG signal are analyzed in various ways in order to produce a set of features – statistical measures which characterize the raw EMG signal. The process of extracting useful information from the EMG signal, and the subsequent use of the extracted information, is explained in the following sections.

2.2.3.1 Data Segmentation

EMG signals have two states – transient and steady state. In the transient state the observed muscles go from rest to a voluntary contraction level, and in the steady state the muscle is in constant force contraction. Transient EMG signals have historically been more difficult to model than steady state signals. To combat this challenge, many classification methods use data segmentation, in which an EMG signal is analyzed in either overlapping or disjoint segments [19]. In this manner, the signal is considered steady state (formally "wide sense stationary") within a segment, but is modeled as changing its properties from segment-to-segment.

Since the EMG signal is desired to be used as a control for robotic systems, real-time constraints require that the total time of the segment length and processing time be 300 ms or less [25]. In *adjacent windowing,* EMG samples do not overlap – the signal is divided into equal segments for which features are extracted. In *overlapped windowing* the new segment slides over the current one with an increment time smaller than the segment length. Englehart and Hudgins investigated how segment increment impacts controller performance in a classification task and found that while smaller segments can produce a redundant stream of decisions, they can also help to improve system accuracy and response time [26]. They also found that through continuous segmentation, the segment length can be significantly reduced without substantial loss of accuracy. In some applications, all but one EMG sample overlaps between adjacent segments.

2.2.3.2 Feature Extraction

Feature extraction is the process of computing pre-selected features of the EMG signal to be fed to a processing scheme (such as a classifier) to improve the performance of an EMG-based control system [25]. The success of the system therefore depends on both the relevance of the feature to the intended motion and the validity of the method used for extracting the feature. In a real system, these features must be able to be extracted in real-time to be used as input signals to the control system.

There are two approaches to feature evaluation: structural and phenomenological. In structural feature evaluation, features are generated based on models (both physiological and physical) and can be evaluated using synthetic signals. This approach is helpful in determining the bias, variance, and level of sensitivity to noise of a given feature. In phenomenological feature evaluation, features are determined more empirically by interpreting the raw EMG signal and evaluating feature performance based on the overall success of an EMG control scheme (e.g. classification). Methods for selecting features involve various search strategies such as: sequential forward and backward selection, sequential floating selection, and random search strategies such as genetic algorithms.

Features fall into one of three categories: time domain, frequency domain, and time-scale (time-frequency) domain.

2.2.3.2.1 Time domain features

Time domain features are the most common type of EMG feature due to the ease with which they can be computed. The EMG signal is amplitude modulated where higher signal amplitudes represent higher muscle contraction levels, thus the piece of information needed is amplitude [27]. EMG amplitude is proportional to the number of active motor units and their rate of activation [25]. It is obtained by estimating the standard deviation of an EMG signal and provides information regarding signal energy, activation level, duration of contraction, and force [28].

Techniques to form an EMG amplitude include analog rectify and smoothing (low pass filter) processing, mean absolute value (MAV) processing, and root mean square (RMS) processing. A Gaussian model has been found to fit the EMG signal at a high level of contraction, while LaPlacian is well suited for low contractions and fatigued muscles. For signals modeled as a Gaussian random process, the RMS theoretically provides the maximum likelihood estimation (MLE) of amplitude in a constant force and non-fatiguing contraction. For those modeled as a LaPlacian random process, MAV provides the MLE of the amplitude. Clancy et al. experimentally found that for EMG signals acquired from constant-force, constant-posture, non-fatiguing contractions, the distribution of experimental data falls between Gaussian and LaPlacian, and that the Gaussian model fits better on average [18]. As such they concluded that there is little reason to argue between the MAV and RMS amplitude estimation methods.

Clancy et al. have developed methods for improving the quality of EMG amplitude estimates. They have shown that signal temporal whitening (decorrelation) and the combination of multiple channel signals to form one amplitude estimate (from a large muscle) reduce the variance in amplitude features without increasing bias. In multiple channel whitening, EMG recordings obtained from adjacent electrodes are combined to improve the signal-to-noise (SNR) ratio. Since the distance from the muscle and electrode gain settings differ per electrode, gain normalization is also performed during this step.

Demodulation and smoothing are performed on the EMG signal. Demodulation rectifies the signal and raises the result to a power (1 for MAV, 2 for RMS). Smoothing filters the resulting signal, thereby increasing the SNR[1]. Relinearization is then performed to return the signal to EMG amplitude by inverting the power law applied during demodulation. If EMG-torque or EMG-force is to be estimated, then the signal is additionally decimated to a frequency relevant to that of the frequency of the measured force.

Other time-domain features of EMG signals include mean absolute value slope (MAVS), zero crossing (ZC), slope sign changes (SSC), and waveform length (WL) [29]. These features provide measures of signal amplitude, frequency, and duration.

2.2.3.2.2 Frequency domain features

Mean and median frequency of a power spectral density (PSD) of an EMG signal are common frequency features, as they provide some basic information about the signal spectrum and its change over time [25]. Various methods of acquiring the mean and median frequency have been proposed, with Farina and Merletti presenting an autoregressive (AR) model outperforming the periodogram method in short segment length under stationary and non-stationary conditions [30].

2.2.3.2.3 Time-frequency features

Since EMG signals are non-stationary, knowledge of both frequency and time is pertinent to EMG control [25]. Spectral analysis uses the Fourier Transform (FT), which provides signal frequency content without reference to timing. Time-

[1] The smoothing step may be omitted when the EMG amplitude obtained is used to estimate torque. Low pass filtering will occur within a later processing stage.

frequency analysis can be used for signal de-noising, identifying fatigue in long term activity, and isolating coordinated muscle activities. Methods to map a signal to a function of both time and frequency include the Short Time Fourier Transform (STFT) and the wavelet transform (WT).

The STFT creates a time-frequency signal, but has limited precision due to the size of the analysis window. Wavelet analysis can de-noise a signal without signal degradation and allows for the analysis of a localized area of a larger signal. This localized analysis reveals trends, breakdown points, discontinuities in higher derivatives, and self-similarity that other methods miss.

In wavelet analysis, a low scale shows the rapidly changing details of a signal (with a high frequency), and a high scale shows the slowly changing coarse features (with a low frequency). One can therefore monitor different parts of a signal by adjusting the focus of a wavelet transform. A generalized form of the WT is the wavelet packet transform (WPT) which allows for the "best" adapted analysis of a signal in a time-scale domain.

STFT, WT, and WPT differ in the way in which they partition the time-scale access. STFT uses fixed partitioning ratios, the WT uses variable aspect ratios where the frequency resolution is proportional to the center frequency, and the WPT provides adaptive partitioning – a complete set of partitions are provided as alternatives, and the best for a given application is selected. Englehart et al. [31], [32] used feature projection to determine the time-frequency feature that best classified EMG data and found WPT to be the best, followed by WT and then STFT.

2.2.3.3 Control Methods

The EMG signal has shown promise as a control signal for robotic prostheses and orthoses by correctly interpreting patient motion intention [19]. Despite its promise, EMG powered control has seen only incremental improvements since the first operable EMG controlled prosthesis was presented in the 1960s [25].

The EMG controller, depicted in Figure 5, generates output commands based on signal patterns and control schemes. EMG controllers should have accurate movement selection, intuitive actuating control for the user, and a response time fast enough that it is not noticeable to the user. Systems must also offer a high degree of dexterous control. One way to create intuitive systems is to reduce the knowledge required by the user to utilize the system. This can be accomplished by developing EMG control systems capable of interpreting muscle activation patterns and using them in a natural way to actuate motions.

EMG-based control methods can be categorized as either pattern recognition based or non-pattern recognition based [19]. Pattern recognition based control methods are more commonly employed in research and have thus far been shown to provide more functionality than simple commercial control schemes. In most methods, the feature extraction is performed on the raw EMG signal and these features are fed to the model.

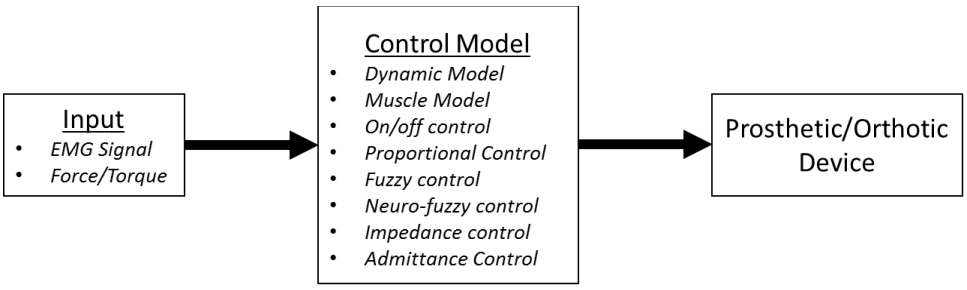

Figure 5: Diagram of EMG methods of EMG control models. Modified from [19].

2.2.3.3.1 Pattern Recognition Based Methods

Pattern recognition of EMG signals has been shown to potentially restore greater functionality than conventional control techniques [5]. The premise of the use of pattern recognition in prostheses and orthoses is that patients can activate repeatable/distinct EMG signal patterns that can be mapped to appropriate prosthesis/orthosis commands. The accuracy of pattern recognition based systems depends on the features, their extraction method, and the classification methods [19].

Classification is the task of assigning objects to one of several predefined categories [31]. When classification is used, a feature set is provided to the classification model, and the output of the model is the class label that the model believes the input came from. A classification model can be used to predict a class label of unknown data – it can be treated as a black box that assigns a label when presented with the feature set.

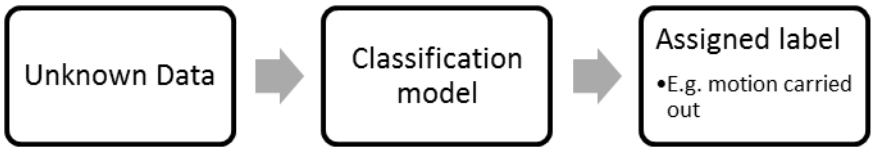

Figure 6: Classification overview.

There are several methods for building classification models, including rule-based classifiers, neural networks, support vector machines, and Bayes classifiers. Each method uses a learning algorithm to identify a model that best fits the relationship between the feature set and class label of the input data [31]. A good classification model fits the input data well, and correctly predicts the class labels of data it has not seen before.

The general classification approach is the following:

- A training set consisting of data with known labels is provided.
- A classification model is built using a training set.
- The classification model is applied to a test set, composed of data with unknown labels.
- An analysis of the accuracy of label determination is conducted by comparing the model output with the true label of the test data.

Performance of classifiers is quantified using a test set with known class labels. A common method for model validation is cross-validation, a technique in which each sample is used the same number of times for training, and once for testing. The data are segmented into partitions. During each run, one or more partitions may be chosen for testing and the rest are used for training. The total error is found by averaging the errors for all runs.

2.2.3.3.2 Non Pattern Recognition Based Methods

Non-pattern recognition based EMG control modeling techniques include proportional control and threshold control [19]. While the majority of assistive robots are currently being developed using classification, proportional control represents the long-term goal for prosthetic and orthotic device control.

The goal of proportionally controlled EMG models is to provide continuous output, e.g. force, for devices such as powered upper limb prostheses [1]. A common approach (in intact subjects) to EMG-torque estimation is to collect force data alongside EMG signals while the muscles under observation produce varying forces [14]. An EMG-torque model is then developed to estimate joint torques needed to perform the intended movement and provide the wearer with a constant fraction of that torque to produce the desired movements [32].

The tension produced by individual muscles cannot be measured non-invasively; thus there is no direct mechanical method to validate the predictions of the model on the level of individual muscles, although predictions about forces generated by the system may still be tested. In addition, the existence of cross-talk (defined as the interfering electrical activity from the surrounding muscles) and the inability to measure this effect add to the difficulties of creating this model. Improved EMG amplitude estimates produce decreased EMG-torque error, as do improvements in system identification (i.e. model selection and fitting procedures).

2.3 Applications of the EMG Signal to Dextrous Hand Control

Upper limb prostheses continue to evolve in both form and functionality [33], [34], [35], offering up to 20 degrees of freedom of movement. However, current EMG control capabilities limit commercially available systems to either three states (open, close, off) or one degree of freedom of proportional control [4], [36]. The control of more degrees of freedom is the greatest desired prosthetic improvement for below elbow amputees [37].

The long-term goal for prosthetic control is to provide a replacement limb with functionality and control similar to that of a (healthy) original limb. A number of techniques are being investigated within the research community to extend control capabilities. Several schemes have been demonstrated in the laboratory for discriminating between a limited set of user functions [38], [39], [29]. Tenore et al. have shown that it is possible to identify flexion and extension movements of individual fingers as well as combined (middle, ring, pinky) movements in a transradial amputee with greater than 90% accuracy [40]. These efforts provide for increased amputee function, but continuous proportional control of movement is not achieved.

Some studies of finger movement have considered proportional control via EMG-based estimation of finger forces or finger joint angles [41], [42], [43]. Liu et al. [1] conducted a preliminary study (N=3) relating EMG activity from forearm flexors and extensors to flexion and extension forces generated during constant posture, slowly force-varying contractions [1]. Spatial filters were used to derive EMG channels and an EMG-force model was generated to relate muscle activity to fingertip force via least squares estimation. The work indicated that multiple degrees of freedom of proportional control may be possible using EMG data collected from the forearm.

3 Methods

This study sought to determine whether the system identification methods of [1] can be used to reliably distinguish between multiple degrees of freedom in the forearm through EMG-force measured at the fingertips. Twenty subjects (10 male, 10 female), ranging in age from 23 to 62 years, successfully completed one experiment each. Data from a 21st subject were discarded due to procedural changes. Subjects had no known neuromuscular deficits of their right hand, arm, or shoulder.

The task for this work was constant-posture slowly force varying contractions of individual fingers and combinations of fingers (termed grips). Each subject was instructed to relax all muscles not involved directly in the task, and to maintain consistent posture and contraction techniques for each finger/grip throughout the study.

The fitting of model parameters was performed through the singular-value-decomposition-based least squares pseudo-inverse approach. A method of eliminating singular values that provide little information but contain noise has been used in other studies [44]. This research studied the effect of various thresholds for discarding such singular values through the identification of optimal model training parameters. Both linear and nonlinear models were explored since it is known that EMG amplitude is not entirely linearly related to force output. After an optimal model had been developed, the selection of subsets of electrodes was explored to determine the practicality of implementing these models in real-world scenarios.

This chapter explains the experimental and data analysis methods employed for the finger and grip EMG-force study. The experimental apparatus is explained in detail, including the acquisition of the EMG and force signals and the manner in which the subject interacted with the apparatus. A subsection detailing clinical procedures is also included.

3.1 Data Acquisition

A low-cost multifunction data acquisition unit was used to collect 16-bit resolution signals from 12 sEMG channels as well as the force output by a load cell. The design of the acquisition of both of these types of signals is detailed below.

3.1.1 EMG Signal

The EMG signal is acquired in a multistage process composed of the detection of raw EMG signals via sEMG electrode amplifiers, signal conditioning with a custom built signal conditioner, and data acquisition at a rate of 4096 Hz per electrode channel via a National Instruments data acquisition (DAQ) unit (NI-PCI 6229) in combination with a LabVIEW VI.

A block diagram of EMG signal acquisition can be seen below.

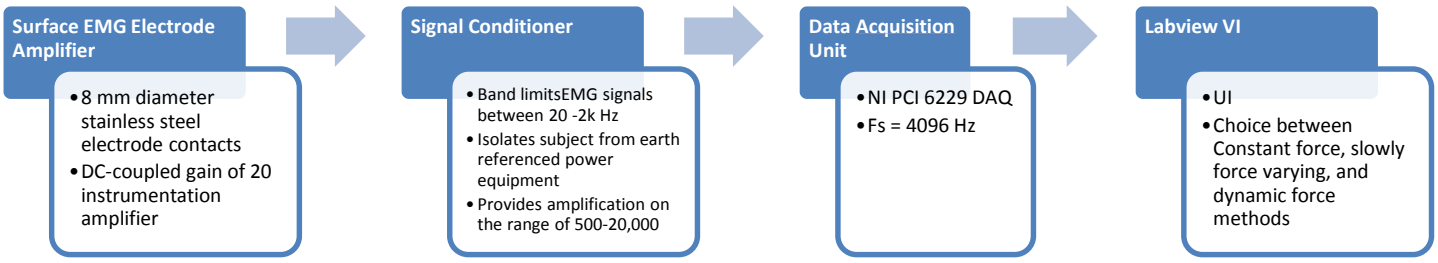

Figure 7: EMG Signal Acquisition

Each electrode-amplifier is a 3x1.5x0.6cm epoxy cast element. Each consists of a pair of eight mm diameter stainless steel electrode contacts separated by a distance of ten mm (edge to edge). These contacts are connected to a DC-coupled (gain of 20) instrumentation amplifier. Data from the electrode amplifiers is transferred to the signal conditioner via Ultra-Flex wire. The circuit diagram for these electrodes is shown below.

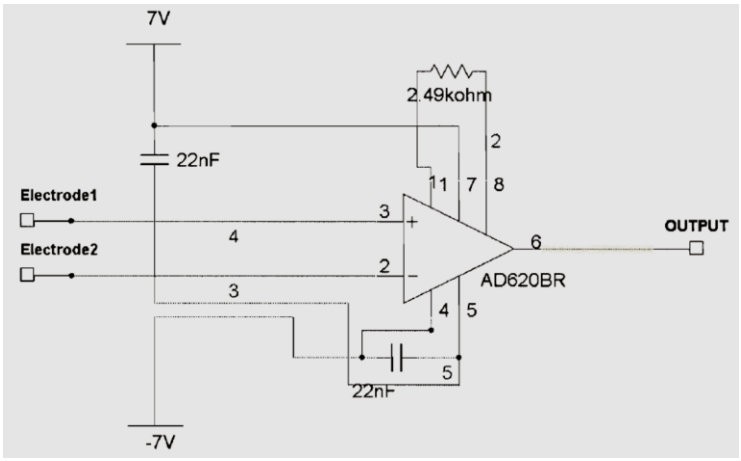

Figure 8: Three-Op-Amp Design of an Instrumentation Amplifier [45].

The signal conditioner serves to bandlimit the EMG signals between 15 and 1800 Hz, isolate the subject from earth referenced power equipment, and amplify EMG signals at gains of 200-25,600. Shown below is the full signal conditioner circuit diagram.

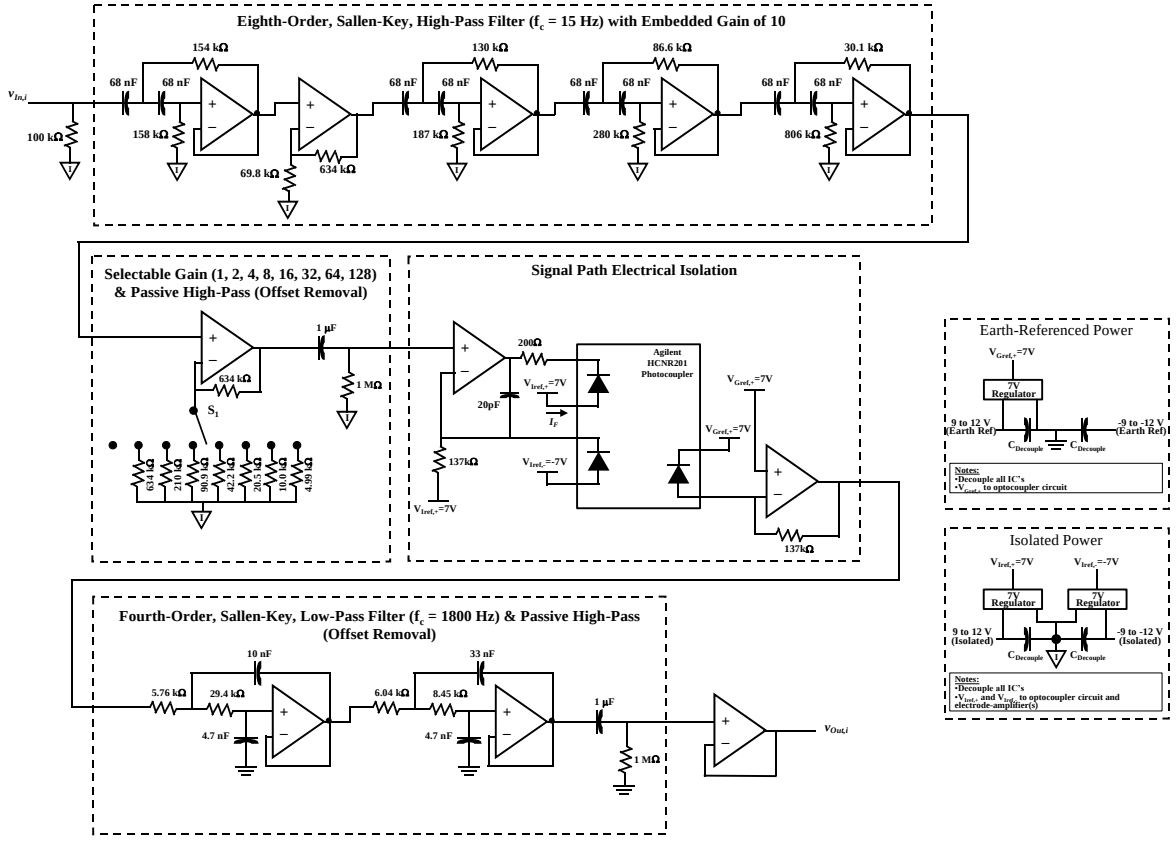

Figure 9: Signal Conditioner circuit diagram [46].

The output of the signal conditioner is acquired by the DAQ at a sampling rate of 4096 Hz at 16-bit resolution for various lengths of time (based on the test type) defined by a LabVIEW Virtual Instrument (VI).

3.1.2 Force Signal

A force transducer (LC101-100 load cell; Omega Engineering, Inc., Stamford, CT, USA) was used to obtain flexion and extension forces of the fingers and grips. The load cell produces output signals on a mV scale (0.3 mV/lb up to 30 mV maximum). A bridge amplifier/signal conditioner module (DMD465-WB; Omega Engineering, Inc., Stamford, CT, USA) was used to amplify the signal to a +5 to -5 Volt scale and filter background noise. The force channel was acquired at a sampling rate of 4096 Hz (16-bit resolution) by the DAQ for various lengths of time (based on the test type) defined by the VI.

A block diagram of the force signal acquisition can be seen below.

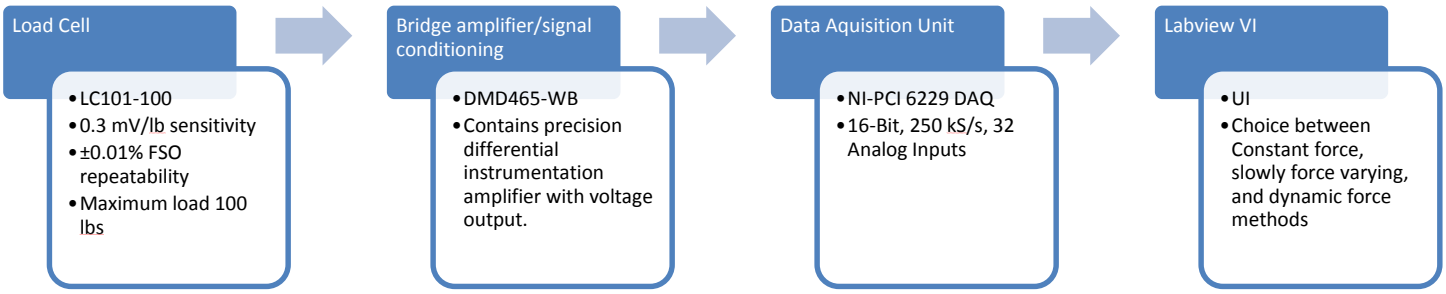

Figure 10: Force Signal Acquisition

3.2 Subject Interface

Of the utmost importance in biomedical studies is the way in which the subject interfaces with study equipment. If the test setup is poorly designed, not ergonomic, or not intuitive to the subject, data acquired during the study may produce poor results, causing researchers to draw false conclusions about the potential for their work. As such, considerable attention was paid to the way in which the subject interfaces with our test setup.

The overall subject interface for this study consisted of 12 surface EMG electrode amplifiers, a hand/finger restraint device, and various LabVIEW interfaces used for both collecting data and providing the user with an interface for each type of contraction trial conducted during testing (constant force, slowly force varying, and dynamic force varying muscular contractions).

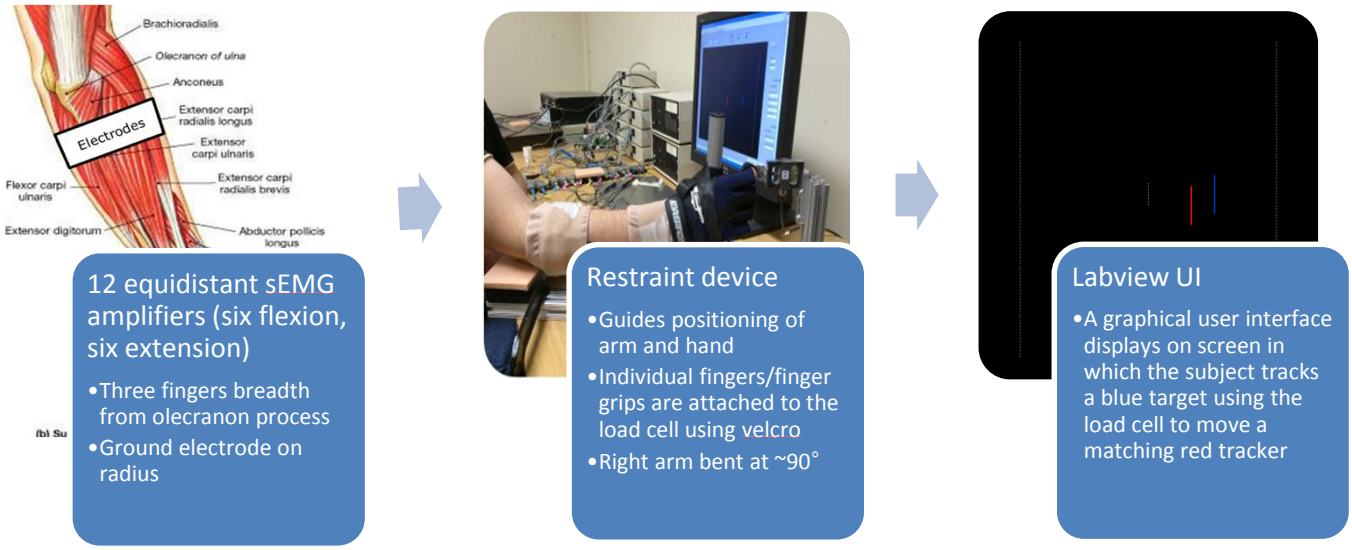

Figure 11: Diagram of subject interface for study [15].

Each part of the subject interface is detailed in the sections below.

3.2.1 Surface EMG Amplifier Placement

The muscles of the forearm can be divided multiple groups including those responsible for moving the wrist, four fingers, and thumb, with the bulkiest portions of the muscles at the proximal forearm. These muscles are divided by fascia into the anterior flexors and posterior extensors, both of which have superficial and deep muscle layers. Most flexors are innervated by the median nerve while the extensors are innervated by the radial nerve. These muscles move fingers via their long tendons with the assistance of the small intrinsic muscles of the hand for more precise movement [15].

A study that mapped the innervation zones of forearm muscles demonstrated the difficulty of targeting electrode positions near innervation zones corresponding to specific muscles. Additionally, studies have shown that targeting specific muscles for pattern recognition control do not make improvements over evenly spacing electrodes around the forearm [5].

A review of EMG studies in the forearm reporting classification accuracies >90% and their related electrode placement was conducted and can be found in Appendix 1. A generalized electrode placement (equidistant spacing of electrodes mounted circumferentially) was used. Muscles detected with these electrodes included:

- **Superficial muscles (directly measured)**
  - Extensor digitorum
  - Flexor carpi ulnaris
  - Extensor carpi radialis longus
  - Extensor carpi radialis brevis
  - Flexor digitorum superficialis
- **Deep muscles (not directly measured)**
  - Extensor digit minimi
  - Extensor pollicis brevis and longus
  - Flexor pollicis longus
  - Adbuctor pollicis longus
  - Extensor Indicis
  - Flexor digitorum profundus

Based on a conservative model of a female forearm, twelve surface EMG amplifiers were used on all subjects for consistency. Electrode 1 was always mounted on brachioradialis, followed by electrodes 2-6 mounted across the anterior forearm muscles (flexor carpi ulnaris, flexor carpi digitorum superficialis) and electrodes 7-12 mounted across the posterior forearm muscles (extensor digitorum, extensor carpi radialis longus and brevis).

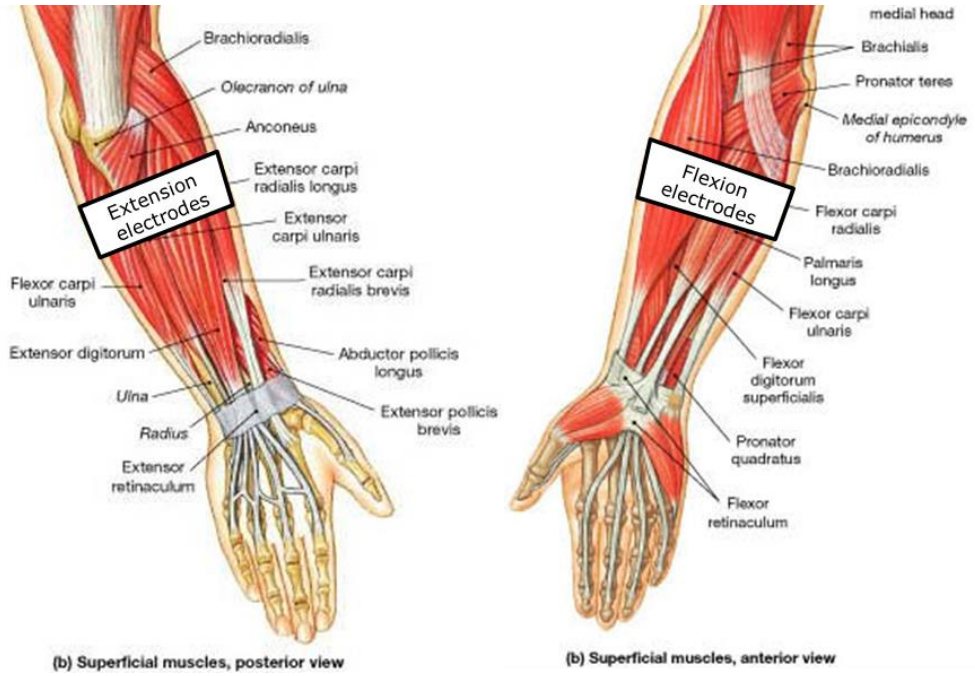

Figure 12: Diagram of flexion and electrode placement with respect to superficial anterior and posterior forearm muscles [15].

To prepare the subject's forearm for electrode placement, it was first scrubbed with an alcohol wipe and then lubricated with conductive gel (Spectra 360 Electrode Gel; Parker Laboratories, Inc., Fairfield, NJ). Then surface EMG amplifiers were placed equidistant from each other and mounted circumferentially around the forearm, parallel to muscle fibers. The proximal edge of each surface electrode was mounted three fingers breadth[2] from the antecubital with a wrist-band reference electrode attached to the distal head of the radius [47]. The minimum distance between the centers of the electrode contacts for the study was 2.66 cm. Electrodes were secured to the arm using ace bandages and medical tape. The outputs of each electrode amplifier were then further amplified and filtered between 15-1800 Hz.

3.2.2 Finger Restraint Apparatus

To facilitate constant-posture finger flexion and extension trials a restraint device was used to ensure proper alignment and angular positioning of the subject's forearm throughout testing. This device was a modification of the restraint device used in previous testing by Liu et al. (2011). The apparatus consisted of a rectangular base built using modular framing (10 Series Profiles, 80/20 Inc., Columbia City, IN, USA) in combination with a one degree of freedom LC101-100[3] load cell (Omega Engineering, Inc., Stamford, CT, USA), and load cell attachments for use with individual fingers, four finger grip and three finger grip[4]. Extensions from the rectangular based allowed the device to be rigidly clamped to the table. A detailed picture of this setup is shown in Figure 13.

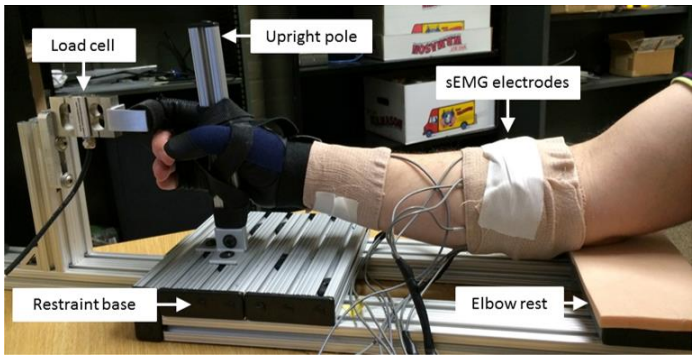

Figure 13: Photograph of arm secured into the restraint device. A Velcro strap is wrapped around a finger (index in this case) to secure it to the load cell, which measures finger or grip flexion/extension force. The gloved hand is attached to the upright pole using Velcro. Twelve surface EMG electrode amplifiers are wrapped around the circumference of the forearm, a ground/reference electrode is mounted on the radius at the wrist.

As seen above, the hand was secured to an upright pole during data acquisition. A cushioned elbow rest plate was mounted at the rear of the base for subject comfort. The height of this rest plate was adjusted for each finger to keep the long axis of the forearm parallel to the table. The subject was seated with their right arm bent at ~90 degrees for the duration of the study; the seat was adjusted to a comfortable height for the subject. Once mounted, the EMG electrodes were never in contact with the finger restraint setup. Shown in Figure 14 are the posterior and aerial view of the apparatus, respectively.

[2] The same researcher performed this measurement and placement throughout the study for consistent placement.
[3] The LC101-100 load cell was selected for use in this study to facilitate the testing of individual finger forces as well as three and four finger combination forces (termed grips).
[4] Testing confirmed that sensitivity of the LC101-100 load cell was equivalent to that of the LCL-040 load cell used in previous studies in our laboratory for individual finger trials.

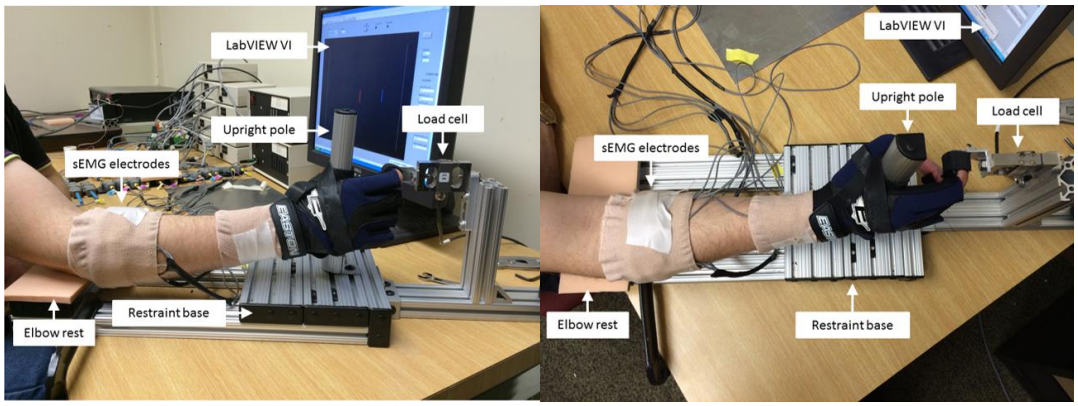

Figure 14: (Left) Posterior view of the hand/arm secured into restraint device. (Right) Aerial view of hand/arm secured into the restraint device.

Apparatuses built for the attachment of either individual fingers or a full four-finger grip to the load cell can be seen below.

Figure 15: (Left) Finger attachment and load cell. (Right) Grip attachment and load cell.

The location of the load cell apparatus and upright pole were adjusted for each subject such that the subject's fingers naturally reached the load cell apparatus for testing. Examples of the use of these pieces with hands in place are shown below.

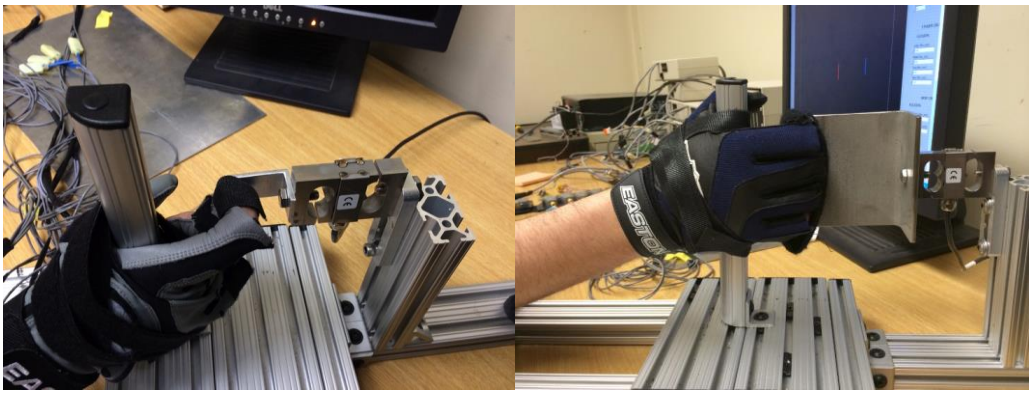

Figure 16: Demonstration of the use of the finger (left) and grip (right) attachments.

3.2.3 Virtual Instruments

Integral to the successful collection of data was the design of the VI used for the testing of flexion and extension constant force contractions and slowly force varying contractions in which the user tracks a moving blue line using their finger force. The following sections detail the way each of these VIs functions. The main screen of the VIs is shown below in Figure 17. For details on their use during clinical operations see Section 3.3.4 below.

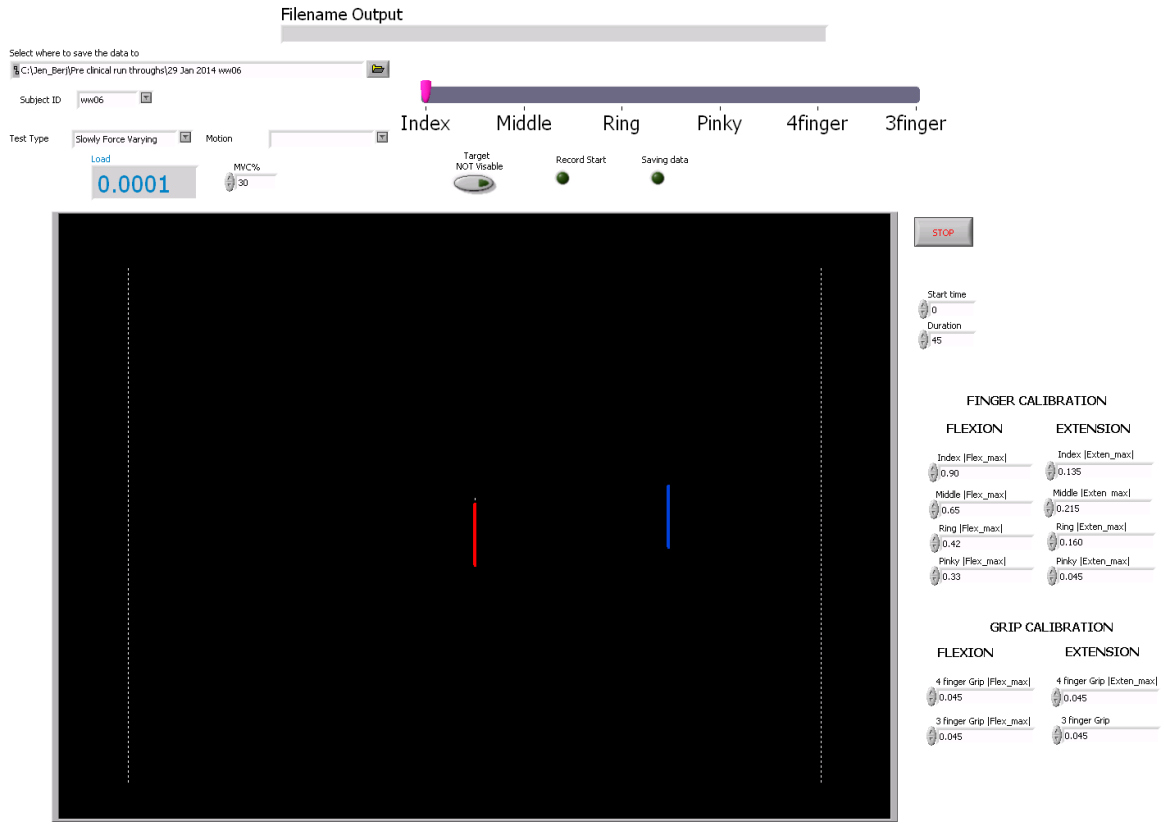

Figure 17: Virtual Instrument Front Panel. The horizontal location of the red line corresponds to the force currently exerted by the subject, while the location of the blue line represents a target force for the subject to match. The subject's goal is to keep the red line in as close proximity as possible to the blue line throughout the entire test.

3.2.3.1 Force Calibration

This VI plots a histogram of the subject's force signal during maximum contractions over a period of ~2-3s. It identifies the mean force exerted by the subject during maximum voluntary force contractions. It is used by the test administrator to identify the subject's maximum voluntary force calibration values for flexion and extension of each finger, and the four and three finger grips. These calibration values allow each test to be run at a specified percentage of 100% MVC.

3.2.3.2 Constant Force Contractions

During a Constant Force (CF) test, the VI presents the subject with a single red line. The subject either pulls (flexes) their red cursor to the left hand side of the test window or pushes (extends) the red cursor to the right hand side of the window, and holds the cursor in that position for a certain amount of time specified by the test administrator. The test administrator selects the type of test being run, and the subject's action (flexion or extension), and data files are automatically saved with the proper file name (thereby reducing potential for user entry error). The VI collects data for the amount of time specified by the test administrator, which allows the administrator to define a delay before data acquisition begins.

Calibration values obtained during force calibration are entered into this VI, which in turn set the limits of the VI window. For example, to test 100% flexion, the MVC percent is set to 100. This setting requires that the subject exert the same voltage value as was entered for calibration to either side of the screen. If MVC is set to 30%, the subject is required to exert only 30% of the calibration value to reach the side of the screen.

3.2.3.3 Slowly Force Varying Contractions

During a slowly force varying (SFV) test, the VI presents the subject with two lines: one blue and one red. The blue line is a moving force target controlled by the VI, while the red line is controlled by the subject's fingertip/grip forces. The red line moves to the right when the subject performs extension movement and to the left when they perform flexion movements. The subject's goal is to keep the red line as close in proximity as possible to the blue line throughout the entire test.

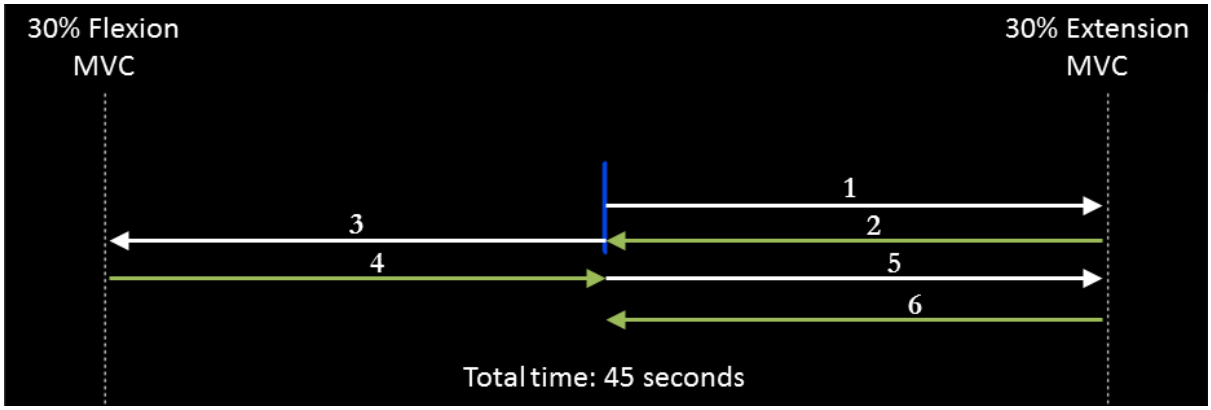

Figure 18: The VI presented to the subject during a SFV test. The blue line moves at a constant rate throughout the 45 second test, during which time it moves from the starting position, to the right of the screen (1), back toward the left of the screen (2, 3), again to the right of the screen (4, 5), and then back to the middle of the screen (6).

The force target (blue line) begins in the center of the screen and moves at a constant rate toward the right side of the screen, set to 30% extension MVC (1). Once the force target reaches the right edge, it travels to the left (2) until it reaches the left side of the screen, set to 30% flexion MVC (3). The force target then returns to the right side of the screen (4, 5), and changes direction one final time to return to the middle of the screen (6). The force target moves at a constant rate throughout the test and the entire test takes 45 seconds.

It is important to note that the center of the screen does not represent zero force. The subject's red tracker is skewed toward the weaker contraction sense (for this dataset it was always extension), to allow for the gain setting of the interface to be uniform across all movements. This results in the subject spending significantly less time in extension than in flexion, as highlighted in the force time-series plot below.

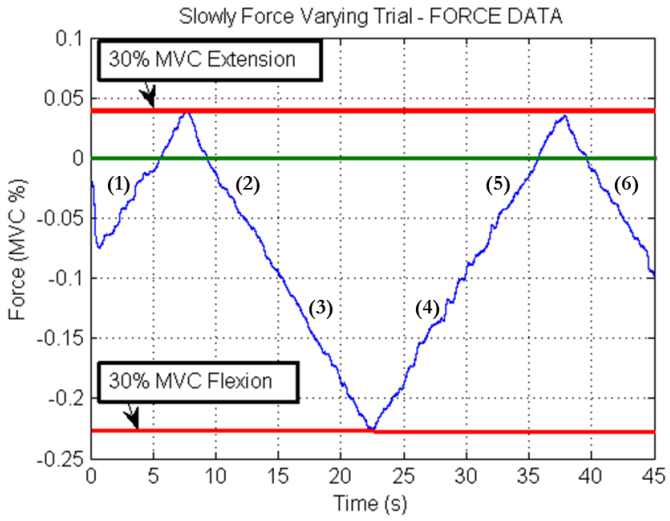

Figure 19: Graph of the load cell output during an SFV test. The labels correspond to the movements of the line from Figure 17. The green line indicates zero percent MVC.

All slowly force varying tests are run at 30% MVC with a zero second startup delay and each test runs for a total of 45 seconds. In order to follow the red line on the display screen, the subject will have to reach 30% MVC for both flexion and extension. In Figure 19 you can see an example graph of the load cell data produced from an SFV test.

3.3 Clinical Procedures

Twenty healthy subjects (ten male, ten female, aged 23-62 years) each completed one experiment. Subjects initially performed two five second MVCs per finger, each in flexion and extension, the averages of which were used as the subject's MVCs for the experiment. Next, they performed a 0% MVC (rest contraction) and separate flexion and extension 30% MVCs (for each finger) for ten seconds each, utilizing force feedback on a computer screen. These contractions were used to calibrate the advanced EMG amp processors [48]. Subjects then performed static (constant-posture, slowly force-varying) and dynamic (constant-posture, random 1 Hz movement) target tracking contractions (for each finger). A computer screen displayed their finger force.

3.3.1 Informed Consent

Before beginning any study procedures, the subject reviewed the informed consent form both privately and then with a test administrator. The test administrator answered any questions the subject had and ensured that the subject fully comprehended the study before enrolling them as a study subject.

3.3.2 Demographics & Survey (20 minutes)

After securing written informed consent, the circumference of the subject's right forearm was measured in order to customize the location of the 12 bipolar electrode amplifiers which would be secured to their arm. The subject then answered a verbal questionnaire reviewing the inclusion/exclusion criteria as well as their demographics such as race, ethnicity, age, height, and weight.

3.3.3 Electrode & Testing Setup (1 hour)

3.3.3.1 Electrode Mounting

The electrodes were mounted on the subject's right arm via the methods detailed in Section 3.2.1 (Surface EMG Amplifier Placement). The minimum electrode distance was 1.86 cm (2.66 cm center to center).

3.3.3.2 Load Cell Contact

After the subject had been seated, the restraint device was fitted to the subject's forearm length and hand size. First, the height of the chair was adjusted to a comfortable height and the subject's right arm was bent at ~90 degrees with their elbow supported at the olecranon process. Subjects wore a fingerless glove to allow the hand to be secured to the restraint device's upright pole without restricting the fingertips. The subject's hand was supinated ("thumb up") and secured to the upright pole using Velcro.

The load cell was then arranged to contact the most distal phalange of one or multiple of the subject's fingers to measure flexion and extension forces. Fingers were secured around the load cell apparatus using a thin Velcro strap. Fingers not in use during a trial were unconstrained, curled passively and extending beyond the upright pole. The height of the hand above the base was adjusted throughout testing so that the distal phalange of any one of the four fingers could be aligned with the load cell. This was done for all tests that the subject performed.

Constant posture flexion force was directed toward the subject (pulling motion), while extension was away from the subject (pushing motion). Force measurement was only made on one finger or grip at a time and subjects were instructed to minimize co-contraction throughout each test. Fingers not in use were assumed to be generating zero fingertip force.

3.3.3.3 Force Calibration (1/2 hour)

Subjects produced maximum contraction of each digit (separately), and combinations of fingers [four fingers (no thumb) and three fingers (middle, ring, pinky)], in both flexion and extension. Each maximum contraction lasted approximately three seconds. Subjects performed each maximum contraction twice, and the average of the force output by the subject for each motion was used as their MVC calibration value for the duration of testing. The force calibration values obtained during this procedure were entered into the VI to be used as a metric throughout testing.

3.3.3.4 Electrode Gain Setting (10 minutes)

After the subject's force calibration values were entered and 2-3 minutes of rest was provided, the gain of each electrode was set. During this portion of the visit, the subject repeated the motions from the force calibration section at 100% MVC for one to two seconds while the researchers adjusted the gain settings on each electrode channel to eliminate the possibility of signal clipping during data acquisition.

3.3.4 Grip Trials (EMG-Force, 1 hour)

Subjects produced flexion and extension signals for two grips.

Grips that were tested were:

1. Four fingers attached to the apparatus: index, middle, ring, & pinky
2. Three fingers attached to the apparatus: middle, ring, & pinky

Approximately two minutes of rest was provided between each trial for grip EMG-force activities to allow muscles to recover between trials. Hand restraints were removed between trials as needed, and test administrators continually checked on the comfort of the subject.

3.3.4.1 Constant Force (100%) (10 minutes)

Subjects produced one set of five second duration constant-posture constant-force contractions against the load cell with each grip. The startup delay was set to two seconds to allow the subject to reach either the flexion or extension side from their baseline. The force level was the same as their calibration trials (100% MVC). Visual feedback of the force was provided. A full explanation of this test is presented in Section 3.2.3.2 Constant Force Contractions.

3.3.4.2 Constant Force (30%) (20 minutes)

Subjects produced two sets of ten second duration constant-posture constant-force contractions against the load cell with each grip. The startup delay was set to two seconds to allow the subject to reach either the flexion or extension side from their baseline. For these trials, the subject was required to maintain 30% MVC. The length of each trial was extended from 5 seconds to 10 seconds due to the ease with which subjects could achieve 30% MVC. Visual feedback of the force was provided. A full explanation of this test is presented in Section 3.2.3.2 Constant Force Contractions.

These contractions were used to calibrate advanced EMG amplitude estimation algorithms [48], [49].

3.3.4.3 Slowly Force Varying Contractions (15 minutes)

Subjects produced three sets of constant-posture slowly force varying contractions with each grip. The startup delay was set to zero seconds so that the force signal would mimic that shown in Figure 19. These trials were conducted to a maximum of 30% MVC and lasted 45 seconds each. There were three contraction sets for both grips, for a total of six trials. The order of the contractions was randomized for each contraction set. For a full description of this test, see Section 3.2.3.3 Slowly Force Varying Contractions.

3.3.4.4 Dynamic Force Varying Contractions (15 minutes)

Note: Dynamic force varying contractions were not analyzed as a part of this thesis; they can be analyzed at a later date. This explanation is being included for full disclosure as this 15-minute session contributes to overall muscle fatigue in future measurements.

Subjects also produced three sets of tracking contractions in which they tracked a randomly moving force target (blue line) on the computer screen for 45 seconds– with each grip. The target moved as a uniform random process bandlimited to 1 Hz, over the range from 30% extension MVC to 30% flexion MVC. There were three contraction sets for both grips, for a total of six trials. The order of the contractions was randomized for each contraction set.

3.3.5 Classification Trials (No force measurement, 20 minutes)

Note: Classification contractions were not analyzed as a part of this thesis; they can be analyzed at a later date. This explanation is being included for full disclosure as this 20-minute session contributes to overall muscle fatigue in future measurements.

In addition to the above force-tracking trials, subjects participated in a short session in which they completed gestures to be used for signal classification. The gestures were as follows:

- Rest
- Wrist flexion
- Wrist extension
- Forearm supination
- Forearm pronation
- Hand close
- Hand open
- Pinch grip
- Three finger grip

Photographs of these gestures are shown below in Figure 20.

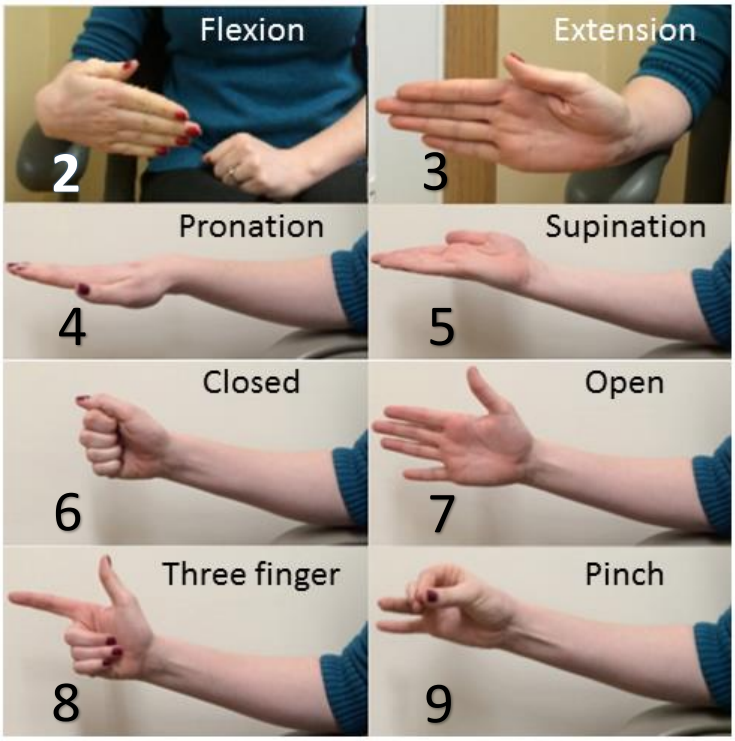

Figure 20: Pictures of all of the classification gestures performed by each subject. Note: Movement 1 was always "REST" in the predetermined classification sequence.

The *rest* 'contraction' was simply a relaxed version of the *hand open* shown in Figure 20.

During this section, subjects were released from the restraint device but remained seated. Subjects were shown a training video on the movements they would perform, and were given time to practice with visual cues.

Once subjects felt confident in their ability to perform the gestures, recordings began. Four 45 second recordings took place; each gesture was held for five seconds. Two of these recordings were in the order that the subject practiced (denoted by the numbers in Figure 20). The other two sequences had a randomized order. Timed video and audio cues were provided throughout all recordings. This design was modeled after similar classification research conducted by Englehart et al [38], which has been employed in numerous classification studies [36], [26].

A schematic of the experimental protocol for classification can be seen below.

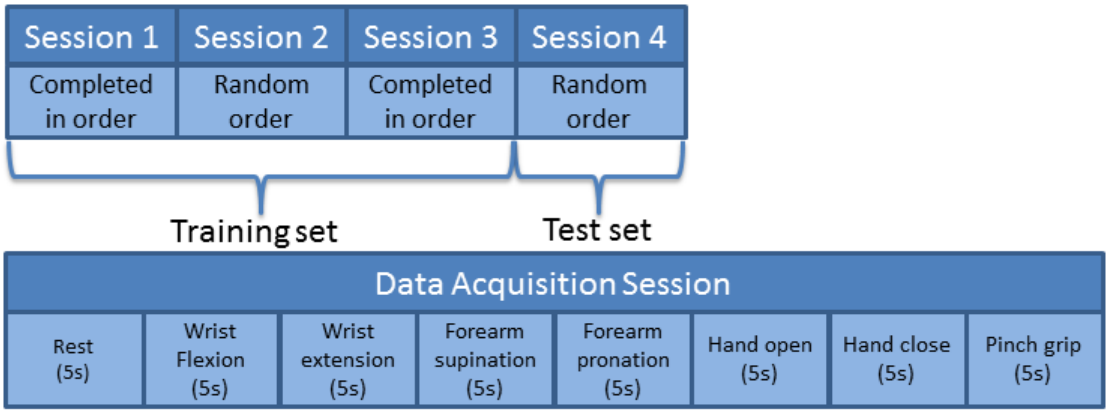

Figure 21: Diagram depicting classification tests

3.3.6 Finger Trials (EMG-Force, 1 hour)

Following the collection of grip EMG-force and classification data, finger EMG-force data were collected. The same series of tests were run for each finger (separately) as were run for each grip in the grip EMG-force portion of data collection. These tests were:

- Constant Force (100% MVC, five seconds)
  - One set of flexion and extension per finger
- Constant Force (30% MVC, ten seconds)
  - Two sets of flexion and extension per finger
- Slowly force varying contractions (30% MVC, 45 seconds)
  - Three sets per finger
- Dynamic force varying contractions (30% MVC, 45 seconds)
  - Three sets per finger

Subjects produced maximum contraction of each of the four fingers (separately).

Thirty seconds of rest was provided between trials to avoid fatigue. Additional rest was provided as needed. The order of contractions for each set of finger trials was randomized. The Velcro hand restraint was removed between trials as needed, and test administrators continually checked on the comfort of the subject.

3.4 Data Analysis

All analysis was performed offline in MATLAB (The MathWorks, Natick, MA). All signal preprocessing and model operations were performed using a stand-alone MATLAB toolbox [50]. The signal processing scheme for this study included a preprocessing stage, in which EMG amplitudes were generated, followed by EMG-force estimation via a polynomial, static FIR EMG-force model. An overview of this process is shown below.

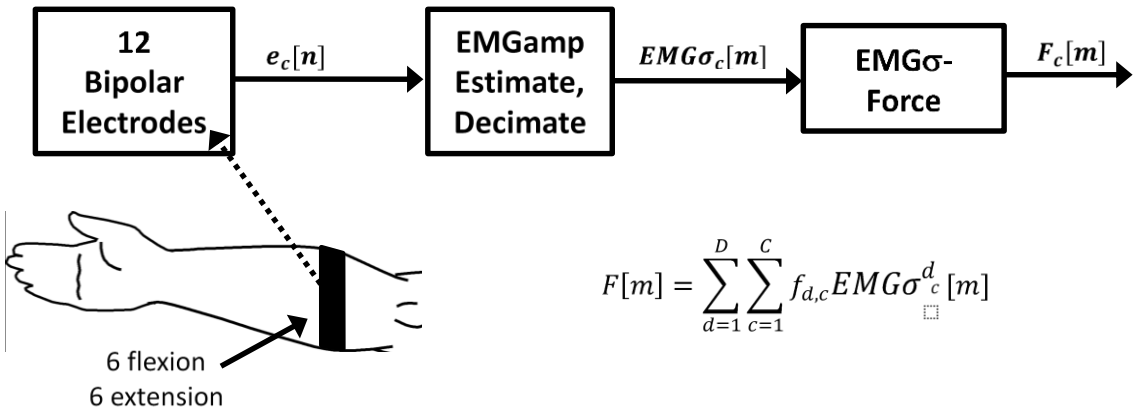

Figure 22: EMG-force model. Each of the bipolar surface EMGs are bandpass filtered between 15-1800 Hz and notch filtered at the power line frequency before performing EMG amplitude estimation at a reduced sampling rate. Least squares estimation is used to simultaneously relate EMG amplitudes to the force of the four finger tips. Sample index *n* denotes signals at the rate of 4096 Hz, while sample index *m* denotes signals at a rate of 4.096 Hz.

3.4.1 Signal Pre Processing (formation of EMG Amplitudes)

The original sampling rate of 4096 Hz is necessary for acquiring the raw EMG, but is not appropriate once an EMG amplitude estimate has been formed. To produce EMG amplitude estimates, the sampled EMG data were highpass filtered (15 Hz) using a fifth-order Butterworth filter, and second-order IIR notch filtered (bandwidth 1 Hz) at the power line frequency and all harmonics (due to the presence of significant power line interference). The narrow notch filter bandwidth eliminated the interference source with a limited decrease in overall statistical bandwidth of the signal [51]. Filtering was applied in the forward, then reverse time directions to achieve zero phase. This filtering was followed by a

first order demodulator for signal rectification. After demodulation, EMG signals were passed through a noncausal (two-pass), low pass 9th order Chebyshev Type 1 filter with an effective cutoff frequency of 0.8 Hz and decimated by a factor of 1000, producing a resampled frequency of 4.096 Hz. This low pass filter served as the smoothing stage of the amplitude estimate. Figure 23 shows an example of these stages.

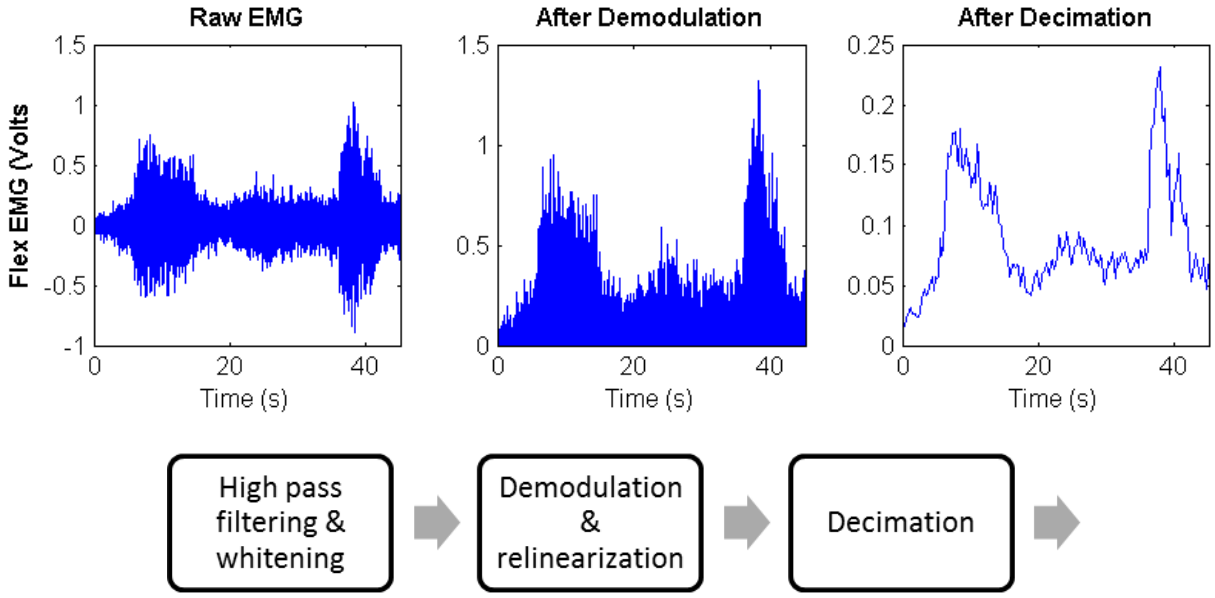

Figure 23: A single channel EMG signal (top plots) passing through steps of EMG amplitude estimation (bottom plot). Data (in 45s duration) were collected from a forearm flexion muscle channel during a slowly force varying contraction.

The force signal was similarly decimated, producing an EMG dataset with a bandwidth approximately 10 times that of the torque signal being estimated [52]. This decimated sampling rate is best for system identification, being large enough to capture the system dynamics (the fundamental period of force variation was 30s) and small enough to avoid noise existing out of the signal band [52], [13].[5] The force data was also normalized to percent MVC to facilitate the reporting of statistics across subjects.

3.4.2 EMG-Force Model

EMG amplitudes were related to force output at the fingertips using both linear and nonlinear FIR EMG-force static model structures. The model form is shown below. The model structure was a polynomial nonlinear model of degree *D*, the equation for which is shown below.

$$F[m] = \sum_{d=1}^{D} \sum_{c=1}^{C} f_{d,c} EMG\sigma_c^d [m]$$

Equation 2: EMG-Force Model.

In the equation, *F[m]* is the measured force at the *m*th decimated sample, $f_{d,c}$ are the fit parameters, *c* is the channel, *d* is the model order and $EMG\sigma_c$ are the EMG amplitude estimates for a given channel.

[5] When the system identification model is oversampled spurious model performance can occur [52]. It is recommended that the sampling rate of the EMG data not be more than 10 times the highest signal frequency.

Regularized (via the pseudo-inverse technique) linear least squares [44] was used to compute sets of fit parameters for the model. Singular value decomposition is used to solve the linear least squares problem. Singular values/vectors whose ratio of singular value to the maximum singular value is less than some tolerance (defined by the researcher) were discarded. A brief explanation of this process is shown in Figure 24: Fit coefficient vector calculation via least squares minimization.Figure 24 below.

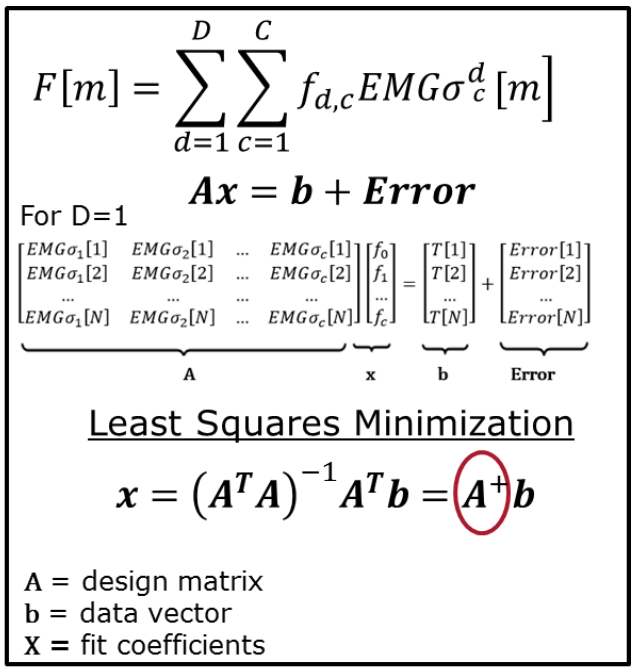

Figure 24: Fit coefficient vector calculation via least squares minimization.

This method is discussed in detail in Section 3.4.4.2 Tolerance and Model Order Selection.

3.4.3 Testing Estimator Performance

Models were formed relating the EMG channels simultaneously to force in all four fingers by combining four trials (one per finger) to form a single analysis record. One model was formed per subject. Three analysis records existed per subject. A train-test evaluation paradigm was utilized in which the model coefficients were fit to the data from a training record (the first record) and then used to "predict" the force from the second and third testing records. Prediction referred to passing the EMG amplitudes from the test record through the EMG-force model calibrated during training to predict the measured finger force during the test recording.

An error signal was formed as the difference between the force from the predicted and actual test record. The first and last 7.5 seconds of data from each error signal was removed (trimmed) since these data were corrupted by the startup transients of the various processing filters [13]. The resulting data contained equal amounts of time at each force level.

The tracking error was computed as the root-mean-square (RMS) error between the actual and predicted force was computed and used as a performance measure [18]. The average of the root mean squared errors was reported as the test error value; one error value was reported per finger. Only test trial results are presented. For statistical analysis, test error values were subjected to paired sign tests [53].

3.4.4 Model Optimization

After initial results across the four fingers were obtained, model parameters such as EMG amplitude resampled frequency, polynomial degree, and pseudo-inverse tolerance were varied to optimize the model performance. These modifications were performed serially such that EMG amplitude frequency was tested while holding tolerance and order constant, etc.

During this exploration the resampled frequency was tested at 4.096 Hz, 8.192 Hz, and 20.48 Hz, the polynomial degree ranged from$1 \leq D \leq 3$, and the pseudo-inverse tolerance ranged from $0.005 \leq Tol \leq 0.1$ in step sizes of 0.005. The first pass at modeling was made with *D = 1, Tol = 0.0056,* and a resampled frequency of 4.096 Hz, based on prior work [1].

3.4.4.1 EMG Amplitude Sampling Frequency

During EMG amplitude estimation, the raw EMG is decimated to a frequency lower than the original sampling frequency. After a first pass at modeling, the initial resampling frequency of 4.096 Hz (decimation by 1000), seemed to present noisy estimates. It was hypothesized that the decimation process during amplitude estimation was missing higher frequency components in the signal due to subject self-adjustments during tracking trials (e.g. moving quickly to catch up with the cursor after a mistake).

To explore whether a higher resampled frequency would improve tracking and reduce noise in the estimated force vectors, EMG amplitude estimates were generated with resampled frequencies of twice (8.192 Hz) and five times (20.48 Hz) the original resampled frequency. Each of these three datasets were modeled with training data and subsequently tested on test data; the original tolerance of 0.0056 and model order of 1 were maintained during this modeling.

3.4.4.1.1 Minimum Resampling Frequency

It was desired to identify the minimum possible resampling frequency for EMG amplitude estimates for slowly force varying contractions. To do this, the power spectral density of the force signal was examined to identify where the majority of signal power occurs, as well as the filter transients from the preprocessing paradigm.

3.4.4.1.1.1 Force power spectral density

To determine the validity of the initial resampling frequency, a power spectral density (PSD) analysis[6] was conducted on the force data. It is expected that the majority of the force power is less than 1 Hz, thus to properly inspect the signal, the spectral resolution must be significantly smaller than 1 Hz.

The maximum spectral resolution was calculated based on the largest possible window[7] size for the analysis using Welch's method. For a 45 second trial collected at 4096 Hz, this resolution is 0.0444 Hz. The calculation of resolution can be seen below.

$$Spectral\ Resolution = \frac{Fs}{WindowSize} = \frac{4096}{45 * 4096} = 0.0222\ Hz$$

Equation 3: PSD spectral resolution calculation for force signal.

The PSD was calculated on all of the force signals for slowly force varying finger data collected during the study (60 trials). The ensemble average was calculated and analyzed for its frequency content. The plot of this can be seen below.

[6] Using *pwelch* in MATLAB.

[7] The maximum possible window size is the full length of the file. MATLAB function *pwelch* divides the input file into overlapping sections the length of the window, and a Hamming window of this length is used for the analysis.

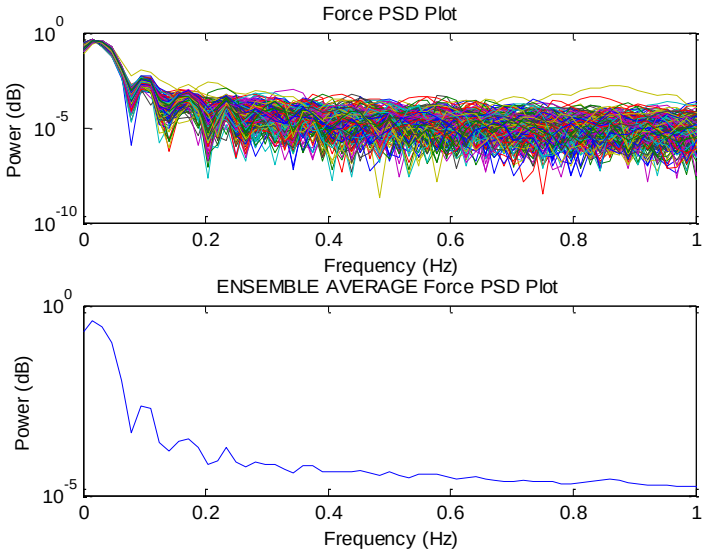

Figure 25: (Top) PSD of each force signal from slowly force varying trials in the study. (Bottom) Ensemble average of slowly force varying force PSDs for the study.

This analysis clearly indicated that the majority of the power in the signal occurs below 0.2 Hz. According to Ljung's rule [52], a resampling frequency of approximately 2 Hz would be acceptable.

3.4.4.1.1.2 Filter transient analysis

The impulse response (which defines the startup transient of the signal processing) of the system model with a resampling frequency of 4.096 Hz was assessed to determine the validity of decreasing resampling frequency below this value. It was found that after 7.5 seconds, the impulse response died down to 1e-03 (0.1%) of the peak response – or 1e-6 (one millionth) the original power. This response is shown in the figure below, with a red sample indicating the sample that occurs at 7.5 seconds.

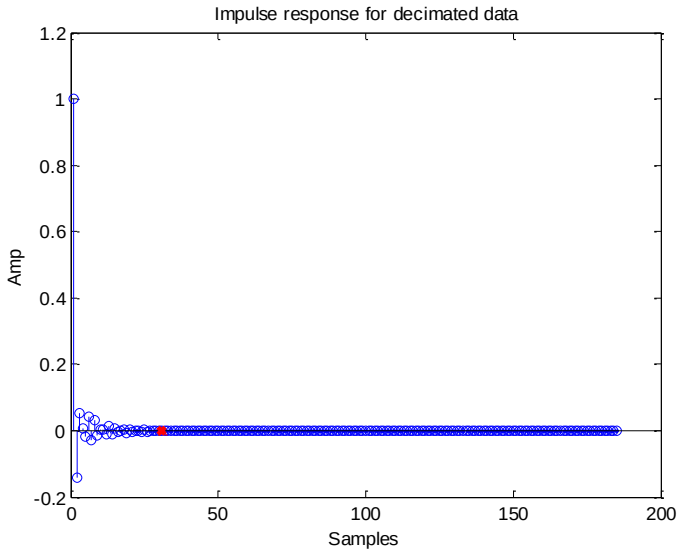

Figure 26: Impulse response of EMG force system. Response was used to determine the impact of filter transients on the dataset.

Since this response already requires eliminating the first 7.5 seconds of data (which is exactly the amount of time it takes for the moving force target to traverse from the center to either side of the screen), it was decided that decreasing the

resampling frequency further (which would increase this startup transient duration) would negatively impact the modeling process by eliminating too much data at times of changing force.

3.4.4.2 Tolerance and Model Order Selection

The pseudo-inverse tolerance and polynomial model order of the EMG-force model were varied across several values each. This generated many models with various combinations of these parameters. The following sections describe the motivation behind parameter modification and the method employed to test these modifications.

3.4.4.2.1 Tolerance

In Equation 2, when D = 1, the model can be written in the form

$$\boldsymbol{Ax = b + Error}$$

Equation 4: Linear least squares model (EMG-Force)

Where

$$\underbrace{\begin{bmatrix} EMG\sigma_1[1] & EMG\sigma_2[1] & \dots & EMG\sigma_c[1] \\ EMG\sigma_1[2] & EMG\sigma_2[2] & \dots & EMG\sigma_c[2] \\ \dots & \dots & \dots & \dots \\ EMG\sigma_1[N] & EMG\sigma_2[N] & \dots & EMG\sigma_c[N] \end{bmatrix}}_{\mathbf{A}} \underbrace{\begin{bmatrix} f_0 \\ f_1 \\ \dots \\ f_c \end{bmatrix}}_{\mathbf{x}} = \underbrace{\begin{bmatrix} T[1] \\ T[2] \\ \dots \\ T[N] \end{bmatrix}}_{\mathbf{b}} + \underbrace{\begin{bmatrix} Error[1] \\ Error[2] \\ \dots \\ Error[N] \end{bmatrix}}_{\mathbf{Error}}$$

Where **A** is the"design matrix", **x** is the fit coefficient vector, and **b** is the output vector [44]. The fit parameters, **x**, are found by minimizing errors in the least square sense by minimizing the square of the distance between the data and signal vectors through a linear combination of the columns of **A** [54]. This means that the **x** values must satisfy:

$$min\|\boldsymbol{Ax - b}\|^2$$

Equation 5: Least squares error minimization.

The solution to this minimization is found by computing

$$\boldsymbol{x = \left(A^T A\right)^{-1} A^T b = A^+ b}$$

Equation 6: Calculation of fit coefficients via singular value decomposition to find the pseudo-inverse.

where $\mathbf{A}^+$ is the Moore-Penrose pseudo-inverse of **A**, which uses singular value decomposition to compute $\mathbf{A}^+$.

Since the fit coefficients (**x**) are the product of $\mathbf{A}^+$ and **b** (the output vector), the values within $\mathbf{A}^+$ impact the fit coefficients. If these values represent noise within the training signal (rather than the signal itself), this noise gets injected into the model via the fit coefficients.

To improve the fit coefficients, singular values within the pseudo-inverse computation believed to represent noise are "removed." This is done by computing the ratio between each individual singular value and the maximum singular value in the design matrix **A** and defining a *tolerance* for that ratio. Any singular values within the pseudo-inverse matrix which fall below the tolerance are replaced with zeroes (e.g. for tol = 0.01, all singular values <0.01 are replaced with a 0).

For this set of data, the extent to which noise in the original signal was being modeled by the fit coefficients was unknown. Tolerance values between 0.005 and 0.01 (in steps of 0.005) were tested to determine whether changing this threshold would decrease the noise in the estimates.

3.4.4.2.2 Model Order

The relationship between force produced by muscles and the amplitude of their EMG signal is not necessarily linear. In small muscles (such as those in the forearm) the relationship is relatively linear [24]. This is because the firing rate of motor units has greater dynamic range and motor unit recruitment is limited to the lower end of the force range.

While linear models have commonly been used to relate EMG amplitude to force, nonlinear models have shown promise in some cases [55]. As such, the polynomial degree within the model was tested from $1 \leq D \leq 3$. The method for nonlinear modeling in this case is to estimate force with a model that simultaneously considers multiple model parameters, the process for which is shown below.

$$F[m] = \sum_{d=1}^{D} \sum_{c=1}^{C} f_{d,c} EMG_c^d[m]$$

$$\boldsymbol{Ax = b + Error}$$

$$\downarrow$$

$$[\boldsymbol{A^1\ A^2\ \ldots AD}] \begin{bmatrix} \boldsymbol{x_{D=1}} \\ \boldsymbol{x_{D=2}} \\ \boldsymbol{\ldots} \\ \boldsymbol{x_{D=D}} \end{bmatrix} = \boldsymbol{b + Error}$$

Figure 27: Explanation of estimating force with a model that simultaneously considers multiple polynomial orders. Note that the b vector remains unchanged.

3.4.5 Reduced Electrode Array Models

While the above research was performed using twelve sEMG electrodes, it is desired that less electrodes be required for real-world implementation. The use of twelve electrodes, in addition to being expensive, may also be a cumbersome approach.

Using the final model design (selected resampling frequency, pseudo-inverse tolerance, and model order), the best electrodes for arrays of sizes 6-12 were found, per subject, via exhaustive search.

Since linear least squares was used to model the data with twelve electrodes, the least squares error (LSE) produced during each generation of the model fit coefficients represents the measure of model fit. This equation can be seen below.

$$Least\ Squares\ Error = \|\boldsymbol{Ax} - \boldsymbol{b}\|^2$$

Equation 7: Least squares error equation.

This method attempts to minimize the square of the distance from the data vector, **b** to the signal model, where the LSE represents the part of the data vector that the signal model cannot describe.

To perform electrode selection, the LSE was calculated for each possible electrode vector for each electrode set (e.g. for the choice of the best 10 electrodes, $\binom{12}{10}$= 66 LSEs were calculated). The model producing the minimum LSE on the training data was chosen as the model for the number of electrodes under consideration. This model was then tested using test data from analysis records two and three.

Since each dataset contains subject-specific physiological data, it was not expected that the best electrodes for any given subject match that of any other subject. Electrode placement was tailored to subject physiology (forearm circumference), and the underlying muscle physiology is expected to vary in size, orientation with respect to the electrodes, and MUAPT activation patterns.

3.4.6 Statistical Methods

Two analysis records per subject were used to test each model, for a total of 40 (20 subjects x 2 test trials) tests of any one modeling configuration. From each of these tests the RMS error, in MVC percent, was output per finger. Thus for any one model, 40 error values for each finger were output representing the performance of the model across the study.

The methods above describe variations of tolerance, model order, and electrode combinations amounting to a total of 67 models to test in 1791 possible comparisons.

For each of these modeling scenarios, it was desired to know the statistical significance of any apparent improvement. This comparison was conducted via a paired sign test with a p-value of 0.05. As it was desired to identify the best performing model among the possible models, for any model comparisons that resulted in statistical significance ($p<0.05$), the higher performing model (i.e., the one with lower errors) was chosen to continue to subsequent comparisons. This method results in either a single model that performs significantly better than all others, or, more commonly, a final group of models that perform significantly better than other models but do not outperform each other. In this case, the "best" model is selected by looking at two items: model order, and average error of the model. This process is illustrated in the figure below.

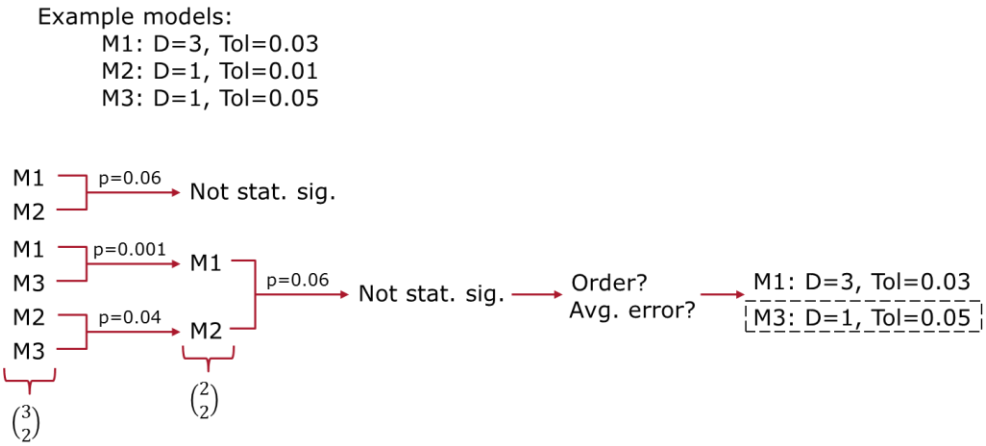

Figure 28: Illustration of "best" model selection.

A model that uses fewer coefficients is a simpler (and therefore less computationally complex to implement) model. If the result of this test is a set of models that are not significantly different from one another, the model with lower model order is selected over a model with high model order. If model orders are the same, then the average error produced by each model is compared, and the model with the lower error is chosen for final selection.

Since we are concerned with the best single model for all four fingers, the statistical significance for each finger was not considered separately. Rather the four error values (index, middle, ring, and pinky) were reshaped to represent one vector, and used in the paired sign test. This prevents us from identifying that different fingers require different models.

3.4.6.1 False Discovery Rate Control

During simultaneous hypothesis testing, the control of increased type I errors (incorrect rejection of a true null hypothesis) is of concern [56]. Methods to control the probability of incorrectly rejecting a true null hypothesis include the familywise error rate (which reduces the probability of even one incorrect assessment) and the false discovery rate (FDR), which produces the proportion of erroneous rejections among all rejections.

For this case, it is more important to control the FDR. When using the FDR approach, the dependency of test statistics must be considered. The Benjamini-Hochberg-Yekutieli FDR procedure controls the FDR for data with positively dependent test statistics; a modification to the thresholding of this procedure allows for its use in all cases of dependency. Data are positively dependent if the test statistics are Gaussian variables that are positively correlated or independent.

To determine which method to use (positive dependence vs. any dependence case), the dependency of each dataset compared was evaluated. The distribution of the data (RMS error in MVC%) within each model was observed and found to be roughly Gaussian (some cases had clear outliers). Next, the correlation between the error data from any two models was computed. Each correlation coefficient was found to be positive, across 1770 comparisons. To be sure, the correlation between each model was plotted. An example graph can be seen below.

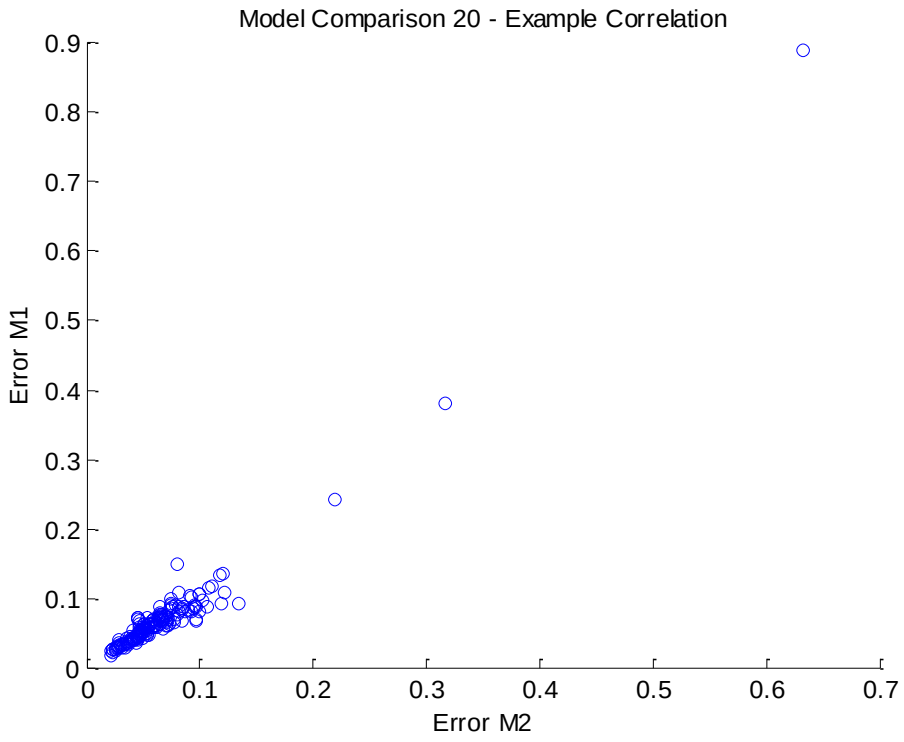

Figure 29: Example of correlation between two models.

This check was performed on the errors resulting from tolerance and model order variations as well as those resulting from models with varying amounts of electrodes. Both produced positively correlated datasets and Gaussian distributions.

4 Results and Discussion

Analysis of the tracking tasks consisted of evaluating the RMS error between the target and the subjects' pursuit path. Statistical analysis was applied to all EMG processors. Demographic results from the study can be found in Appendix 5.

4.1 EMG Amplitude Resampling Frequency

The base EMG-force model produced relatively noisy estimates, even with 12 electrodes. To investigate whether the resampling frequency of the EMG amplitudes impacts the noise of the estimation, models were generated with EMG amplitude resampling frequencies of 4.096 Hz, 8.192 Hz, and 20.48 Hz.

A box plot of the modeling error across the study (per finger) at each sampling rate can be seen below (left). A closer look at the data with error <15% is also shown (right).

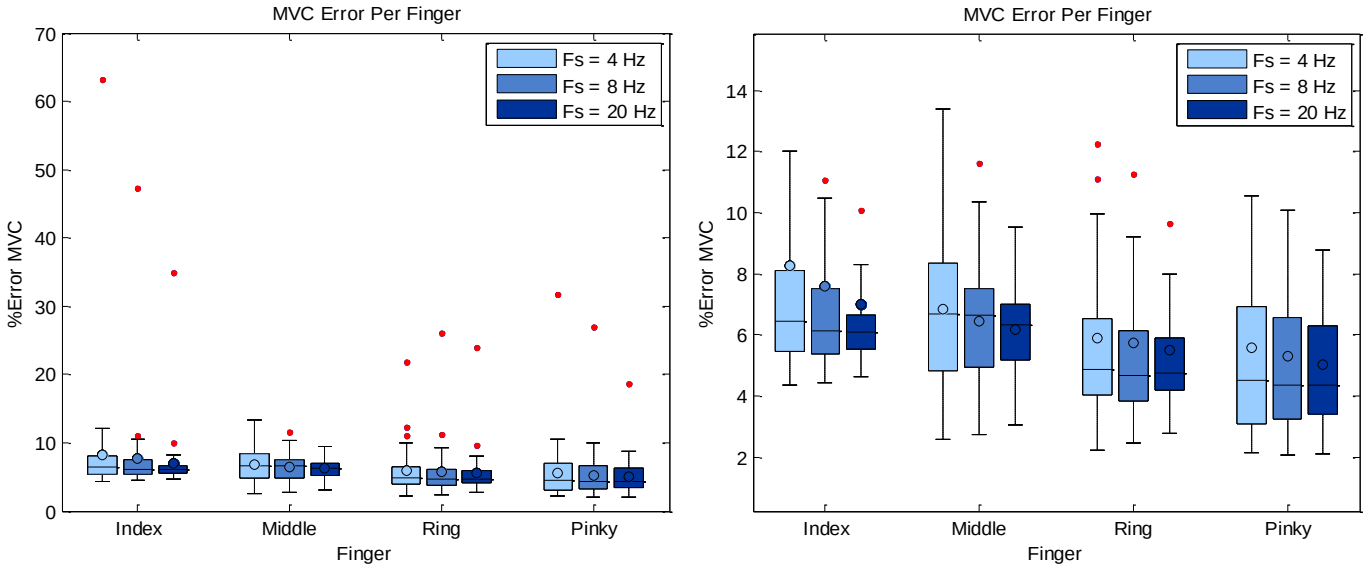

Figure 30: (Left) Box and whisker plot of MVC error per finger based on original model with sampling frequencies of 4.096, 8.192, and 20.48 Hz. Red dots represent outliers (>3/2*upper quartile, <3/2 lower quartile), the upper and lower bounds of the boxes represent the 75th & 25th percentile, respectively, the line within the box represents the median, the whiskers represent the maximum and minimum point excluding outliers, and the circles (filled with the same color as the boxes) represent the mean error. (Right) Same plot as (Left) zoomed in to see errors <15%.

From the above it can be seen that with increase in sampling frequency:

- Mean error of the estimates decreases
- Distribution of errors tightens
- Minimum/maximum error tightens
- Median error does not uniformly decrease

These results were surprising in contrast to the plots of estimated and measured force. Visual inspection indicates that the tracking was not actually improved by increasing sampling frequency – rather the estimates are a noisier version of the 4.096 Hz tracking line. A direct comparison between the middle finger identification at the time of largest force change for 4.096 Hz and 20.48 Hz is shown below.

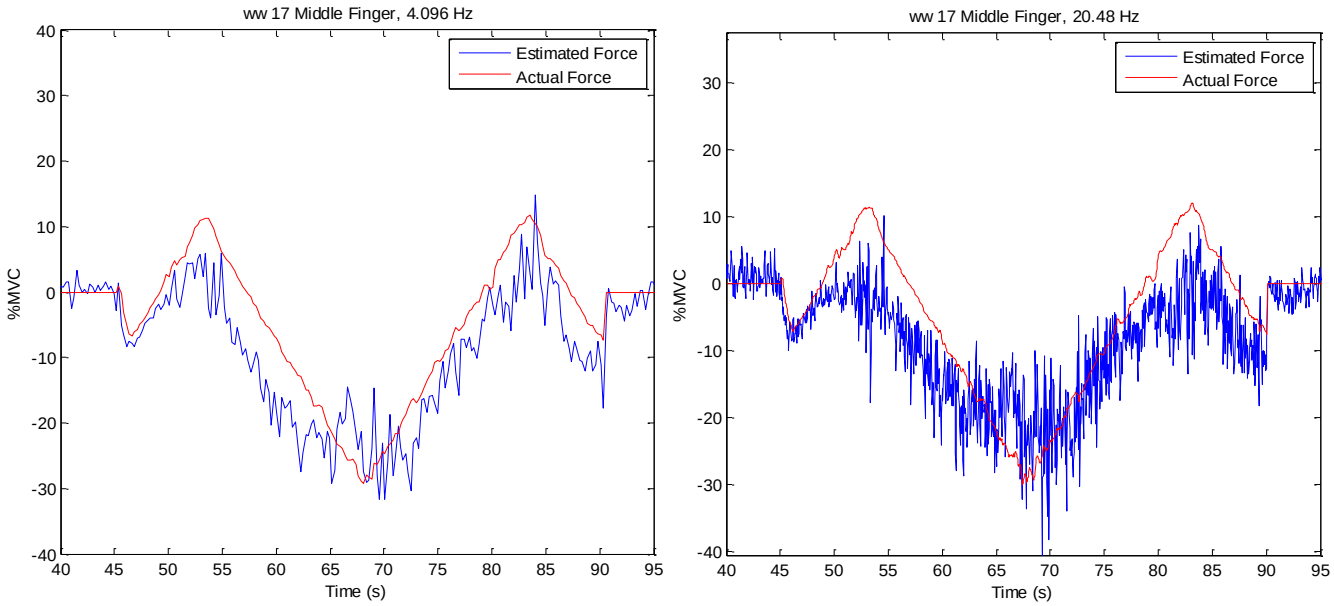

Figure 31: (Left) Tracking at 4 Hz (Right) Tracking at 20 Hz.

The trend of the errors is generally the same across all three datasets. This suggests that changing the sampling frequency would not necessarily change the overall way in which a prosthetic or orthotic would respond to the current model.

From a practical viewpoint – one would much rather implement the model shown on the left in Figure 31 for the control of a prosthesis or orthosis. The resampling frequency of choice for modeling was thus 4.096 Hz; this optimal decimation factor was used in all further analysis and results [13].

4.2 Pseudo-inverse Tolerance and Model Order

Tolerance and model order were co-varied according to the scheme outlined in Section 3.4.4.2 Tolerance and Model Order Selection. Shown below are plots of the average errors per finger (presented in average MVC% error) across the study for each model. Tolerance is shown on the x-axis and a different line color and marker style indicates the performance of the models at each tolerance for the three model orders.

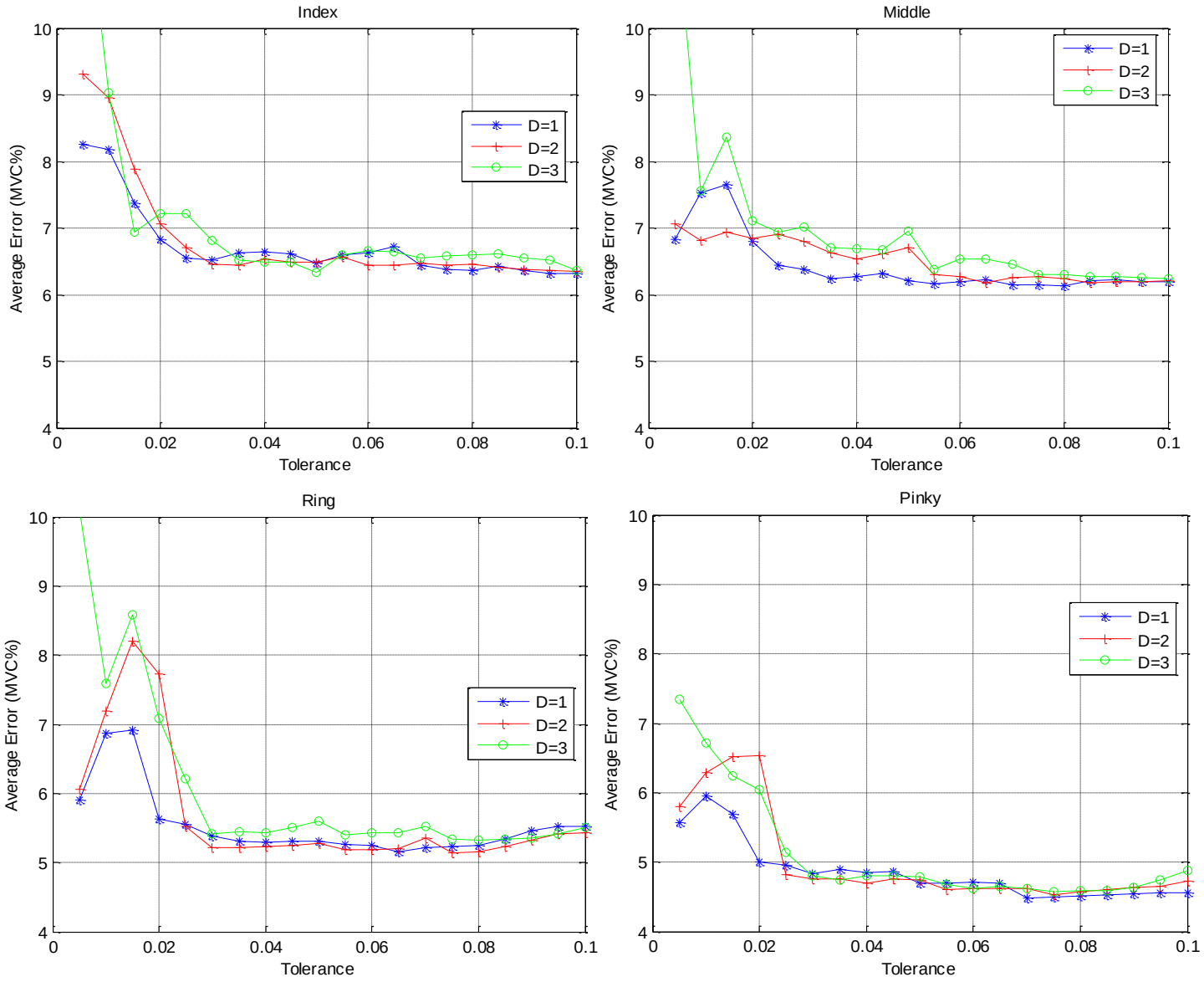

Figure 32: Mean error (in MVC%) per finger across the study for each model. (Upper left) Index finger, (Upper right) Middle finger, (Bottom left) Ring finger, (Bottom right) Pinky finger.

For all four fingers, tolerances lower than ~0.025 clearly result in worse performance than higher tolerances. After a tolerance of 0.025, the best tolerance and model order to select are not immediately evident.

The paired sign test with a p-value of 0.05 was used in concert with the Benjamini–Hochberg–Yekutieli procedure for FDR control ($q<0.05$) to compare the 1770 models above, as described in Section 3.4.6 Statistical Methods.

This method provided the following models for consideration:

- D=1, Tol=0.055
- D=1, Tol=0.050
- D=2, Tol=0.030
- D=3, Tol=0.035[8]
- D=2, Tol=0.045

To make a decision with regards to model selection, the average MVC error for each finger with a given model was considered. This table is shown below.

Table 1: Average MVC% Error ± SD for models under consideration. Cells highlighted in green represent the minimum error for that finger. The greyed out row is the model that FDR control methods eliminated.

Model	*Index*	*Middle*	*Ring*	*Pinky*
D=1 Tol =0.055	6.59 ± 1.0%	6.17 ± 1.2%	5.27 ± 1.5%	4.69 ± 2.0%
D=1 Tol= 0.05	6.48 ± 1.0%	6.20 ± 1.2%	5.30 ± 1.7%	4.69 ± 2.0%
D=2 Tol =0.030	6.46 ± 1.1%	6.80 ± 2.8%	5.22 ± 1.9%	4.75 ± 2.1%
D=3 Tol= 0.035	6.52 ± 0.6%	6.70 ± 3.7%	5.44 ± 2.2%	4.75 ± 2.1%
D=2 Tol =0.045	6.48 ± 0.8%	6.62 ± 2.9%	5.25 ± 2.0%	4.75 ± 2.2%

The models with *D=1 Tol = 0.055* and *D=2 Tol = 0.030* both contained the best performance for two fingers. Since models of higher order are more complex to implement (larger number of fit coefficients), the first order model with a pseudo-inverse tolerance of 0.055 was selected for final results. The full results of all model comparisons can be found in Appendix 6.

An example of improved performance from the original model is shown below.

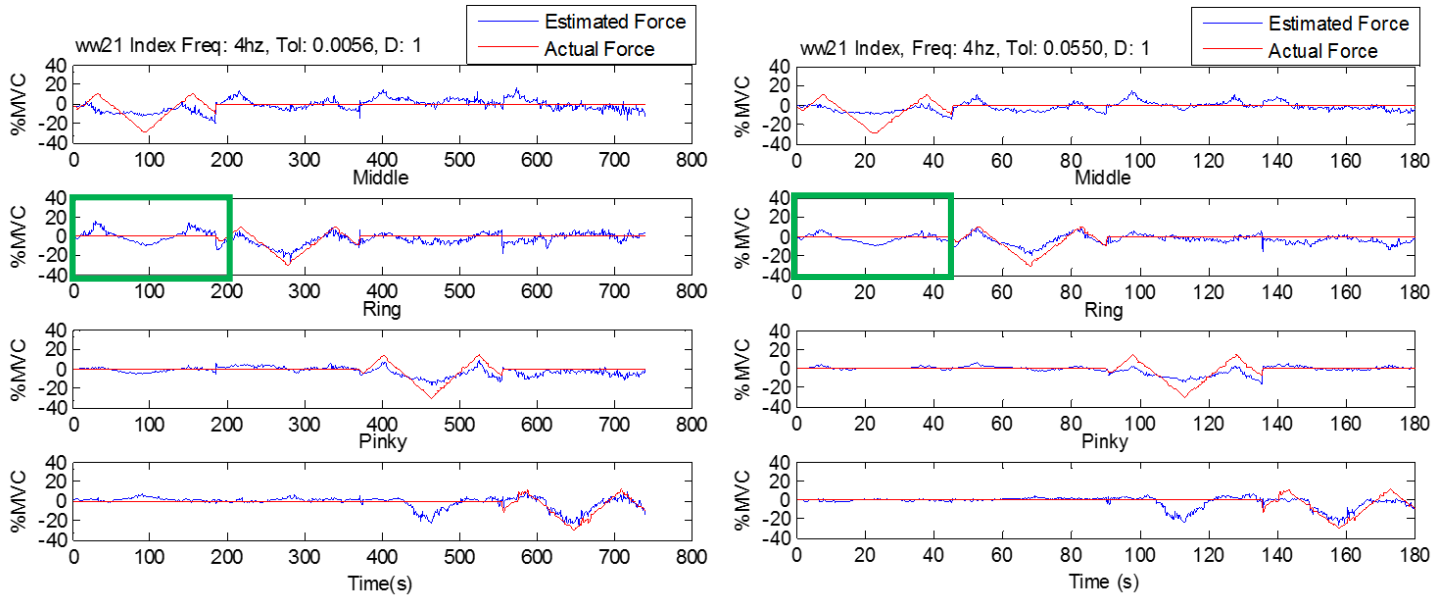

Figure 33: (Left) Original model performance with 4.096 Hz, D = 1, Tol = 0.0056, (Right) Final model performance for the same subject and trial with 4.096 Hz, D = 1, Tol = 0.055.

[8] This model was found via FDR control to have falsely rejected the null hypothesis.

While this method does offer improvement across the entire study, it is important to consider that increasing the tolerance in subjects for whom estimation worked well with the original model results in a loss of information about their signal, and thus less accurate tracking. An example of this phenomenon is shown below.

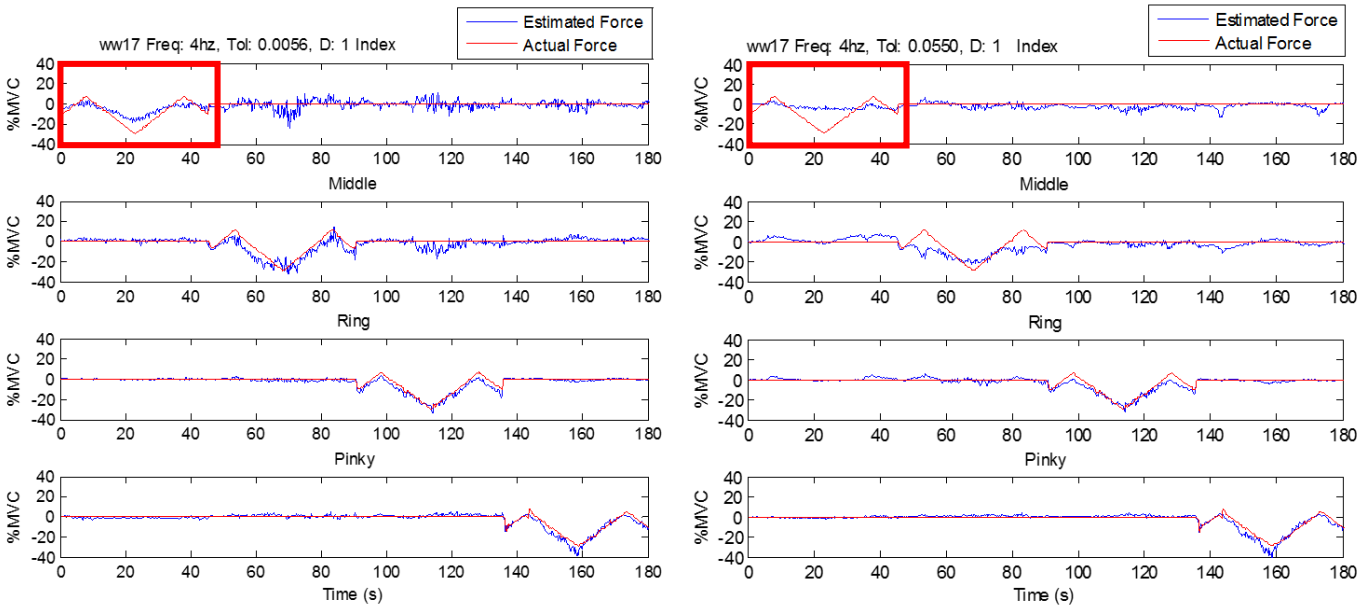

Figure 34: (Left) Original model performance with 4.096 Hz, D = 1, Tol = 0.0056, (Right) Final model performance for the same subject and trial with 4.096 Hz, D = 1, Tol = 0.055.

The performance across the study using the original and selected models is shown below in Figure 35 and Table 2.

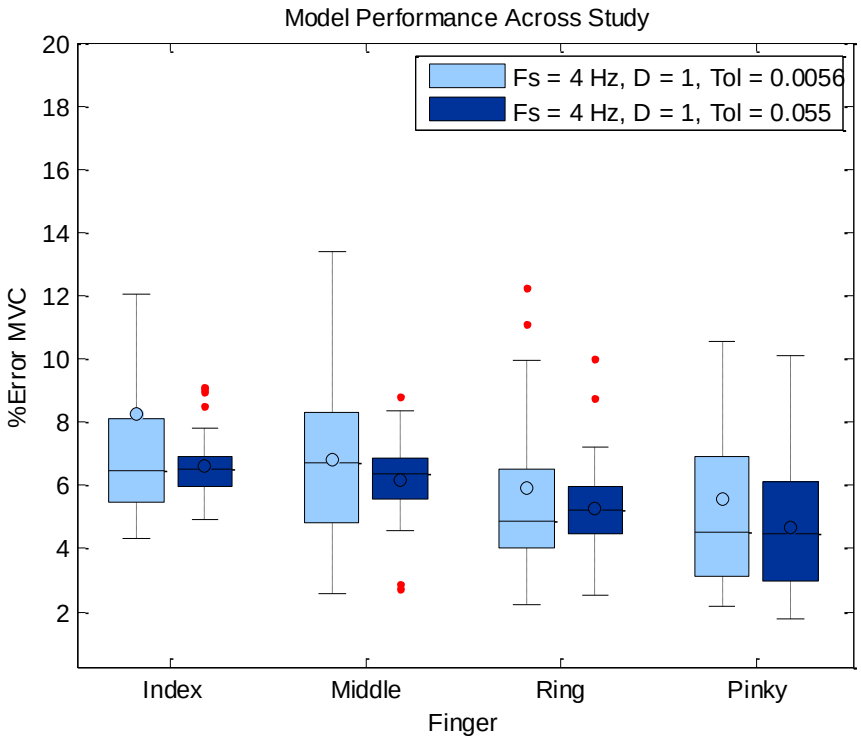

Figure 35: Study performance for the original and final model parameters.

Table 2: Mean error and standard deviation (in MVC%) for each finger for the original and final models.

	Model	*Index*	*Middle*	*Ring*	*Pinky*
Mean ± SD (MVC%)	***D=1 Tol = 0.0056***	8.25 ± 9.1%	6.83 ±2.5%	5.9 ± 3.5%	5.57 ±4.8%
	D=1 Tol=0.055	6.59 ± 1.0%	6.17 ± 1.2%	5.27 ± 1.5%	4.69 ± 2.0%

As can be seen in the above, the median error (line) did not show a dramatic difference, but the average error (circles) and distribution decreased with the change in tolerance.

The final parameters of choice were thus a resampling frequency of 4.096 Hz, a polynomial order of 1, and a pseudo-inverse tolerance value of 0.055.

4.3 Reduced Electrode Array Models

Since the use of 12 sEMGs may be both expensive and cumbersome to implement in practice, the final objective of this thesis was to determine whether reduced sensor sets produce models with acceptable levels of performance. A plot of the study performance in terms of MVC% error is shown below for electrode sets of sizes 6 through 12. The performance of each finger is shown on a separate line.

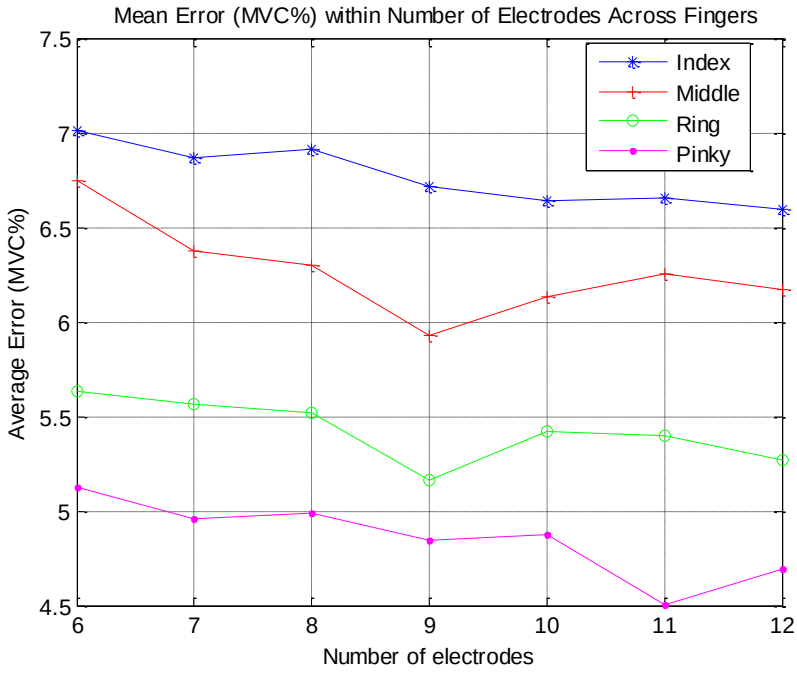

Figure 36: Mean error in MVC% for the study for electrode arrays of various sizes.

The above shows that in general the average error decreases as the number of electrodes in the model increases, with the exception of the performance of the middle and ring pinky for nine electrodes. The table below shows the mean and standard deviation of the error across the study in MVC% for each electrode array.

Table 3: Mean and standard deviation of error across the study in MVC% for each electrode array size.

Number of Electrodes	Finger			
	Index	Middle	Ring	Pinky
6	7.01 ± 1.3%	6.75 ± 2.0%	5.63 ± 1.8%	5.13 ± 1.7%
7	6.87 ± 1.2%	6.38 ± 1.6%	5.57 ± 1.7%	4.96 ± 1.7%
8	6.91 ± 1.3%	6.30 ± 1.4%	5.52 ± 1.8%	4.99 ± 1.9%
9	6.72 ± 1.2%	5.93 ± 1.1%	5.16 ± 1.3%	4.85 ± 2.0%
10	6.64 ± 1.1%	6.14 ± 1.2%	5.42 ± 1.6%	4.87 ± 1.9%
11	6.66 ± 1.0%	6.25 ± 1.2%	5.40 ± 1.8%	4.51 ± 1.7%
12	6.59 ± 1.0%	6.17 ± 1.2%	5.27 ± 1.5%	4.69 ± 2.0%

The performance of models with less than six electrodes was not pursued during analysis as less electrodes resulted in an unrealistic fit. Since this study attempts to achieve four independent degrees of freedom, it can be expected that at least four electrodes are required for modeling. There are several flexion and extension muscles within the forearm, which may make a case for using as many as eight electrodes (minimum) in models.

A paired sign test ($p<0.05$) was conducted to compare all models according to the scheme described in Section 3.4.6 Statistical Methods. The FDR used a control rate of $q<0.05$. The table below shows which models each electrode configuration performed significantly better than in decreasing order from 12 to 6 electrodes.

Table 4: Statistical comparison of reduced electrode array models.

Number of electrodes	Significantly better than
12	11, 10, 8, ~~7~~, 6
11	8, 7, 6
10	8, 7, 6
9	8, 7
8	6
7	6
6	None

All other comparisons were not significantly different. Despite the significant difference in performance of the electrode configurations when compared with six electrodes, the mean and standard deviation of the error in MVC% present a relatively small difference in average error (<0.6% across all fingers) between the full 12 electrode configuration and six electrode configuration. The performance of this model is put in perspective in the box plot below.

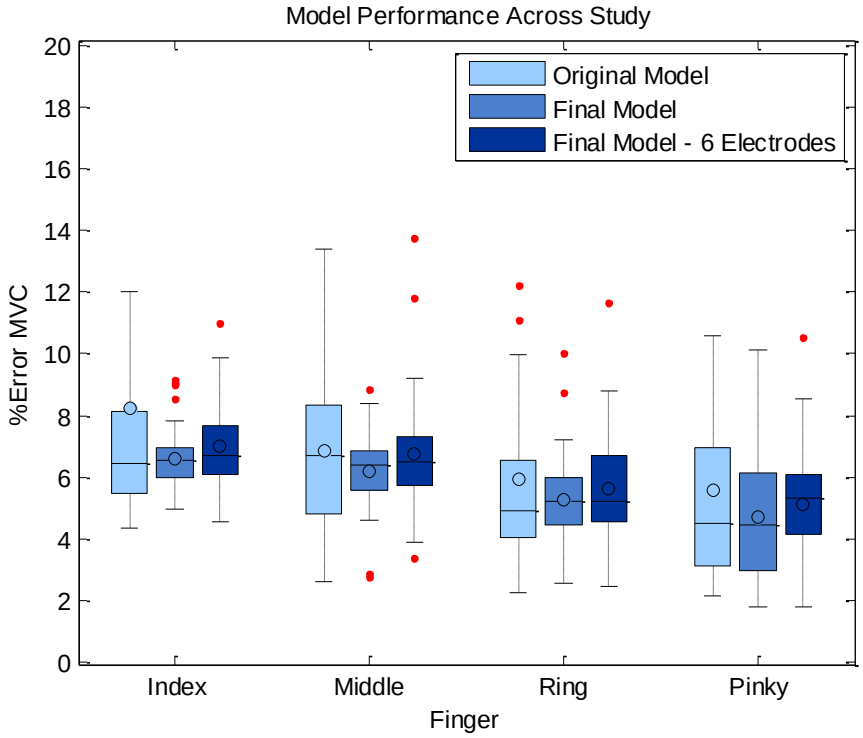

Figure 37: Study performance for the original, final, and 6 electrode models.

The table of errors for each finger is shown below for each of these models. The lowest error is highlighted in green.

Table 5: Mean and standard deviation of error across the study in MVC% for the original, final and 6 electrode models.

	Model	*Index*	*Middle*	*Ring*	*Pinky*
Mean ± SD	***Original***	8.25 ± 9.1%	6.83 ±2.5%	5.9 ± 3.5%	5.57 ±4.8%
	Final – 12 Electrodes	6.59 ± 1.0%	6.17 ± 1.2%	5.27 ± 1.5%	4.69 ± 2.0%
	Final - 6 Electrodes	7.01 ±1.3%	6.75 ± 2.0%	5.63 ± 1.8%	5.13 ± 1.7%

4.4 Model Fit and Error Characterization

The error characterization for this study does not produce accurate results in all cases. In the case of a “flat model fit” (described below), the error percentage produced would be approximately 6.42% per finger. This calls the accuracy of the above reporting and the goodness of fit achieved across the study into question. The goodness of fit was investigated for both the final model parameters and original model parameters and is described below in Section 4.4.1 Model Fit Investigation. Methods of coping with the flat fit are proposed in Section 4.4.3, including future data collection techniques, improved system identification methods, and improved error characterization methods for the continued use of least squares estimation.

4.4.1 Model Fit Investigation

The estimates produced for each test record with the final model parameters were subjectively investigated by the researcher. A binary method of fit determination was used to characterize the true performance of the study in which a ”1” was marked for a finger within a record that appeared to track for a given model and a ”0” was marked for those that did not. Of the models that fit, many track incredibly well. Based on this method of analysis, the percentage of tracking trials that fit, per finger, are shown below in Table 6.

Table 6: Percent of records that exhibited a fit for the study based on D = 1, tol = 0.055 (subjective assessment).

Finger	Percent of Records
Index	10.00%
Middle	40.00%
Ring	65.00%
Pinky	70.00%

These results are surprising for the index and middle fingers. Prior to model optimization, considerably more index and middle fingers exhibited fit curves. The same method of assessment was conducted on data from the original model parameters, with D = 1 and tol = 0.0056. The percentage of tracking trials that fit, per finger, for these parameters are shown below.

Table 7: Percent of records that exhibited fit for study based on D = 1, tol = 0.0056 (subjective assessment).

Finger	Percent of Records
Index	57.50%
Middle	57.50%
Ring	77.50%
Pinky	85.00%

The difference in results shows that the manner in which the estimates were denoised and optimized resulted in a significant decrease in the amount of models that tracked per finger.

4.4.2 The "Flat Fit" Problem

A "flat fit" occurs when all fingers not involved in the tracking task use the same constant force level. In this study that constant level was an assumed zero force. The example trial below shows a relatively flat fit for the index and middle fingers, but tracking for the ring and pinky fingers.

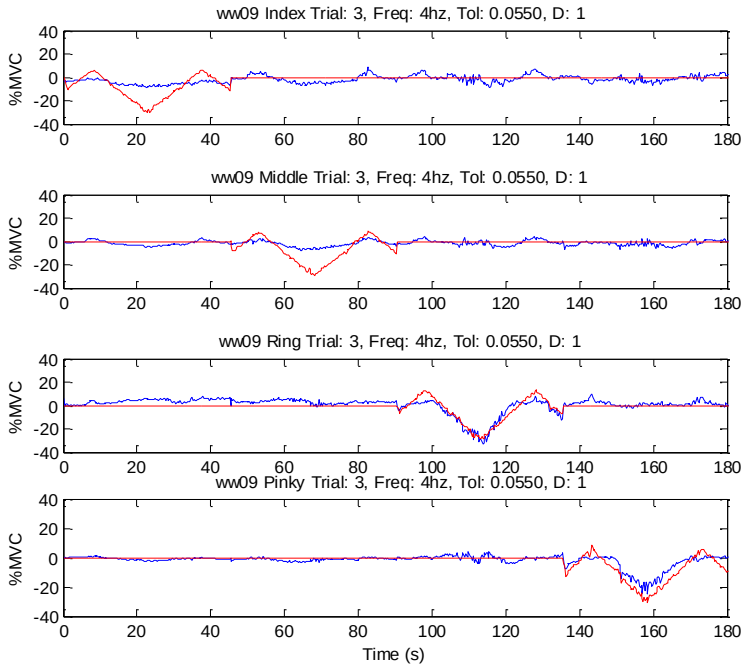

Figure 38: Example trial in which two fingers exhibit flat fit while the other two exhibit tracking.

The model does not exhibit the ability to track the movement of the index or middle fingers. Since 75% of the data for each finger (three out of four 45 second trials) is at a constant zero force, the error calculated for such a fit is still rather small (roughly 6.42 MVC% per finger[9] for a completely flat fit). This means that when statistics are computed low errors are being taken into account when, in fact, tracking was not successful. Thus the current method of estimation error analysis is not appropriate for this dataset.

4.4.3 Coping with Flat Fit

To improve system identification methods as well as our ability to discern poorly performing models, it is desired that such a fit not indicate good performance. The use of the "flat fit" error was considered as a comparator to compensate for this problem, but this method is still lacking as it does not provide an indication of the shape of the fit. A model that oscillates around zero force when the force is zero, and then oscillates around the changing forces during the changing period, can produce a higher error than a flat fit, but actually represents better modeling success.

Potential methods for coping with the flat fit are described below.

4.4.3.1 Techniques for future data collection

A possible solution to this problem would be to have multiple fingers moving simultaneously. However, it is assumed that subjects would experience difficulty tracking two targets at the same time.

A more feasible solution for future studies is to incorporate the force measurement of each finger (via four different load cells) and to vary the "background" force level across trials. In this method, the four fingers could be brought to a baseline level of force (e.g. 10% flexion, 5% extension, etc) for each trial. Once the four fingers have reached baseline force, the tracking trial could be carried out for the finger of interest. Each trial for this finger would use a different baseline force level. Then, when performing a model fit, all trials would be merged together to form a single model. Since there would be no single constant background force level, the possibility of a flat fit falsely representing good performance would be eliminated.

This work could be performed via simulation followed by system identification to validate its potential for success with a real dataset, prior to completing the clinical data collection.

4.4.3.2 Improved system identification techniques

To facilitate the use of least squares estimation, developing models to fit less than four outputs will progressively minimize this problem (with three fingers the percent of time spent at zero force is 67%, and so on).

Additionally, models that consider a different measure of model fit than least squares error should be considered.

4.4.3.3 Error Characterization

While the use of least squares estimation for this study exhibits promising results in that there are many trials for which fingers are clearly tracked, the method of determining model accuracy and therefore the method of improving models does not provide the desired information.

If it is desired to continue using least squares for generating fit coefficients of a four output model, a proposed method of error calculation is the following:

- Calculate a **zero force error –** This is the performance (per finger) in the regions in which that finger is assumed to have exerted zero force. The error is calculated as the RMS error between the actual force signal and the

[9] This value was arrived at theoretically by plotting an expected force curve for a single finger using %MVC values and determining the error between a completely flat estimation and the hypothetical force curve.

estimated signal. This error can be considered separately from the tracking error and evaluated as the potential contribution of co-contractions.

- Calculate a **changing force error –** This is the performance (per finger) in the region in which the moving finger is exerting a changing force. The error is calculated as the RMS error between the actual force signal and the estimated signal. This error can be compared to the flat fit performance for this region and be used to characterize our ability to track finger movement.

The plot below demonstrates the suggested error calculation methods.

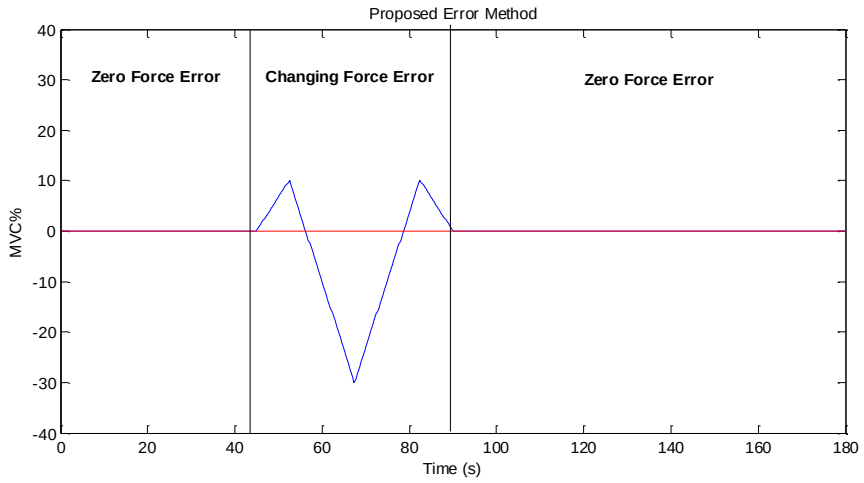

Figure 39: Suggested error calculation methods with zero force error and changing force error outlined.

This error characterization should be completed per model fit, with two errors reported per finger: zero force error and changing force error. Study performance and model optimization methods should then consider minimizing both of these errors as best possible.

This method of error estimation does not help the method of modeling – only the evaluation of the estimates produced by models using least squares to compute fit coefficients.

5 Limitations of this work

There are several limitations to this study approach, each of which will be considered in detail in this section. These limitations pertain to both the physical test setup and data acquisition methods as well as the signal processing methods employed.

The current methods of data collection may lead to inconsistent data collection.

- *The current process involves a lot of physical involvement from the researchers throughout testing.* Individual fingers and grips are attached to the load cell apparatus using a piece of Velcro. The hand is additionally attached to the upright pole using Velcro. These pieces of Velcro are removed and replaced several times throughout the study. While the application of this Velcro was completed in as repeatable a fashion as possible by the researchers, it is impossible to avoid variability with such methods.
- *The current process involves constant subject observation and correction.* The best example of this is posture. Since the study visit lasted anywhere from three to four hours, it was common for subjects to begin slouching throughout the testing. Study researchers corrected slouching as best they could, but it cannot be guaranteed that all subjects maintained the same posture throughout testing.
- *The method of electrode placement is not robust.* While the electrodes are placed circumferentially about the arm, and every effort is made to provide equal distance between them, the manner in which electrodes are assembled for mounting and the manner in which they are mounted is not ideal.
    1. Electrodes are adhered to a piece of medical tape on which the researcher has drawn lines for electrode placement. This method is a less exact than desired and can sometimes lead to the need to remove electrodes and readjust their placement.
    2. Since the electrodes are secured to the subject with this medical tape and an ace bandage, sometimes the ace bandage loosens throughout the duration of the study visit. This bandage may be tightened, but the electrodes may not be removed and replaced as the repeatability of electrode placement is unknown.
- *The current finger restraint design may contribute to co-contraction.* Several subjects noted that with their hand wrapped around the upright pole, they had a hard time not using their thumb for support during data collection trials. Researchers and subjects attempted to minimize this occurrence, however it is expected that some data exhibit co-contraction as a result of this arrangement.
- *Subjects' muscles may have been fatiguing during finger trials.* During this data collection the grips and classification data were collected first. This sequencing meant that the finger data tended to be in the third hour of data collection. While rest was provided throughout testing, there were subjects that noted muscle fatigue.

The current method of modeling assumes that fingers move separately from one another.

In order to identify individual muscle activity responsible for the movement of a single finger, fingers were moved individually. However, to form a multiple degree of freedom model, the results from these individual finger trials had to be combined. This meant that forces of fingers not in use during data collection trials were defined to be zero for the purposes of modeling. While these forces are expected to be small, the anatomy and physiology of the forearm, wrist, and hand place limitations on the degree to which fingers can be moved individually. As such, it is likely that when subjects attempt to move an individual finger, muscles related to moving other fingers (e.g. the pinky and ring finger) are activated regardless of efforts not to co-contract. This means that muscle activation levels for fingers unrelated to the movement being studied will be observed. The modeling method then attempts to correlate these data with zero force, which is not necessarily true.

The current method of modeling utilizes a single background force.

With the current dataset, the force of each finger not performing tracking is assumed to be zero. When performing modeling, this results in 75% of the EMG dataset being tied to a zero force value. This often results in a flat fit model, which can easily exhibit low modeling error (roughly 6.42 MVC% per finger). These flat fits are incorporated into the statistical analysis without adequate penalty for failed modeling.

The current method of model optimization optimizes performance for a limited number of subjects.

Based on the impact that changing model parameters such as pseudo-inverse tolerance and model order had on individual subjects' data, it seems that the signal-to-noise ratio differs across subjects. While an increase in tolerance improved some subjects' performance, it actually decreased the performance of others, indicating that singular values unrelated to noise had been discarded in an attempt to produce higher performance across the whole study with a single set of model parameters. Future research might consider optimizing the pseudo-inverse tolerance for each subject.

The current method of estimating error does not form an appropriate representation of model fit.

The data collection scheme has an impact on the validity of commonly used error characterization methods. The test data for each trial is composed, for each finger, of 75% zero force data. This results in a flat fit falsely exhibiting good model performance – achieving an error of 6.42% if the resulting model does not stray from the zero force line during the test. This suggests that the method of determining error for this study is not adequate. An improved error performance measure was proposed in Section 4.4.3.3 Error Characterization.

6 Future Work

Recommendations for future work are stated with respect to the identified study limitations in Section 5 Limitations of this work.

To improve methods of data collection

- A different approach to data collection, such as a two visit scheme or a decreased amount of data to collect is recommended to reduce the potential of muscle fatigue and posture relaxation.
- An ergonomic study/human factors analysis is suggested for the test apparatus. New methods should seek to both minimize researcher interaction in fingertip and hand placement, and increase the repeatability of such actions through exact settings rather than objective analysis of the similarity of attachment methods.
    - An evaluation of the extent to which co-contraction occurs using the current setup and a comparison across other possible setups should be completed. Such an analysis could be conducted by devising alternative designs and testing these designs with the same subject. In the study, the power of signals achieved by electrodes expected to represent co-contraction should be analyzed across test setups. The test setup resulting in the lowest amount of co-contraction should be chosen for use.
- Measure the force from multiple fingers at the same time.
- A study for the improvement of electrode setup is recommended.
- A study of the repeatability of electrode placement is recommended.
- A better method for securing electrodes to subjects' forearm to reduce slip throughout study is recommended.
- Consider a study design in which fingers exert force simultaneously, to limit the time spent in zero force mode.
    - Study subjects' ability to control force in multiple fingers at the same time.
- Consider a study design in which the force is measured at each fingertip, and fingers not performing tracking are brought to a baseline force level (e.g. 10% flexion for one trial, 15% extension for another trial, etc). Once the four fingers have reached baseline force, the tracking trial could be carried out for the finger of interest. Each trial for this finger would use a different baseline force level. Then, when performing a model fit, all trials would be merged together to form a single model. Since there would be no single constant background force level, the possibility of a flat fit falsely representing good performance would be eliminated.
    - This work could be performed via simulation followed by system identification to validate its potential for success with a real dataset, prior to completing the clinical data collection.

To improve methods of modeling

- This work did not have the opportunity to explore model cross validation. As such it is recommended that this is performed on the existing dataset to determine if improvement in modeling can be achieved.
- This work utilized a single trial for training and two trials for testing estimation. A separate paradigm in which two trials are used for training and one is used for test would likely improve modeling results.
- A study aimed at identifying fewer degrees of freedom is recommended. Modeling results indicate that there are pairs of fingers that may act as a single degree of freedom together, e.g. the pinky and ring finger.
- To facilitate the use of least squares estimation, developing models to fit less than four outputs will progressively minimize this problem (with three fingers the percent of time spent at zero force is 67%, and so on).
- Models that consider a different measure of model fit than least squares error should be considered.

To improve methods of model optimization

- During this investigation it was observed that subjects performed better with differing tolerance and model order values. Modeling methods should therefore consider the ideal parameters per subject, rather than the setting of a single parameter across the study.
- Consider the use of alternative error calculation methods such as the zero-force/changing-force error method proposed in Section 4.4.3.3 Error Characterization.

7 Conclusions

The results of this thesis are supportive that multiple degrees of freedom of proportional control information are available from the surface EMG of the forearm, at least in intact subjects. EMG-based estimation of finger forces yield low force errors, with many trials exhibiting tracking of each of the four fingers.

An EMG amplitude sampling frequency of 4.096 Hz was found to produce models which allowed for good EMG amplitude estimates. Although a higher frequency (20.48 Hz) produced the lowest mean error and distribution of error, visual inspection indicated nosier overall estimation which would be impractical in control implementations. In addition, the median error was not distinguishable between sampling rates.

Least squares regularization with a pseudo-inverse tolerance of 0.055 resulted in significant improvement in modeling results, for an average error of 4.69% MVC-6.59% MVC across the four fingers. Increasing polynomial order was not found to significantly improve modeling results, thus linear models appear to be satisfactory for this work. When considering smaller electrode arrays, results remained fairly good with as few as six electrodes, with the average %MVC error ranging from 5.13%-7.01% across the four fingers. The average %MVC error was lower for nine electrodes compared to ten, which identifies a potential cost tradeoff for commercial implementation.

Across all modeling efforts (varying pseudo-inverse tolerance, model order), the EMG-force estimates for the pinky and ring finger produced superior results (4.69 ±2% and 5.27 ± 1.5%, respectively) and demonstrated excellent tracking. Force estimates of the index and middle finger produced higher errors (6.59 ± 1% and 6.17 ±1.2%, respectively) and consistently tracked poorly. In practical implementations it is likely more desirable to have better performance in the index finger than the pinky and thus the model should be optimized based on finger prioritization.

This work identified important limitations to the current study design. The current design actuates fingers individually, however this biases the results when analyzing performance. The majority of the data (~75%) analyzed for each finger is during a “rest” time where the fingers are assumed to be producing zero force. The signal of interest occurs when the finger is exerting a changing force (~25% of the signal). The current design optimized the entire model (including the time of rest) rather than just the changing force. Methods such as actuation of multiple fingers during tracking trials, a change in baseline force for fingers not tracking, and new modeling methods are suggested for combatting this issue.

8 Bibliography

[1] P. Liu, D. R. Brown, F. Martel, D. Rancourt and E. A. Clancy, "EMG-to-force Modeling for Multiple Fingers," in *Proc. of Bioengineering Conference (NEBEC), 2011 IEEE 37th Annual Northeast*, New York, Troy.

[2] I. M. Delph, S. Fischer, P. Gauthier, L. C. Martinez, E. Clancy and G. Fischer, "A Soft Robotic Exomusculature Glove with Integrated sEMG Sensing for Hand Rehabilitation," in *13th International Conference on Rehabiliation Robotics (ICORR)*, Seattle, WA, 2013.

[3] Amputee Coalition, "Limb Loss Statistics," Limb Loss Resource Center. [Online]. [Accessed 30 March 2014].

[4] F. Tenore, A. Ramos, A. Fahmy, S. Acharya, R. Etienne-Cummings and N. Thakor, "Towards the Control of Individual Fingers of a Prosthetic Hand Using Surface EMG SIgnals," *Engineering in Medicine and Biology Society,* vol. 29th Annual International Conference of the IEEE, pp. 6145, 6148, 2007.

[5] A. Young, L. J. Hargrove and T. A. Kuiken, "The Effects of Electrode Size and Orientation on the Sensitivity of Myoelectric Pattern Recognition Systems to Electrode Shift," *IEEE Transactions on Biomedical Engineering,* pp. 2537-544, 2011.

[6] "KNOWSTROKE: KNOW THE SIGNS. ACT IN TIME," NINDS Know Stroke Capaign. [Online]. [Accessed 28 March 2014].

[7] N. Dancause, S. Barbary, S. Frost, E. Plautz, D. Chen, E. Zoubina, A. Stowe and R. Nudo, "Extensive cortical rewiring after brain injury," *J Neurosci,* vol. 25, pp. 10167-10179, 2005.

[8] E. Taub, G. Uswatte, D. King, D. Morris, J. Crago and A. Chatterjee, "A placebo-controlled trial of constraint-induced movement therapy for upper extremity after stroke," *Stroke,* vol. 37, pp. 1045-1049, 2006.

[9] S. Page, P. Levine and A. Leonard, "Modified constraint-induced therapy in acute stroke: A randomized controlled pilot study," *Neurorehabil Neural Repair,* vol. 19, pp. 27-32, 2005.

[10] S. Fasoli, H. Krebs, J. Stein, W. Frontera and N. Hogan, "Effects of robotic therapy on motor impairment and recovery in chronic stroke," *Arch Phys Med Rehabil,* vol. 84, pp. 477-82, 2003.

[11] E. Frick and J. Alberts, "Combined use of repetitive task practice and an assistive robotic device in a patient with subacute stroke," *Physical Therapy,* vol. 86, no. 10, pp. 1378-13, 2006.

[12] L. Rosenstein, A. L. Ridgel, A. Thota, B. Samame and J. L. Alberts, "Effects of combined roboic therapy and repetitive-task practice on upper-extremity function in a patient with chronic stroke," *Am. J. Occup. Ther.,* vol. 62, pp. 28-35, 2008.

[13] E. A. Clancy, O. Bida and D. Rancourt, "Influence of advanced electromyogram (EMG) amplitude processors on EMG-to-torque estimation during constant-posture, force-varying contractions.," *Journal of Biomechanics,* vol. 39, pp. 2690-8, 2006.

[14] P. Liu, L. Liu, F. Martel, D. Rancourt and E. A. Clancy, "Influence of joint angle on EMG-torque model during

constant-posture quasi-constant-torque contractions.," *Journal of Electromyography and Kinesiology,* vol. 23, pp. 1020-1028, 2013.

[15] E. N. Marieb, "10: The Muscular System," in *Anatomy & Physiology. 5th ed*, Boston, Pearson.

[16] J. Basmajian and C. De Luca, Muscles Alive (5th edition), Baltimore, MD: Williams and Wilkins, 1985.

[17] A. Merlo, D. Farina and R. Merletti, "A fast and reliable technique for muscle activity detection from surface EMG signals.," *IEEE Trans. Biomed. Eng.,* vol. 47, no. 6, pp. 748-756, 2000.

[18] E. A. Clancy, E. L. Morin and R. Merletti, "Sampling, noise-reduction and amplitude estimation issues in surface electromyography," *Journal of Electromyography and Kinesiology,* vol. 12, no. 1, pp. 1-16, 2002.

[19] R. A. R. C. Gopura, D. S. V. Bandara, J. M. P. Gunasekara and T. S. S. Jayawardane, "Chapter 12: Recent Trends in EMG-Based Control Methods for Assistive Robots," in *Electrodiagnosis in New Frontiers of Clinical Research*, 2013.

[20] C. J. De Luca, A. Adam, R. Wotiz, L. D. Gilmore and S. H. Nawab, "Decomposition of Surface EMG Signals," *J Neurophysiol,* vol. 96, pp. 1646-1657, 2006.

[21] SENIAM, "Introduction to the Special Issue on the SENIAM European Concerted Action," *Journal of Electromyography and Kinesiology,* vol. 10, pp. 283-86, 2000.

[22] H. J. Hermens, B. Freriks, C. Disselhorst-Klug and G. Rau, "Development of Recommendations for sEMG Sensors and Sensor Placement Procedured," *Journal of Electromyography and Kinesiology,* vol. 10, pp. 361-74, 2000.

[23] D. F. Stegeman and H. J. Hermens, "Standards for Surface Electromyography: The European Project," *Surface EMG for Non-invasive Assessment of Muscles (SENAIM),* pp. 108-12.

[24] Carlo J. DeLuca, "Surface Electromyography: Detection and Recording," DelSys Incorporated, Boston, MA, USa, 2002.

[25] M. A. Oskoei and H. Hu, "Myoelectric control systems - a survey," *Elselvier - Biomedical Signal Processing and Control,* vol. 2, no. 4, pp. 275-294, October 2007.

[26] K. Englehart and B. Hudgins, "A robust, real-time control scheme for multifunction myoelectric control," *IEEE Trans. Biomed. Eng,* vol. 52, no. 11, pp. 848-854, 2003.

[27] N. Hogan and R. W. Mann, "Myoelectric signal processing: Optimal estimation applied to electromyography - Part II: experimental demonstration of optimal myoprocessor performance," *IEEE Trans. Biomed Eng.,* Vols. BME-27, pp. 396-410, 1980.

[28] E. A. Clancy and N. Hogan, "Relating agonist-antagonist electromyograms to joint torque during isonmetric, quasi-isotonic, non-fatiguing contractions.," *IEEE Transactions in Biomedical Engineering,* vol. 44, pp. 1024-8, 1997.

[29] B. Hudgins, P. A. Parker and R. N. Scott, "A New Strategy for Multifunction Myoelectric Control," *IEEE Trnas. Biomed. Eng.,* vol. 40, pp. 82-94, 1993.

[30] D. Farina and R. Merletti, "Comparison of algorithms for estimation of EMG variables during voluntary isometric contractions," *J. Electromyogr. Kinesiol.,* vol. 10, pp. 337-349, 2000.

[31] P.-N. Tan, M. Steinbach and V. Kumar, "Classification: Basic Concepts, Decision Trees, and Model Evaluation," in *Introduction to Data Mining*, Boston, Addison-Welsey, 2005, pp. 145-202.

[32] T. Lenzi, S. De Rossi, N. Vitiello and M. Carrozza, "Proportional EMG control for upper-limb powered exoskeletons," in *33rd Annual International Conference of the IEEE EMBS*, Boston, MA, 2011.

[33] "Dextrous Hand," Shadow Robot Company, 2014. [Online]. Available: http://www.shadowrobot.com/products/dexterous-hand/. [Accessed 25 April 2014].

[34] "CyberHand Project - Bio-inspired Mechatronic Hand," CyberHand, [Online]. Available: http://www-arts.sssup.it/Cyberhand/introduction/biomechand.htm. [Accessed 25 April 2014].

[35] "DLR - Institute of Robotics and Mechatronics - DLR/HIT Hand," 2007. [Online]. Available: http://www.dlr.de/rm/en/desktopdefault.aspx/tabid-3802/6102_read-8918/. [Accessed 24 April 2014].

[36] P. Parker, K. Englehart and B. Hudgins, "Myoelectric Signal Processing for Control of Powered Limb Prostheses," *Journal of Electromyography and Kinesiology,* vol. 16.6, pp. 541-48, 2006.

[37] D. Atkins, C. Y. Heard and W. H. Donovan, "Epidemiologic overview of individuals with upper-limb loss and their reported research priorities," *J. Prosthet. Orthot.,* vol. 8, pp. 2-11, 1996.

[38] K. Englehart, B. Hudgins and P. A. Parker, "A Wavelet-Based Continuous Classification Scheme for Multifunction Myoelectric Control," *IEEE Trans. Biomed. Eng.,* vol. 48, pp. 302-311, 2001.

[39] B. Karlik, M. O. Tokhi and M. Alci, "A Fuzzy Clustering Neural Network Architecture for Multifunction Upper-Limb Prostheses," *IEEE Trans. Biomed. Eng.,* vol. 50, pp. 1255-1261, 2003.

[40] F. V. G. Tenore, A. Ramos, A. Fahmy, S. Acharya, R. Etienne-Cummings and N. V. Thakor, "Decoding of Individuated Finger Movements Using Surface Electromyography," *IEEE Transactions on Biomedical Engineering,* vol. 56.5, pp. 1427-434, 2009.

[41] C. Castellini and P. van der Smagt, "Surface EMG in Advanced Hand Prosthetics," *Bio. Cyber,* vol. 100, pp. 35-47, 2009.

[42] R. J. Smith, D. Huberdeau, F. Tenore and N. V. Thakor, "Real-Time Myoelectric Decoding of Individual Finger Movements for a Virtual Target Task," *Proc. 31st Ann. Int. Conf. IEEE EMBS,* pp. 2376-2379, 2009.

[43] R. J. Smith, F. Tenore, D. Huberdeau, R. Etienne-Cummings and N. V. Thakor, "Continuous Decoding of Finger Position from Surface EMG Signals for the Control of Powered Prostheses," *Proc. 30th An. Int. Conf. IEEE EMBS,* pp. 197-200, 2008.

[44] W. H. Press, S. A. Teukolsky, W. T. Vetterling and B. P. Flannery, Numerical Recipies in C, 2 ed., New York: Cambridge University Press, 1994, pp. 671-681.

[45] C. A. Salini, J. A. Tranquilli and P. Prakash, "Adaptive whitening in electromyogram amplitude estimation for epoch-based applications," Worcester Polytechnic Institute, Worcester, MA, 2003.

[46] E. A. Clancy, "Design of a High-Resolution, Monopolar, Surface Electromyogram (EMG) Array Electrode-Amplifier and its Associated Signal Conditioning Circuit," Worcester, MA.

[47] A. O. Perotto, Anatomical Guide for the Electromyographer, 3 ed., Sprinfield, IL: Charles C Thomas, 1994, pp. 30-73.

[48] E. A. Clancy and K. A. Farry, "Adaptive Whitening of the Electormyogram to Improve Amplitude Estimation," *IEEE Transactionf on Biomedical Engineerin,* vol. 47, no. 6, pp. 709-719, 2000.

[49] P. Prakash, C. Salini, J. Tranquilli, D. Brown and E. Clancy, "Adaptive whitening in electromyogram amplitude estimation for epoch-based applications," *IEEE Trans Biomed Eng,* vol. 52, pp. 331-334, 2005.

[50] E. A. Clancy, "EMG Amplitude Estimation Toolbox: User's Guide," 2014. [Online]. Available: http://ece.wpi.edu/~ted/emg_tool.htm.

[51] J. Bendat and A. Piersol, Random data: analysis and measurement procedures., New York: John Wiley and Sons, Inc., 1971.

[52] L. Ljung, System identification: theory for the user., Upper Saddle River, NJ: Prentice-Hall, 1999, pp. 143-6, 444-52, 491-519.

[53] F. J. Miller I, Probability and statistics fo rengineers., Englewood Cliffs, NJ: Prentice-Hall, Inc., 1977, pp. 272-5.

[54] S. M. Kay, "Chapter 8: Least Squares: 8.5 Geometrical Interpretations," in *Fundamentals of Statistical SIgnal Processing: Estimation Theory*, vol. 1, A. V. Oppenheim, Ed., Upper Saddle River, NJ: Prentice Hall PTR, 1993, pp. 227-229.

[55] E. A. Clancy, O. Bida and D. Rancourt, "Influence of advanced electromyogram (EMG) amplitude processors on EMG-to-torque estimation during constant posture force varying contraction," *J. Biomech,* vol. 39, no. 14, pp. 2690-2698, 2006.

[56] Y. Benjamini and D. Yekutieli, "The control fo the false discovery rate in multiple testing under dependency," *The Annals of Statistics,* vol. 29, no. 4, pp. 1165-1188, 2001.

[57] O. Bida, E. A. Clancy, D. R. Brown and D. Cyganski, "Influence of Electromyogram (EMG) Amplitude Processing in EMG-Torque Estimation," The Electrical & Computer Engineering Department at Worcester Polytechnic Institute, Worcester, MA, 2005.

[58] R. J. Nudo, "Plasticity," *NeuroRx,* vol. 3, no. 4, pp. 420-7, 2006.

[59] M. Moon, "DARPA Developing Muscle-controlled Prosthetic Limbs That Can Feel (video)," Engadget, 30 May 2013. [Online]. [Accessed 31 March 2014].

[60] K. A. Farry, I. D. Walker and R. G. Baraniuk, "Myoelectric Teleoperation of a Complex Robotic Hand," *IEEE Trans.*

Robot. Automat., vol. 12, pp. 775-788, 1996.

[61] P. Shenoy, K. J. Miller, B. Crawford and R. P. Rao, "Online Electromyographic Control of a Robotic Prostheses," *IEEE Trans. Biomed. Eng.,* vol. 55, pp. 1128-1135, 2008.

[62] M. Zecca, S. Micera, M. C. Carrozza and P. Dario, "Control of Multifunctional Prosthetic Hands by Processing the Electromyographic Signal," *Crit. Rev. Biomed. Eng.,* vol. 30, pp. 459-485, 2002.

[63] K. Saitou, M. Okada and T. Sadoyama, "Effect on surface EMG waveforms of electrode location with respect to the neuromuscular junctions: Its significance in EMG-muscle length relation," in *In Proc. 8th Congr. Int. Soc. Electrophysiology and Kinesiology*, Baltimore, MD, 1990.

[64] T. Xueyan, L. Yunhui, L. Congyi and S. Dong, "Hand Motion Classification Using a Mutli-Channel Surface Electromyography Sensor," *Sensors,* vol. 12, pp. 1130-147, 2012.

[65] B. Sebastian and P. van de Smagt, "Learning EMG Control of a Robotic Hand: Towards Active Prostheses," in *Proc. of IEEE International Conference on Robotics and Automation*, Florida, Orlando, 2006.

[66] J. L. Birdwell, L. J. Hargrove and F. R. Weir, "Quantification of Isolated Muscle Compartment Activity in Extrinsic Finger Muscles for Potential Prosthetic Control Sites," in *Proc. of 33rd Annual International Conference of the IEEE EMBS*, Boston, Massachusetts, USA, 2011.

[67] A. Wege and A. Zimmermann, "Electromyography Sensor Based Control for a Hand Exoskeleton," in *Proc. of IEEE International Conference on Robotics and Biomimetrics*, China, Sanya, 2008.

[68] D. K. Kumar, S. P. Arjunan and V. P. Singh, "Towards Identification of Finger Flexions Using Single Channel Surface Electromyography -- Able Bodied and Amputee Subjects," *Journal of Neuroengineering and Rehabilitation,* vol. 50, no. 10.1, 2013.

[69] K.-J. You, K.-W. Rhee and H.-C. Shin, "Finger Motion Decoding Using EMG Signals Corresponding Various Arm Postures," *Experimental Neurobiology,* vol. 19, pp. 54-61, 2010.

[70] Y. Itoh, H. Uematsu, F. Nogata, T. Nemoto, A. Inamori, K. Koide and H. Matsuura, "Finger Curvature Movement Recognition Interfaec Technique Using sEMG Signals," *Journal of Achievements in Materials and Manufacturing Engineering,* vol. 23.2, pp. 43-46, 2007.

[71] S. W. Lee, K. M. Wilson, B. A. Lock and D. G. Kamper, "Subject-specific Myoelectric Pattern Classification of Functional Hand Movements for Stroke Survivors," *IEEE Transactions on Neural Systems and Rehabilitation Engineering,* vol. 19.5, 2011.

[72] X. Lou, S. Xiao, Y. Qi, X. Hu, Y. Wang and X. Zheng, "Corticomuscular Coherence Analysis on Hand Movement Distinction for Active Rehabilitation," *Computational and Mathematical Methods in Medicine,* 2013.

[73] H. S. Ryait, A. S. Arora and R. Agarwal, "Study of Issues in the Development of Surface EMG Controlled Human Hand," *Journal of Materials Science: Materials in Medicine,* vol. 20, pp. 107-14, 2009.

[74] A. D. C. Chan and K. Englehart, "Continuous Classification of Myoelectric Signals for Powered Prosthesis Using Gaussian Mixture Models," in *Proc. of 25th Engineering in Medicine and Biology Society International Conference*, Mexico, Cancun.

[75] Y. Huang, K. B. Englehart, B. Hudgins and A. D. C. Chan, "A Gaussian Mixture Model Based Classification Scheme for Myoelectric Control of Powered Upper Limb Prostheses," *IEEE Transactions on Biomedical Engineering,* vol. 52.11, pp. 182-811, 2005.

[76] K. Englehart, B. Hudgins and A. D. C. Chan, "Continuous multifunction myoelectric control using pattern recognition," *Techo. Disability,* vol. 15, no. 2, pp. 95-103, 2003.

[77] P. A. Bendat JS, Random data: analysis and measurement procedures., New York: John Wiley and Sons, Inc., 1971.

[78] E. A. Clancy, L. Liu, P. Liu and D. V. Zandt Moyer, "Identification of Constant-Posture EMG-Torque Relationship About the Elbow Using Nonlinear Dynamic Models," *IEEE Transactions on Biomedical Engineering,* vol. 59, no. 1, pp. 205-212, 2012.

[79] L. J. Hargrove, G. Li, K. B. Englehart and B. S. Hudgins, "Principle component analysis for improved classification accuracies in pattern recognition-based myoelectric control.," *IEEE Trans. biomed Eng.,* vol. 56, no. 6, pp. 1407-1414, 2009.

[80] G. Li, A. E. Schultz and T. A. Kuiken, "Quantifying pattern recognition-based myoelectric control of multfunctional transradial prosthesis.," *IEEE Trans. Neural Sys. Rehab. Eng.,* vol. 18, no. 4, pp. 185-192, 2010.

[81] D. Graupe and W. K. Cline, "Functional separation of EMG sinals via ARMA identification methods for prosthesis control purposes," *IEEE Trans. Sys. Man Cuber.,* vol. 5, no. 2, pp. 252-259, 1975.

[82] R. Boostani and M. H. Moradi, "Evaluation of forearm EMG signal features for the control of a prosthetic hand," *Physio. Meas.,* vol. 24, pp. 309-319, 2003.

[83] D. Staudenmann, K. Roeleveld, D. F. Stegeman and J. H. van Dieen, "Methodological aspects of SEMG recordings for force estimation - A tutorial and review.," *Journal of Electromyography and Kinesiology,* vol. 20, pp. 375-387, 2010.

Appendix 1 Electrode Placement Recommendations

WPI

Anatomical surface EMG placement on the forearm

Research concerning WPI IRB Protocol #13-141: Relating Arm Muscle Electrical Activity to Hand/Finger Forces for use in Prosthesis Control and Stroke Rehabilitation Devices

Jennifer Keating

11/16/2013

Table of Contents

Table of Tables

Table of Figures

1 Executive Summary

The proposed research by Clancy et al will involve the use of 16 bipolar surface electrode amplifiers. Due to the anticipated variation in physical properties (length, diameter) of the forearms of human subjects, electrodes will be placed in targeted anatomical locations as opposed to generalized placement at 20 mm intervals as recommended by SENIAM. To determine these locations, research regarding the muscles and nerves responsible for activating the motions of interest (individual finger flexion/extension) was conducted. This research included both consultation of anatomy and physiology textbooks and an overview of literature focused on the use of surface EMG electrodes for the control of prostheses and exoskeleton gloves for rehabilitative purposes using the forearm. Four example electrode orientations are detailed, with the main recommendation being that electrodes are grouped in sets of two, longitudinally, rather than groups of four, wrapped circumferentially. A group meeting is needed to discuss how to proceed.

2 Motivation

The research conducted this year for both slowly-varying and dynamic contractions of the fingers and finger combinations will involve the use of 16 bipolar surface electrode amplifiers, each consisting of a pair of 8-mm diameter, stainless steel, electrode contacts separated by 10 mm (edge to edge), connected to a DC-coupled (gain of 20) instrumentation amplifier. To maximize the value of the information provided by electrodes during clinical data collection, electrodes will be placed on subjects' forearms according to anatomic location.

3 General Electrode Orientation and Location Recommendations

The SENIAM project was initiated to solve problems preventing a useful exchange of data in the area of sEMG research, and to establish standards that allow for European cooperation in this area of research [1]. Of its primary objectives was to develop recommendations on sensors and sensor placement procedures. Authors identified 352 electrode location descriptions in 144 papers in which surface EMG was utilized. Most descriptions were found to be generic and indicating muscle belly, motor point, or midpoint of muscle as location of choice; these locations often coincide with innervation zones which have effects on EMG signal features such as frequency characteristics [3].

Factors that influence the stability of EMG recordings include the presence of motor units/muscle tendons, the presence of other active muscles nearby [7] and the location of innervation zones in relation to the recording electrodes [3]. It was recommended that bipolar electrodes be positioned parallel to muscle fibers with a spacing of 20 mm between centers of electrode poles [2]. This placement is small enough to avoid most crosstalk but large enough to pick from a pool of motor units [3]. While sEMG sensors have traditionally been placed on top of the muscle belly over the motor endplate zone due to the ease with which large signals can be obtained, it has been found that the sEMG pattern in this region is not stable or reproducible [7]. It is therefore recommended that sensors be placed halfway between the most distal motor endplate zone and distal tendon, and that the geometrical distance of the electrode from other muscles be maximized (i.e. place electrodes at the muscle surface away from the edge of the muscle) [2,7]. These recommendations have been reconfirmed by research conducted on the effect of electrode size and orientation on the sensitivity of myoelectric pattern recognition systems in which electrodes oriented parallel to muscle fibers outperformed perpendicular ones significantly [3].

4 Forearm Anatomy & Physiology

A barrier to using EMG signals as a command interface for prosthetic hands is measuring independent muscle control sites in the residual limb [12]. Though sEMG electrodes are commonly used to detect muscle activity in the forearm, the muscles are close together, small, and sometimes deep within the forearm. These electrodes therefore often detect the summation of simultaneous activity from several muscles. A study by Saitou et al demonstrated the difficulty of targeting electrode positions near innervation zones corresponding to specific muscles in the forearm [5]. Through careful selection of electrode placement our study aims to remove as many of these known issues as is reasonably possible.

The forearm muscles are divided into muscles responsible for wrist movement and muscles responsible for hand movement [4]. Of concern for this study are those causing the movement of the fingers and the thumb. The larger portions of the forearm muscles are located at the proximal forearm and taper to long insertion tendons at the wrist. They are divided by fascia into the anterior flexors (largely innervated by the median nerve) and posterior extensors (supplied by the radial nerve), each with superficial and deep muscle layers. Muscles that operate the fingers are located in the forearm and move fingers via their long tendons.

Human Anatomy & Physiology by Eliane N. Marieb covers, in detail, the muscles of the forearm, movements of the wrist, hand, and fingers. The information provided within the sections *Summary of the actions of muscles acting on the arm, forearm, and hand* and *Intrinsic muscles of the hand: fine movements of the fibers* was used to derive the table below. References noted next to muscles indicate studies involving finger and grip identification which have had positive outcomes using sensors on the specified muscle. Pictures taken from [4] with the relevant muscles highlighted are included following the table.

Table 1: Table of relevant muscles. Includes location, description, origin/insertion, action, and nerve supply.

Muscle	Category	Location	Description	Origin (O) and insertion (I)	Action	Nerve supply	Type
Extensor carpi radialis brevis [8, 9, 10] Extensor carpi radialis longus [8, 9, 10]	Superficial	Posterior	Shorter than extensor carpi radialis longus and lies deep to it	O-lateral epicondyle of humerus, I-base of third metacarpal	Extends and abducts wrist; acts synergistically with extensor carpi radialis longus to steady wrist during finger flexion	Deep branch of radial nerve	Unrelated to fingers
Extensor digitorum [6, 8, 9, 10, 11, 13, 15] Extensor digit minimi [6,8, 10]	Superficial	Posterior	Lies medial to extensor carpi radialis brevis; a detached portion of this muscle, called extensor digiti minimi extends the pinky	O-lateral epicondyle of humerus, I-by four tendons into extensor expansions and distal phalanges of fingers 2-5	Prime mover of finger extension; extends wrist; can abduct (flare) fingers	Posterior interrosseous nerve, a branch of radial nerves C5 and C6	Extension
Adbuctor pollicis longus	Deep	Posterior	Lateral and parallel to extensor pollicus longus; just distal to supinator	O-posterior surface of radius and ulna; interosseous membrane, I-base of first metacarpal and trapezium	Abducts and extends thumb	Posterior interosseous nerve	Abduction & Extension
Extensor pollicis brevis and longus [6, 8, 10, 11, 13,15]	Deep	Posterior	Deep muscle pair with a common origin and action; overlain by extensor carpi ulnaris	O-dorsal shaft of radius and ulna; interosseous membrane, I-base of proximal (brevis0 and distal (longus) phalanx of thumb	Extends thumb	Posterior interosseous nerve	Extension

Muscle	Category	Location	Description	Origin (O) and insertion (I)	Action	Nerve supply	Type
Extensor Indicis [6, 8, 10, 11, 13, 15]	Deep	Posterior	Tiny muscle arisin close to wrist	O-posterior surface of distal ulna; interosseous membrane, I-extensor expansion of index finger; joins tendon of extensor digitorum	Extends index finger and assists in wrist extension	Posterior interosseous nerve	Extension
Flexor carpi ulnaris [8, 9, 10]	Superficial	Anterior	Most medial muscle of group; two headed; ulnar nerve lies lateral to its tendon	O-medial epicondyle of humerus; olecranon process and posterior surface of ulna, I-pisiform and hamate bones and base of fifth metacarpal	Powerful flexor of wrist; also adducts hand in concert with extensor carpi ulnaris (posterior muscle); stabilizes wrist during finger extension	Ulnar nerve (C7 and C8)	Flexion
Flexor digitorum superficialis [8, 10, 11,12, 13, 14]	Superficial	Anterior	Two headed muscle; more deeply placed (therefore, actually forms an intermediate layer); overlain by muscles above but visible at distal end of forearm	O-medial epicondyle of humerus, coronoid process of ulna; shaft of radius, I-by four tendons into middle phalanges of fingers 2-5	Flexes wrist and middle phalanges of fingers 2-5; the important finger flexor when speed and flexion against resistance are required	Median nerve (C7, C8 and T1)	Flexion
Flexor pollicis longus [8, 9, 10, 13]	Deep	Anterior	Partly covered by flexor digitorum superficialis; parallels flexor digitorum profundus laterally	O-anterior surface of radius and interosseous membrane, I-distal phalanx of thumb	Flexes distal phalanx of thumb	Branch of median nerve (C8, T1)	Flexion
Flexor digitorum profundus [8, 10, 12]	Deep	Anterior	Extensive origin; overlain entirely by flexor digitorum superficialias	O-coronoid process, anteromedial surface of ulna, and interosseous membrane, I-by four tendons into distal phalanges of fings 2-5	Slow acting flexor of any or all fingers; assists in flexing wrist; the only muscle that can flex distal interphlanageal joints	Medial half by ulnar nerve; lateral half by median nerve	Flexion

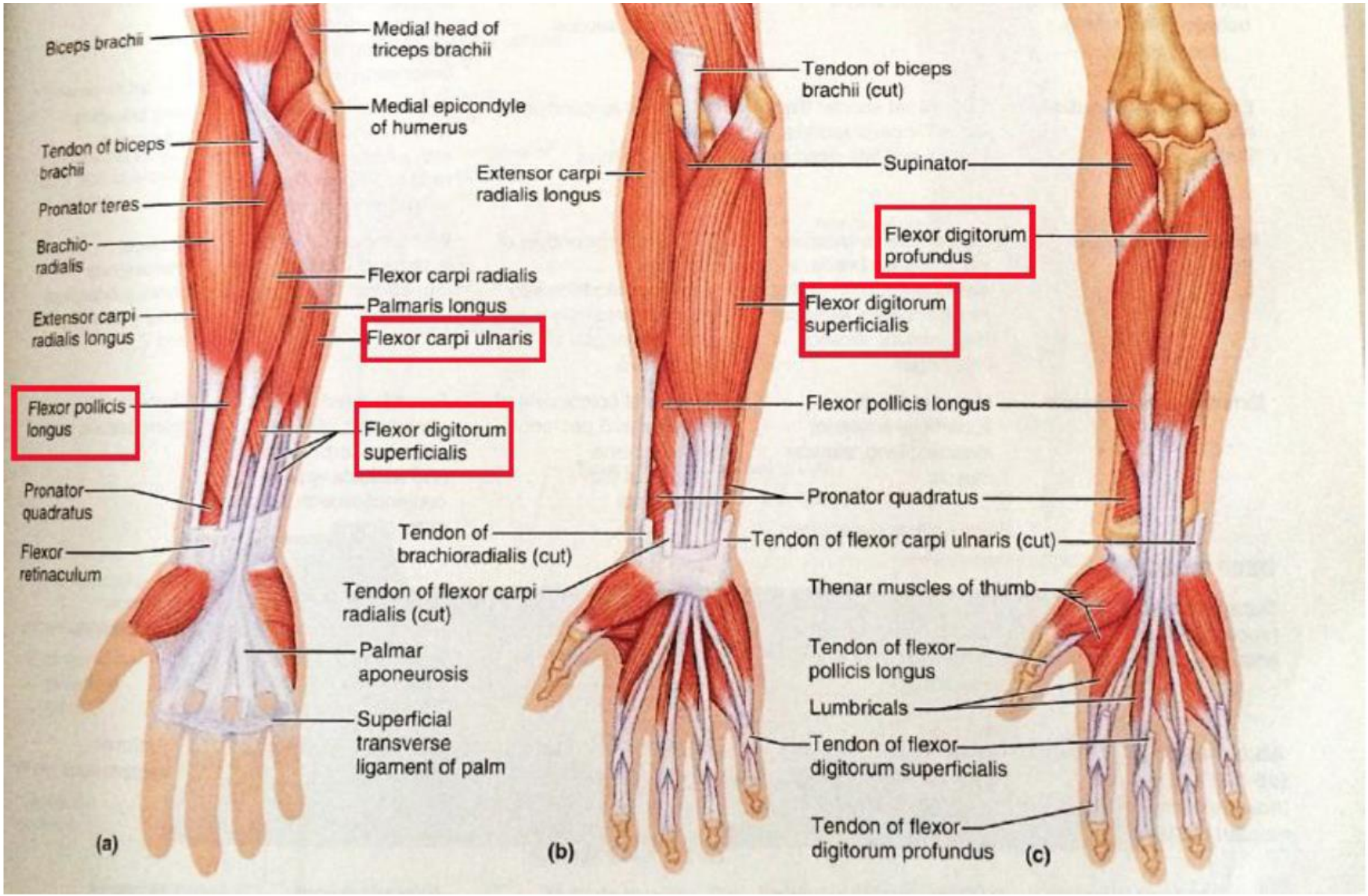
Biceps brachii
Medial head of triceps brachii
Medial epicondyle of humerus
Tendon of biceps brachii
Pronator teres
Brachio-radialis
Extensor carpi radialis longus
Flexor carpi radialis
Palmaris longus
Flexor carpi ulnaris
Flexor pollicis longus
Flexor digitorum superficialis
Pronator quadratus
Flexor retinaculum
Palmar aponeurosis
Superficial transverse ligament of palm
(a)
Tendon of biceps brachii (cut)
Extensor carpi radialis longus
Supinator
Flexor digitorum profundus
Flexor digitorum superficialis
Flexor pollicis longus
Pronator quadratus
Tendon of brachioradialis (cut)
Tendon of flexor carpi radialis (cut)
Tendon of flexor carpi ulnaris (cut)
(b)
Thenar muscles of thumb
Tendon of flexor pollicis longus
Lumbricals
Tendon of flexor digitorum superficialis
Tendon of flexor digitorum profundus
(c)

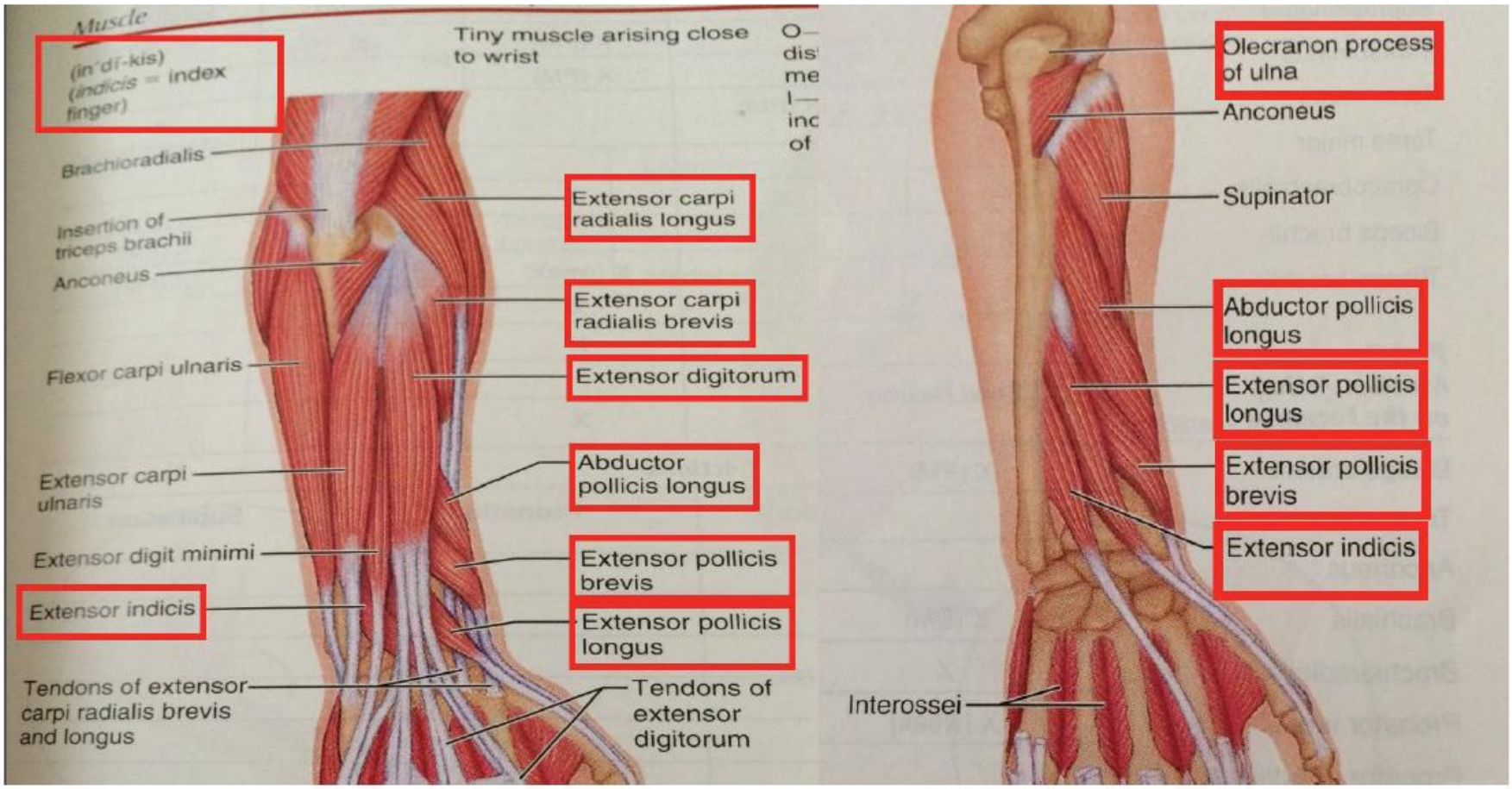
Muscle
(in'dĭ-kis)
(indicis = index finger)
Tiny muscle arising close to wrist
Brachioradialis
Insertion of triceps brachii
Anconeus
Flexor carpi ulnaris
Extensor carpi ulnaris
Extensor digit minimi
Extensor indicis
Tendons of extensor carpi radialis brevis and longus
Extensor carpi radialis longus
Extensor carpi radialis brevis
Extensor digitorum
Abductor pollicis longus
Extensor pollicis brevis
Extensor pollicis longus
Tendons of extensor digitorum
Olecranon process of ulna
Anconeus
Supinator
Abductor pollicis longus
Extensor pollicis longus
Extensor pollicis brevis
Extensor indicis
Interossei

5 sEMG placement in successful studies focusing on finger and grip movements

5.1 Example 1: Redundant multi-channel sensor ring

A study conducted by Tang et al on hand motion classification utilized an electrode orientation in which a multi-channel sensor ring was oriented about the wrist, covering the posterior side of the forearm, as shown in Figure 1 below [6].

Muscles used:

- Extensor digitorum
- Extensor policis longus & brevis
- Extensor indicis
- Extensor digiti minimi

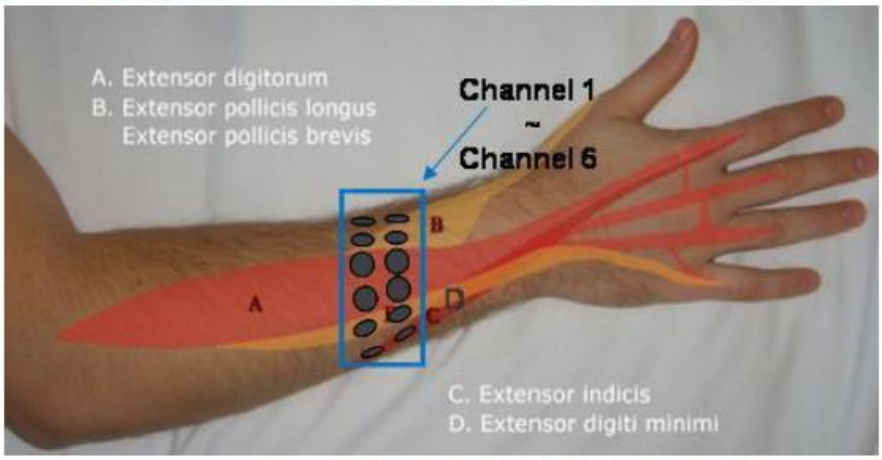

Figure 1: Electrode orientation for study completed by Tang et al [6].

This study proposed a new cascaded-structure classifier which was able to identify eleven types of hand gestures accurately (98% success rate) using new features developed by the research team.[1] Gestures included individual finger extension and predefined gestures such as ball grasp and lateral grasp.

A second study that placed electrodes in a similar way for finger motion decoding using sEMG used only four channels, as shown below [15].

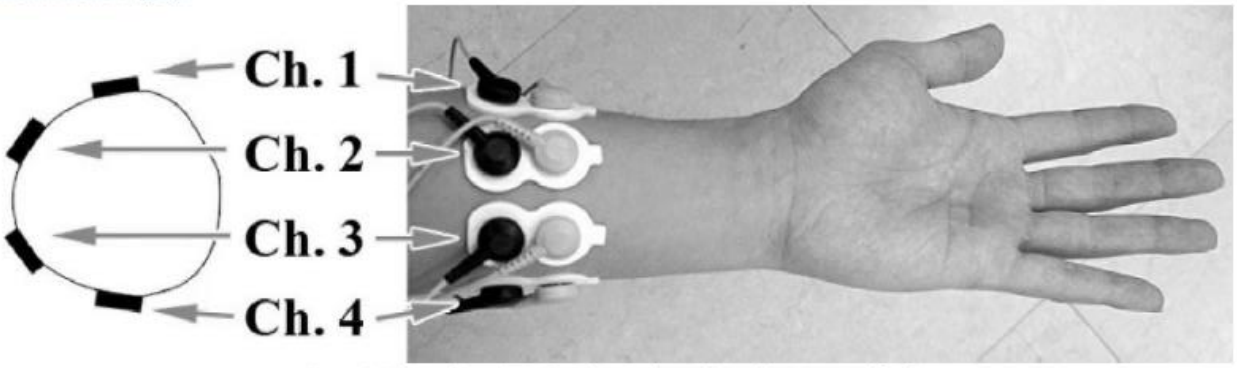

Figure 2: Electrode orientation for study conducted by You et al [15].

This study was able to achieve 97.75% accuracy for flexion of the thumb, index finger, middle finger, ring finger, and little finger, and three multi-finger motions. MLE was used to infer finger motions.

[1] Features included energy ratio features in the time domain and concordance correlation features describing the relationship between very two channels of the multi-channel sEMG sensor system.

5.2 Example 2: Individually placed 32-channel system – 5 bands around the forearm

A study by Tenore, Ramos et al conducted in 2007 utilized a much more complex electrode orientation than the above study, in which electrodes were placed according to SENIAM recommendations throughout the forearm by following physical landmarks of the subject [8]. The research team presented a framework for decoding myoelectric signals from natural hand/finger movements naturally for use in upper limb prostheses. The setup and electrode orientation for an array of 32 bipolar electrodes, with a reference electrode placed on the distal part of the olecranon and a ground electrode on the clavicle is shown below. The team was able to show that 12 individuated flexion/extension movements of the fingers and groups of fingers can be decoded with accuracy >98% (used neural networks).

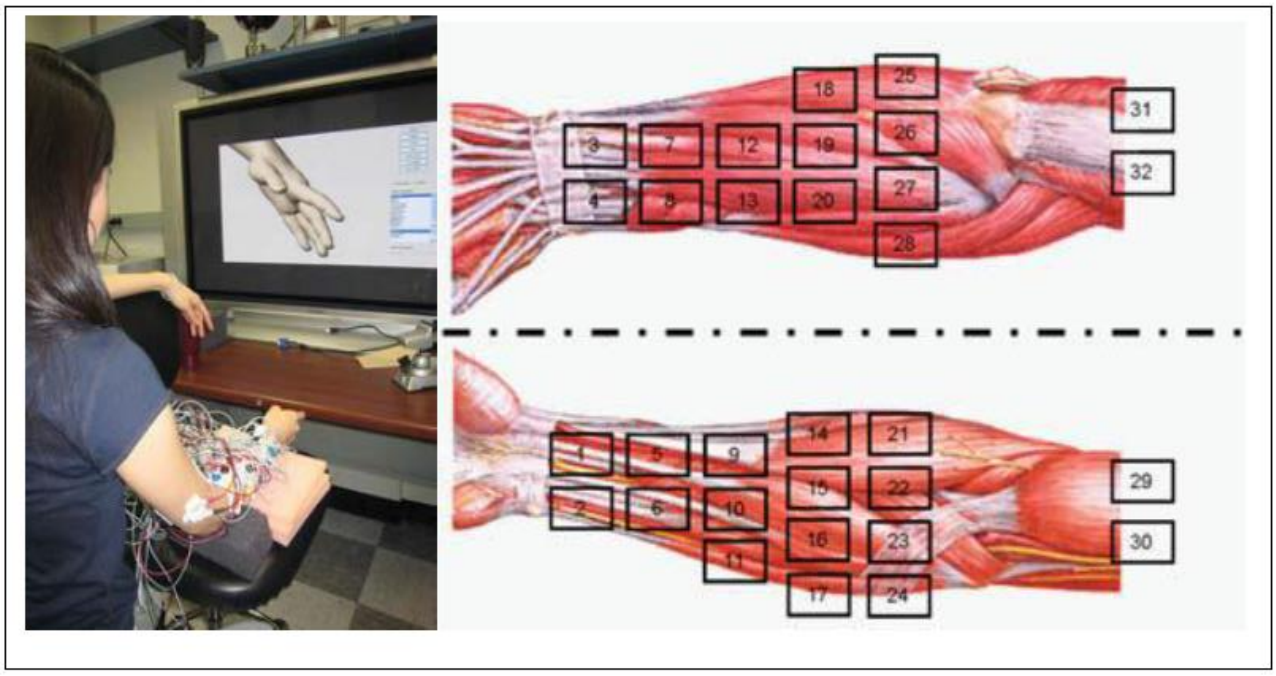

Figure 3: Physical setup and electrode orientation for study conducted by Tenore, Ramos et al [8].

Muscles used:

- Flexor carpi ulnaris
- Extensor carpi ulnaris
- Extensor digit minimi
- Extensor pollicis brevis & longus
- Extensor inicis
- Extensor digitorum
- Extensor carpi radialis Brevis
- Extensor carpi radialis longus
- Pronator quadratus (overlain by wrist)
- Flexor digitorum superficialis (overlain by wrist)
- Flexor pollicus longus
- Flexor digitorum sperficialis & profundus
- Palmaris longus
- Flexor carpi radialis
- Brachioradialis
- Pronator teres

5.3 Example 3: Two rings consisting of 15 sEMG channels

A study conducted by Smith et al in 2008 for the continuous decoding of finger position from sEMG signals for the control of powered prostheses utilized an electrode orientation that appears to be a compromise between choices 1 and 2 [9]. This setup used fifteen bipolar Ag/AGCl electrodes placed on the subject's right forearm with reference and ground electrodes placed on the olecranon process and clavicle, respectively. The electrode locations were chosen based on potential MES recording sites for transradial amputees, and were arranged in two rings, as shown below. Research was able to show that it is possible to continuously decode finger position from sEMG signals collected from a generalized electrode placement in an able bodied subject.

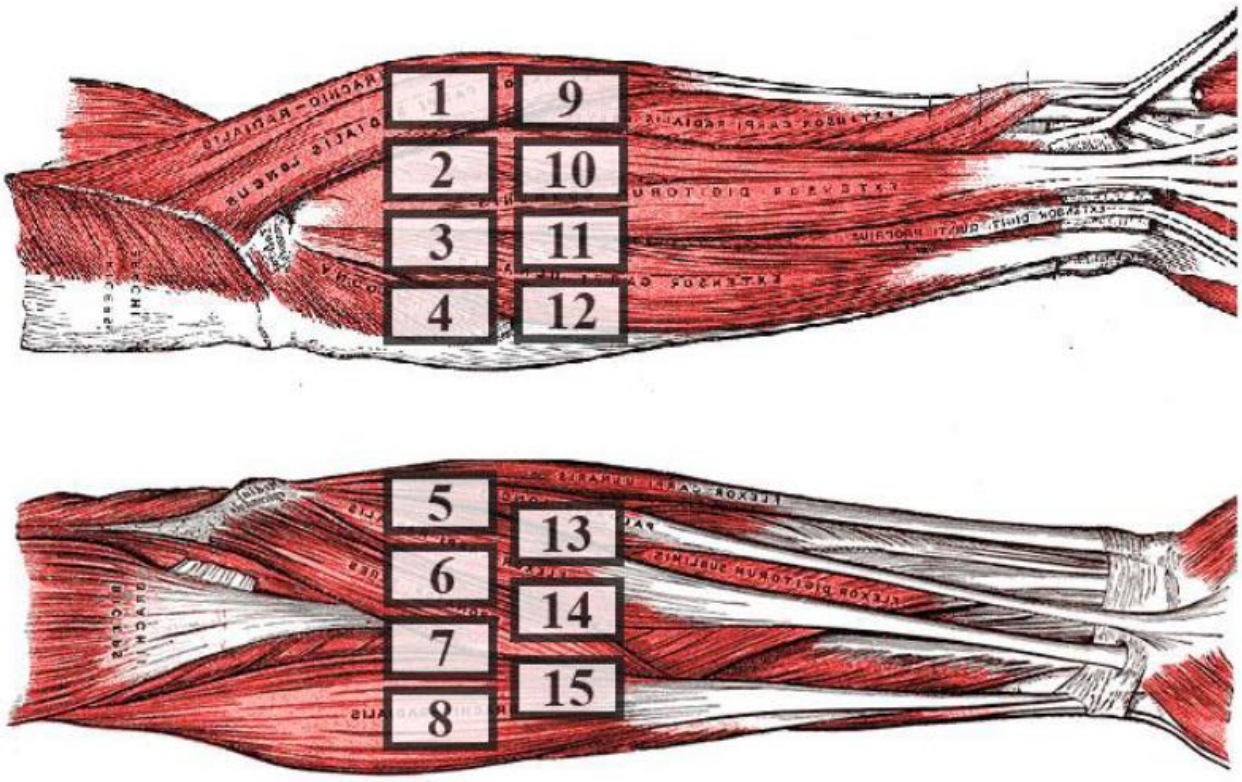

Figure 4: Arrangement of electrodes for study by Smith et al [9]. Electrode notation is laid over diagrams from Gray's anatomy. {REFERENCE}

Muscles used:

- Brachioradialis
- Flexor carpi ulnaris
- Flexor carpi radialis
- Palmaris longus / Flexor carpi ulnaris
- Flexor pollicus longus
- Extensor carpi radialis longus & brevis
- Extensor carpi ulnaris
- Extensor digitorum

5.4 Example 4: Individually placed 32-channel system – follow up to previous work

Another study by Tenore et al in 2009 demonstrated that it is possible to decode individual flexion/extension movements of each finger with >90% accuracy in transradial amputees using sEMG signals [10]. Electrodes were placed on the forearm by following SENIAM recommendations and using the orientation in the figure below.

Muscles used:

- Flexor carpi ulnaris
- Extensor carpi ulnaris
- Extensor digit minimi
- Extensor pollicis brevis & longus
- Extensor inicis
- Extensor digitorum
- Extensor carpi radialis Brevis
- Extensor carpi radialis longus
- Pronator quadratus (overlain by wrist)
- Flexor digitorum superficialis (overlain by wrist)
- Flexor pollicus longus
- Flexor digitorum sperficialis & profundus
- Palmaris longus
- Flexor carpi radialis
- Brachioradialis
- Pronator teres
- Biceps brachii
- Triceps brachii

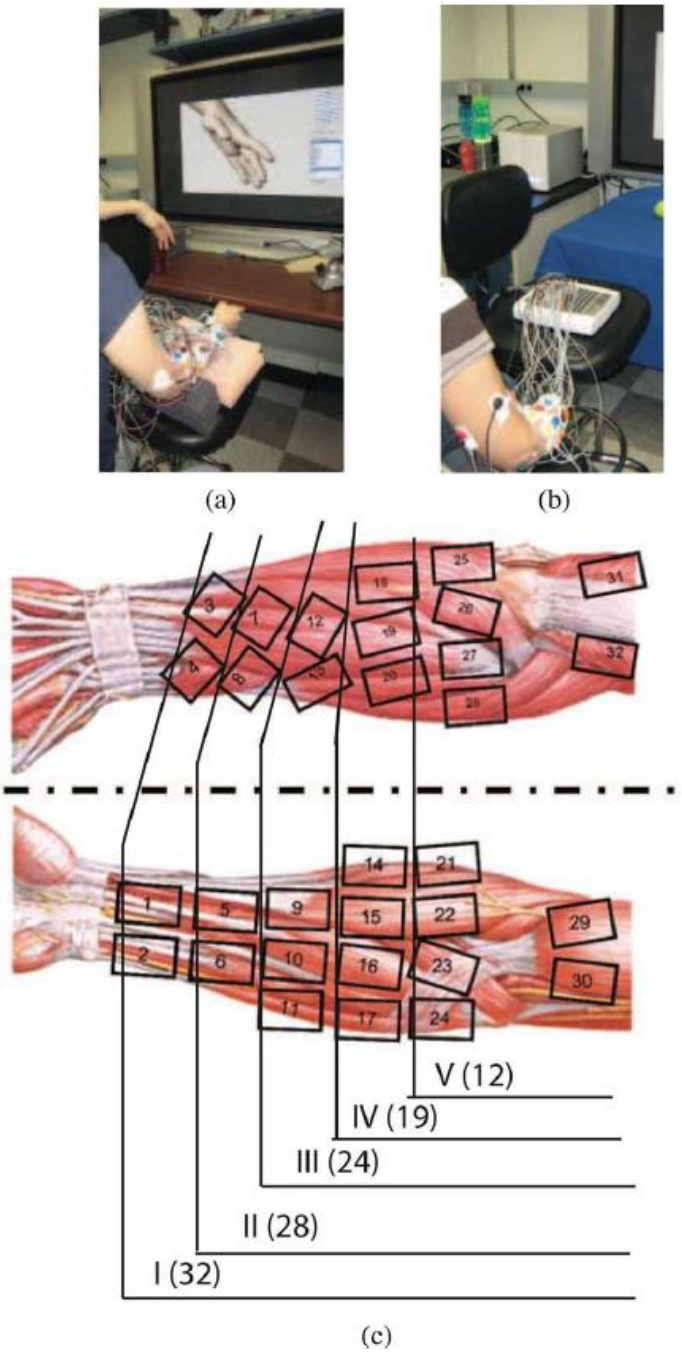

Figure 5: Electrode orientation for study by Tenore et al in which individual flexion/extension movements of each finger were decoded with >90% accuracy in transradial amputees using sEMG signals [10].

6 Recommended Electrode Placement

The placement of all 16 electrodes has not been completed. Placement will adhere to the following as much as possible.

- Electrode contacts of each electrode-amplifier will be oriented along the long axis of the forearm.
- Electrodes will be placed three fingers breadth from the olecranon process of the elbow.
- The distance between adjacent electrode amplifiers will be ~1.75 cm.

Muscles related to finger flexion and extension were selected using [4]. The electrode orientation was determined by forming criteria for the expected quality of results that the research team can obtain from a specific muscle. These criteria are shown below. Criteria were ranked against each other using a weighted objectives chart to later facilitate muscle ranking.

6.1 Criteria

Table 2: Criterion used for muscle selection, shown in weighted objectives chart

	Objective	A	B	C	D	E	F
A	Accessibility	*	1	1	1	1	0
B	Multiple successful studies used it	0	*	0	0.5	0.5	0
C	Can be positioned parallel to muscle fibers	0	1	*	1	1	0
D	Can be placed halfway between the most distal motor endplate zone and distal tendon	0	0.5	0	*	**0**	0
E	Geometrical distance of electrode from other muscles can be maximized	0	0.5	0	1	*	**0**
F	Controls finger flexion or extension	1	1	1	1	1	*

Table 3: Weighted importance of each criteria

Objective	Score	Weighted importance
Controls finger flexion or extension	5	33.33%
Accessibility	4	26.67%
Can be positioned parallel to muscle fibers	3	20.00%
Geometrical distance of electrode from other muscles can be maximized	1.5	10.00%
Multiple successful studies used it	1	6.67%
Can be placed halfway between the most distal motor endplate zone and distal tendon	0.5	3.33%

6.2 Muscle ranking

Muscles were ranked against the above criteria using '1' to indicate the answer 'yes', '0' to indicate the answer 'no', and '0.5' to indicate the answer 'maybe'. These values were then multiplied by the weighted importance percentages in the chart above to determine the extent to which a particular muscle is expected to comply by the criteria set forth. Muscles were ranked using only superficial anatomical diagrams to allow for accessibility & geometry related questions to be answered properly.

Table 4: Muscles ranked by compliance with criteria

Muscle	Overall compliance
Extensor digitorum [6, 8, 9, 10, 11, 12, 13, 15]	94.70%
Flexor carpi ulnaris [8, 9, 10]	83.20%
Extensor carpi radialis longus [8, 9, 10]	73.20%
Extensor digit minimi [deep muscle] [6,8, 10]	73.05%
Extensor carpi radialis brevis [8, 9, 10]	71.55%
Flexor digitorum superficialis [8, 10, 11,12, 13, 14]	63.00%
Extensor pollicis brevis and longus [deep muscle] [6, 8, 10, 11, 13,15]	59.90%
Flexor pollicis longus [deep muscle] [8, 9, 10, 13]	56.55%
Adbuctor pollicis longus [deep muscle]	41.70%
Extensor Indicis [deep muscle][6, 8, 10, 11, 13, 15]	39.70%
Flexor digitorum profundus [deep muscle] [8, 10, 12]	39.70%

6.3 Electrode orientation

Rectangular shapes indicating the anticipated size and location of electrodes have been overlain on the superficial views of both sides of the forearm. The table below indicates the muscle, its overall compliance with the above criteria, which electrode numbers represent this muscle, and comments/questions regarding electrode placement for this muscle.

Table 5: Muscle compliance and assigned electrode numbers, with questions/comments regarding electrode placement.

Muscle	Overall compliance	Electrode numbers	Questions/comments
Extensor digitorum	94.70%	1,2	
Flexor carpi ulnaris	83.20%	3,4	
Extensor carpi radialis longus	73.20%	5	
Extensor digit minimi	73.05%	6	Difficult not to overlap. Can overlap extensor carpi ulnaris if not a problem.
Extensor carpi radialis brevis	71.55%	7	
Flexor digitorum superficialis	63.00%	8	Where is the best place to put this one?
Extensor pollicis brevis and longus	59.90%	9	Not sure if we want this. Maybe just do other muscles again, these are both related to the thumb
Flexor pollicis longus	56.55%	10	Not sure if we want this. Maybe just do other muscles again, these are both related to the thumb
Adbuctor pollicis longus	41.70%	11	Not sure if we want this. Maybe just do other muscles again, these are both related to the thumb
Extensor Indicis	39.70%	12	What does having all the tendons there do?
Flexor digitorum profundus	39.70%	None	Not able to be found on superficial diagrams

Keating, 14

Figures 6 and 7 indicate the anticipated placement for electrodes to capture signals from the muscles discussed above. Those in blue relate directly to flexion or extension of fingers 2-5, while those in green relate to thumb movement. No muscles related to wrist movement have been selected for use. Based on these images it is recommended that electrodes are grouped in sets of two, longitudinally, rather than groups of four, wrapped circumferentially.

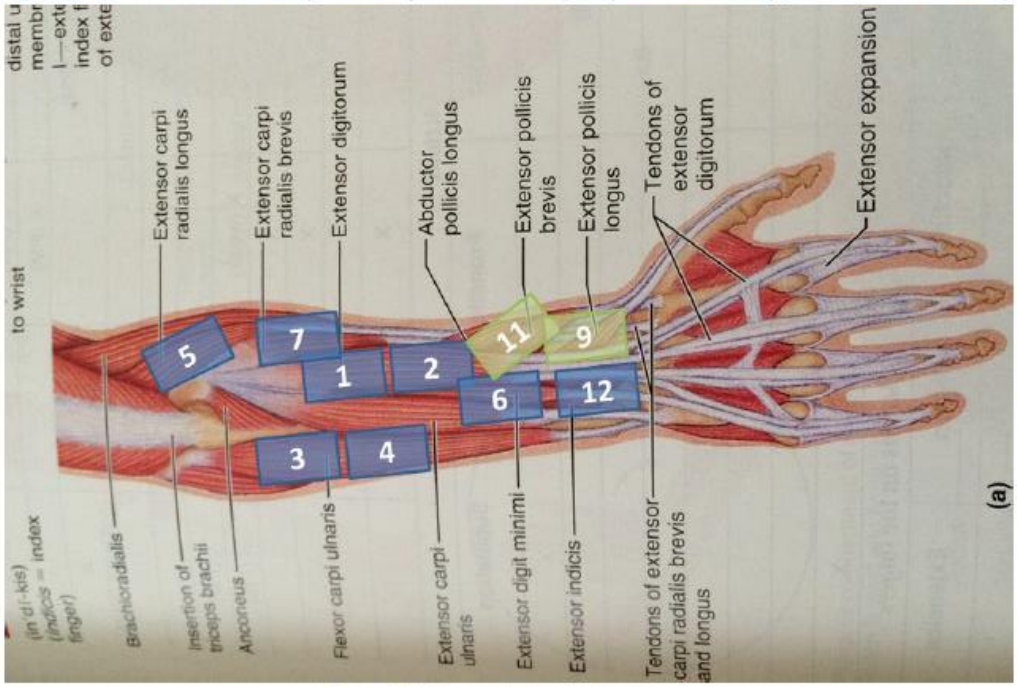

Figure 6: Extensor electrode placement.

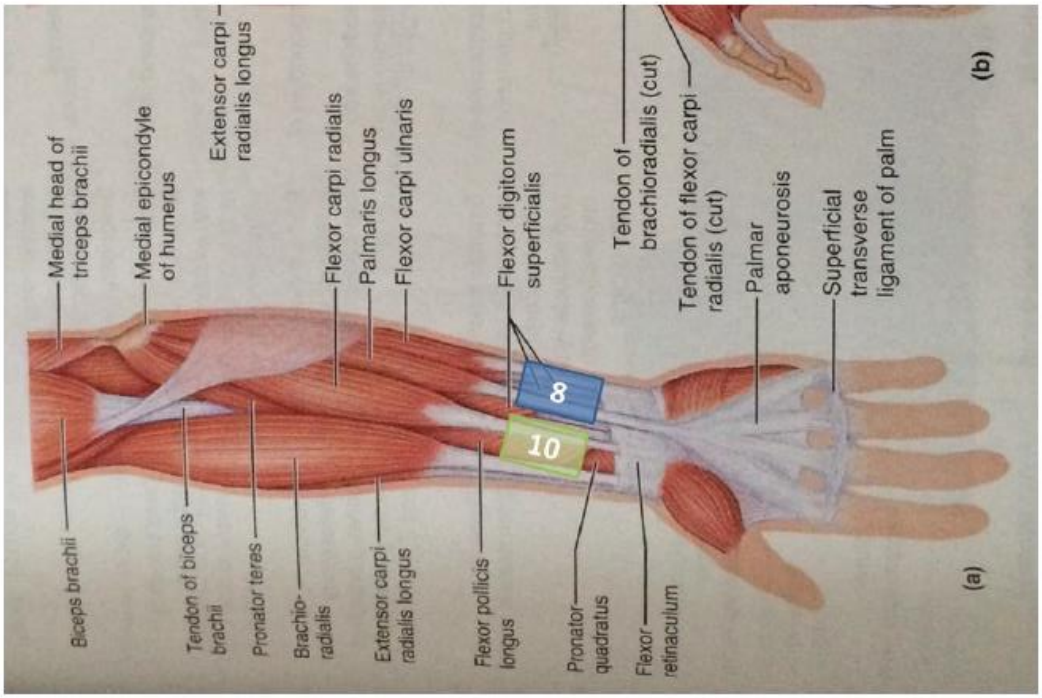

Figure 7: Flexor electrode placement

8 References

[1] "Introduction to the Special Issue on the SENIAM European Concerted Action." *Journal of Electromyography and Kinesiology* 10 (2000): 283-86. Print.

[2] Stegeman, D. F., and H. J. Hermens. "Standards for Surface Electromyography: The European Project "Surface EMG for Non-invasive Assessment of Muscles (SENIAM)"." (n.d.): 108-12. Print.

[3] Young, Aaron J., Levi J. Hargrove, and Todd A. Kuiken. "The Effects of Electrode Size and Orientation on the Sensitivity of Myoelectric Pattern Recognition Systems to Electrode Shift." *IEEE Transactions on Biomedical Engineering* 58.9 (2011): 2537-544. Print.

[4] Marieb, Elaine N. "10: The Muscular System." Anatomy & Physiology. 5th ed. Boston: Pearson, n.d. N. pag. Print.

[5] Saitou, K., M. Okada, and T. Sadoyama. "Effect on surface EMG waveforms of electrode location with respect to the neuromuscular junctions: Its significance in EMG-muscle lengthrelation." *In Proc. 8th Congr. Int. Soc. Electrophysiology and Kinesiology*, Baltimore, MD, 1990, pp 27-30.

[6] Tang, Xueyan, Yunhui Liu, Congyi Lv, and Dong Sun. "Hand Motion Classification Using a Multi-Channel Surface Electromyography Sensor." *Sensors* 12 (2012): 1130-147. Print.

[7] Hermens, Hermie J., Bart Freriks, Catherine Disselhorst-Klug, and Gunter Rau. "Development of Recommendations for SEMG Sensors and Sensor Placement Procedures." *Journal of Electromyography and Kinesiology* 10 (2000): 361-74. Print.

[8] Tenore, Francesco, Ander Ramos, Amir Fahmy, Soumyadipta Acharya, Ralph Etienne-Cummings, and Nitish V. Thakor. *Towards the Control of Individual Fingers of a Prosthetic Hand Using Surface EMG Signals*. Proc. of 29th Annual International Conference of the IEEE EMBS, France, Lyon. Lyon, France: n.p., 2007. 6145-148. Print.

[9] Smith, Ryan J., Francesco Tenore, David Huberdeau, Ralph Etienne-Cummings, and Nitish V. Thakor. "Continuous Decoding of Finger Position from Surface EMG Signals for the Control of Powered Prostheses." *30th Annual International IEEE EMBS Conference*. Proc. of 30th Annual International IEEE EMBS Conference, Britich Columbia, Canada, Vancouver. N.p.: n.p., 2008. 197-200. Print.

[10] Tenore, F.V.G., A. Ramos, A. Fahmy, S. Acharya, R. Etienne-Cummings, and N.V. Thakor. "Decoding of Individuated Finger Movements Using Surface Electromyography." *IEEE Transactions on Biomedical Engineering* 56.5 (2009): 1427-434. Print.

[11] Bitzer, Sebastian, and Patrick Van De Smagt. *Learning EMG Control of a Robotic Hand: Towards Active Prostheses*. Proc. of IEEE International Conference on Robotics and Automation, Florida, Orlando. N.p.: n.p., 2006. 2819-823. Print. – Was able to develop a robust method based on SVM to detect opening/closing actions of fingers.

[12] Birdwell, J. Lexander, Levi J. Harvrove, and Richerd F. Weir. *Quantification of Isolated Muscle Compartment Activity in Extrinsic Finger Muscles for Potential Prosthesis Control Sites*. Proc. of 33rd Annual International Conference of the IEEE EMBS, Massachusetts, USA, Boston. Boston, MA: n.p., 2011. 4104-107. Print.

[13] Wege, Andreas, and Armin Zimmermann. *Electromyography Sensor Based Control for a Hand Exoskeleton*. Proc. of IEEE International Conference on Robotics and Biomimetics, China, Sanya. N.p.: IEEE, 2008. 1470-475. Print.

[14] Kumar, Dinesh Kant, Sridhar Poosapadi Arjunan, and Vijay Pal Singh. "Towards Identification of Finger Flexions Using Single Channel Surface Electromyography – Able Bodied and Amputee Subjects." *Journal of Neuroengineering and Rehabilitation* 50th ser. 10.1 (2013): n. pag. Print.

[15] You, Kyung-Jin, Ki-Won Rhee, and Hyun-Chool Shin. "Finger Motion Decoding Using EMG Signals Corresponding Various Arm Postures." *Experimental Neurobiology* 19 (2010): 54-61. Print.

Other references reviewed:

Itoh, Y., H. Uematsu, F. Nogata, T. Nemoto, A. Inamori, K. Koide, and H. Matsuura. "Finger Curvature Movement Recognition Interface Technique Using SEMG Signals." *Journal of Achievements in Materials and Manufacturing Engineering* 23.2 (2007): 43-46. Print.

Lee, S. W., K. M. Wilson, B. A. Lock, and D. G. Kamper. "Subject-specific Myoelectric Pattern Classification of Functional Hand Movements for Stroke Survivors." *IEEE Transactions on Neural Systems and Rehabilitation Engineering* 19.5 (2011): n. pag. Print.

Lou, Xinxin, Siyuan Xiao, Yu Qi, Xiaoling Hu, Yiwen Wang, and Xiaoxiang Zheng. "Corticomuscular Coherence Analysis on Hand Movement Distinction for Active Rehabilitation." *Computational and Mathematical Methods in Medicine* 2013.Article ID 908591 (2013): n. pag. Print.

Ryait, Hardeep S., A. S. Arora, and Ravinder Agarwal. "Study of Issues in the Development of Surface EMG Controlled Human Hand." *Journal of Materials Science: Materials in Medicine* 20 (2009): 107-14. Print.

Zecca, M., Silvestro Micera, M. C. Carrozza, and P. Dario. "Control of Multifunctional Prosthetic Hands by Processing the Electromyographic Signal." *Critical Reviews? in Biomedical Engineering* 30.4-6 (2002): 459-85. Print.

9 Appendices

9.1 Muscle Compliance to criteria

9.1.1 Extensor carpi radialis brevis

Criteria	Extensor carpi radialis brevis [8, 9, 10]	Importance	Compliance to criteria	Comments
Is easily accessible from the surface	1	26.70%	26.70%	
Multiple successful studies used it	1	6.70%	6.70%	
Controls finger flexion/extension	0.5	33.00%	16.50%	Steadies wrist during finger flexion
Electrodes can be positioned parallel to muscle fibers	1	20.00%	20.00%	
Electrodes can be placed halfway between the most distal motor endplate zone and distal tendon	0.5	3.30%	1.65%	Small amount of space, can try to be away from but is near
Geometrical distance of electrode from other muscles can be maximized	0	10.00%	0.00%	Very small amount of space here, will just have to deal with what we have
		TOTAL COMPLIANCE	71.55%	

9.1.2 Extensor carpi radialis longus

Criteria	Extensor carpi radialis longus [8, 9, 10]	Importance	Compliance to criteria	Comments
Is easily accessible from the surface	1	26.70%	26.70%	
Multiple successful studies used it	1	6.70%	6.70%	
Controls finger flexion/extension	0.5	33.00%	16.50%	Steadies wrist during finger flexion
Electrodes can be positioned parallel to muscle fibers	1	20.00%	20.00%	
Electrodes can be placed halfway between the most distal motor endplate zone and distal tendon	1	3.30%	3.30%	Small amount of space, can try to be away from but is near
Geometrical distance of electrode from other muscles can be maximized	0	10.00%	0.00%	Very small amount of space here, will just have to deal with what we have

TOTAL COMPLIANCE	73.20%	

9.1.3 Extensor digitorum

Criteria	Extensor digitorum [6, 8, 9, 10, 11, 13, 15]	Importance	Compliance to criteria	Comments
Is easily accessible from the surface	1	26.70%	26.70%	
Multiple successful studies used it	1	6.70%	6.70%	
Controls finger flexion/extension	1	33.00%	33.00%	
Electrodes can be positioned parallel to muscle fibers	1	20.00%	20.00%	
Electrodes can be placed halfway between the most distal motor endplate zone and distal tendon	1	3.30%	3.30%	
Geometrical distance of electrode from other muscles can be maximized	0.5	10.00%	5.00%	Not particularly wide and is above deeper muscles also controlling actions. Is very close to extensor carpi ulnaris as well.
TOTAL COMPLIANCE			94.70%	

9.1.4 Extensor digit minimi

Criteria	Extensor digit minimi [6,8, 10]	Importance	Compliance to criteria	Comments
Is easily accessible from the surface	0.5	26.70%	13.35%	Small and not quite superficial, will likely have data from other muscles
Multiple successful studies used it	1	6.70%	6.70%	
Controls finger flexion/extension	1	33.00%	33.00%	
Electrodes can be positioned parallel to muscle fibers	1	20.00%	20.00%	
Electrodes can be placed halfway between the most distal motor endplate zone and distal tendon	0	3.30%	0.00%	Limited space, not really up for debate
Geometrical distance of electrode from other muscles can be maximized	0	10.00%	0.00%	Limited space, not really up for debate

TOTAL COMPLIANCE	73.05%	

9.1.5 Abductor pollicus longus

Criteria	Adbuctor pollicis longus	Importance	Compliance to criteria	Comments
Is easily accessible from the surface	1	26.70%	26.70%	Small and not quite superficial, will likely have data from other muscles
Multiple successful studies used it	0	6.70%	0.00%	
Controls finger flexion/extension	0	33.00%	0.00%	Is for thumb
Electrodes can be positioned parallel to muscle fibers	0.5	20.00%	10.00%	With some difficulty due to angle, depends on how we do the setup
Electrodes can be placed halfway between the most distal motor endplate zone and distal tendon	0	3.30%	0.00%	Limited space
Geometrical distance of electrode from other muscles can be maximized	0.5	10.00%	5.00%	Limited space
		TOTAL COMPLIANCE	41.70%	

9.1.6 Extensor pollicis brevis & longus

Criteria	Extensor pollicis brevis and longus	Importance	Compliance to criteria	Comments
Is easily accessible from the surface	1	26.70%	26.70%	Small and not quite superficial, will likely have data from other muscles
Multiple successful studies used it	1	6.70%	6.70%	
Controls finger flexion/extension	0.5	33.00%	16.50%	Is for thumb
Electrodes can be positioned parallel to muscle fibers	0.5	20.00%	10.00%	With some difficulty due to angle, depends on how we do the setup
Electrodes can be placed halfway between the most distal motor endplate zone and distal tendon	0	3.30%	0.00%	Limited space
Geometrical distance of electrode from other muscles can be maximized	0	10.00%	0.00%	Limited space, also note it lies over tendons

TOTAL COMPLIANCE	59.90%	

9.1.7 Extensor indicis

Criteria	Extensor Indicis [6, 8, 10, 11, 13, 15]	Importance	Compliance to criteria	Comments
Is easily accessible from the surface	0	26.70%	0.00%	Deep muscle
Multiple successful studies used it	1	6.70%	6.70%	Not sure how studies have differentiated it before
Controls finger flexion/extension	1	33.00%	33.00%	Index finger
Electrodes can be positioned parallel to muscle fibers	0	20.00%	0.00%	Very difficult to access, will have to make do with what we can fit
Electrodes can be placed halfway between the most distal motor endplate zone and distal tendon	0	3.30%	0.00%	Very difficult to access, will have to make do with what we can fit
Geometrical distance of electrode from other muscles can be maximized	0	10.00%	0.00%	Very difficult to access, will have to make do with what we can fit
		TOTAL COMPLIANCE	39.70%	

9.1.8 Flexor carpi ulnaris

Criteria	Flexor carpi ulnaris [8, 9, 10]	Importance	Compliance to criteria	Comments
Is easily accessible from the surface	1	26.70%	26.70%	
Multiple successful studies used it	1	6.70%	6.70%	
Controls finger flexion/extension	0.5	33.00%	16.50%	
Electrodes can be positioned parallel to muscle fibers	1	20.00%	20.00%	
Electrodes can be placed halfway between the most distal motor endplate zone and distal tendon	1	3.30%	3.30%	
Geometrical distance of electrode from other muscles can be maximized	1	10.00%	10.00%	

TOTAL COMPLIANCE	83.20%	

9.1.9 Flexor digitorum superficialis

Criteria	Flexor digitorum superficialis [8, 10, 11,12, 13, 14]	Importance	Compliance to criteria	Comments
Is easily accessible from the surface	0	26.70%	0.00%	Not sure why it is called superficial, lies deep to multiple muscles
Multiple successful studies used it	1	6.70%	6.70%	Yes but not sure how it is differentiated
Controls finger flexion/extension	1	33.00%	33.00%	
Electrodes can be positioned parallel to muscle fibers	1	20.00%	20.00%	Yes, but not directly on top
Electrodes can be placed halfway between the most distal motor endplate zone and distal tendon	1	3.30%	3.30%	Yes, but not directly on top
Geometrical distance of electrode from other muscles can be maximized	0	10.00%	0.00%	No. Other muscles will interfere
		TOTAL COMPLIANCE	63.00%	

9.1.10 Flexor pollicis longus

Criteria	Flexor pollicis longus [8, 9, 10, 13]	Importance	Compliance to criteria	Comments
Is easily accessible from the surface	0.5	26.70%	13.35%	
Multiple successful studies used it	1	6.70%	6.70%	
Controls finger flexion/extension	0.5	33.00%	16.50%	Thumb
Electrodes can be positioned parallel to muscle fibers	1	20.00%	20.00%	
Electrodes can be placed halfway between the most distal motor endplate zone and distal tendon	0	3.30%	0.00%	What you see is what you get
Geometrical distance of electrode from other muscles can be maximized	0	10.00%	0.00%	What you see is what you get

TOTAL COMPLIANCE	56.55%	

9.1.11 Flexor digitorum profundus

Criteria	Flexor digitorum profundus [8, 10, 12]	Importance	Compliance to criteria	Comments
Is easily accessible from the surface	0	26.70%	0.00%	
Multiple successful studies used it	1	6.70%	6.70%	
Controls finger flexion/extension	1	33.00%	33.00%	
Electrodes can be positioned parallel to muscle fibers	0	20.00%	0.00%	Can't find in superficial images
Electrodes can be placed halfway between the most distal motor endplate zone and distal tendon	0	3.30%	0.00%	Can't find in superficial images
Geometrical distance of electrode from other muscles can be maximized	0	10.00%	0.00%	Can't find in superficial images
		TOTAL COMPLIANCE	39.70%	

Appendix 2 Test Setup Validation

A-2.1 Electrode Amplifier

WORCESTER POLYTECHNIC INSTITUTE

Electrode Amplifier Validation

Berj Bardizbanian

10/19/2013

1 Table of Contents

2 Table of Figures

3 Executive Summary

The circuitry of the electrodes was tested at different stages during the manufacturing process: At the initial stage before soldering conductors, after soldering conductors, after pouring the epoxy, after connecting to male DB9 connectors, and after connecting male DB9 to female DB9-RJ45 assembly cable.

All signals were observed as expected, with no additive noise. The following sections detail the electrode design, the testing of the electrodes, and the testing of the DB9 and RJ45 connector.

4 Electrode Design

Before describing the methodology used to validate test results, below is the circuit that the electrodes are made of.

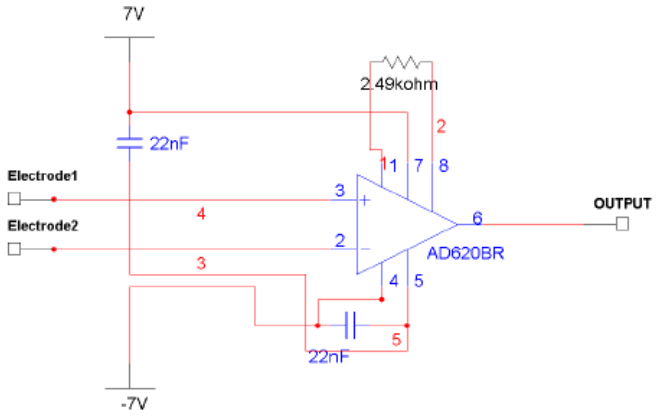

Fig. 1: Electrode circuitry

Electrodes form the input to AD620 instrumentation amplifier with power-line decoupling capacitors. The circuit is supplied by +/- 7 V DC and the output is taken at terminal 6. Ultra-Flex wire is used to connect the circuit to DB9. These ultra-flex wire contains four different colored wires (Red, Green, White and Black), and 5 mils PVC insulated Ultraminiature conductors sandwiched inside a tinned copper braided shield. The whole assembly is covered with a flexible PVC jacket, as shown in Fig. 2.

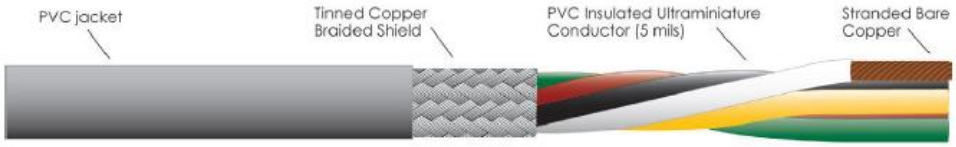

Fig. 2: Ultra-flex cable configuration

The red and green conductors are used for +7V and -7V, respectively, while the white and black conducts are for the output and ground, respectively.

The full assembly can be seen below in Figure 3.

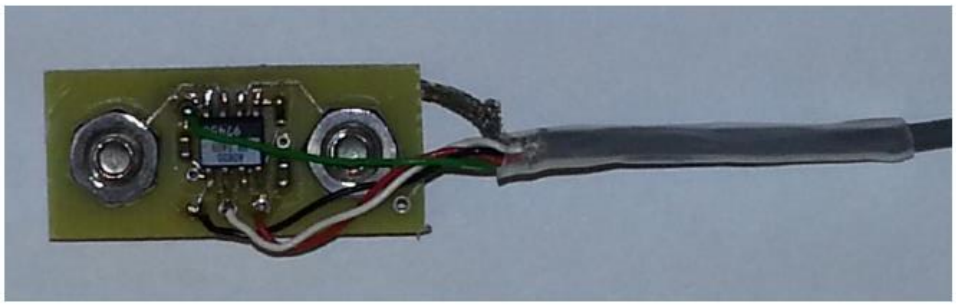

Fig. 3: PCB with electronic components, electrode assemblies, and ultra-flex cable

5 Testing the Soldered PCB

The following steps were taken to test the soldered PCB before continuing with connecting the electrodes to the rest of the assembly.

- Connect the red conductor on the other end of the cable (away from the PCB) to +7V DC
- Connect the green conductor on the other end of the cable to –7V DC
- Connect the white conductor to the oscilloscope.
- Use the signal generator to generate a sinusoid signal with 80 Hz and 150 mV_{PP}.
- Input the generated signal to the circuit by placing the probes on each of the tightened screws or nuts.
- Observe the output signal on the oscilloscope.
    - The result should be a magnified sinusoid signal with amplitude around 6 V_{PP} and the same frequency as the input signal.
- Change the input signal amplitude and frequency and verify the response of the circuit.
- The output should be sinusoid signal as long the output V_{pp} is within the supply voltage range below +/- 7V and should get "chopped" signal when exceeds that range.

6 DB9 and RJ45 Connector Testing

Testing the circuit from DB9 and RJ45 connectors was completed by following the same test methodology described in *Section 5 – Testing the Soldered PCB* above. The only difference was that the oscilloscope connection was through the pins of DB9 and RJ45 instead of the ultra-flex wire conductors. These connections are shown in the wiring diagrams in Figs. 4 and 5 below.

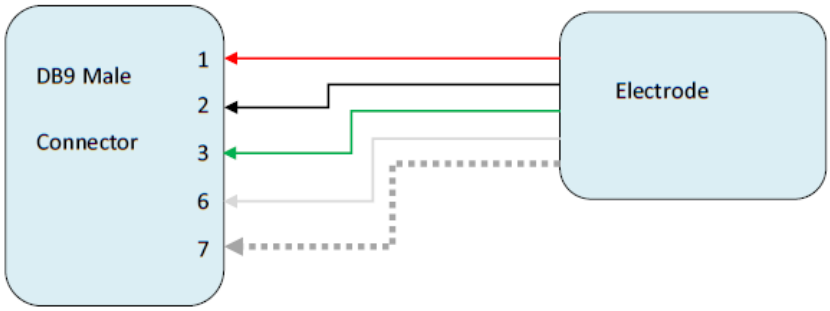

Fig. 4: Electrode to DB9 male connector wiring Diagram

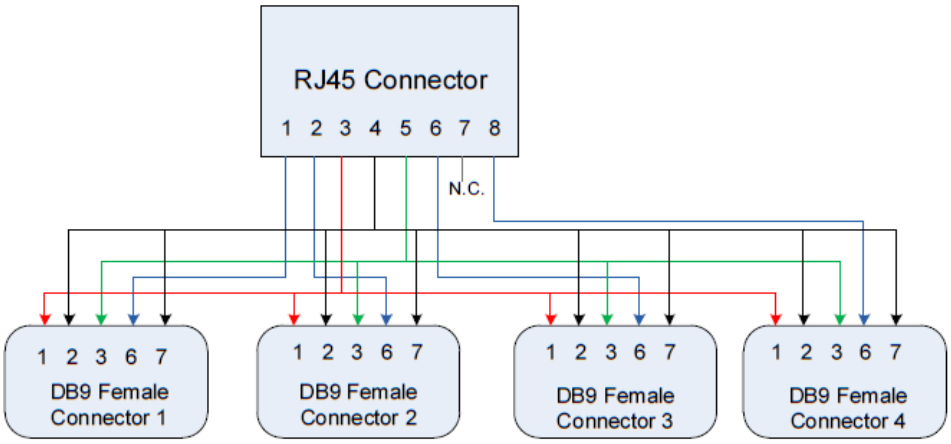

Fig. 5: RJ45 to DB9 Female connector wiring Diagram

A-2.2 Load Cell

CONFIDENTIAL

WORCESTER POLYTECHNIC INSTITUTE

Load Cell Accuracy & Repeatability

Jennifer Keating

26 November 2013

2 Table of Contents

3 Executive Summary

Pulling data was collected using a 500g calibrated weight. The data acquired was used to calculate the sensitivity of the LC101-100 load cell, in mV/lb, as well as to determine the repeatability of the baseline and the voltage achieved when force was applied to the cell.

The sensitivity of the load cell was found to be approximately -0.3 mV/lb, which is not far from the datasheet's expected value of 0.3 mV/lb.

The repeatability of the baseline was found to be good, with a standard deviation of 4.4721e-006 V, which amounts to ~2.13% of the signal when 500g is applied (and therefore much less when in use during the study). The repeatability of voltage achieved reached similar statistics, with a standard deviation across of about ~1% with 500g applied.

Conclusion: The LC101-100 load cell can be used for both gripping and individual finger EMG-force research.

4 Introduction

The proposed EMG study will relate the electrical activity of the forearm muscles that control forces in the fingers to the forces produced by the hand. As such, the accuracy and repeatability of the load cell used to measure force are vital to the success of the study.

A testing setup was developed to allow for determination of the accuracy and repeatability of the LC101 load cell to a known applied weight. The NI-USB 6211 and LabVIEW Signal Express were used for data acquisition.

Data collection consisted of 40 second trials of load cell voltage acquisition with approximately 3 applications of weight. During each trial baseline data was nominally collected for 3 seconds, while weight was applied for approximately 10 seconds per repetition. Five trials were conducted.

Data analysis consisted of extracting the voltages of the baseline and applied weight for each trial and determining the standard deviation of these values.

5 Equipment

5.1 Hardware

- LC101-100 load cell (Omega)
- NI6211 USB DAQ
  - 16-bit 250kS/s M series Multifunction DAQ with 16 AIs 2AOs
- Laboratory Calibration Mass Set
  - 500 g (±100 mg)
- Load cell test setup
  - Composed of optical rod and ¼-28" set screws (Thorlabs)

5.2 Software

- LabVIEW Signal Express
- MATLAB

6 Methods

6.1 Test Setup

6.1.1 Load Cell Voltage: NI-USB 6211 DAQ

The NI-USB 6211 DAQ was connected via USB to the computer and the load cell was connected to the DAQ. The NI6211 was used to supply the load cell with 5V, and the load cell outputs were connected to the signal input pins of the NI6211 to record voltage data directly to the computer.

Figure 1: NI-USB 6211 DAQ with load cell leads connected.

LabVIEW Signal Express was used to collect voltage data from the NI6211 for a 40 second time period, at a sampling rate of 1000 Hz, for each trial.

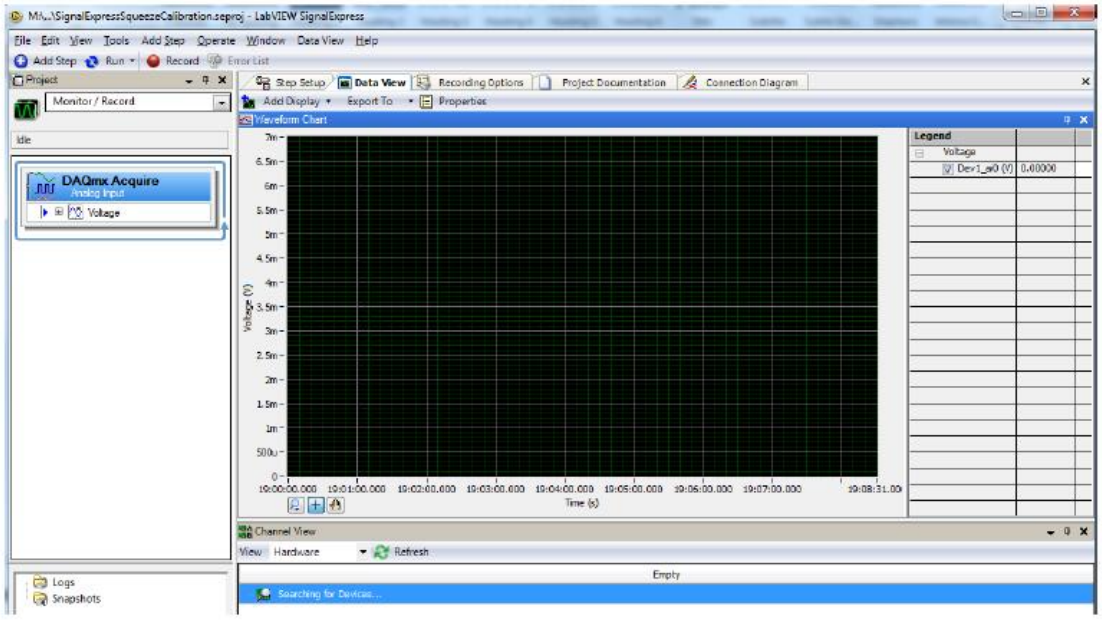

Figure 2: LabVIEW Signal Express VI for load cell data collection.

6.1.2 Force Application

The LC101-100 is an S type load cell which provides both tension and compression output readings. During this study, the load cell is mounted to a restraint device for constant-posture finger flexion-extension. The subject's finger is secured to the load cell apparatus via a Velcro strap. The subject then performs both *pushing* and *pulling* motions in which they move their finger away from and toward the palm of their hand, respectively.

The setup for the pulling scenario consisted of the LC101-100 kg load cell apparatus, an optical rod, a mounting base (to accommodate the ¼"-28 threading) and set screw.

Figure 3: Mounting of the LC101-100

To mimic the pulling motion a small cable was tied around each weight and a loop was created at the top to allow for attachment to the load cell. The load cell was attached to the optical rod (which was attached to an optical breadboard) via the set screw. This setup can be seen below.

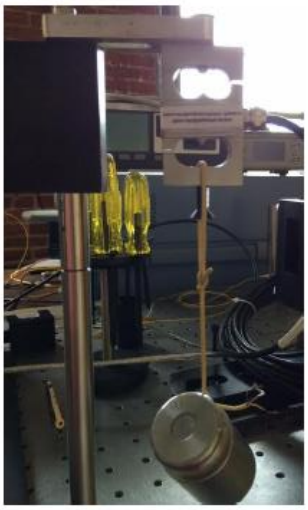

Figure 4: 500g weight suspended by one of the LCL-040 load cells.

To produce baseline data, the test operator lifted the weight such that the loop around the load cell had enough slack as to exert negligible force. The weight was then gently released for each pulling application.

6.2 Data Collection

A calibrated weight of 500g was used to apply a known force (later converted to lbf) to the load cell. The procedure for completing a trial with a certain weight was as follows. Five trials were completed with the 500g weight.

Figure 5: Calibrated mass set.

1. Connect the load cell to the NI6211
2. Open NI Signal Express Project for 40 second load cell data collection
3. Manually lift the 500g weight up so as to minimize weight applied to the load cell
4. Hit 'Run continuously' on the NI SE Project
5. Manually release the weight such that it is hanging from the load cell after 3 seconds[1]
6. Remove weight from load cell after 10 seconds
7. Repeat steps 5-6 twice more
8. Stop the Signal Express Project
9. Save the voltage data with the following name scheme "*LC#_<weight>g_Trial#*"

10. Table 1: Data collection table.

Weight (g)	Pound-force	Number of weight applications	Baseline time (s)	Weight application time (s)	Number of Trials
500	1.10	3	3	10	5

An example time series and density plot from this data is shown below.

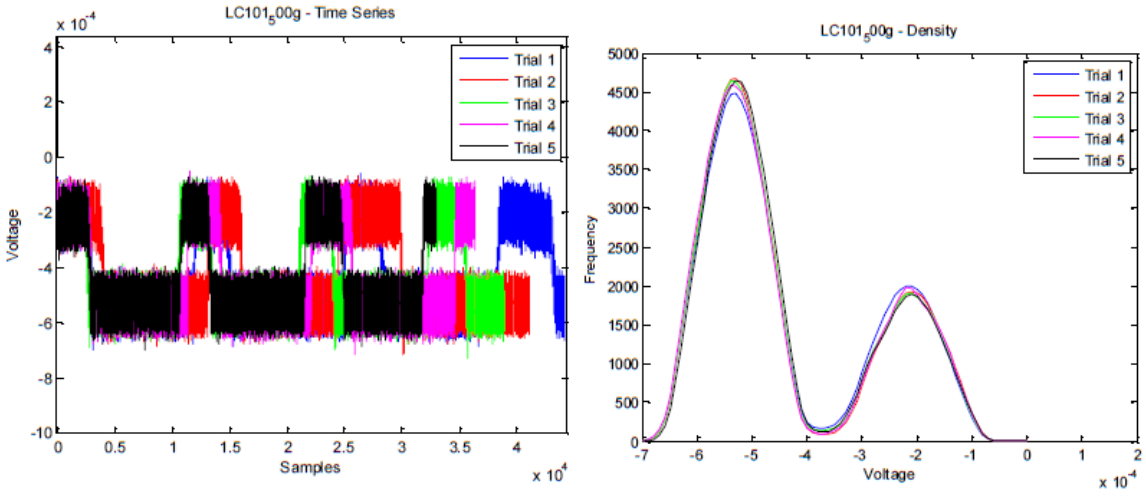

[1] The manual completion of this testing results in more variable signals than would be observed with a machine operated test.

6.3 Data Analysis

The data analysis used here was the same as for LCL-040 load cell testing. Example data is from LCL-040 load cells.

6.3.1 Baseline & Weight Voltage Data Extraction

The function ***plotLoadCellData*** takes the names of the raw data files to be used in analysis, and requests a name for the dataset, which is used to label saved figures and .mat files.

```
>> plotLoadCellData('LC1_1kg_1.xlsx', 'LC1_1kg_2.xlsx', 'LC1_1kg_3.xlsx', 'LC1_1kg_4.xlsx', 'LC1_
Enter the name of the dataset (use quotes): 'LC1 1kg (pulling)'
```

After the data title is entered, the program loads the data, indicating a new ellipse each time a file has been parsed. Once the data from all files has been loaded, a time series plot is displayed, with a prompt for the user to enter the maximum and minimum voltage in the dataset.

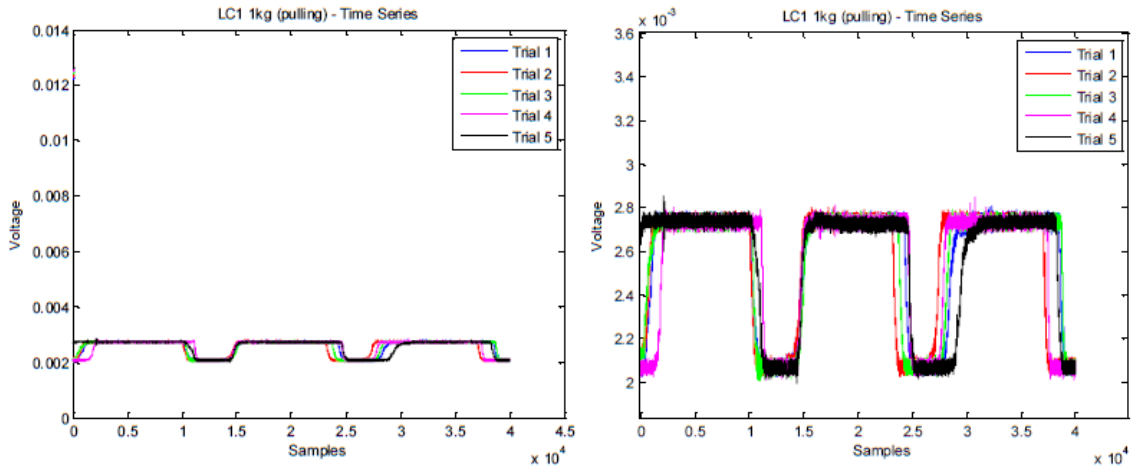

Figure 6: Time series data for LC1 1kg trials

```
>> plotLoadCellData('LC1_1kg_1.xlsx', 'LC1_1kg_2.xlsx', 'LC1_1kg_3.xlsx', 'LC1_1kg_4.xlsx',
Enter the name of the dataset (use quotes): 'LC1 1kg (pulling)'
Loading data.............
What is the maximum voltage to be used for this signal?
[default: 0.007000]: 0.0028
What is the minimum voltage to be used for this signal?
[default: 0.000000]: 0.002
```

Note: The time series data will not necessarily line up perfectly as weight placement was completed manually using a stopwatch during testing.

A density plot is then generated containing the density of each trial, with the limits of the density analysis being the minimum and maximum voltage entered by the user.[2] Such a plot can be seen below.

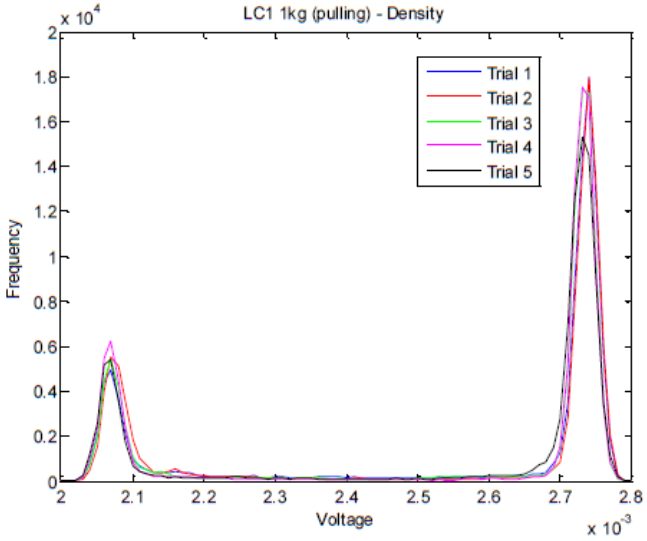

Figure 7: Density plot for load cell 1 tests with 1kg weight.

The density plot shows the distribution of the baseline data (smaller peak) and weight application data (larger peak). The reason that it is known which peak is baseline and which is weight is because of the way the data collection was conducted: weights were applied for 10 seconds per repetition while baseline was only collected for 3 seconds, resulting in a high concentration of voltage values at baseline, but a noticeably higher concentration at weight application. The function ***plotLoadCellData*** then identifies the voltage value at the peak of both density curves and stores that value as the value of the baseline and weight application for each trial. The code for this is shown below.

```
% Compute the densities of the data
     [trial1_Y, trial1_X] = ksdensity(trial1, minVoltage:0.00001:maxVoltage);
    [pks, locs] = findpeaks(trial1_Y, 'sortstr', 'descend');
    if USE_WEIGHTS == 1
        trial1Baseline = locs(2);
        trial1Baseline = trial1_X(trial1Baseline);
    end
    trial1Weight = locs(1);
    trial1Weight = trial1_X(trial1Weight);
```

The trial weights and trial baselines data is saved to a .mat file, and the standard deviation of both sets is saved as a representation of the variance of the data. All figures and statistics are automatically saved as .fig and .mat files, respectively.

6.3.2 Sensitivity calculation

The function ***loadCellSensitivity*** is used to calculate the sensitivity of the load cell, in mV/lb. It takes as its inputs the weight used in the trials being loaded and the .mat file containing the data saved during load cell analysis (***plotLoadCellData***). To make use of the function easy, the user inputs the weight applied in grams, and the function translates this into pounds for later comparisons. From this it calculates the average voltage for each weight application (as well as standard deviation). This value is used to calculate load cell sensitivity using the voltage corresponding to the used weight.

---

[2] The reason for this is that if there are outliers to any of the trials used in data analysis, the density plot may appear skewed as it tries to fit the entire dataset.

Three load cell sensitivities are output for each load cell – one per weight used. The standard deviation of this is also output as a measure of the variance of the calculations.

The calculation for expected load cell sensitivity is shown below.

$$Expected\ Sensitivity = \frac{Full\ Scale\ Range}{Maximum\ Load} \quad (1)$$

Where

$$Full\ Scale\ Range = Rated\ Output * Excitation\ Voltage \quad (2)$$

The constant values for these load cells are:

Maximum load *= 40 lbs*
Rated output *= 4 mV/V*
Excitation Voltage *= 5 Vdc*

A plot is then generated to compare the calculated sensitivity for each weight application to that expected based on the load cell's datasheet.

As completed with the ***plotLoadCellData*** function, the user enters the name of a dataset so that the sensitivities and related statistics can be saved to an appropriately named .mat file. Statistics include:

- *Differences* – a measure of the difference between the application of weight and the baseline
  - This is the raw data, not averaged.
- *Voltage response* –the average voltages of the differences
- *Sensitivity* – voltage response / weight applied (in lbs)

The sensitivity is converted to mV, which is a more useful measure given the magnitude of the load cell responses.

7 Results

7.1 Load Cell Sensitivity

The sensitivity of each load cell report for the applied weight can be seen in the graphs below.

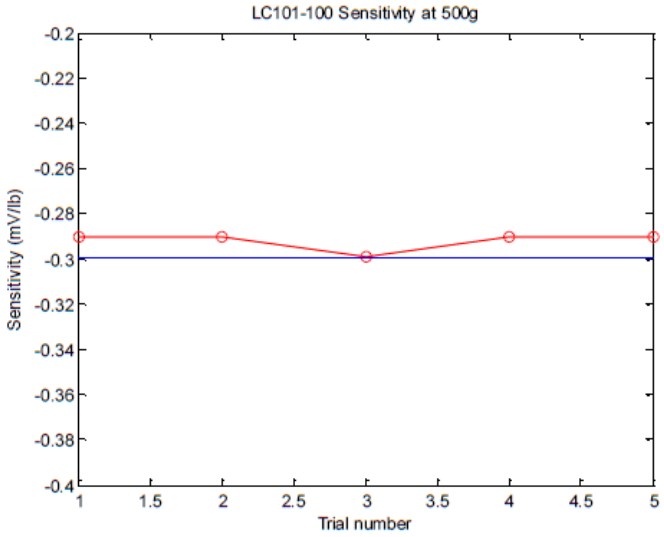

Figure 8: Load cell sensitivities for pulling action

As can be seen from the above the sensitivities of the load cells are clustered around approximately -0.3 mV/lb for the pushing action. These sensitivities are fairly similar across varying weight applications. Variability in this data is suspected to be a result of the manual method of testing.

7.2 Baseline repeatability

The standard deviation of all baseline values is shown below in Table 2.

Table 2: Baseline averages and standard deviation table.

Trial	Baseline (mV)
1	-0.21
2	-0.21
3	-0.21
4	-0.21
5	-0.21
AVERAGE	-0.21
STDEV	0.0044721

The standard deviation of the baselines is approximately 4.5 μV.

7.3 Weight application repeatability

The repeatability of weight application for both methods was found to be similarly consistent than that of the baselines. Table 3 below indicates the voltage acquired for each weight application and the standard deviation of the dataset.

Table 3: Load Cell 1 Weight Table

Trial	Voltage (mV)
1	-0.53
2	-0.53
3	-0.54

4	-0.54
5	-0.53
AVERAGE	**-0.534**
STDEV	**0.0054772**

Based on this result it has been concluded that the LC101-100 lb load cell provides equivalent sensitivity to the LCL-040 load cell. The LC101-100 lb load cell will therefore be used for both finger and grip trials.

ALL STAINLESS STEEL "S" BEAM LOAD CELLS

HIGH ACCURACY, ECONOMICAL PRICE

STANDARD AND METRIC MODELS

Tension/Compression
0-25 lb to 0-40,000 lb
0-10 kgf to 0-10,000 kgf

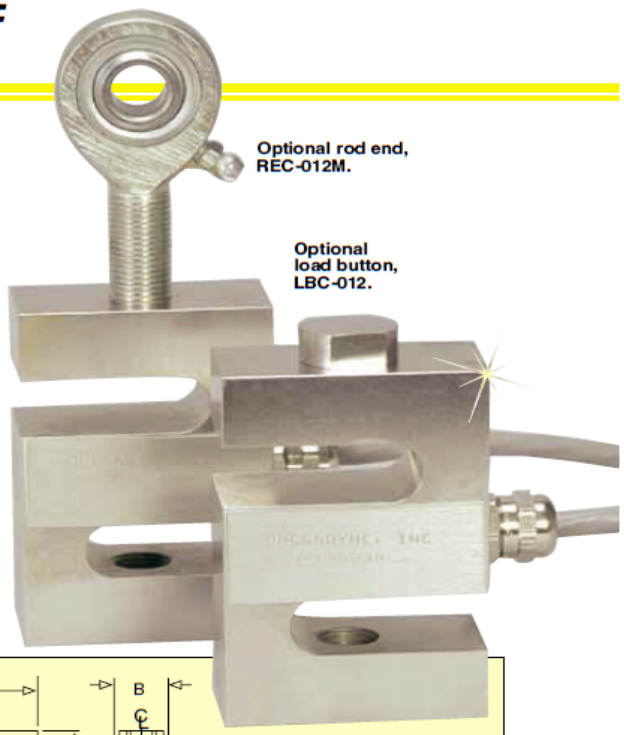

STANDARD
LC101-2K shown slightly smaller than actual size.

LC101/LCM101 Series
LC111/LCM111 Series

MADE IN USA NIST RoHS
Standard

- All Stainless Steel for Harsh Industrial Applications
- 0.25% Interchangeability for Multiple Load Cell Applications
- 5-Point Calibration Provided (in Tension)

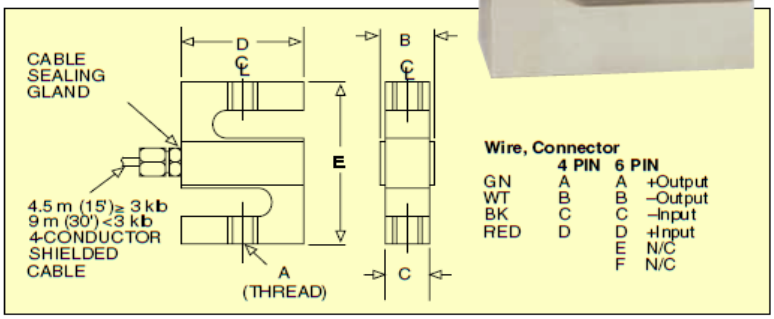

SPECIFICATIONS

Excitation: 10 Vdc, 15 Vdc maximum
Output: 3 mV/V ±0.0075 mV/V
Linearity: ±0.03% FSO (0.1% 40 K)
Hysteresis: ±0.02% FSO (0.1% 40 K)
Repeatability: ±0.01% FSO (0.05% 40 K)
Zero Balance: ±1% FSO
Operating Temp Range: -40 to 93°C (-40 to 200°F)
Compensated Temp Range: 17 to 71°C (60 to 160°F)
Thermal Effects:
Zero: 0.002% FSO/°C
Span: 0.002% FSO/°C
Safe Overload: 150% of capacity
Ultimate Overload: 300% of capacity
Input Resistance: 350 ±10 Ω
Output Resistance: 350 ±10 Ω
Full Scale Deflection: 0.010 to 0.020"
Construction: 17-4 PH stainless steel

Electrical (LC101/LCM101) (4-Conductor Shielded Cable):
<100 kgf/250 lb: 9 m (30') 24 AWG
250 to 1000 kgf/250 to 2000 lb: 9 m (30') 20 AWG
≥1500 kgf/3000 lb: 4.5 m (15') 20 AWG

Mating Connector (LC111/LCM111):
≤100 kgf/200 lb: PT06F8-4S, sold separately
≥250 kgf/250 lb: PT06F10-6S, sold separately

Dimensions: mm (inch)

CAPACITY	A	B	C	D	E	WEIGHT kg (lb)
lb						
25 to 200	¼-28	19 (0.75)	13 (0.50)	38 (1.5)	64 (2.5)	0.45 (1.0)
250 to 2.5K	½-20	32 (1.25)	25 (1.0)	51 (2.0)	76 (3.0)	1.1 (2.5)
3K to 5K	⅝-18	32 (1.25)	25 (1.0)	51 (2.5)	89 (3.5)	1.6 (3.5)
10K to 20K	1-14	44 (1.75)	38 (1.5)	76 (3.0)	108 (4.3)	2.0 (4.5)
25K to 30K	1-14	57 (2.25)	51 (2.0)	102 (4.0)	108 (4.3)	4 (9)
40K	1¼-12	83 (3.25)	76 (3.0)	102 (4.0)	140 (5.5)	6 (13)
kgf						
10 to 100	M6 x 1.00	19 (0.75)	13 (0.50)	38 (1.5)	64 (2.5)	0.45 (1.0)
250 to 1000	M12 x 1.75	32 (1.25)	25 (1.0)	51 (2.0)	76 (3.0)	1.1 (2.5)
1500 to 2000	M16 x 2.0	32 (1.25)	25 (1.0)	51 (2.5)	89 (3.5)	1.6 (3.5)
5K to 10K	M24 x 2.00	44 (1.75)	38 (1.5)	76 (3.0)	108 (4.3)	2.0 (4.5)

ALL STAINLESS STEEL "S" BEAM LOAD CELLS HIGH ACCURACY, ECONOMICAL PRICE

STANDARD AND METRIC MODELS

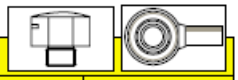

To Order *Visit omega.com/lc101 for Pricing and Details*

CAPACITY lb	CAPACITY kgf	MODEL CABLE	MODEL CONNECTOR	COMPATIBLE METERS*	LOAD BUTTON MODEL NO.	ROD END MODEL NO.
STANDARD MODELS						
25	—	LC101-25	LC111-25	DP41-S, DP25B-S	LBC-014	REC-014M
50	—	LC101-50	LC111-50	DP41-S, DP25B-S	LBC-014	REC-014M
100	—	LC101-100	LC111-100	DP41-S, DP25B-S	LBC-014	REC-014M
200	—	LC101-200	LC111-200	DP41-S, DP25B-S	LBC-014	REC-014M
250	—	LC101-250	LC111-250	DP41-S, DP25B-S	LBC-012	REC-012M
500	—	LC101-500	LC111-500	DP41-S, DP25B-S	LBC-012	REC-012M
1000	—	LC101-1K	LC111-1K	DP41-S, DP25B-S	LBC-012	REC-012M
2000	—	LC101-2K	LC111-2K	DP41-S, DP25B-S	LBC-012	REC-012M
3000	—	LC101-3K	LC111-3K	DP41-S, DP25B-S	LBC-058	REC-058M
5000	—	LC101-5K	LC111-5K	DP41-S, DP25B-S	LBC-058	REC-058M
10,000	—	LC101-10K	LC111-10K	DP41-S, DP25B-S	LBC-100	REC-100M
20,000	—	LC101-20K	LC111-20K	DP41-S, DP25B-S	LBC-100	REC-100M
25,000	—	LC101-25K	LC111-25K	DP41-S, DP25B-S	LBC-100	REC-100M-1
30,000	—	LC101-30K	LC111-30K	DP41-S, DP25B-S	LBC-100	REC-100M-1
40,000	—	LC101-40K	LC111-40K	DP41-S, DP25B-S	LBC-114	REC-114M
METRIC MODELS						
—	10	LCM101-10	LCM111-10	iSeries, DP41-S, DP25B-S	MLBC-M6	MREC-M6M
—	25	LCM101-25	LCM111-25	iSeries, DP41-S, DP25B-S	MLBC-M6	MREC-M6M
—	50	LCM101-50	LCM111-50	iSeries, DP41-S, DP25B-S	MLBC-M6	MREC-M6M
—	100	LCM101-100	LCM111-100	iSeries, DP41-S, DP25B-S	MLBC-M6	MREC-M6M
—	250	LCM101-250	LCM111-250	iSeries, DP41-S, DP25B-S	MLBC-M12	MREC-M12M
—	500	LCM101-500	LCM111-500	iSeries, DP41-S, DP25B-S	MLBC-M12	MREC-M12M
—	1000	LCM101-1K	LCM111-1K	iSeries, DP41-S, DP25B-S	MLBC-M12	MREC-M12M
—	1500	LCM101-1.5K	LCM111-1.5K	iSeries, DP41-S, DP25B-S	MLBC-M16	MREC-M16M
—	2000	LCM101-2K	LCM111-2K	iSeries, DP41-S, DP25B-S	MLBC-M16	MREC-M16M
—	5000	LCM101-5K	LCM111-5K	iSeries, DP41-S, DP25B-S	MLBC-M24	MREC-M24M
—	10,000	LCM101-10K	LCM111-10K	iSeries, DP41-S, DP25B-S	MLBC-M24	MREC-M24M

STANDARD LOAD BUTTONS

MODEL NO.	THREAD
LBC-014	¼-28
LBC-012	½-20
LBC-058	⅝-18
LBC-100	1-14
LBC-114	1¼-12

METRIC LOAD BUTTONS

MODEL NO.	THREAD
MLBC-M6	M6 x 1.0
MLBC-M12	M12 x 1.75
MLBC-M16	M16 x 2.0
MLBC-M24	M24 x 2.0

Load Button Dimensions

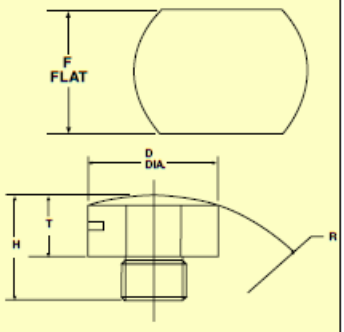

See omege.com for dimensions.

Rod End Dimensions

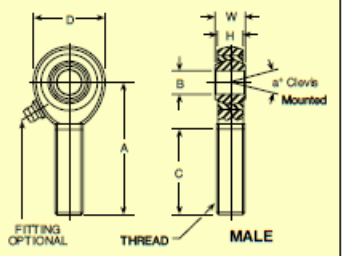

ACCESSORIES

MODEL NO.	DESCRIPTION
PT06F8-4S	Mating connector for LC111/LCM111 series load cells, 200 lb, <100 kg
PT06F10-6S	Mating connector for LC111/LCM111 series load cells, 250 lb, >250 kg
CA-4PC24-2A-015	LC111/LCM111 series load cells, 200 lb, < 100 kg, cable assembly with 4 pin connector
CA-4PC24-2-015	LC111/LCM111 series load cells, 250 lb, > 250 kg, cable assembly with 6 pin connector

Comes complete with 5-point NIST-traceable calibration and 59 kΩ shunt data.

** Visit **omega.com** for compatible meters.*
*To order connector style, change model number to **LC111**, no extra charge. Mating connector sold separately.*

***Ordering Examples: LC111-200,** 200 lb capacity connector-style load cell.*
***LCM111-100,** 100 kgf capacity connector-style load cell. **PT06F8-4S,** mating connector, **REC-014M,** matching rod end, **LBC-014,** matching load button.*
***LC101-5K,** 5000 lb capacity cable-style load cell. **REC-058M,** matching rod end.*

ROD ENDS

To Order *Visit omega.com/lc101 for Pricing and Details* — Dimensions: mm (inch)

MALE ROD ENDS	THREAD	B	W	H	A	D	C	a°	STATIC LOAD lb
REC-014M	¼-28 UNF	5 (0.190)	8 (0.312)	6 (0.250)	40 (1.562)	19 (0.750)	25 (1.000)	10	2158
REC-012M	½-20 UNF	11 (0.4375)	14 (0.562)	11 (0.437)	62 (2.438)	33 (1.312)	38 (1.500)	12	23,452
REC-058M	⅝-18 UNF	13 (0.5000)	16 (0.625)	13 (0.500)	67 (2.625)	38 (1.500)	41 (1.625)	10	31,390
REC-100M	1-14 UNF	25 (1.000)	35 (1.375)	25 (1.000)	105 (4.125)	70 (2.750)	545 (2.120)	14	43,541
REC-114M	1¼-12 UNF	32 (1.250)	28 (1.093)	24 (0.937)	105 (4.125)	70 (2.750)	54 (2.125)	7	44,500
MREC-M6M	M6 x 1.0	6 (0.236)	9 (0.354)	7 (0.275)	36 (1.417)	19 (0.748)	22 (0.866)	13	17,720
MREC-M12M	M12 x 1.75	12 (0.472)	16 (0.630)	12 (0.472)	54 (2.126)	30 (1.181)	33 (1.300)	17	44,490
MREC-M16M	M16 x 2.0	16 (0.630)	21 (0.826)	14.25 (0.561)	66 (2.598)	38 (1.496)	40 (1.575)	23	76,291
MREC-M24M	M24 x 2.0	25 (0.984)	31 (1.220)	22 (0.866)	95 (3.740)	60 (2.362)	57 (2.244)	19	251,780

A-2.3 Bridge Amplifier

WPI

Calibrating DMD-465WB Bridgesensor

AC Powered Signal Conditioner

Keating & Bardizbanian

11/30/2013

1 TABLE OF CONTENTS

2 DESCRIPTION OF THE DEVICE

DMD-465WB is bridgesensor that is used to amplify the signal generated by the load cell. It consists of 13 terminals and 5 tuning ports. Figure 1 shows simplified block diagram of the unit.

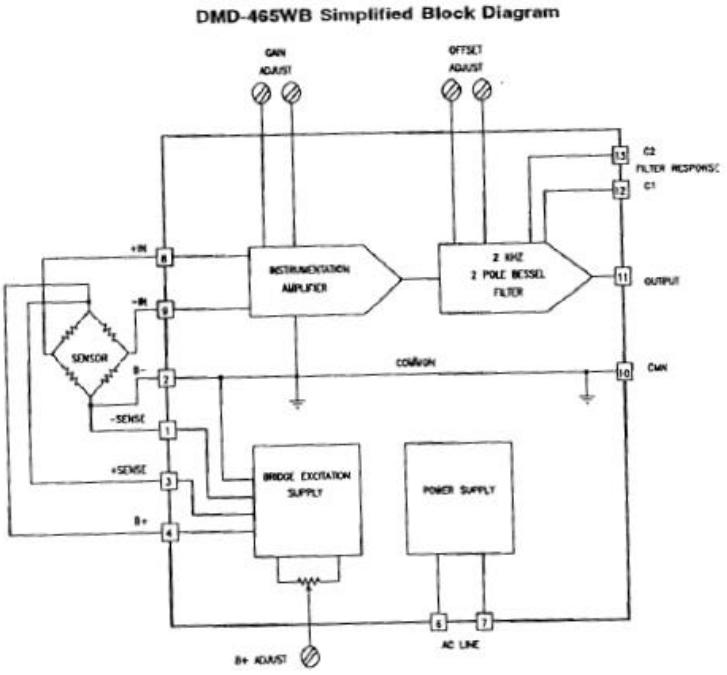

Figure 1: Block diagram of the DMD-465WB bridge sensor.

The top view of the unit with the location of all terminals and ports is shown on the next page.

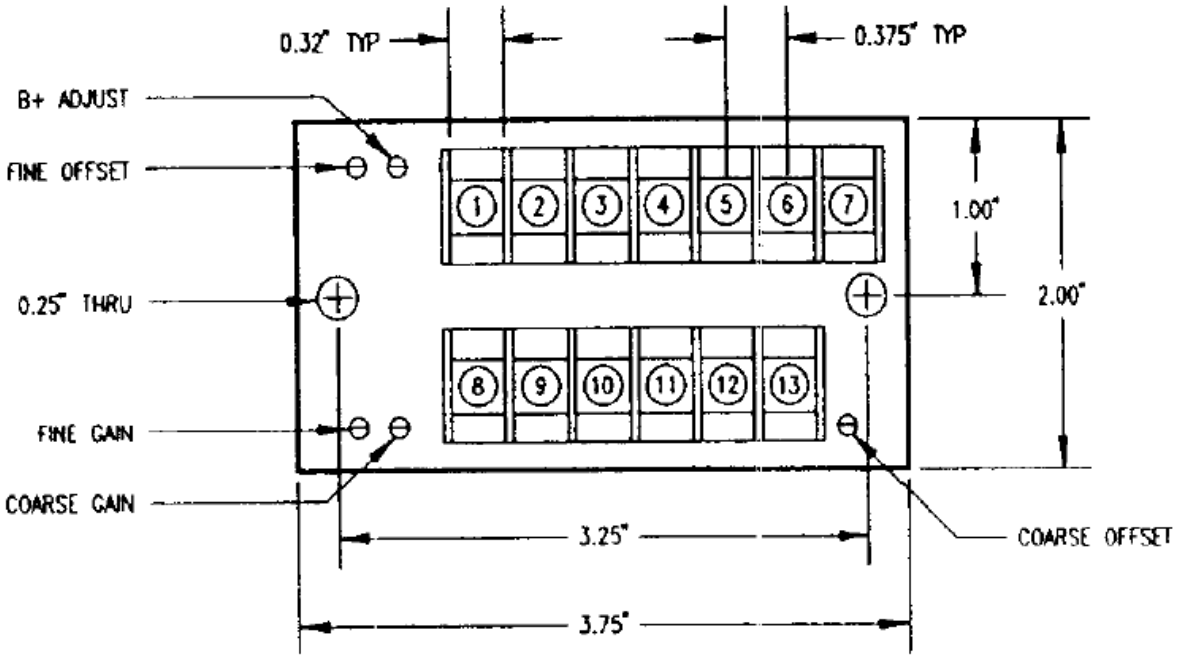

Terminal Strip Assignments			
Screw Terminal	Function	Screw Terminal	Function
1	-SENSE	8	+INPUT
2	B-	9	-INPUT
3	+SENSE	10	AMPLIFIER CMN
4	B+	11	AMPLIFIER OUTPUT
5	NOT USED	12	FILTER - C1
6	AC	13	FILTER - C2
7	AC		

Figure 2: Top view of bridge amplifier/signal conditioner with terminal strip assignment table.

3 CALIBRATION STEPS

Calibration of the DMD-465WB must be conducted before any trial. This includes adjusting the offsets and verifying the gains. Before initial calibration, the full scale of the load cell in use must be verified in Vdc and Vac. In our test, the load cell is the LC101-100 with a full scale range of 30mVdc.

Sections **Error! Reference source not found.** **Error! Reference source not found.** and 3.2 Calibration Procedure for Zero Adjustment detail how to calibrate the offset and gain of the DMD-465WB.

3.1 REQUIRED HARDWARE CONNECTIONS

To connect the LC101-100 to the DMD-465WB all connections should be as follows:

1. Connect the **+out** of LC101-100 to **+INPUT** of DMD-465WB.
2. Connect the **-out** of LC101-100 to **-INPUT** of DMD-465WB.

Table 1: LC101-100 and Omega DMD-465WB Configuration

LC101-100 Output Line	Color	Omega DMD-465WB Input
+Input (excitation)	Red	4 (B+), a small wire bridges 3&4
- Input (excitation)	Black	2 (B-), a small wire bridges 1&2
+Output	Green	8 (+input)
-Output	White	9 (-input)

Shown below are the Omega DMD-465WB pin diagram and an overhead view of the LC101-100 load cell connected to the DMD-465WB. In the overhead view inputs to the DMD-465WB are outlined in orange while its outputs are outlined in green.

Figure 3: Omega DMD-465WB diagram.

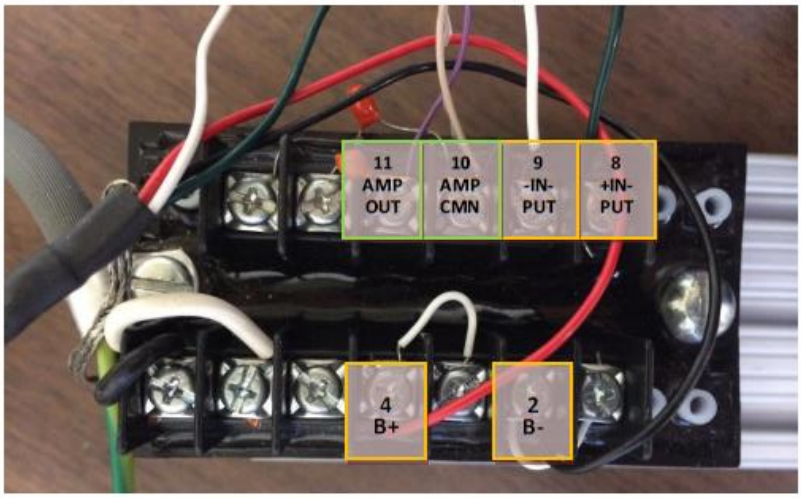

Figure 4: Overhead view of the LC101-100 load cell connected to the DMD-465WB

Note that the above figure also includes the setup of the DMD-465WB as well as the output of the DMD-465WB to the NI-PCI 6229, the connections for which are described below.

3.2 CALIBRATION PROCEDURE FOR ZERO ADJUSTMENT

1. Connect the VAC power supply.
2. Turn on the power supply and set the **EXCITATION** to +5V which is the required excitation of LC101-100
3. Adjust the power using **B+**.
1. Connect the **+INPUT** and **–INPUT** terminals with a temporary jumper.
2. Connect a voltmeter across the output pins 11 **(AMPLIFIER OUTPUT)** and 10 **(AMPLIFIER CMN)**
3. Adjust the **Coarse Offset** and the **Fine Offset** ports until the voltmeter shows zero or close to .001

3.3 FULL SCALE VOLTAGE ADJUSTMENT

1. Remove the jumper between **+INPUT** and **–INPUT** terminals and apply known load to LC101-100
    - Known load would ideally be full scale (30 mV)
    - This can also be accomplished by applying Vdc equal to full scale from calibration certs to the INPUT terminals
2. Adjust the **Coarse gain** and **Fine gain** knobs until you reach the desired voltage output.
    - The desired output is the maximum gain possible
    - The output of DMD-465WB cannot exceed 15 Volts (this will result in signal clipping)
    - For the purposes of our testing the output voltage achieved was 6.44 V (so gain = 195).

A-2.4 NI PCI 6229 DAQ Channels

PCI 6229 Validation

To determine whether the PCI-6229 was suitable for use in future experiments the following validation was performed:

- A function generator was used to input a 1 Hz sin wave into each channel
- The output of the channel was measured using a VI in LabVIEW 2009 made by Sabah Razavi
    - The VI is called *data_get.vi* and can be found at *C:\Jen_Berj\DAQ_Validation* on the lab computer in AK220
- The output signal for each channel was characterized according to the frequency and amplitude of the output signal, noise characteristics, and any other issues that are noticed by the tester.
- *ALL DATA WAS SAVED TO THE LAB COMPUTER IN AK220, at: C:\Jen_berj\DAQ_Validation* with the format *ChannelName_Frequency_Amplitude.csv*, e.g. *AI13_10hz_5V.csv.*

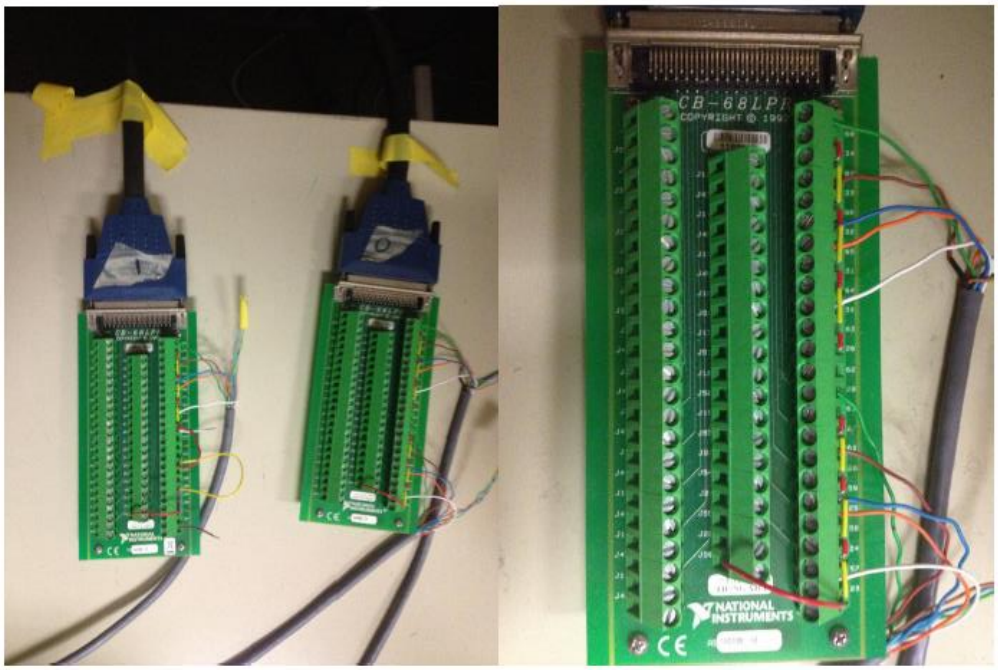

Figure 1:The NI 6B-68LPR, a screw terminal accessory for use with the NI PCI-6229, which is installed in the lab computer.

Detailed Procedure

- Ensure that nothing is connected to the NI 6229.
- Open the *data_get.vi* found at *C:\Jen_Berj\DAQ_Validation*, the following *Front Panel* will open up.

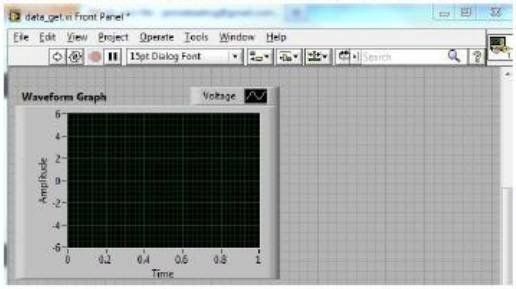

- Open the *block diagram*, the following window will open
  - Click the tab "*Window*" → Click "*Show block diagram*"

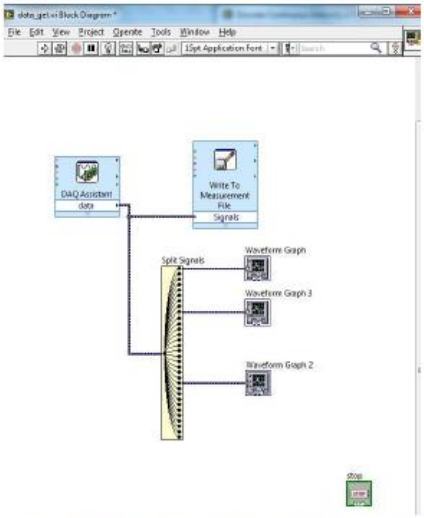

- Double click the "*DAQ Assistant*" block, the following window will open

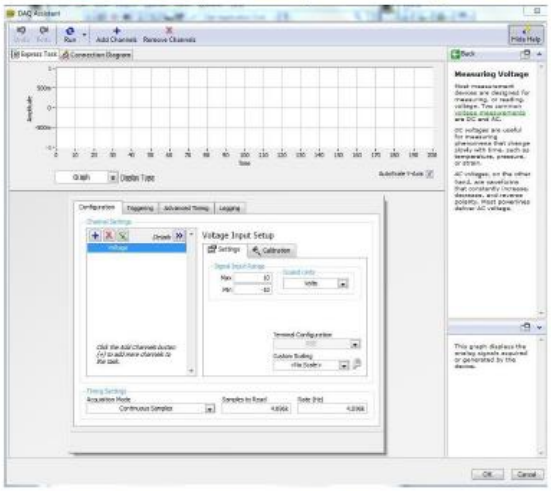

- Under the *Channel Settings* portion of the *Configuration* window, click the **+** symbol to see a dropdown of properties that can be measured.

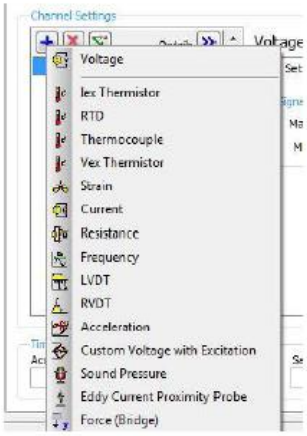

- Click the *Voltage* portion of the list
  - A window will pop up with the channels available for reading. Select the channels you wish to plot.

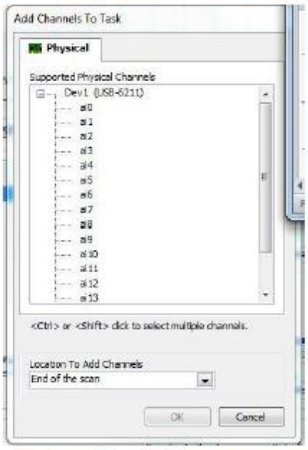

  - Here is what it will look like once you select voltage channels

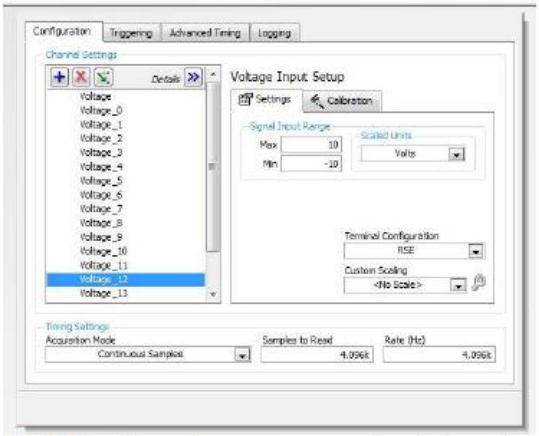

NOTE: For this testing we want to select 1 channel at a time because you will input a signal to only 1 channel at a time.

- Hit *'Run'* from the top options on the DAQ assistant. You should see the sin wave show up in the plot now.

- Let the program run for ~10s. The program will automatically stop.
- A prompt to save the data will come up.
    - Change the file type to "All files" (from .lvm)
- Save the data with the following naming scheme:
    - *ChannelName_Frequency_Amplitude* e.g. *AI13_10hz_5V*
- The data will automatically save in *C:\Jen_Berj\DAQ_Validation*
    - Check that the data file saved with the correct name in the correct location.
- Move the function generator to the next channel for testing.
- Select the next channel for testing in LabVIEW
    - Change the *physical channel* by clicking the green arrow button; a window will appear.

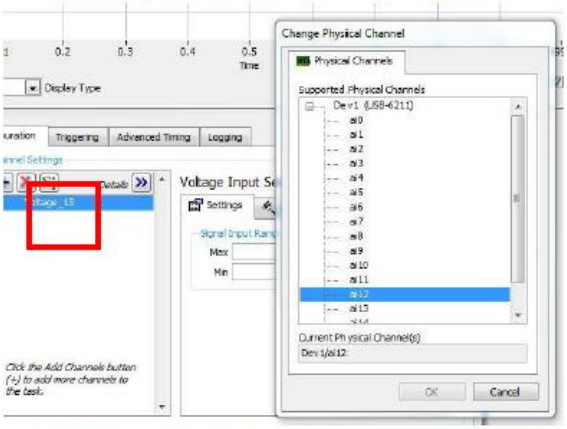

- Collect the data for this channel by following the instructions in *Section 1.1 Data Collection.*
- *Repeat for all channels*

Results

A summary of the testing of each channel of the DAQ is below. The function generator was set to output a 4V 1Hz sin wave for this testing. Testing was conducted with AI GND respective to each tested channel. In cases where multiple graphs appear per channel, repeat testing was required to obtain a clean signal. All channels eventually exhibited a clean signal. The raw data collected from all channels is displayed below, including failed trials. In the cases where the initial test run failed, issues were noted, and subsequent passing test results are shown.

AI0

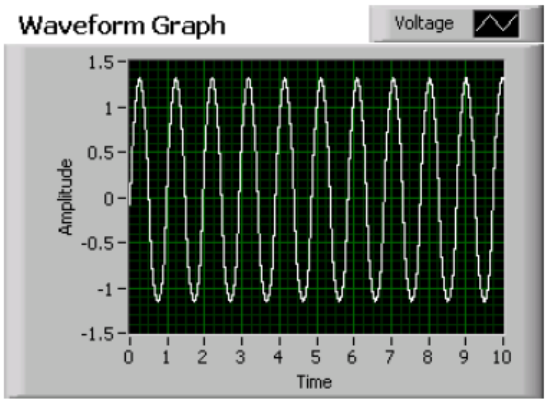

AI3 (64 & 30)

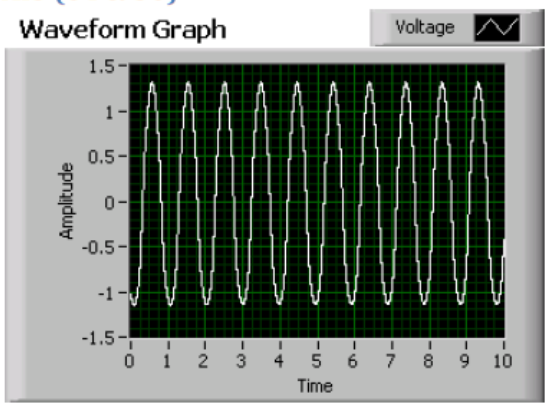

AI1 (67 & 33)

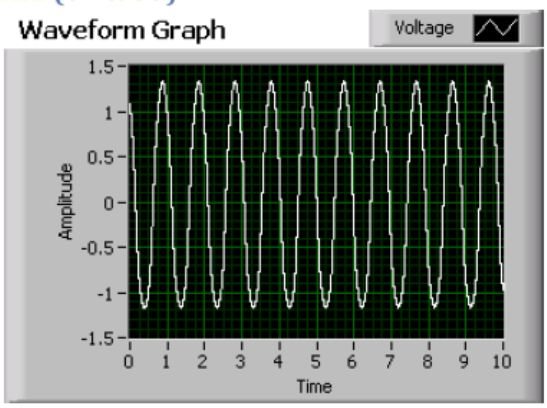

AI4 (28 & 29)

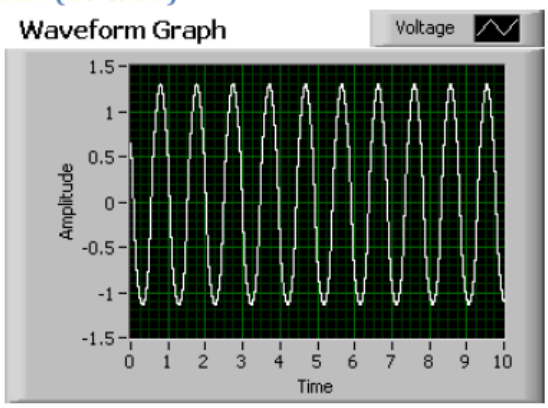

AI2 (64 & 32)

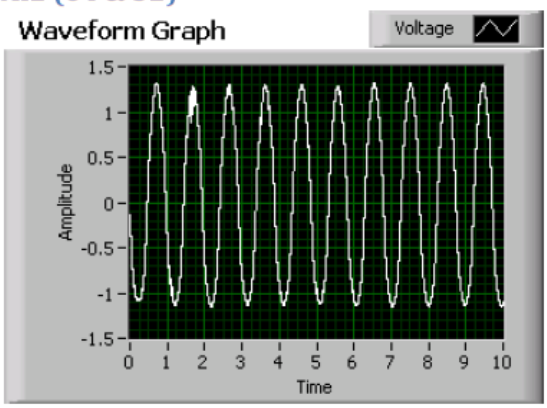

AI5 (60 & 27)

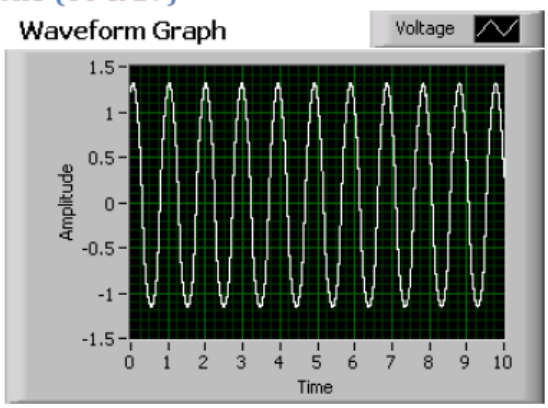

AI6 (25 & 59)

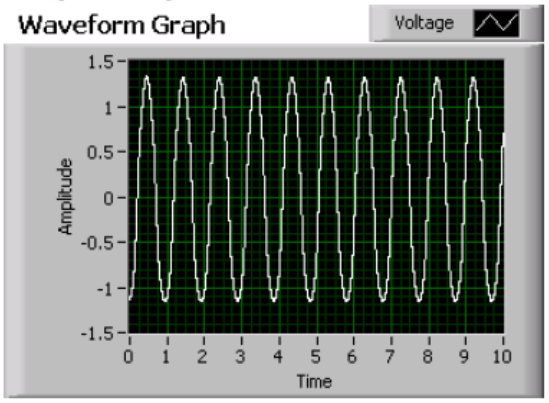

AI7 (24 & 57)

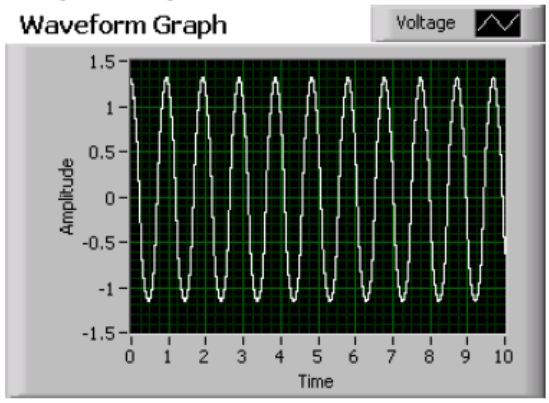

AI8 (34 & 67)

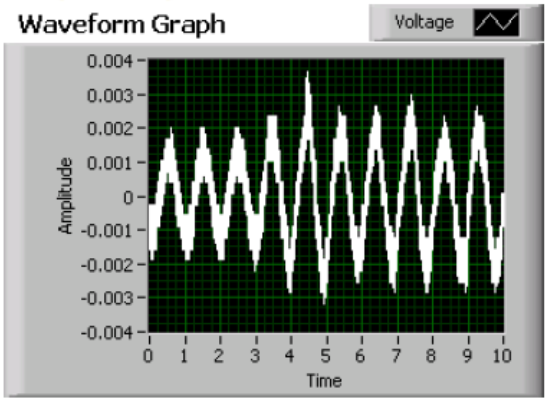

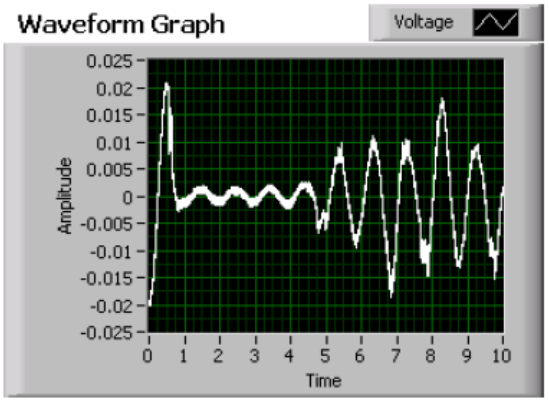

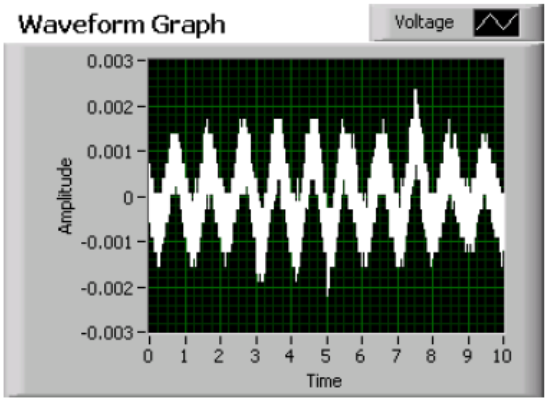

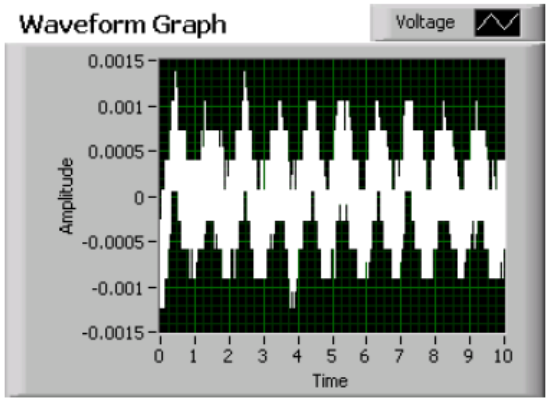

Initial testing showed there were shorts between channels 8 and 10. The results after this short was removed can be seen below

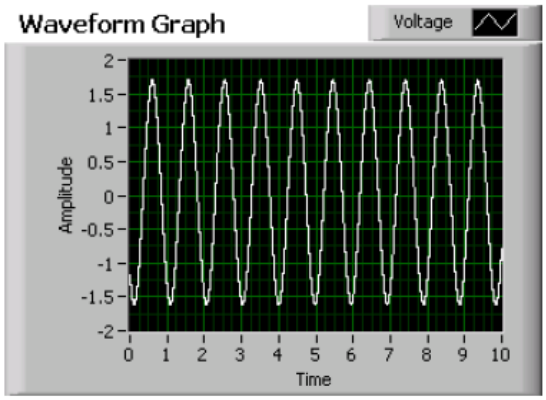

AI9 (32 & 66)

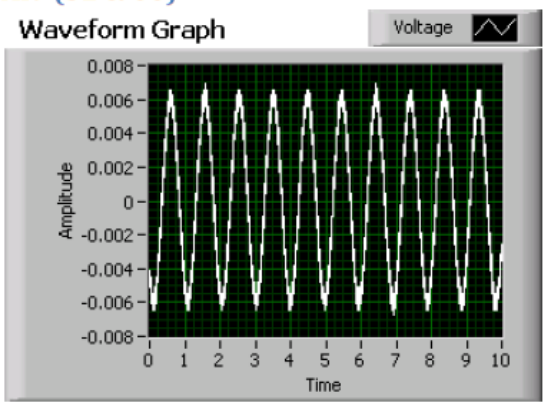

AI10 (31 & 64)

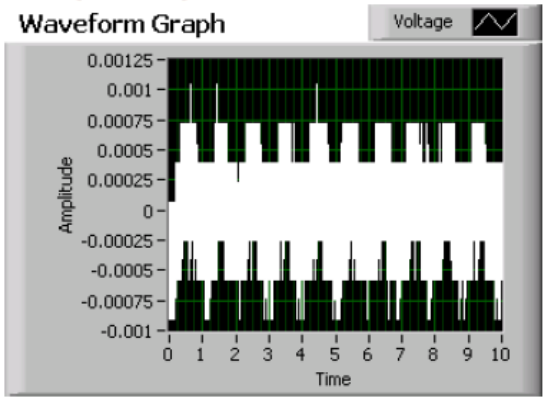

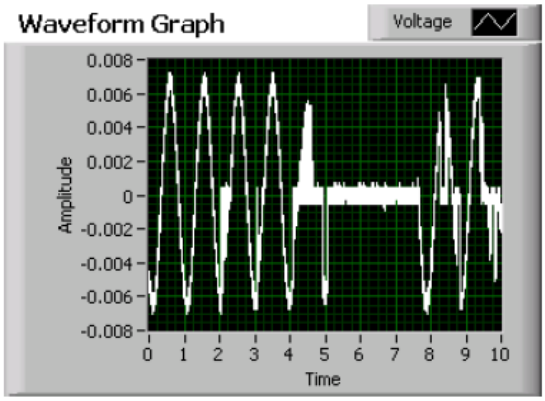

Based on these results, an attempt was made to use a different method of contact (direct rather than alligator clips). These results can be seen below.

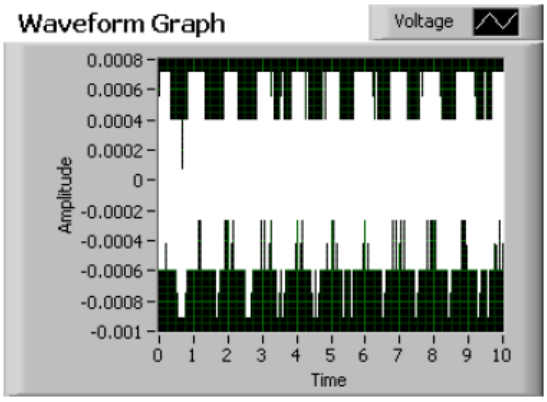

The results were not improved by the deviation in function generator connection method. At this time, the testers identified a short between channels 8 and 10. The improved results can be seen below.

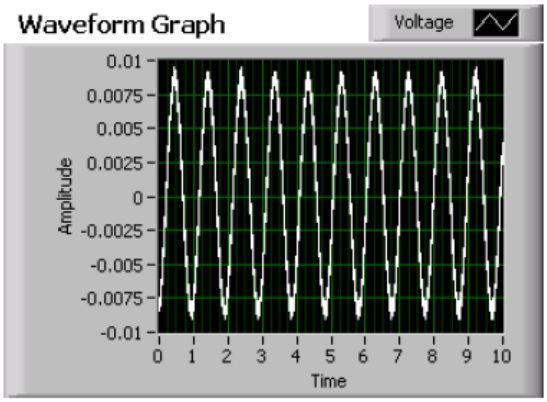

AI11 (63 & 29)

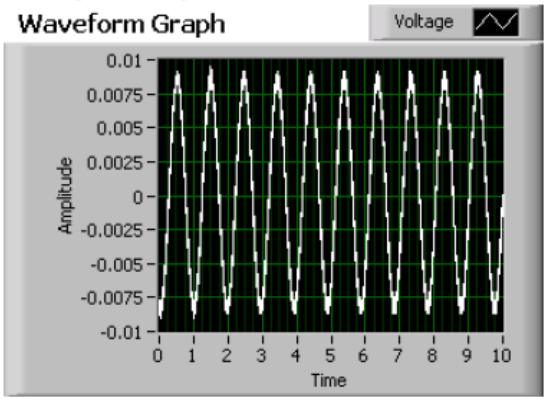

AI12 (27&61)

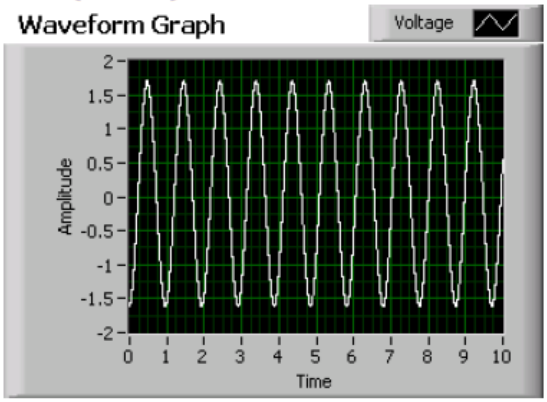

AI13 (26 & 59)

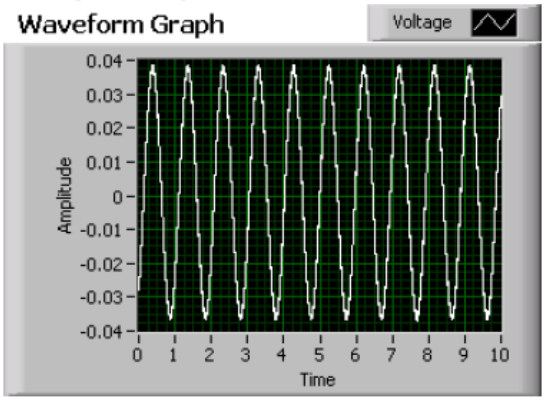

AI16 (67&68)

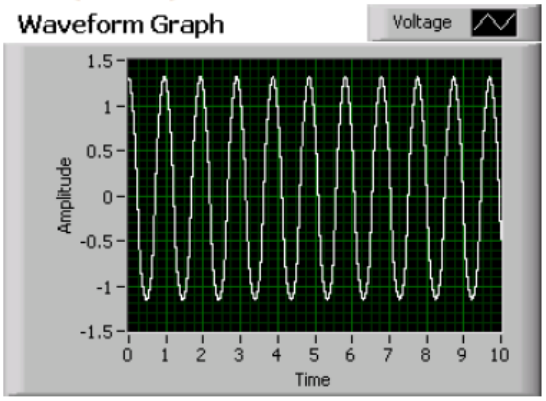

AI14 (24 & 58)

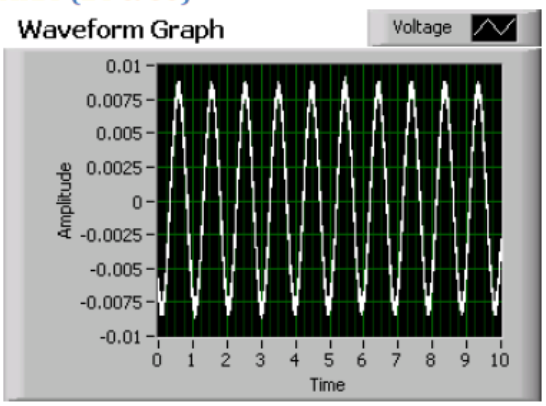

AI17 (67&33)

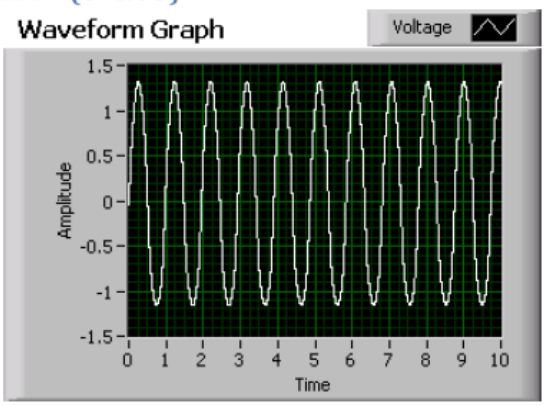

AI15 (23&56)

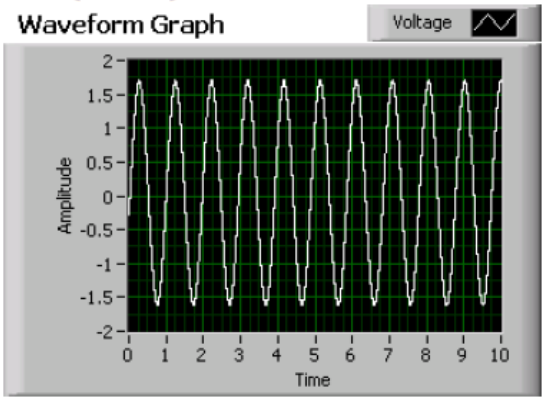

AI18 (32 & 65)

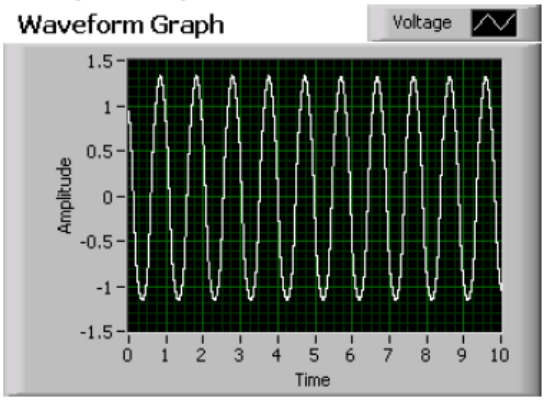

AI19 (64&30)

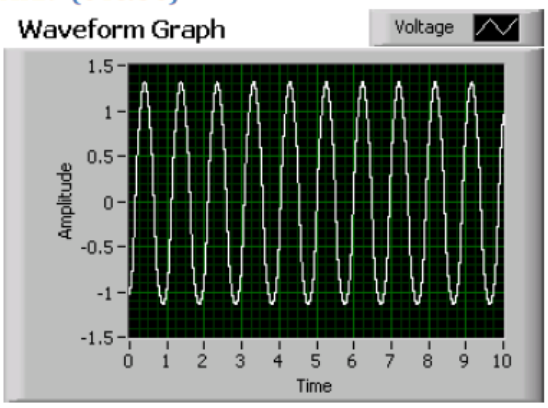

AI21 (27&60)

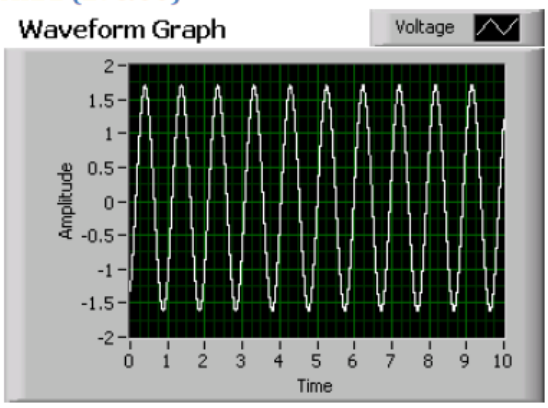

AI20 (29 & 28)

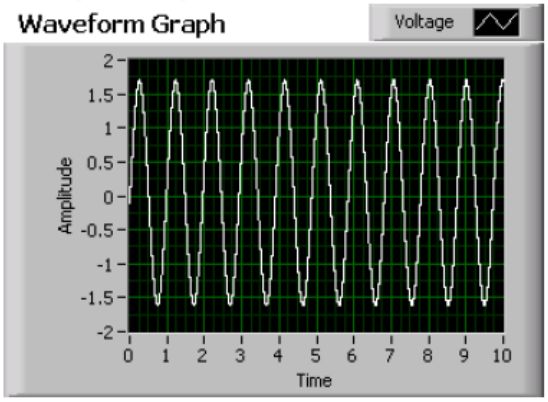

AI22 (59 & 25)

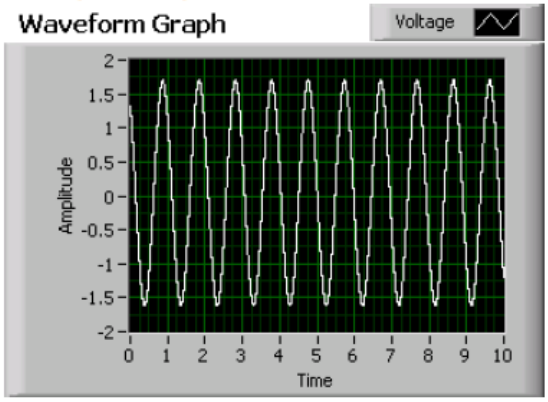

AI23 (24&57)

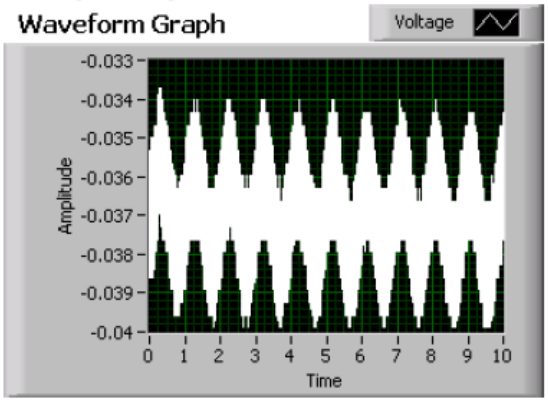

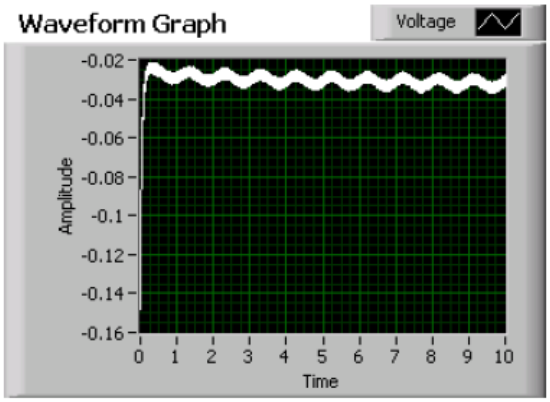

Testers hypothesized connection to the function generator error and attempted a root cause investigation by changing the connection method and using thin wires. The noisier results are shown below.

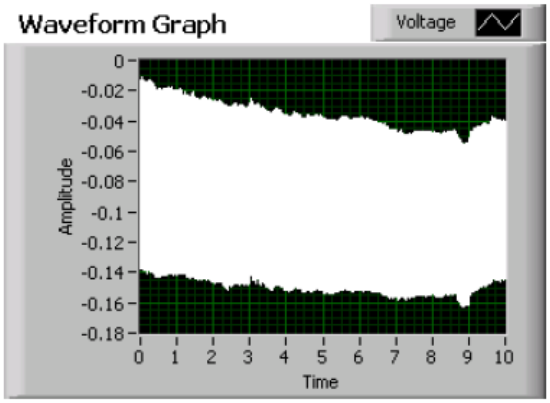

Additional root cause investigation at a later date corrected the error and demonstrated AI Channel 23 passed validation.

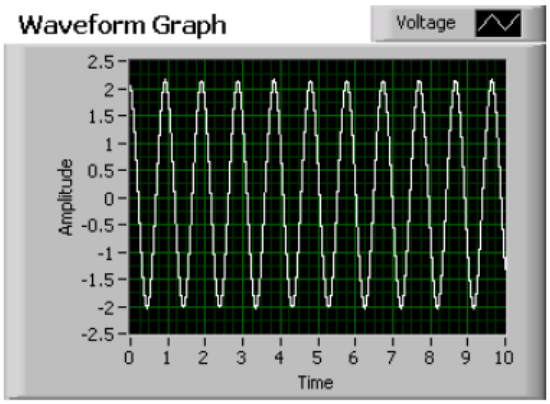

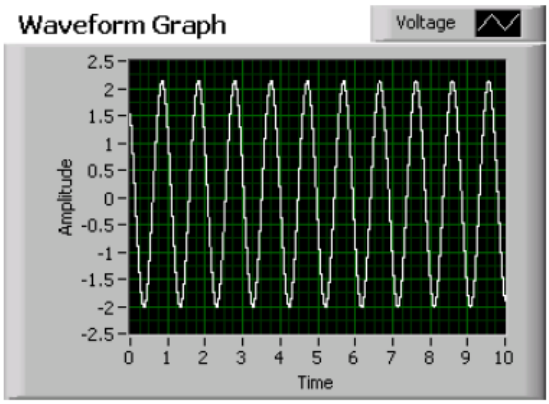

AI24 (67&34)

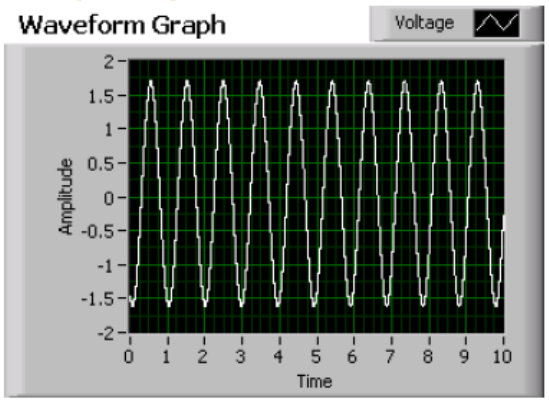

AI25(32&66)

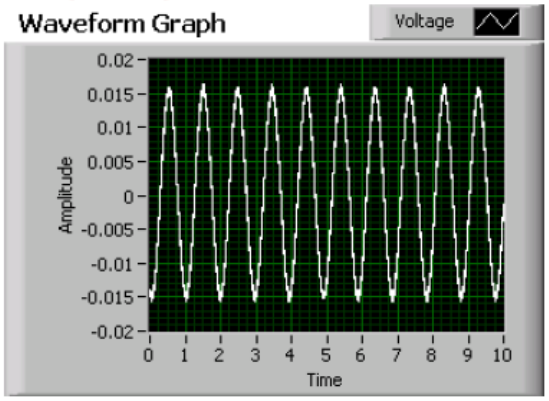

AI26(64&31)

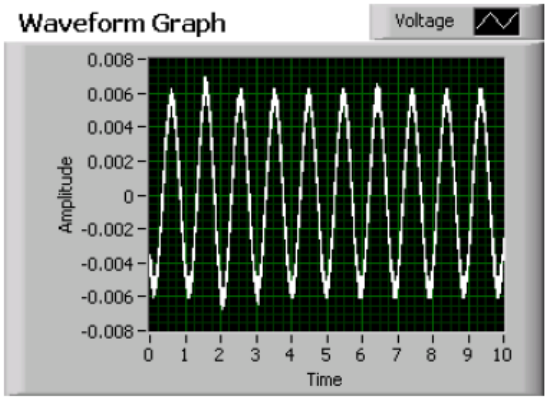

AI27(29&63)

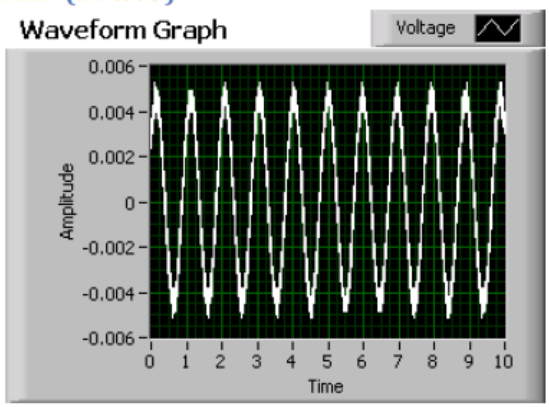

AI28(27&61)

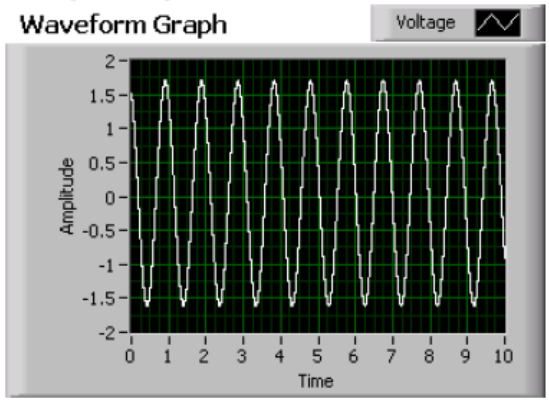

AI29(59&26)

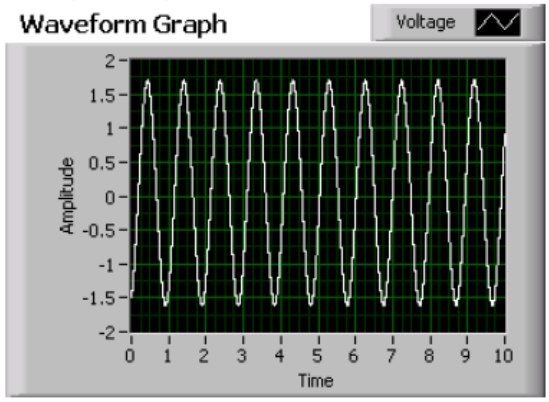

AI30(24&58)

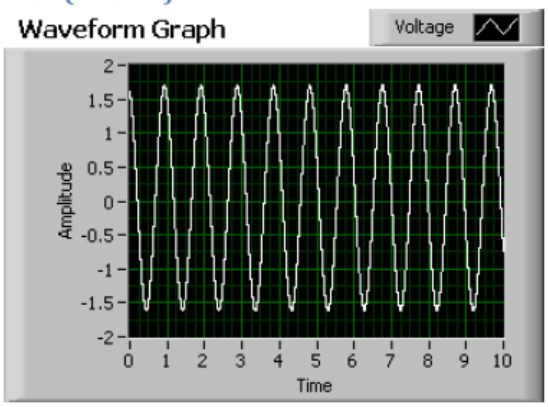

AI31(56&23)

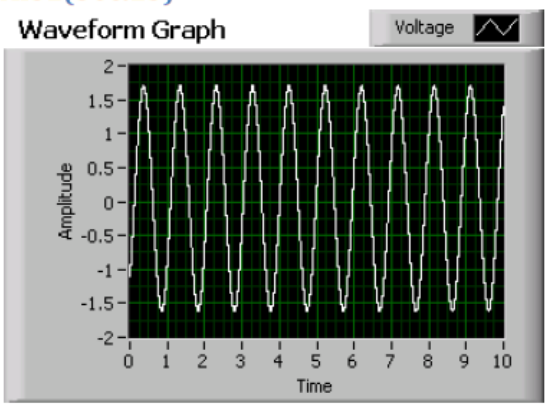

Appendix 3 Design Documentation

A-3.1 Slowly Varying Force VI

WPI – L(SP)^2

Slowly Force Varying EMG for Finger & Grips LabVIEW VI

Design & Troubleshooting Document

Jennifer Keating

4/29/2014

1 TABLE OF CONTENTS

TABLE OF FIGURES

TABLE OF TABLES

1 SLOWLY FORCE VARYING CONTRACTIONS VI - SUMMARY

The LabVIEW interface needed to complete Slowly Force Varying contraction testing can be found under the following path:

C:\Jen_Berj\Finger Labview Data Collection

And is called:

Slowly_Force_Varying.vi

This LabVIEW VI

- Provides a user interface in which
  - A blue line, dubbed the 'target', moves back and forth across a black screen at a tester defined rate.
  - A red line represents the force output by the subject on the load cell.
    - The subject tracks the blue target with their red line by flexing and extending against the load cell.
  - Accepts selection of the finger/grip in use.
    - This is a slider that simply selects which finger/grip the subject is going to use for the current trial in order to take their maximum flexion/extension values into account during the trial.
- Accepts "calibration" values for each finger/grip
  - Each subject will have a different maximum force that they can exert for flexion and extension with each finger and grip being tested during clinical trials. Calibration testing is conducted to identify these voltage values.
  - These voltage values are entered into the VI to adjust the VI screen limits for each subject.
- Records force and EMG data while the subject tracks the target.
- Allows the test administrator to turn off the target indicator.
- Displays the real-time load cell voltage, as read by the NI-PCI 6229.

A screenshot of the user interface (Front Panel) is shown below.

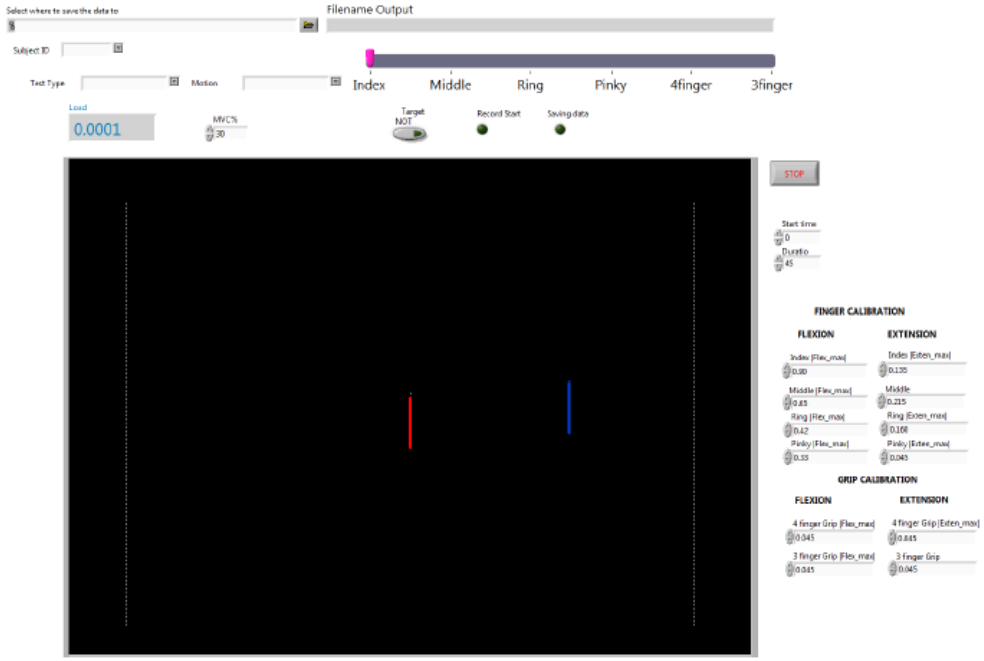

Figure 1: VI Front Panel view

This LabVIEW VI saves discrete voltage data from the LC101-100 load cell and 12 electrodes in LVM format.

The name of this VI is somewhat of a misnomer as it is also used to conduct Constant Force and Rest contractions.

1.1 REQUIRED HARDWARE CONNECTIONS

This LabVIEW program reads the analog signal of the LC101-100 load cell and the EMG electrodes using the NI-PCI 6229 via the DAQ assistant tool, which converts all of the signals from analog to digital domain.

To connect the LC101-100 to the NI-PCI 6229 DAQ, the output of the load cell must be connected to the Omega DMD-465WB AC powered bridge sensor. The output of the DMD-465WB must then be connected to the NI-PCI 6229. All connections should be as follows:

Table 1: LC101-100 and Omega DMD-465WB Configuration

LC101-100 Output Line	Color	Omega DMD-465WB Input
+Input (excitation)	Red	4 (B+), a small wire bridges 3&4
- Input (excitation)	Black	2 (B-), a small wire bridges 1&2
+Output	Green	9 (-input)*
-Output	White	8 (+input)*

***Note this was changed in order to make flexion move the cursor to the right and extension move it to the left, as mentioned by Professor Clancy. Correct orientation should be Green to 8, White to 9.**

Shown below are the Omega DMD-465WB pin diagram and an overhead view of the LC101-100 load cell connected to the DMD-465WB. In the overhead view inputs to the DMD-465WB are outlined in orange while its outputs are outlined in green.

Figure 2: Omega DMD-465WB diagram.

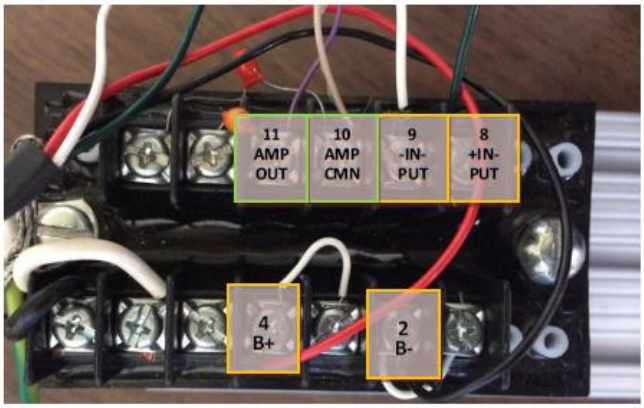

Figure 3: Overhead view of the LC101-100 load cell connected to the DMD-465WB

The above figure also includes the setup of the DMD-465WB, as well as the output of the DMD-465WB to the NI-PCI 6229, the connections for which are described below.

Table 2: Omega DMD-465WB and NI-PCI 6229 configuration

Omega DMD-465WB Output	Color	NI-PCI 6229 Input Channel(s)
11 (AMPL OUTPUT)	Purple	J68
10 (AMPL CMN)	Beige	J67

Shown below in Figures 3 and 4 are the DMD-465WB output connections and the NI-PCI 6229 input connections.

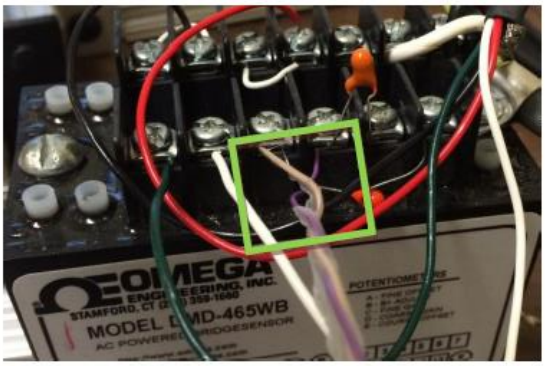

Figure 4: Side view of DMD-465WB with all connections. The amplifier output and common connections are located centrally in beige and purple.

Figure 5: AMPL CMN and AMPL OUTPUT connected to J68 and J67 respectively. The green wire connected is unrelated to the load cell output.

Note: Each of the channels on the NI-PCI 6229 DAQ is labeled as shown in Table 2 above – with a J followed by a number. These channel labels are all associated with various analog inputs and outputs. When adding a voltage source to a VI, these channels are referred to as their function (e.g. AI30). The image below, taken from NI documentation, shows the appropriate labeling.

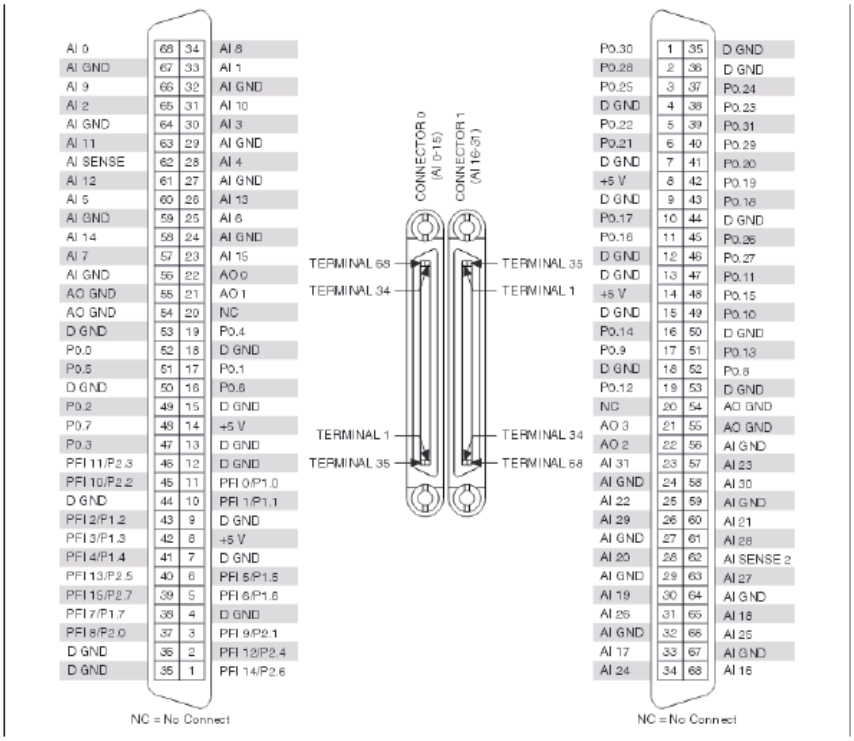

Figure 6: PCI/PXI-6229 Pinout provided by National Instruments.

2 SLOWLY FORCE VARYING RAMP CONTRACTIONS VI – DETAILED DESIGN

This LabVIEW VI (*Slowly_Force_Varying.vi*) is designed so that the test administrator can enter calibration values for finger and grip flexion and extension. The test administrator can then select the finger or grip that the subject will use to complete a contraction trial. This selection associates the calibration value for that finger or grip with the trial, resulting in an adjustment to the required force output on the load cell for the subject to move the tracker to the left most and right most vertical dotted lines. The amount of effort required to reach these lines is determined by the % MVC entered by the test administrator for testing[1]. The test administrator additionally has the option to make the blue target invisible and still record EMG and load cell data from the subject's actions.

The subject interacts with this VI differently than the test administrator. During a clinical session the subject has 12 electrodes mounted on their arm and is connected to the load cell setup. The subject pulls or pushes on the load cell in order to demonstrate muscle contraction during flexion or extension activities. A red indicator line represents the load cell output, and the subject uses this indicator to try and track the target (the blue line) during contractions.

The real-time load cell voltage is shown in the upper left – above the subject's interaction zone.

Shown below is a screenshot of the Front Panel of the VI.

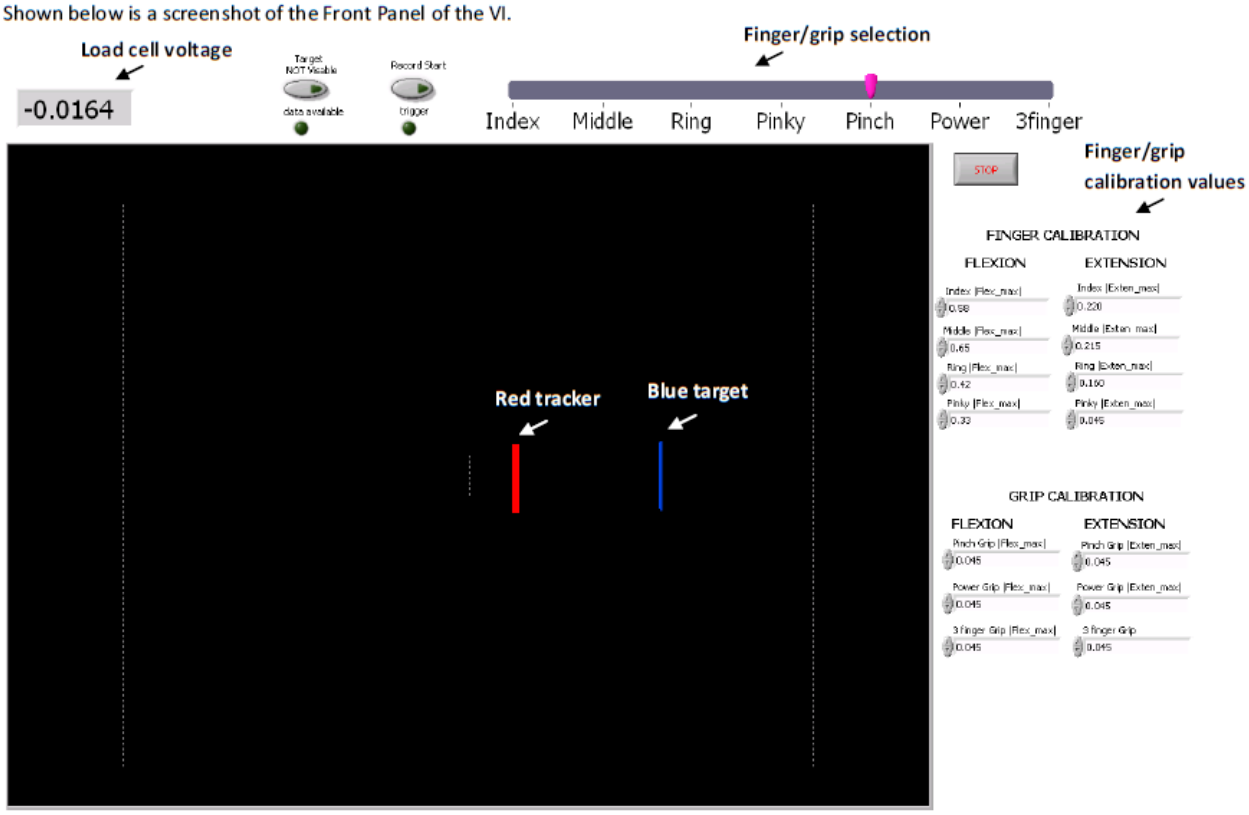

Figure 7: Front panel of the Slowly_Force-Varying.vi

The block diagram for this VI can be seen on the following page. Individual sections of the block diagram will be discussed in detail in the following sections.

[1] For most finger testing, this percentage is set to 30% MVC.

2.1 BLOCK DIAGRAM

The Block Diagram of the VI can be accessed via **Window → Show Block Diagram (or CTRL+E)**. The following sections detail the functionality of this VI.

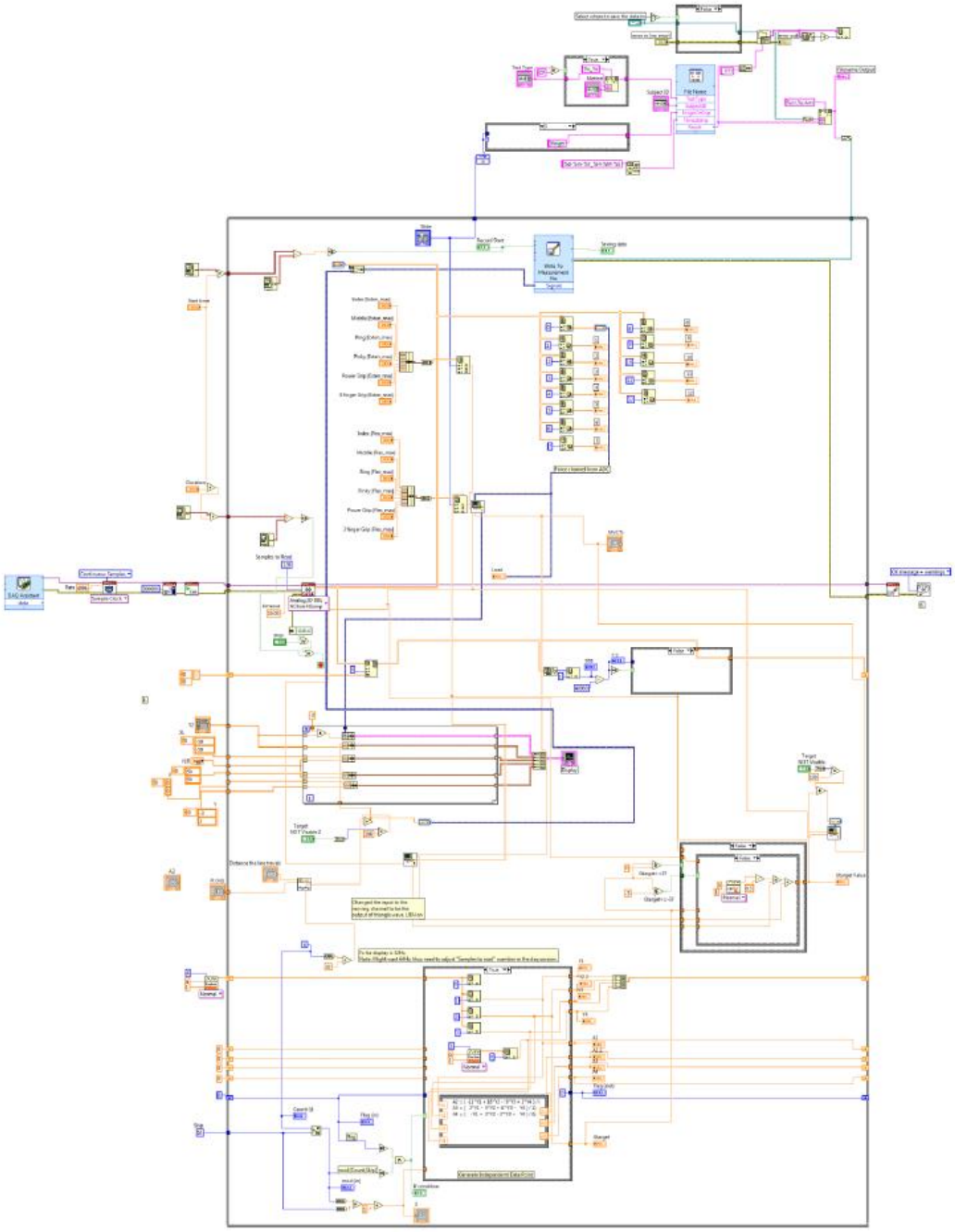

Figure 8: Full block diagram of slowly_force_varying.vi

2.2 DATA ACQUISITION & RECORDING

This section describes how the signals are acquired and the path they take through the VI, the general path for which is shown below.

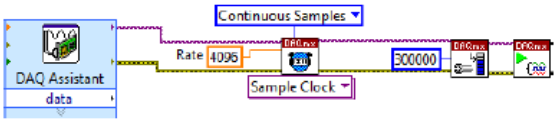

Figure 9: Data acquisition stage.

First, a DAQ assistant block is used to acquire the signals from the NI PCI-6229.

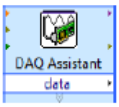

Figure 10: DAQ Assistant icon

The DAQ assistant is setup with the following parameters.

- Signal input range from -5 to 5 volts.
- Terminal configuration of RSE
- No scaling
- Acquisition mode of 1 sample (on demand)

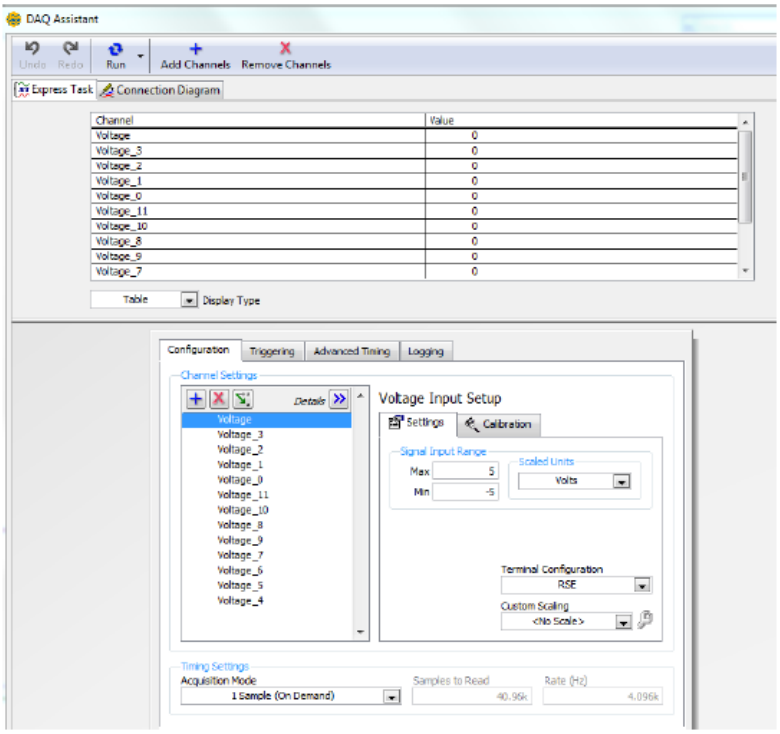

Figure 11: Detailed view of the DAQ assistant settings within the VI.

The details of each channel including order referenced by LabVIEW, the physical channel, and device type can be seen by clicking the double blue arrow.

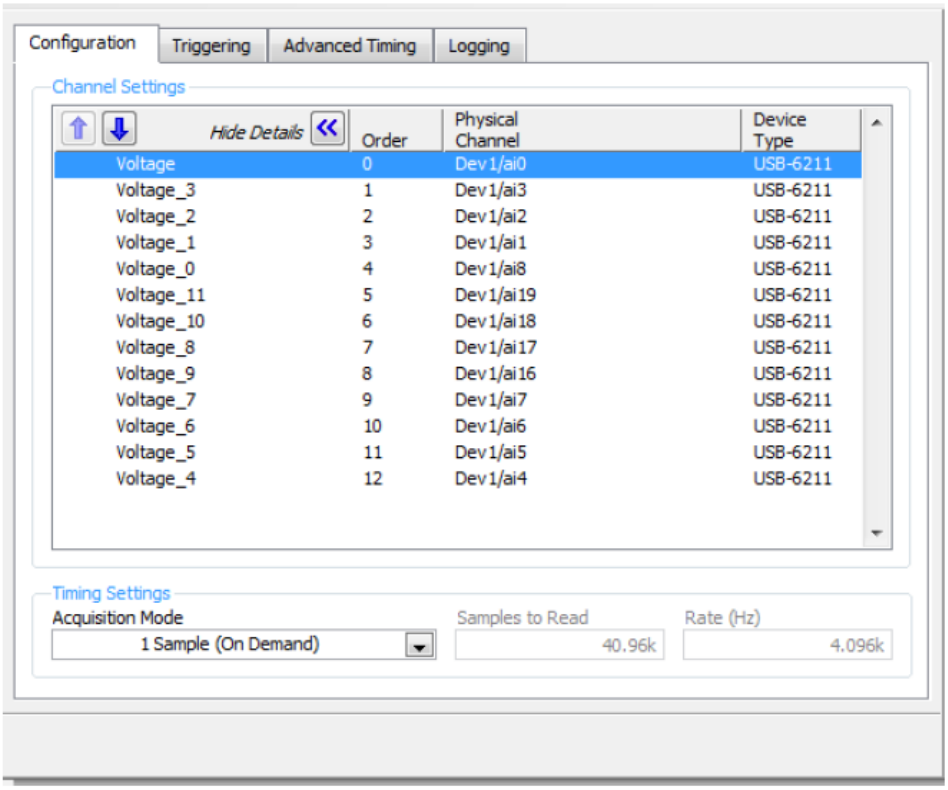

Figure 12: Expanded channel information view. Note that the order of the electrodes is listed 0-12 per the configuration in the lab in AK220. However, these voltage values are NOT sequential (e.g.3, 2, 1, 0, 11, 10, etc). This is due to the manner in which the electrodes are connected to the NI PCI-6229. Play close attention to this detail! (NOTE: The device type listed here is the USB-6211 because this document was written while connected to another NI DAQ. The correct device is the NI PCI-6229).

WARNING: When looking at the channel information, you will see that the order of the electrodes is listed 0-12 per the configuration in the lab in AK220. However, these voltage values are NOT sequential (e.g.3, 2, 1, 0, 11, 10, etc). This is due to the manner in which the electrodes are connected to the NI PCI-6229. Play close attention to this detail!

The connection of each voltage source can be checked by viewing the connection diagram. The diagram for Voltage_0 (the load cell) can be seen below.

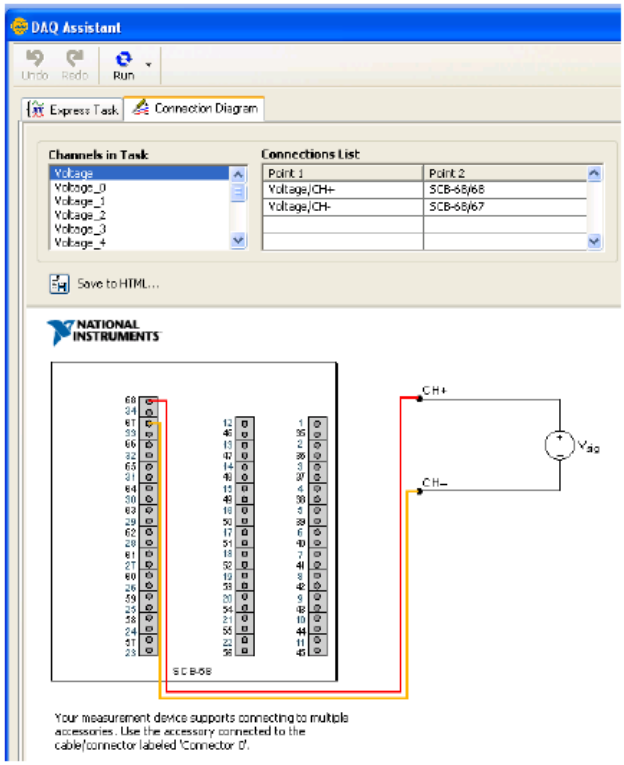

Figure 13: Connection diagram for channel 0.

After the signals are acquired using the DAQ assistant they are sampled at a rate of 4096 Hz.

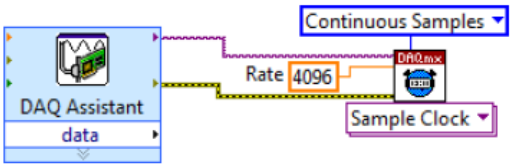

Figure 14: Sampling of data from DAQ assistant.

As seen above, the DAQ assistant is set to "One sample (on demand)" for data acquisition. Here, the data read in is output as a task (purple line) to a DAQmx block. The **task out** is a reference to the task (in this case data acquisition from 13 channels [12 EMG and 1 load cell]). An **error out** line (yellow) is also connected between the DAQ assistant and DAQmx blocks. This line indicates the error status that the DAQ assistant express VI produces.

The first DAQmx block that the data is passed to is a **sample clock** where the number of samples to acquire (continuous) and the rate of the sample clock (4096 Hz) are set. Since the data contains 13 channels, this means that each channel is sampled at 4096 Hz. The input-output diagram of a Sample Clock DAQmx block is shown below.

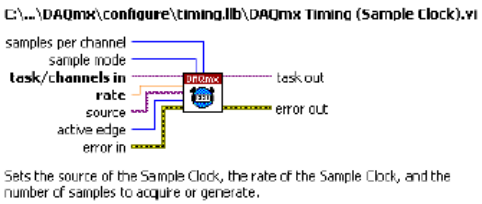

Figure 15: Inputs and outputs of a Sample Clock DAQmx block.

The **task out** of the **Sample Clock DAQmx** is then wired to a **Configure input Buffer DAQmx VI,** which is used to override the automatic input buffer allocation that NI-DAQmx performs. Here, the buffer size (in samples per channel) is set to 300,000. This is the number of samples the buffer can hold for each channel in the task.

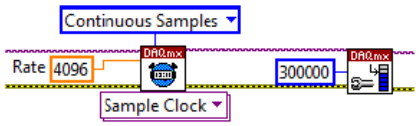

Figure 16: Sample clock and input buffer configuration stage.

Shown below is an input-output diagram of the **Configure Input Buffer DAQmx VI.**

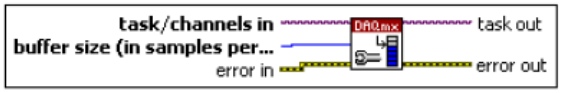

Figure 17: Inputs and outputs of a Configure Input Buffer DAQmx block.

After buffering, the data is sent to a **Start Task NI-DAQmx VI** which transitions the task to the running state to begin measurement. This step is performed to improve the performance of the application[2].

Figure 18: Buffering and start task stage.

Shown below is an input-output diagram of the **Start Task NI-DAQmx VI.**

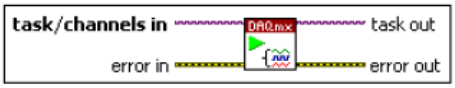

Figure 19: inpust and outputs of a Start Task DAQmx block.

The data is then passed to the while loop responsible for moving the target cursors and writing data, which executes until stopped by the test administrator, or until the required number of samples has been acquired if the "Record Start" button has been selected at the beginning of the session. This condition will be discussed in a later section.

[2] Without the use of this VI, a measurement task starts automatically when **DAQmx Read** and **DAQmx Write** are used. If these VIs are used in a loop, the task is started and stopped repeatedly, which reduces the performance of the application.

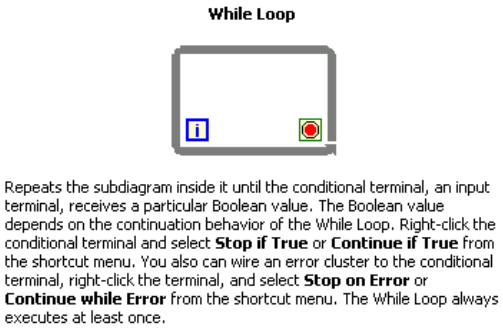

Figure 20: National Instruments' description of the while loop function.

The data's first stop in the while loop is another DAQmx VI – the **Analog 2D DBL NChan NSamp** block. This block reads one or more floating point samples from a task that contains one or more analog input channels to output a 2D array of data. In our particular instance it takes the task (our 13 channels), the number or samples to read per channel (1, continuously), any incoming errors, and a timeout. The timeout is the amount of time (in s) to wait for samples to become available. If more than this amount of time (10s in our case) elapses without incoming samples, the VI returns an error. Ten seconds is the default amount of time that a VI will wait.

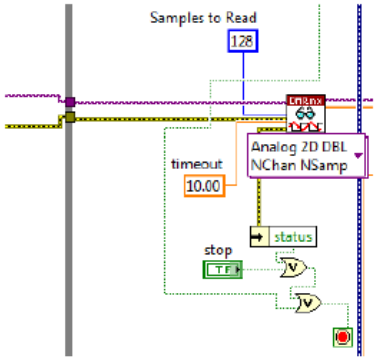

Figure 21: Converting data to a 2D array.

This block *outputs* the task (our channels) and a **2D array of data**, each row corresponding to a channel in the task and each column corresponding to a sample from each channel. The order of the channels in the array corresponds to the order we added the channels to the task. As usual, the DAQmx block also outputs an **error out** with any error information.

The 2D array of data and task split ways here. We will first cover the path of the 2D array of data.

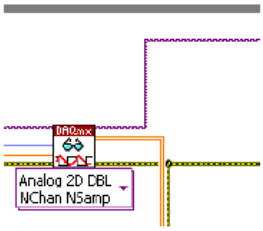

Figure 22: Output of the Analog 2D DBL NChan NSamp Block, showing both the channel array (orange) and error out (purple).

The array of data is first converted to a dynamic data type for use with Express VIs. The dynamic data type will now be a blue thick wire.

Figure 23: The conversion of the channel array to a dynamic datatype.

The data is then merged with data from the moving target (detailed in Section 2.4.4 The Target). This merging is shown in the above diagram, where the moving target dynamic data line comes from the bottom left. After this merge there are 14 channels within the dynamic data line – 12 EMG channels, 1 force channel, and 1 channel representing the coordinates of the moving target (blue) line.

The dynamic data is then passed to the **Write to Measurement File** express VI. This VI writes data to either text based (.lvm) or binary (.tdm or .tdms) measurement files. In this VI the **Write to Measurement File** is configured to save .lvm files.

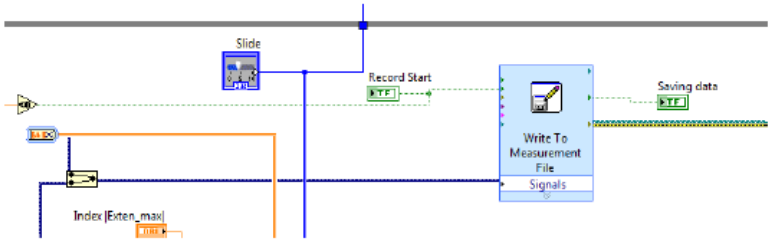

Figure 24: Dynamic data being passed to Write to Measurement File express VI.

The settings of the **Write to Measurement File** express VI are shown below.

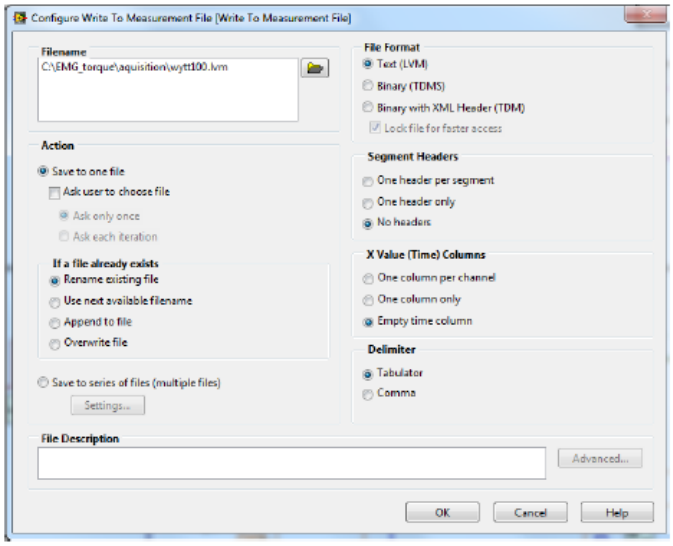

Figure 25: Write to measurement file express VI settinsg.

Aside from being used to record EMG and load cell signals, this dynamic data is used throughout the while loop for control of the Tracker (red line).

The VI operates until the condition for ending the while loop is met. This condition is defined by the test administrator through the entry of *Start time* and *Duration.* The front panel portion of this is shown below.

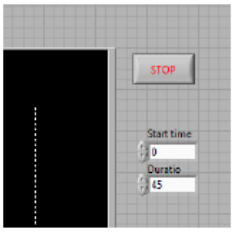

Figure 26: Start time and duration entry boxes.

The way that this information is used in the block diagram is the following.

The *Duration* and *Start Time* are added together to form the full time for which the VI should run. Once the start time has elapsed, the VI begins recording the EMG and force data for the contraction trial.

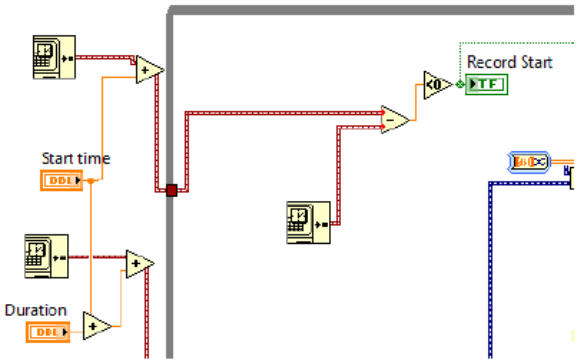

Figure 27: VI operation length formation via duration and start time.

The record command is sent to the **Write To Measurement File** express VI explained above. Once the difference between the *End Time* (projected using the test administrator's *duration* and *start-time* settings) and the current time is 0, the test is stopped.

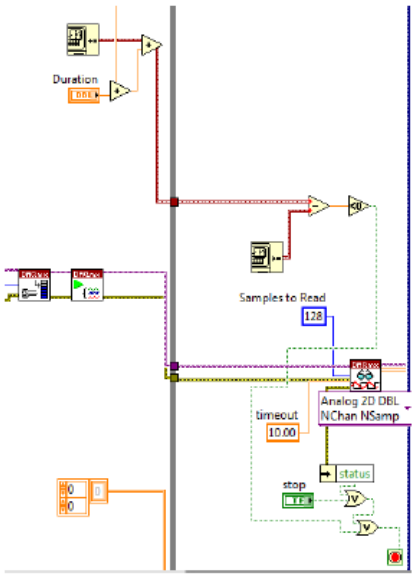

Figure 28: Block diagram showing the comparison between current time and end time.

Since the process of writing the file takes a few seconds after the VI has stopped, an indicator light on the front panel shows when the VI is actively saving data. It is lit up in green when recording, and off when not recording. The block diagram indicates this light with the T/F toggle "Saving Data" shown in the **Write To Measurement File** block.

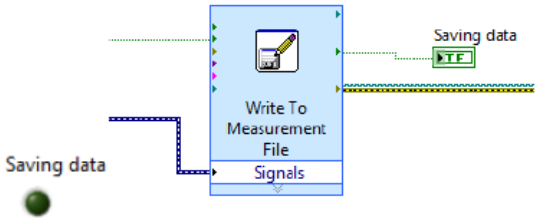

Figure 29: Front Panel and Block Diagram representation of saving data indicator.

2.3 AUTOMATED FILE SAVING

The data captured during the Data Acquisition & Recording (Section 2.2) is automatically saved by the VI to avoid user entry error during the data saving process. The Front Panel section in which information pertaining to the data being collected is entered is shown below.

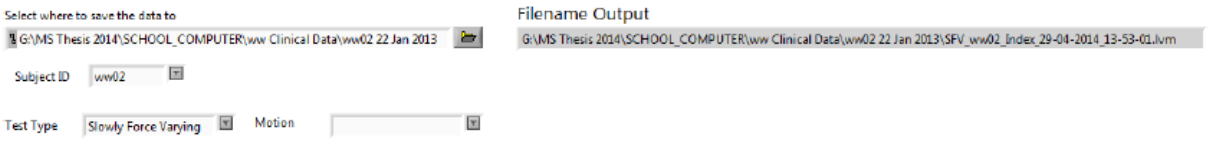

Figure 30: Front panel portion in which the test administrator enters information related to the contraction trial.

This VI is used for three kinds of tests: Slowly force varying (SFV) contractions, constant force (CF) contractions, and rest (REST) contractions. The information that the test administrator must enter includes:

- The folder to save all test data in
  - This should be the data folder created for the subject undergoing clinical testing
- The subject ID
  - This should be an ID generated using the experiment code (in this case 'ww') and the enrollment number[3] (in this case 02)
- The test type
  - This is a dropdown menu from which the test administrator can select "Slowly Force Varying", "Rest", or "Constant Force"
- Motion
  - This is a dropdown menu for the conduct of Constant Force contractions. The options are "Flexion" or "Extension". It should be left blank when Slowly Force Varying or Rest contractions are being measured.

This information is used to generate the filename for the current contraction trial. The filenames are constructed as follows:

TestType_SubjectID_FingerOrGripSelected_Date_Timestamp.lvm

In which the test types are either SFV, CF, or REST, the finger or grip selected is obtained from the slider, and the date is in DD-MM-YYYY format, and the timestamp is in 24 hour clock format.

Once the test administrator hits *run* on the trial, the **Filename Output** box will show the test administrator both the path to the data that will be saved, and the name that that the data will have. For the above settings, this name is "SFV_ww02_Index_29-04-2014_13-53-01.lvm".

The portion of the block diagram which accomplishes this is shown below.

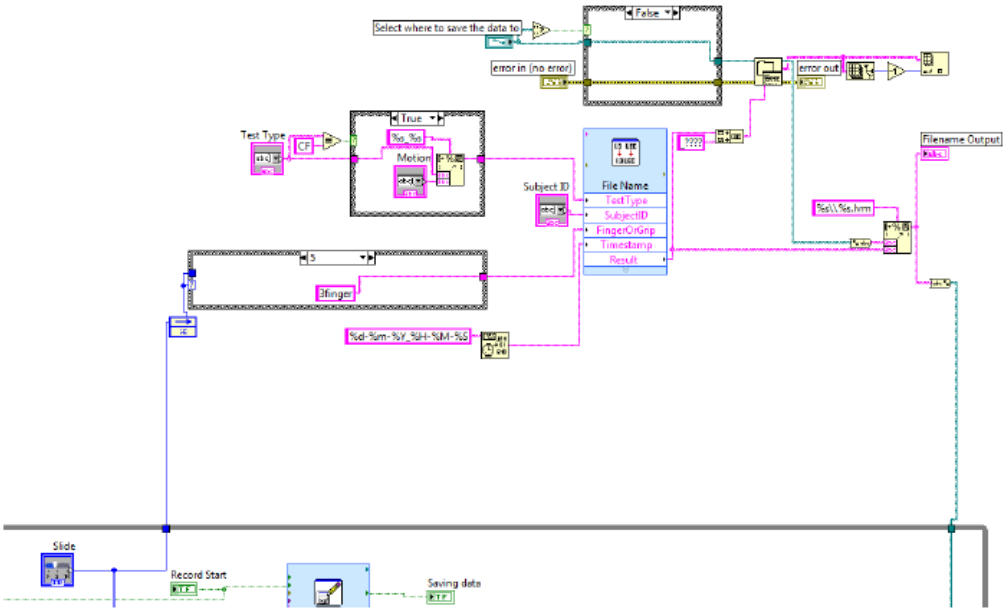

Figure 31: Block diagram portion responsible for automated file naming and data saving.

[3] Enrollment number is a 2 digit number indicating the chronological enrollment of subjects into the study. The 3rd subject in the study with the experiment code 'ww' would be denoted 'ww03'.

2.4 SUBJECT INTERFACE

The subject interface consists of the black screen which has the blue target, red tracker, and three vertical white dotted lines. The line on the right represents the ***extension line,*** the line on the left represents the ***flexion line***. The center line represents the midway point across the screen but is not where zero force occurs as this depends on the subject's strength in either flexion or extension. Shown below is the portion of the *Front Panel* which is relevant to the subject during testing.

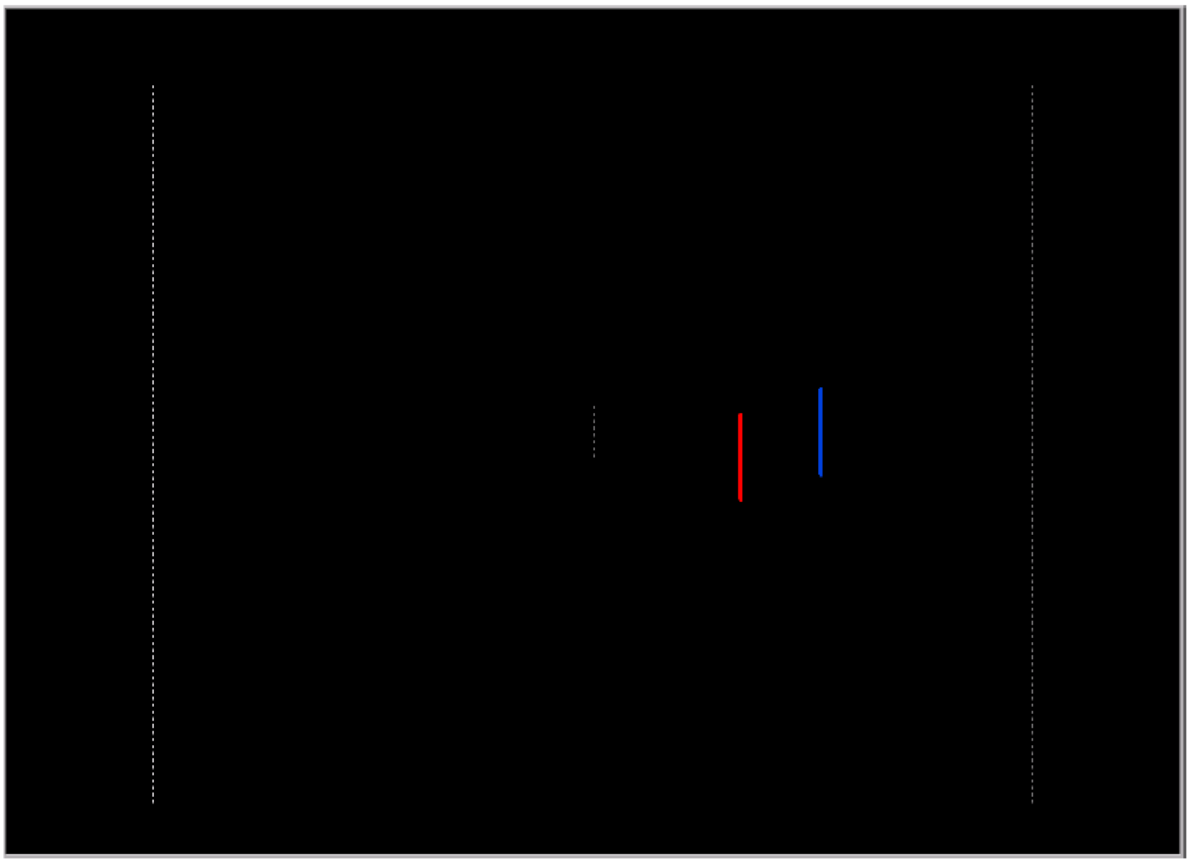

Figure 32: Subject interface portion of the VI

The way in which this graphical area is defined, including the target and tracker are explained in the following sections. To understand these methods, the entry of force calibration data and finger/grip selection is also explained.

2.4.1 DEFINITION OF GRAPHICAL AREA

The graphical area that the user interfaces with is defined using a coordinate system. The figure below shows the definitions for the location and length of the flexion, extension, and center lines.

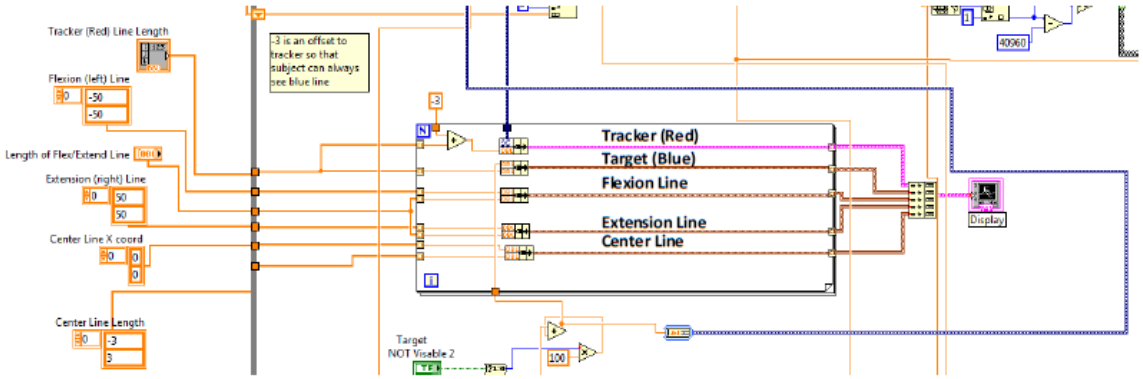

Figure 33: Graphical area definition.

These values are fed to a for loop where the data from the moving tracker and target is combined with the static definition lines to form an interactive UI. The lines responsible for each function are labeled in Figuer 26.

The display VI is responsible for displaying the information on the front panel.

The properties of the 

icon are shown in the figure below.

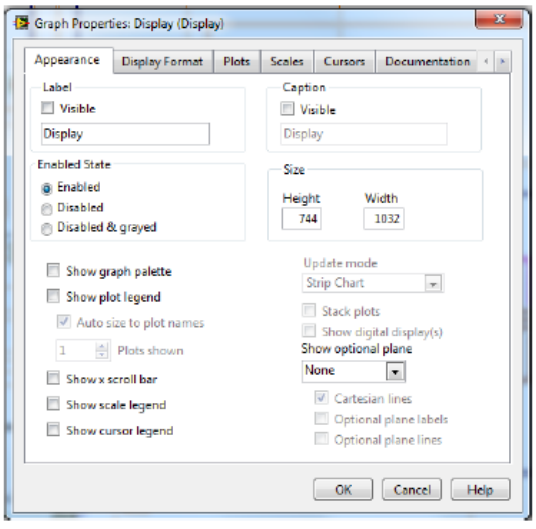

Figure 34: Display icon properties.

2.4.2 CALIBRATION ENTRY (100% MVC VALUES)

Calibration data is collected using the VI *Calibration_100MVC.vi*. The absolute value of the average voltage value for each finger/grip obtained from this testing are the **FINGER CALIBRATION** and **GRIP CALIBRATION** sections on the front panel. The front panel view of this section is shown alongside the relevant part of the block diagram in Figure 35: Finger and grip calibration portions of the VI. below.

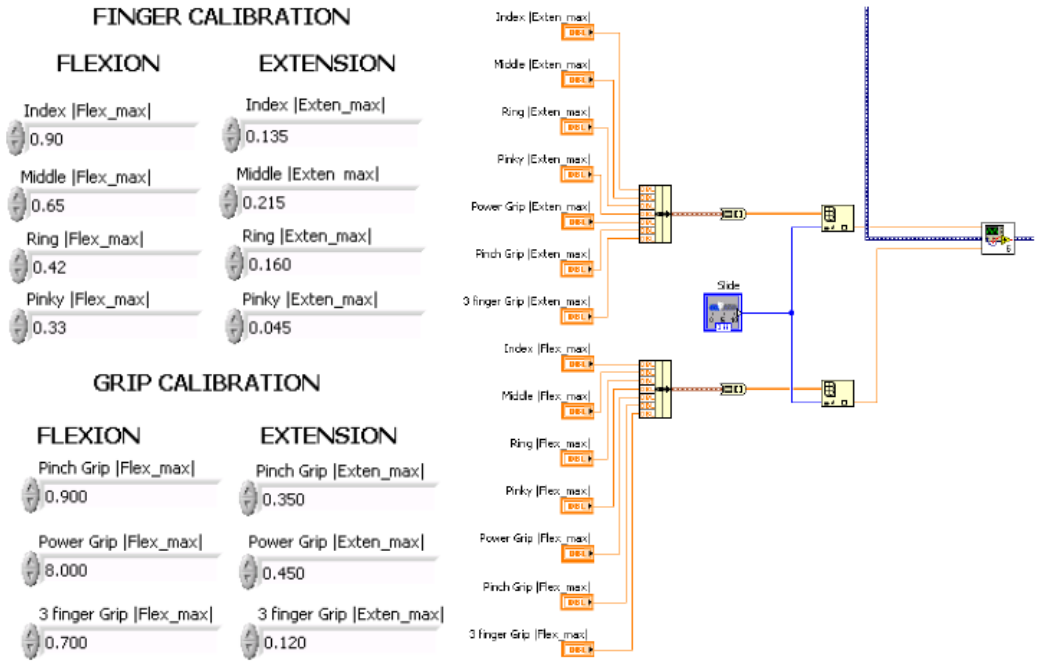

Figure 35: Finger and grip calibration portions of the VI.

Here, a slider is used to select the finger or grip calibration information relevant to the trial the test administrator desires to run. The Front Panel of the slider is shown below.

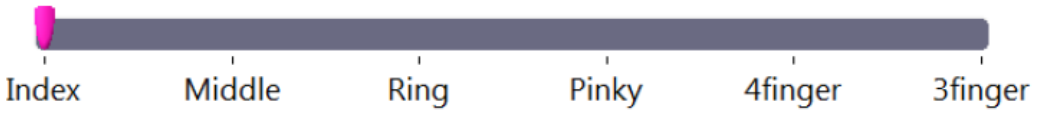

Figure 36: Slider used to select finger or grip for testing.

In the block diagram, the calibration values for extension and flexion are grouped into a cluster using a **bundle**.

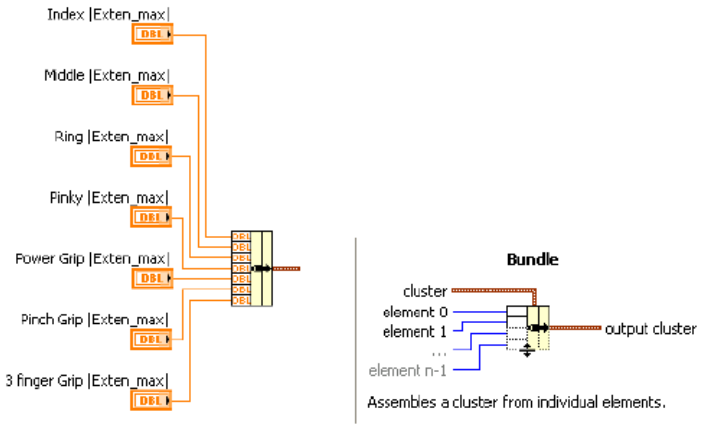

Figure 37: Block diagram for finger values alongside inputs and outputs of bundle block.

The cluster of either extension or flexion values is converted to a 1D array of elements of the same data type. This 1D array is then fed to an **Index Array**, which when combined with the **slider** detailed in Section 2.4.3 Finger & Grip Selection, returns the element at the index indicated by the slider.

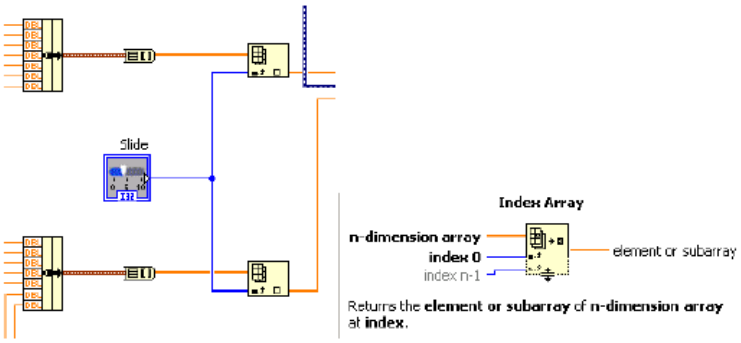

Figure 38: Slider selection explanation.

The output for the index arrays pertaining to flexion and extension are then fed to the "Scaling and Offset (Finger)" sub VI. The use of this information is detailed in Section **Error! Reference source not found.** 2.4.5 The Tracker.

2.4.3 FINGER & GRIP SELECTION

A simple N=6 slider is used for selection of any of the four fingers or three grips being tested. It takes the voltage values obtained during calibration for flexion and extension and provides them to the "Scaling and Offset (Finger)" sub VI to allow for proper Data Output to the red tracking piece.

Figure 39: Slider front panel view

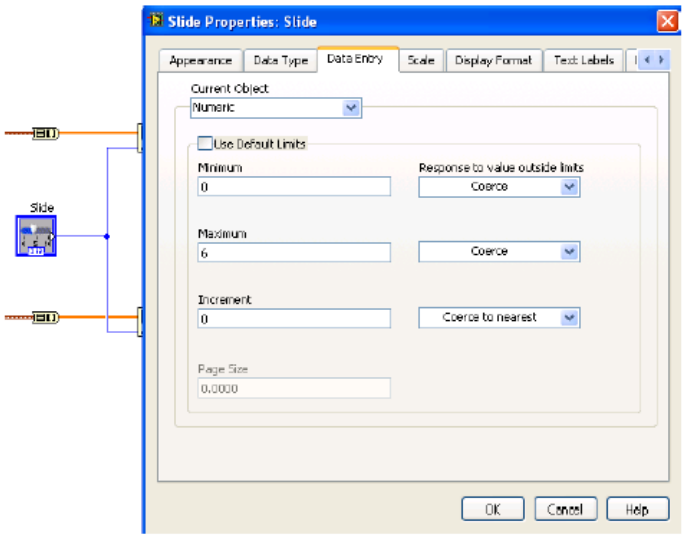

Figure 40: Slider settings

2.4.4 THE TARGET

The target (blue line) is created within the graphical area definitions. This line is indicated in the figure below.

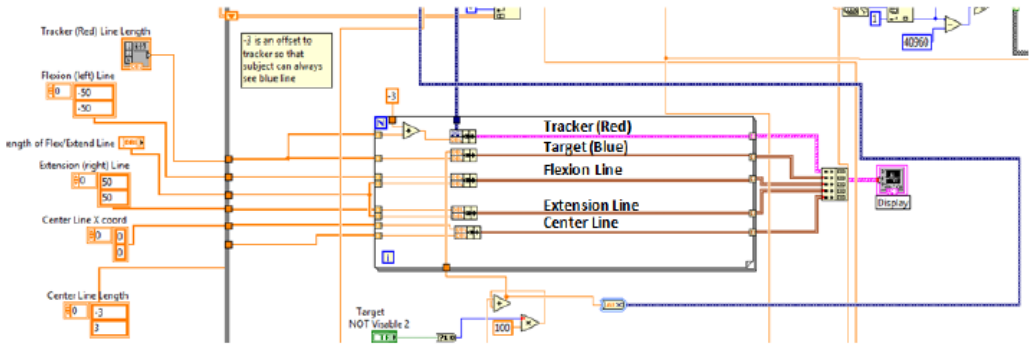

Figure 41: Block diagram of graphical definitions with the target line indicated.

The vertical length of the target line is defined by the item labeled "Tracker (Red Line Length)". This is a misnomer as both the target and tracker lines are the same length. The visibility of this tracker (sometimes turned off for the conduct of Constant Force testing) can be toggled on and off using the "Target Not Visible" button, shown in the above block diagram. The front panel button for this is shown below.

The movement of the target between flexion and extension is defined using a triangle wave function. This function controls the speed and distance that the target moves. This takes in a distance for the line to travel (for this test this value must be defined to be '30'), the frequency of movement (0.033 Hz), and time. A closeup of the triangle wave function is shown below.

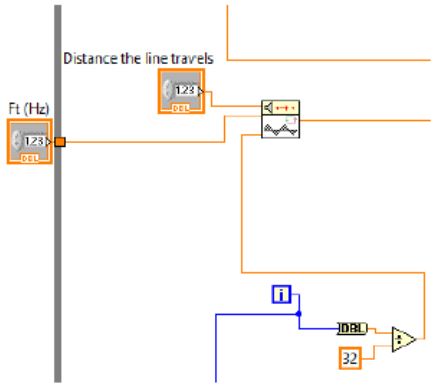

Figure 42: Triangle wave used to create the target line.

National Instruments' help on triangle waves is shown below for further clarification.

Triangle Wave PtByPt VI

Owning Palette: Signal Generation PtByPt VIs

Requires: Full Development System

Generates a triangle wave point by point.

This VI is similar to the Triangle Wave VI.

Details

Add to the block diagram Find on the palette

amplitude is the amplitude of **triangle wave**. The default is 1.0.

frequency is the frequency of **triangle wave** in Hz. The default is 1.

phase is the shift of the waveform, in degrees.

time is the independent variable.

triangle wave is the output triangle wave.

Triangle Wave PtByPt Details

triangle wave = **amplitude** × triangle (q)

where

$$\text{triangle}(q) = \begin{cases} \frac{q}{90} & \text{if } 0 \le q < 90 \\ 2 - \frac{q}{90} & \text{if } 90 \le q < 270 \\ \frac{q}{90} - 4 & \text{if } 270 \le q < 360 \end{cases}$$

and

q = (360 · **frequency** · **time** + **phase**) mod (360), phase in degrees.

Figure 43: Triangle wave help by National Instruments.

These two things work in concert to form the moving target line. Shown below, the output of the triangle wave function is combined with the state of the target visibility and then fed to the display system.

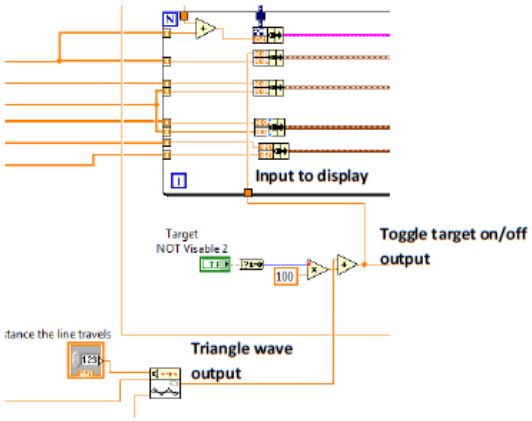

Figure 44: Triangle wave output, Target toggle on/off output, and input to display system.

The motion of the target is converted to a dynamic datatype ad joined with the force and EMG channels to facilitate later comparison between subject force output and tracker motion. This step is shown below.

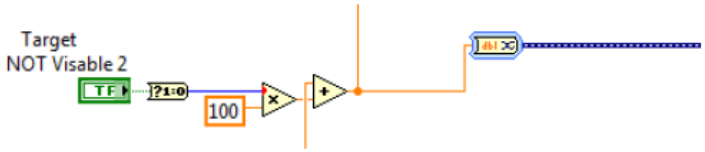

Figure 45: Conversion of target motion to dynamic datatype for writing to measurement file.

The combination of this dynamic data with the EMG and force data is shown below.

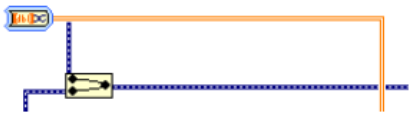

Figure 46: The conversion of the channel array to a dynamic datatype.

2.4.5 THE TRACKER

Most important to the subject interface is the control of the red tracker, which represents the force output by the subject. While the dynamic data bundle containing the EMG data, force data, and triangle wave motion is written to file, a divergent path containing the force data is sent to the user interface for control of the red tracker. The overview of this process is shown in the block diagram below.

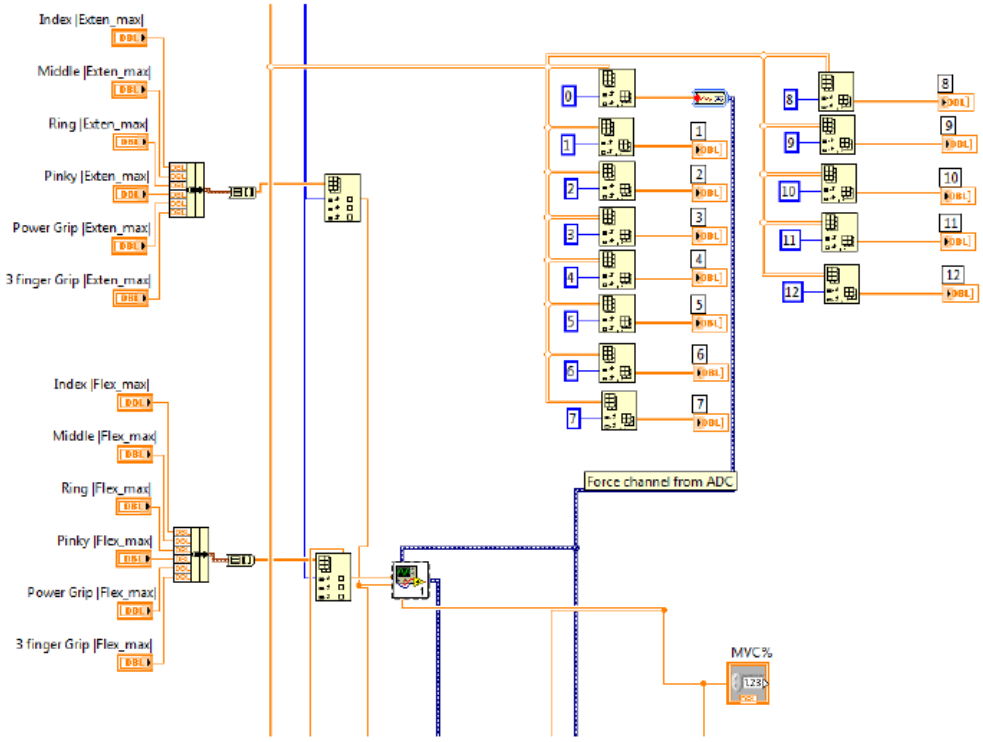

Here it can be seen that the force channel from the NI PCI-6229 is fed to a subVI, which also takes in the calibration information for the finger or grip selected and the %MVC that the subject is intended to reach at the flexion and extension limits. This subVI, called "TrackerLocation_WithOffset.vi", is responsible for moving the red tracker on screen. The block diagram for this VI can be seen below.

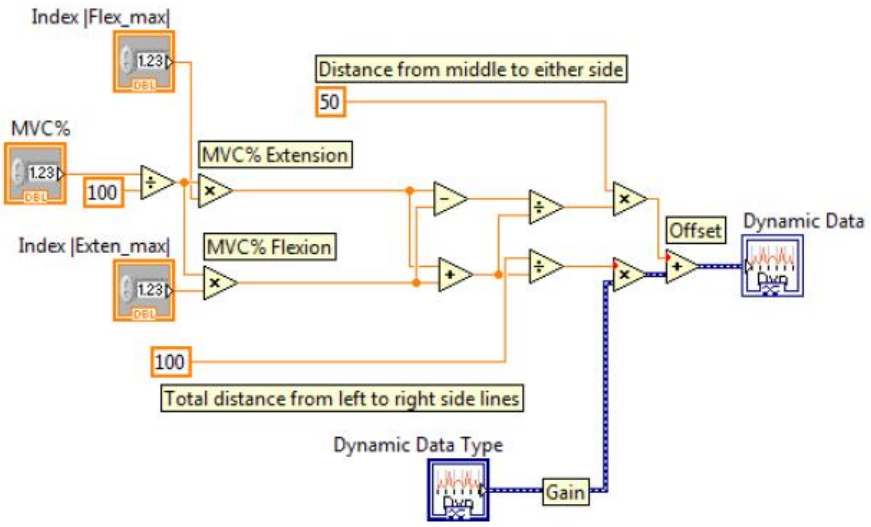

Figure 47: Tracker location and offset subVI

In the figure above, the slider has selected the index finger for the contraction trial. The equations for this system are detailed below.

$$Dyanmic\ Data\ Output = Dynamic\ Data\ Input * Gain + Offset$$

Where

$$Gain = \frac{\left(Flexion\ Max * \left(\frac{MVC}{100}\right) + Extension\ Max * \left(\frac{MVC}{100}\right)\right)}{Distance\ from\ Flexion\ to\ Extension}$$

And

$$Offset = \left(\frac{Flexion\ Max * \left(\frac{MVC}{100}\right) - Extension\ Max * \left(\frac{MVC}{100}\right)}{Flexion\ Max * \left(\frac{MVC}{100}\right) + Extension\ Max * \left(\frac{MVC}{100}\right)} * Distance\ from\ Center\ to\ Edge\right)$$

This method allows for the user to experience constant gain during both flexion and extension activities.

The output of this sub VI is then sent to the for loop described in Section 2.4.1 Definition of Graphical area.

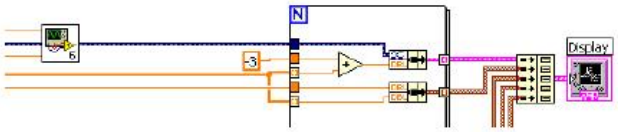

Figure 48: Output of tracker location and offset subVI as input to the display block.

3 EXTRA NOTES

3.1 RSE CONFIGURATION

Grounded or Ground-Referenced Measurement System
A grounded or ground-referenced measurement system is similar to a grounded source in that the measurement is made with respect to ground. Figure 7 depicts an 8-channel grounded measurement system. This is also referred to as a *single-ended measurement system*.

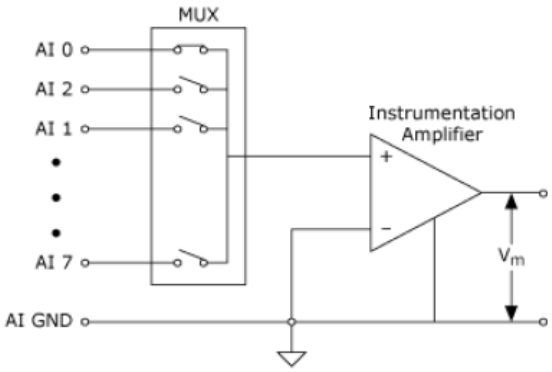

Figure 7. An 8-Channel Ground-Referenced Single-Ended (RSE) Measurement System

3.2 IRRELEVANT SECTIONS

This same VI was used to generate the target motion used for dynamic force testing. As such there are sections within the block diagram that do not apply to slowly force varying, constant force, or rest contraction trials. An example of this is shown below.

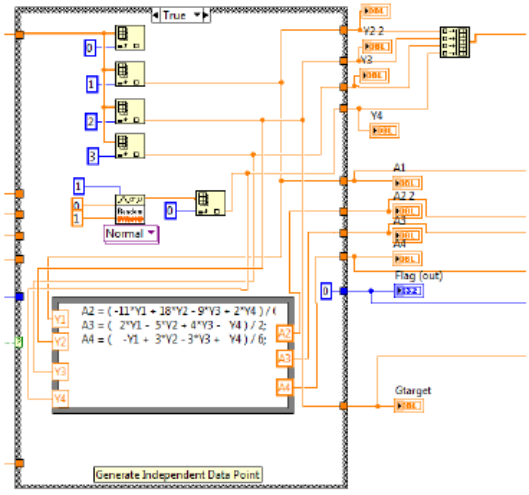

This portion of the VI is not explained within this document as this thesis did not cover dynamic contractions.

A-3.2 Force Calibration VI

WPI

Calibration (100%MVC) for Finger & Grips LabVIEW VI

Design & Troubleshooting Document

Keating & Bardizbanian

11/30/2013

This document outlines the way in which the calibration virtual instrument works for determining a subject's maximum force exerted on the load cell. The subject has all electrodes attached to them and pulls (flexes) and pushes (extends) on the load cell at 100% of their maximum voluntary contraction (MVC) level for 3-5 seconds. The VI "SlowlyForceVarying_Calibration.vi" is used to complete this data collection.

TABLE OF CONTENTS

TABLE OF FIGURES

TABLE OF TABLES

1 CALIBRATION VI – CURRENTLY NAMED SLOWLYFORCEVARYING_CALIBRATION.VI

WARNING: THE OFICIAL NAME OF THIS VI IS CURRENTLY SlowlyForceVarying_Calibration.vi. FOR THE SAKE OF ACCURACY, THIS NAME IS NOT BEING CHANGED AS IT WAS THE VI USED TO COLLECT DATA THROUGHOUT THIS THESIS. FOR FUTURE WORK THIS VI SHOULD BE RENAMED!

The LabVIEW interface needed to complete individual finger and grip calibration can be found under the following path:

C:\Jen_Berj\Finger Labview Data Collection

And is called:

SlowlyForceVarying_Calibration.vi

The only portion of this VI used in clinical sessions is the histogram displayed on the *Front Panel* which shows real-time load cell voltage.

During this testing the test administrator instructs the subject to pull (flex) or push (extend) against the load cell setup as hard as they can for a 3-5 second period of time. During this time the load cell voltage is measured, and the average voltage while force is being applied is calculated and recorded as their maximum voluntary contraction (100% MVC). This is completed twice for each finger and grip involved in testing. The two numbers obtained for each finger/grip are averaged and recorded on the source document.

1.1 REQUIRED HARDWARE CONNECTIONS

This LabVIEW program reads the analog signal of the LC101-100 load cell and the EMG electrodes using the NI-PCI 6229 via the DAQ assistant tool, which converts all of the signals from analog to digital domain.

To connect the LC101-100 to the NI-PCI 6229 DAQ, the output of the load cell must be connected to the Omega DMD-465WB AC powered bridge sensor. The output of the DMD-465WB must then be connected to the NI-PCI 6229. All connections should be as follows:

Table 1: LC101-100 and Omega DMD-465WB Configuration

LC101-100 Output Line	Color	Omega DMD-465WB Input
+Input (excitation)	Red	4 (B+), a small wire bridges 3&4
- Input (excitation)	Black	2 (B-), a small wire bridges 1&2
+Output	Green	9 (-input)*
-Output	White	8 (+input)*

***Note this was changed in order to make flexion move the cursor to the right and extension move it to the left, as mentioned by Professor Clancy. Correct orientation should be Green to 8, White to 9.**

Shown below are the Omega DMD-465WB pin diagram and an overhead view of the LC101-100 load cell connected to the DMD-465WB. In the overhead view inputs to the DMD-465WB are outlined in orange while its outputs are outlined in green.

Figure 1: Omega DMD-465WB diagram.

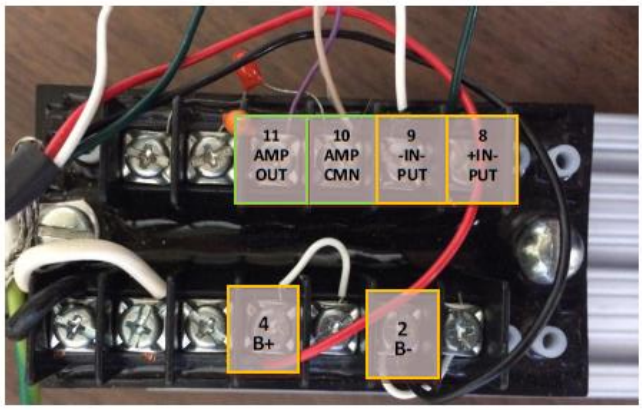

Figure 2: Overhead view of the LC101-100 load cell connected to the DMD-465WB

The above figure also includes the setup of the DMD-465WB, as well as the output of the DMD-465WB to the NI-PCI 6229, the connections for which are described below.

Table 2: Omega DMD-465WB and NI-PCI 6229 configuration

Omega DMD-465WB Output	Color	NI-PCI 6229 Input Channel(s)
11 (AMPL OUTPUT)	Purple	J68
10 (AMPL CMN)	Beige	J67

Shown below in Figures 3 and 4 are the DMD-465WB output connections and the NI-PCI 6229 input connections.

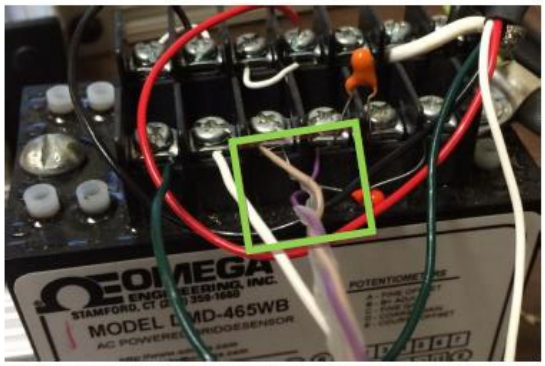

Figure 3: Side view of DMD-465WB with all connections. The amplifier output and common connections are located centrally in beige and purple.

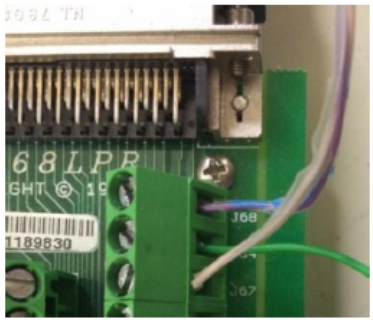

Figure 4: AMPL CMN and AMPL OUTPUT connected to J68 and J67 respectively. The green wire connected is unrelated to the load cell output.

Note: Each of the channels on the NI-PCI 6229 DAQ is labeled as shown in Table 2 above – with a J followed by a number. These channel labels are all associated with various analog inputs and outputs. When adding a voltage source to a VI, these channels are referred to as their function (e.g. AI30). The image below, taken from NI documentation, shows the appropriate labeling.

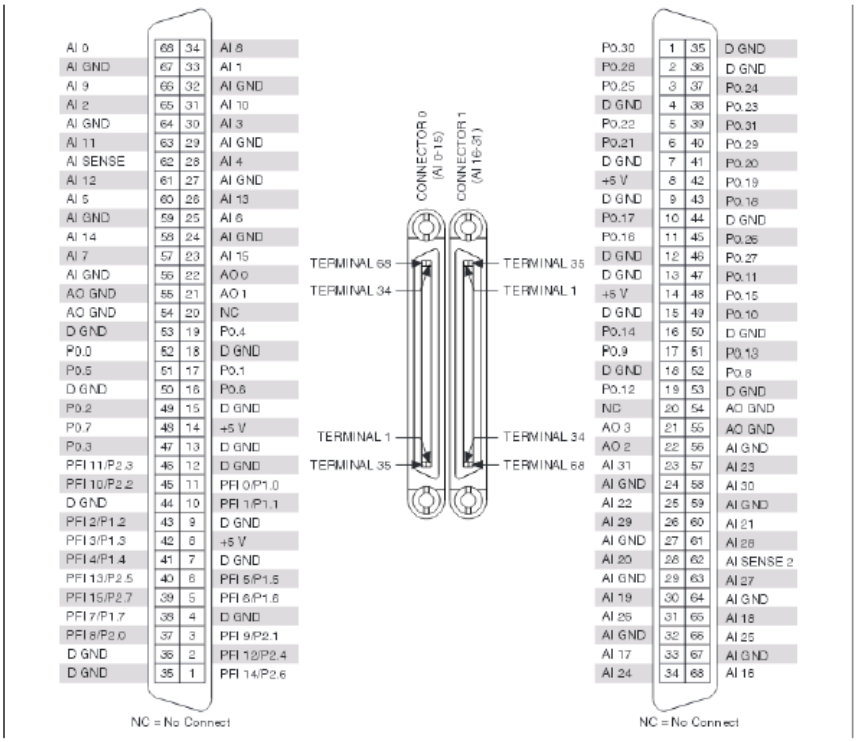

Figure 5: PCI/PXI-6229 Pinout provided by National Instruments.

1.2 CALIBRATION (100% MVC) VI

This LabVIEW VI (*SlowlyForceVarying_Calibration.vi*) is designed so that the test operator can instruct the subject to exert maximum force, either flexion or extension, on the load cell, in order to obtain the maximum value exerted by the subject. The VI uses the voltage from the load cell as measured by the NI6229 on Channel 0 to display a real-time histogram of the maximum force. While the histogram is being displayed, the average force (in voltage) applied by the subject is calculated by finding the voltage value associated with the highest peak in the histogram.

Shown below is a screenshot of the Front Panel of the VI.

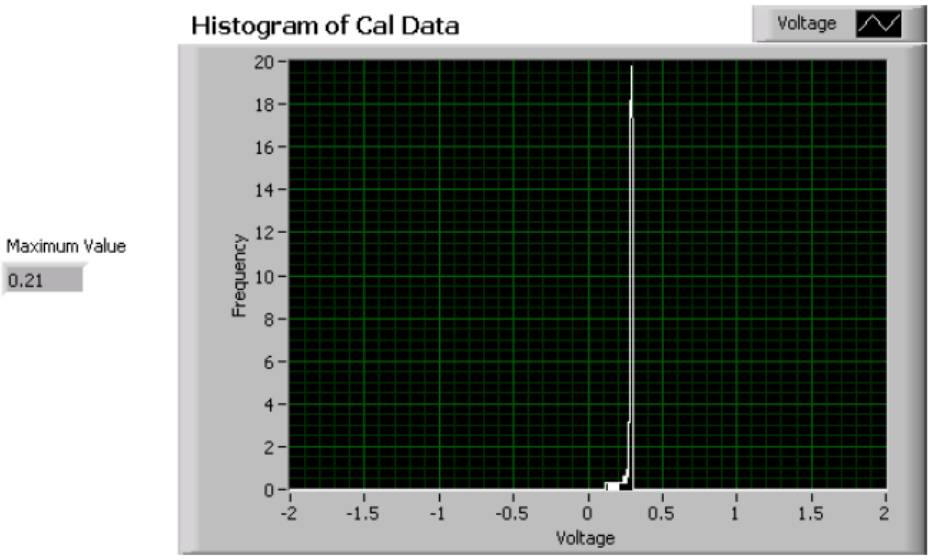

Figure 6: Calibration_MVC100.vi LabVIEW VI Frontal Panel Window

The Maximum Value shown is the voltage at the peak in the histogram. The functionality of each of these blocks can easily be explored for modification or understanding and is not detailed in this document.

1.2.1 BLOCK DIAGRAM

The Block Diagram of the VI can be accessed via **Window → Show Block Diagram (or CTRL+E).** The following sections detail the functionality of this Block Diagram.

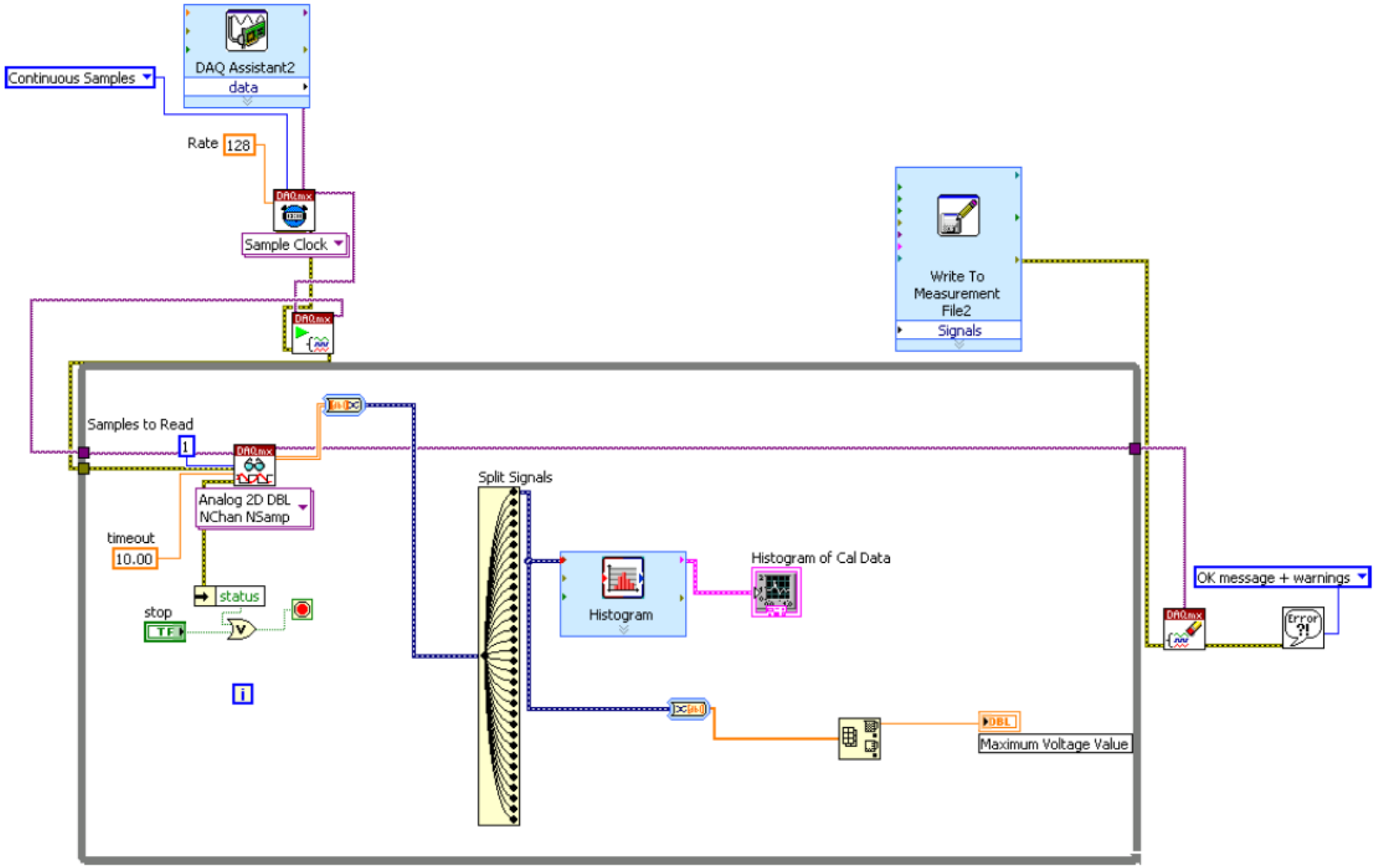

Appendix 4 Clinical Documents

A-4.1 Informed Consent

INFORMED CONSENT TO TAKE PART IN A RESEARCH STUDY

TITLE OF THIS STUDY: **Relating Arm Muscle Electrical Activity to Hand/Finger Forces for use in Prosthesis Control and Stroke Rehabilitation Devices**

STUDY PRINCIPAL INVESTIGATOR: **Edward A. Clancy, Ph.D.**
508-831-5778

PROJECT SPONSOR: **Worcester Polytechnic Institute (WPI)**

Introduction
You are being asked to participate in a research study to be conducted at Worcester Polytechnic Institute. It is important that you read the following explanation of the proposed procedures. This form describes the purpose, procedures, benefits, risks, discomforts and precautions of the study. It also describes the alternative procedures that are available to you and your right to withdraw from the study at any time.

Purpose of the Study
When muscles in your forearm contract, they produce a small electrical signal that can be recorded. Some individuals who wear a prosthetic hand are able to control their hand using the electrical activity of remnant muscles from their forearm. Some people who have a stroke lose some of their ability to move their hands properly. In each condition, electrical activity in the forearm is related to forces produced in the hand/fingers. In this project, we are trying to develop a new technique for using these electrical signals to control a hand prosthesis and/or to aid therapy in stroke victims. This particular study will collect forearm muscle electrical activity and hand/wrist force recordings. These recordings will be used to develop our new technique in able-bodied people, such as yourself, who do not wear a hand prosthesis and have not experienced a stroke. If successful, the new technique may be tested in the future by prosthesis users and/or stroke patients. A total of up to 50 able-bodied people will volunteer as subjects in this experiment.

Experimental Protocol
You will be asked to complete a short subject questionnaire. After completing this questionnaire, you will be seated in a chair and secured using quick-release belts (similar to tightly worn seat-belts in an automobile). Your arm will be held in front and the side of you, supported at the elbow. Your hand and fingers will be tightly secured into a measurement device. Your forearm will be wiped with an alcohol wipe and then approximately 16 surface recording electrodes will be secured around your forearm. These electrodes measure the electrical activity as represented at the surface of your skin. Then, you will be asked to perform a variety of muscle force tasks by pushing/pulling with your fingers, hand and/or wrist against the measurement device. A few of the tasks will require your maximum possible effort for a few seconds. Most tasks will require much less effort. Rest (2–3 minutes) will be provided between tasks, as necessary, so that you can easily maintain your muscle effort while competing all of the contraction tasks. Your participation will last for about four hours.

Benefits
There is no direct benefit to you for participating in this study.

Risks
There is some possibility of minor discomfort due to the postural restraints. There is a risk of skin irritation from the skin preparation required for the electrodes and from the tape used to secure the electrodes to your skin. You should expect some muscle soreness to develop as a consequence of contracting your muscles. You may also experience mental fatigue from the concentration required to complete the tasks. The risks to pregnant women and fetuses are unknown and therefore pregnant women should not participate in the study.

Medical Care if Injured
WPI assumes no responsibility to pay for any injuries that you might receive as a result of participating in this research study. No funds have been set aside for payments or other forms of compensation (such as for lost wages, lost time, or discomfort). If you suffer a physical injury as a result of your participation in this study, you may chose to seek medical care in the same way as you would normally. If your insurance does not cover the cost then you may be responsible for this cost. However, you do not give up any of your legal rights by signing this consent form.

Participation
Your participation in the study is voluntary. You are free to withdraw consent and discontinue participation at any time without penalty. You are free to seek further information regarding the experiment at any time. The project investigators retain the right to cancel or postpone the experimental procedures at any time they see fit.

Confidentiality
Records of your participation in this study will be held confidential so far as permitted by law. However, the study investigators and, under certain circumstances, the Food and Drug Administration (FDA) and the Worcester Polytechnic Institute Institutional Review Board (WPI IRB) will be able to inspect and have access to confidential data that identify you by name. Any publication or presentation of the data will not identify you.

Withdrawal
Data obtained in this experiment will become the property of the investigators and WPI. If you withdraw from the study, data already collected from you will remain in the study.

Data Reuse and Contribution of Your Data to a Public Data Archive
The data from this experiment will also be contributed to publicly available databases and/or reused by the study investigators in future research. The purpose of this data reuse is to share your data with other researchers (or reuse the data ourselves) to make further advances in medicine, science and teaching. Your data could be used for many different purposes. Most researchers will gain access to your data over the Internet. Before contributing your data, all information that identifies you as a subject in this experiment (including your name) will be coded using a random code. The only way to relate the code to yourself is by a "key" that the study investigators will maintain private. We will never reveal your identity, unless required to do so by law. The public database will not provide any direct access to your identity.

Questions
This study will be directly supervised by Edward A. Clancy. Questions or comments about participation should be directed to Edward A. Clancy at (508) 831-5778 (E-mail: ted@wpi.edu). You may also contact

the Chair of the WPI IRB, Professor Kent Rissmiller at (508) 831-5019 (E-mail: kjr@wpi.edu); or the University Compliance Officer, Michael J. Curley at (508) 831-6919 (E-mail: mjcurley@wpi.edu).

Cost/Payment
You will receive $25 for completion of the study. If the experimental session is not completed, you will be paid $8 per completed hour (not to exceed $25).

For Employees of WPI:
Your participation in this study is voluntary. You are free to withdraw your consent and discontinue participation in this study at any time without prejudice or penalty. Your decision to participate or not participate in this study will in no way affect your continued employment or your relationship with individuals who may have an interest in this study. _____initials
(*Please note you will be participating in this study on your own time; not during regular working hours*)

VOLUNTEER'S STATEMENT:

I have been given a chance to ask questions about this research study. These questions have been answered to my satisfaction. I may contact Dr. Clancy if I have any more questions about taking part in this study.

I understand that my participation in this research project is voluntary. I know that I may quit the study at any time without losing any benefits to which I might be entitled. I also understand that the investigator in charge of this study may decide at any time that I should no longer participate in this study.

If I have any questions about my rights as a research subject in this study I may contact:

Prof. Kent J. Rissmiller, Chair
WPI Institutional Review Board
100 Institute Road
Worcester, MA 01609
(508) 831-5296 [E-mail: irb@wpi.edu]

By signing this form, I have not waived any of my legal rights.

I have read and understand the above information. I agree to participate in this study. I have been given a copy of this signed and dated form for my own records.

Study Participant (signature) _____ Date _____

Print Participant's Name _____

Approved by
WPI IRB 1
10/2/13-10/1/2014

Person who explained this study (signature) _____ Date _____

A-4.2 SOP-001 Procedure for Conducting an Informed Consent with a Potential Subject

Procedure for Conducting an Informed Consent with a Potential Subject	SOP Number Clinical-001	Page 1 of 3
	Supersedes NA	Effective Date 1 December 2013

PROCEDURE FOR CONDUCTING AN INFORMED CONSENT WITH A POTENTIAL SUBJECT

Prepared by:_____
Jennifer Keating, MS Thesis Candidate

Procedure for Conducting an Informed Consent with a Potential Subject	SOP Number Clinical-001	Page 2 of 3
	Supersedes NA	Effective Date 1 December 2013

1. **CHANGES:**
   Not applicable, original document.

2. **PURPOSE:**
   To describe the standard operating procedure (SOP) to be followed during the informed consent process.

3. **SCOPE:**
   This procedure applies to all data collection procedures involving potential subjects for which L(SP)^2, is responsible, unless otherwise outlined in the delegation of responsibilities.

4. **APPLICABLE TO:**
   This SOP applies to L(SP)^2 study staff and/or all agents of L(SP)^2 who are overseeing the informed consent procedure.

5. **DEFINITIONS:**
   Informed consent –Consent by a subject to participate in an experiment after the subject understands the risks involved in participation.
   Informed consent form (ICF) – The document that provides a summary of the trial. It should describe the purpose of the trial, the procedures involved, the potential study risks and benefits, and patient confidentiality to potential subjects. Once signed the potential subject is now a subject in the study.
   Principal investigator – The individual primarily responsible for the taking, importation and export of data, and any related activities conducted under a permit issued for scientific research. In the case of clinical trials this person is often a medical doctor (MD).
   Potential subject – Any person who enters the data collection area with the intent of volunteering for the L(SP)^2 sponsored data collection visits but has not yet provided written informed consent.
   Qualified staff member –A member of the L(SP)^2, staff who has completed the necessary training to perform an informed consent procedure and has official documentation indicating that he/she is qualified to conduct the consent process.
   Screening visit – A visit occurring at the beginning of a study which serves to identify whether a particular subject is suitable for current data collection needs. Information gathered at a screening visit will be kept on file in the event of a change in data collection needs.
   Subject – A person who has completed the informed consent process and is entered as a volunteer for L(SP)^2 's data collection visits.
   Written informed consent –Official documentation of a subject's agreement to participate in L(SP)^2 's data collection via the subject's signature, printed name, and date and time of signature.

Procedure for Conducting an Informed Consent with a Potential Subject	SOP Number Clinical-001	Page 3 of 3
	Supersedes NA	Effective Date 1 December 2013

6. **PROCEDURE:**

WARNING: If the subject is not a native English speaker and cannot fully understand the document/your conversation with them, they need to be consented with an informed consent document that is in their native language. At this time L(SP)^2 does not provide multilingual consent forms and such a subject would not be able to participate in the study.

Note: This procedure is to be carried out only by qualified staff members.

6.1. Distributing the Informed Consent Document

6.1.1. When the potential subject has arrived for their screening visit, explain that he/she will be given the informed consent form (ICF) to read thoroughly, without signing. This document will explain the purpose of the study, all study procedures, contact information, and compensation.

6.1.2. Give the potential subject a blank copy of the ICF to read.
IMPORTANT NOTE: Remind the potential subject not to sign anything while reading – signing will take place after the consent process has been completed with a qualified staff member.

6.1.3. Instruct the potential subject to notify staff when he/she has finished reading.

6.2. Reviewing the Informed Consent Document

6.2.1. Review the consent form with the potential subject; discuss the document and make sure that the potential subject verbally comprehends the study. At each study visit, site contact information, IRB contact information, study personnel contact information, and any questions the potential subject has should be discussed.

6.2.2. If needed, call the Principal Investigator (PI)/Sub Investigator to address any other issues the staff member cannot answer fully.

6.3. Obtaining Written Consent

6.3.1. Once the potential subject agrees that he/she understands the document and indicates that he/she would like to volunteer to participate in the trial, obtain written consent.

6.3.1.1. Have the potential subject sign the consent form in pen with printed first and last name, signature and date.

Note: If the subject makes a mistake, have the subject cross out the incorrect information with a single line and rewrite the correct information. Once the information is correct, make a note next to the correction indicating the reason for the mistake and include your initials and date in the DDMonYY format.

6.3.1.2. As the qualified staff member responsible for the informed consent procedure, sign the consent form in pen with printed first and last name, signature and date. The potential subject is now a subject of L(SP)^2's data collection studies.

6.4. Study Enrollment

6.4.1. Review the informed consent document in order to be sure that all procedures were followed properly.

6.4.2. Photocopy the subject's ICF and provide them with the copied version of the form. Let them know that they should take this form home with them and keep it in a safe place.

6.4.3. Place the original signed copy of the ICF in a locked cabinet containing the subject's ICF and any other forms and/or data related to this subject.

6.4.4. Study enrollment is now complete and the study visit may now commence.

7. **REFERENCES:**

None.

ATTACHMENTS:

Informed consent document.

A-4.3 Subject Questionnaire

Subject Questionnaire and Data Collection Sheet
(Completed by Verbal Interview After Informed Consent)

Relating Arm Muscle Electrical Activity to Hand/Finger Forces for use in Prosthesis Control and Stroke Rehabilitation Devices

Subject Identification Code: _____
(to be filled out by study staff)

Age (in years):	Height: _____ ft _____ in
Weight (in lbs):	Gender (circle one): Male Female
Ethnic category (circle one): Hispanic or Latino Not Hispanic or Latino Not reported	Racial category (circle one): American Indian/Alaska Native Asian Native Hawaiian or Other Pacific Islander Black or African American White More Than One Race Not reported

Do you have any condition affecting the function of your hands, arms or shoulders? Yes No If yes, please describe:
Do you have any past injuries to your right elbow or shoulder? Yes No If yes, please describe:
Do you have any limitations to your range of motion in your right elbow or shoulder? Yes No If yes, please describe:

TURN

Do you have any scars on your arms? Yes No If yes, please describe:
Do you have any physical limitations that would hinder your ability to complete this experimental work? Yes No If yes, please describe:
If female: Are you pregnant or could you be pregnant? Yes No [If yes, exclude as subject.]

A-4.4 Source Document for Clinical Procedures

Protocol Number: 13-141	**Subject ID #:** _____
Sponsor: WPI	**Operator ID #s:** _____/_____
Investigator: Dr. Edward Clancy	**Date:** ___/_____/_____

Before Experiments

- Power up all equipment
  - LabVIEW Computer & monitors
  - EMG power
  - Load cell (attached to same power strip as monitors)
- Assign subject number, data file ID
- Measure subject forearm
  - Record measurement
  - Generate proper distances with macro
- Put up "experiment in progress" signs
- Set finger/grip apparatus on experimental table
- Generate order of experiments sheet using MATLAB script

When subject arrives

- Confirm subject information, check for access to forearm
- Obtain written informed consent

Experimental setup

- Complete subject questionnaire
- Instruct subject to use the bathroom now
- Stow belt, wallet, etc if desired
- Shut off all cell phones (subject and experimenters)

Subject instructions during a trial

- Maintain arm/fingers in the experimental position
- Contact with fingers/grip should only be at the finger/grip cuff attachment
- **Relax all muscles not directly involved with pushing, pulling, rotating, etc.**
- Push, pull, rotate only in the directions to/from the cuff attachments
- Maintain a consistent posture/contraction technique during and throughout all trials
- For constant force trials (30, 100% MVC), move to target level gradually (0.5-1s)

ZERO THE LOAD CELL BEFORE ATTACHING THE FINGER! Check throughout testing!

Protocol Number: 13-141	**Subject ID #:** _____
Sponsor: WPI	**Operator ID #s:** _____/_____
Investigator: Dr. Edward Clancy	**Date:** ___/_____/_____

Electrode mounting

- Measure the circumference of the subject's forearm, 3 fingers breadth from the antecubital.
- Use the excel document "populate", to determine electrode placement.

Arm circumference: _____

Space between electrodes: _____

Calibration (FINGER EMG) Trials

- Configure/measure finger apparatus in relation to the subject's arm, THEN secure to the table.
- Make sure the elbow is at 90 degrees.
- Instruct the subject to increase force over 2-3 seconds to achieve maximum effort.
- Ask subject to exert maximum effort (MVC) for ~3s per finger. Record this portion of the trial.
- Instruct the subject to relax.
- Record the voltage output by the subject in the appropriate slot in the LabVIEW VI.

Finger	Action	Voltage Value	Average (V)
Index	Flexion		
Index	Flexion		
Index	Extension		
Index	Extension		
Middle	Flexion		
Middle	Flexion		
Middle	Extension		
Middle	Extension		
Ring	Flexion		
Ring	Flexion		
Ring	Extension		
Ring	Extension		
Pinky	Flexion		
Pinky	Flexion		
Pinky	Extension		
Pinky	Extension		

Startup time (s): 0

Recording time (s): 5

VI	Did you enter all calibration values?
Slowly_Force_Varying.vi	
Dynamic_Force_Varying.vi	

Protocol Number: 13-141	**Subject ID #:** _____
Sponsor: WPI	**Operator ID #s:** _____/_____
Investigator: Dr. Edward Clancy	**Date:** ___/_____/_____

Calibration (GRIP EMG) Trials

- Instruct the subject to increase force over 2-3 seconds to achieve maximum effort.
- Ask subject to exert maximum effort (MVC) for ~3s per finger. Record this portion of the trial.
- Instruct the subject to relax.
- Record the voltage output by the subject in the appropriate slot in the LabVIEW VI.

Grip	Action	Voltage Value	Average
3 finger	Flexion		
3 finger	Flexion		
3 finger	Extension		
3 finger	Extension		
4 finger	Flexion		
4 finger	Flexion		
4 finger	Extension		
4 finger	Extension		

Startup time (s): 0

Recording time (s): 5

VI	Did you enter all calibration values?
Slowly_Force_Varying.vi	
Dynamic_Force_Varying.vi	

Electrode Gain Setting

- Set the MVC in the **Slowly_Force_Varying.vi** to 100%.
- Select "Target NOT Visible"
- Ask the subject to flex until they reach the white line. Hit pause when white line is reached.
- Check EMG signals. Adjust gain as required.
- Repeat for extension.

Constant Force – 100% MVC – 5 second (GRIP EMG) Trials

- Open **Slowly_Force_Varying.vi**
- Double check that calibration values for grips have been entered into the VI!
- Mount EMG Electrodes
- Test EMG gains for saturation
- Select "Target NOT Visible"
- Have subject practice 100% MVCs.

Startup time (s): 2

Recording time (s): 5

Protocol Number: 13-141
Sponsor: WPI
Investigator: Dr. Edward Clancy

Subject ID #: _____
Operator ID #s: _____/_____
Date: ___/_____/_____

Finger	Action	Timestamp	Comments
4 finger	Flexion		
4 finger	Extension		
3 finger	Flexion		
3 finger	Extension		

Constant Force – 30% MVC – 10 second (GRIP EMG) Trials

- Open **Slowly_Force_Varying.vi**
- Double check that calibration values for grips have been entered into the VI!
- Mount EMG Electrodes
- Test EMG gains for saturation
- Select "Target NOT Visible"
- Have subject practice 100% MVCs.

Startup time (s): 2

Recording time (s): 10

Finger	Action	Timestamp	Comments
3 finger	Flexion		
3 finger	Extension		
4 finger	Flexion		
4 finger	Extension		
3 finger	Flexion		
3 finger	Extension		
4 finger	Flexion		
4 finger	Extension		

Protocol Number: 13-141	**Subject ID #:** _____
Sponsor: WPI	**Operator ID #s:** _____/_____
Investigator: Dr. Edward Clancy	**Date:** ___/_____/_____

Slowly Force Varying (GRIP EMG) Trials

Startup time (s): 0

Recording time (s): 45

- Make target visible
- Double check that calibration values for grips have been entered into the VI!
- Have subject practice tracking with all grips
- 30 seconds of rest between trials
- Each trial includes BOTH flexion and extension
- Range to 30% MVC.
- **WARNING: Remember to properly select the finger being tested each time the grip is changed!**

Grip	Trial	Timestamp	Comments
3finger	1		
4finger	1		
3finger	2		
4finger	2		
3finger	3		
4finger	3		

Dynamic Force (GRIP EMG) Trials

Startup time (s): 2

Recording time (s): 45

- Open ***Dynamic_Force_Varying.vi***
- Double check that calibration values for grips have been entered into the VI!
- Have subject practice tracking with all grips
- 30 seconds of rest between trials
- Each trial includes BOTH flexion and extension
- Range to 30% MVC.
- **WARNING: Remember to properly select the finger being tested each time the grip is changed!**

Grip	Trial	Timestamp	Comments
3finger	1		
4finger	1		
3finger	2		
4finger	2		
3finger	3		
4finger	3		

Protocol Number: 13-141	**Subject ID #:** _____
Sponsor: WPI	**Operator ID #s:** _____/_____
Investigator: Dr. Edward Clancy	**Date:** ___/_____/_____

Classification

Recording	Timestamp	Comments
1		
2 (randomized)		
3		
4 (randomized)		

Startup time (s): 0

Recording time (s): 45

Test Setup Changeout

- Release subject's hand from setup
- Switch the load cell finger adapter out with the load cell grip adapter
- Move the load cell pole location according to subject's arm length
- Secure subject back into setup

Protocol Number: 13-141	**Subject ID #:** _____
Sponsor: WPI	**Operator ID #s:** _____/_____
Investigator: Dr. Edward Clancy	**Date:** ___/_____/_____

Constant Force – 100% MVC – 5 second (FINGER EMG) Trials

Startup time (s): 2

Recording time (s): 10

- Open **Slowly_Force_Varying.vi**
- Mount EMG Electrodes
- Test EMG gains for saturation
- Double check that calibration values for fingers have been entered into the VI!
- Select "Target NOT Visible"
- Have subject practice 30% MVCs.
- 30 sec between trials

Finger	Action	Timestamp	Comments
Index	Flexion		
Index	Extension		
Middle	Flexion		
Middle	Extension		
Ring	Flexion		
Ring	Extension		
Pinky	Flexion		
Pinky	Extension		

Protocol Number: 13-141
Sponsor: WPI
Investigator: Dr. Edward Clancy

Subject ID #: _____
Operator ID #s: _____/_____
Date: ___/_____/_____

Constant Force – 30% MVC – 10 second (FINGER EMG) Trials

Startup time (s): 2

Recording time (s): 10

- Open **Slowly_Force_Varying.vi**
- Mount EMG Electrodes
- Test EMG gains for saturation
- Double check that calibration values for fingers have been entered into the VI!
- Select "Target NOT Visible"
- Have subject practice 30% MVCs.
- 30 sec between trials

Finger	Action	Timestamp	Comments
Index	Flexion		
Index	Extension		
Index	Flexion		
Index	Extension		
Middle	Flexion		
Middle	Extension		
Middle	Flexion		
Middle	Extension		
Pinky	Flexion		
Pinky	Extension		
Pinky	Flexion		
Pinky	Extension		
Ring	Flexion		
Ring	Extension		
Ring	Flexion		
Ring	Extension		

Protocol Number: 13-141	**Subject ID #:** _____
Sponsor: WPI	**Operator ID #s:** _____/_____
Investigator: Dr. Edward Clancy	**Date:** ___/_____/_____

Slowly Force Varying (FINGER EMG) Trials

Startup time (s): 0

Recording time (s): 45

- Make target visible
- Double check that calibration values for fingers have been entered into the VI!
- Have subject practice tracking on all fingers
- 30 seconds of rest between trials
- Each trial includes BOTH flexion and extension
- Range to 30% MVC.
- **WARNING: Remember to properly select the finger being tested each time the finger is changed!**

Finger	Trial	Timestamp	Comments
Index	1		
Middle	1		
Ring	1		
Pinky	1		
Index	2		
Middle	2		
Ring	2		
Pinky	2		
Index	3		
Middle	3		
Ring	3		
Pinky	3		

Protocol Number: 13-141	**Subject ID #:** _____
Sponsor: WPI	**Operator ID #s:** _____/_____
Investigator: Dr. Edward Clancy	**Date:** ___/_____/_____

Dynamic Force (FINGER EMG) Trials

Startup time (s): 2

Recording time (s): 45

- Open ***Dynamic_Force_Varying.vi***
- Double check that calibration values for fingers have been entered into the VI!
- Have subject practice tracking on all fingers
- 30 seconds of rest between trials
- Each trial includes BOTH flexion and extension
- Range to 30% MVC.
- **WARNING: Remember to properly select the finger being tested each time the finger is changed!**

Finger	Trial Number	Timestamp	Comments
Index	1		
Middle	1		
Pinky	1		
Ring	1		
Index	2		
Middle	2		
Pinky	2		
Ring	2		
Index	3		
Middle	3		
Pinky	3		
Ring	3		

Protocol Number: 13-141	**Subject ID #:** _____
Sponsor: WPI	**Operator ID #s:** _____/_____
Investigator: Dr. Edward Clancy	**Date:** ___/_____/_____

Post experimental data

- Make notes on electrode locations
- Amount of arm spanned by electrodes, gap size
- Record gains of EMG amplifiers

Electrode	Gain Setting
1	
2	
3	
4	
5	
6	
7	
8	
9	
10	
11	
12	

When subject completes trials

- Remove electrodes
- Pay subject ($25 for completion; else $8 per completed hour not to exceed $25)
- Give subject copies of payment voucher, questionnaire, informed consent document
- Subject departs

After subject departs

- Clean electrode amplifiers, clean up lab
- Back up all data

Signature of lab member(s) performing electrode placement: _____

_____

Signature of lab member performing trial conduct:_____

Appendix 5 Study Demographics

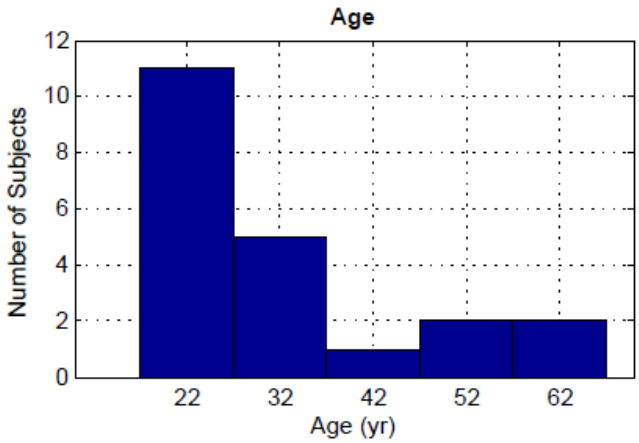

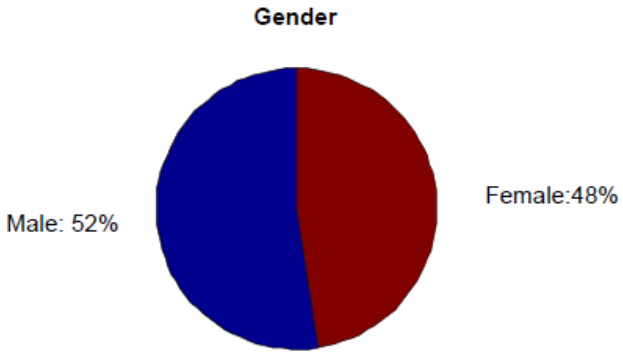

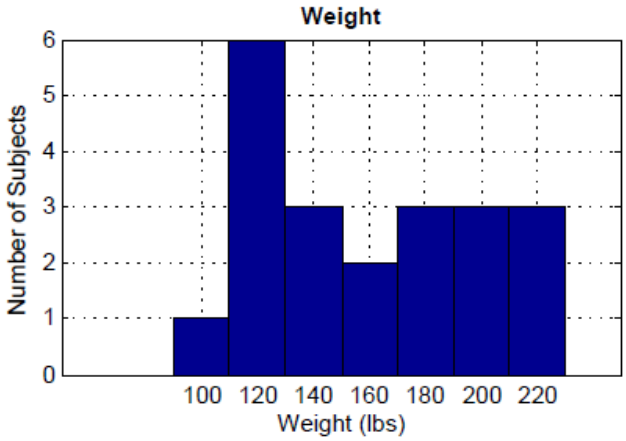

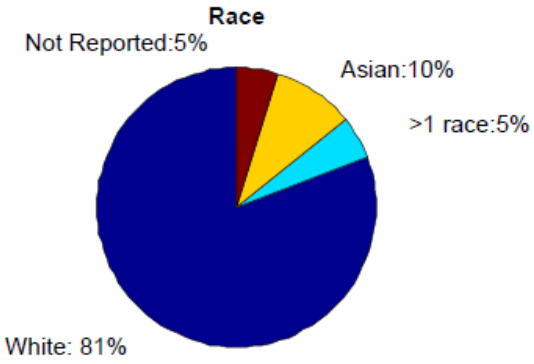

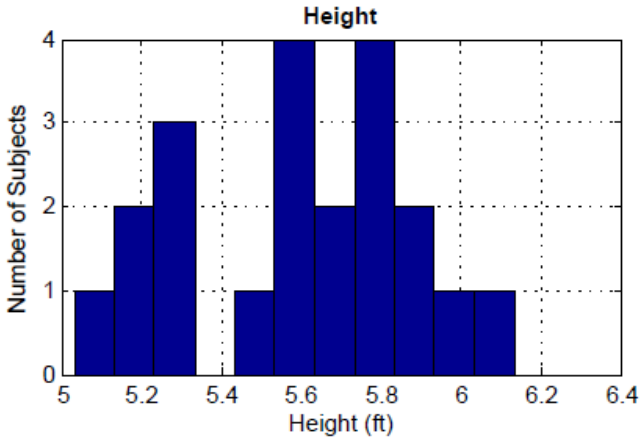

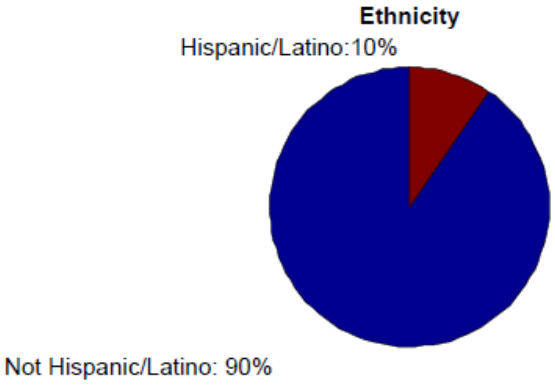

Appendix 6 Tolerance and Model Order Model Comparison Tables

Index Finger

	Model Order (D)		
Tol	**1**	**2**	**3**
0.005	8.25 ± 9.1%	9.31 ± 13.1%	12.39 ± 33.6%
0.01	8.18 ± 8.7%	8.95 ± 13.5%	9.04 ± 15.6%
0.015	7.37 ± 4.7%	7.88 ± 8.0%	6.93 ± 1.9%
0.02	6.83 ± 2.1%	7.06 ± 4.4%	7.21 ± 3.3%
0.025	6.56 ± 1.5%	6.71 ± 1.6%	7.21 ± 2.9%
0.03	6.52 ± 1.3%	6.46 ± 1.1%	6.82 ± 1.2%
0.035	6.62 ± 1.2%	6.44 ± 1.0%	6.52 ± 0.6%
0.04	6.64 ± 1.1%	6.54 ± 1.1%	6.49 ± 0.7%
0.045	6.61 ± 1.1%	6.48 ± 0.8%	6.48 ± 0.7%
0.05	6.48 ± 1.0%	6.49 ± 0.7%	6.33 ± 0.6%
0.055	6.59 ± 1.0%	6.56 ± 0.7%	6.60 ± 1.3%
0.06	6.62 ± 1.0%	6.45 ± 0.6%	6.65 ± 1.3%
0.065	6.72 ± 1.0%	6.44 ± 0.7%	6.65 ± 1.3%
0.07	6.45 ± 0.8%	6.47 ± 0.6%	6.55 ± 1.2%
0.075	6.38 ± 0.6%	6.43 ± 0.5%	6.58 ± 1.2%
0.08	6.37 ± 0.5%	6.46 ± 0.5%	6.59 ± 1.2%
0.085	6.43 ± 0.5%	6.41 ± 0.4%	6.61 ± 1.2%
0.09	6.36 ± 0.5%	6.37 ± 0.4%	6.55 ± 1.2%
0.095	6.32 ± 0.5%	6.36 ± 0.4%	6.51 ± 1.2%
0.1	6.32 ± 0.5%	6.35 ± 0.4%	6.37 ± 0.4%

MIDDLE Middle Finger

	Model Order (D)		
Tol	**1**	**2**	**3**
0.005	6.83 ± 2.4%	7.06 ± 2.3%	11.94 ± 32.9%
0.01	7.53 ± 4.5%	6.82 ± 2.3%	7.57 ± 5.2%
0.015	7.66 ± 6.3%	6.94 ± 3.4%	8.36 ± 9.6%
0.02	6.80 ± 2.1%	6.84 ± 2.7%	7.11 ± 3.7%
0.025	6.44 ± 1.7%	6.91 ± 2.8%	6.94 ± 3.1%
0.03	6.39 ± 1.5%	6.80 ± 2.8%	7.01 ± 3.8%
0.035	6.24 ± 1.4%	6.63 ± 2.3%	6.70 ± 3.7%
0.04	6.28 ± 1.4%	6.53 ± 2.3%	6.69 ± 3.3%
0.045	6.32 ± 1.4%	6.62 ± 2.9%	6.68 ± 3.3%
0.05	6.20 ± 1.2%	6.70 ± 2.9%	6.96 ± 4.4%
0.055	6.17 ± 1.2%	6.30 ± 1.3%	6.38 ± 1.3%
0.06	6.20 ± 1.2%	6.27 ± 1.2%	6.53 ± 1.2%
0.065	6.22 ± 1.1%	6.18 ± 1.2%	6.53 ± 1.2%
0.07	6.15 ± 1.1%	6.26 ± 1.0%	6.46 ± 1.2%
0.075	6.15 ± 1.1%	6.27 ± 1.0%	6.31 ± 0.9%
0.08	6.13 ± 1.1%	6.25 ± 1.0%	6.30 ± 0.9%
0.085	6.22 ± 1.0%	6.17 ± 0.9%	6.27 ± 1.0%
0.09	6.22 ± 1.0%	6.19 ± 0.9%	6.27 ± 0.9%
0.095	6.19 ± 1.0%	6.20 ± 0.9%	6.26 ± 0.9%
0.1	6.19 ± 1.0%	6.21 ± 0.9%	6.25 ± 0.9%

Ring Finger

	Model Order (D)		
Tol	**1**	**2**	**3**
0.005	5.91 ± 3.5%	6.06 ± 3.6%	10.18 ± 30.1%
0.01	6.87 ± 8.7%	7.20 ± 10.5%	7.60 ± 13.9%
0.015	6.92 ± 9.4%	8.19 ± 16.3%	8.58 ± 19.2%
0.02	5.64 ± 2.1%	7.72 ± 14.0%	7.09 ± 9.1%
0.025	5.55 ± 1.9%	5.52 ± 2.1%	6.21 ± 5.5%
0.03	5.39 ± 1.7%	5.22 ± 1.9%	5.42 ± 2.2%
0.035	5.30 ± 1.6%	5.22 ± 1.8%	5.44 ± 2.2%
0.04	5.29 ± 1.7%	5.23 ± 1.9%	5.43 ± 2.2%
0.045	5.30 ± 1.7%	5.25 ± 2.0%	5.50 ± 2.3%
0.05	5.30 ± 1.7%	5.28 ± 2.1%	5.61 ± 2.5%
0.055	5.27 ± 1.5%	5.18 ± 1.9%	5.40 ± 2.0%
0.06	5.25 ± 1.5%	5.18 ± 1.9%	5.43 ± 2.0%
0.065	5.16 ± 1.4%	5.20 ± 1.8%	5.43 ± 2.0%
0.07	5.21 ± 1.2%	5.35 ± 1.7%	5.52 ± 1.9%
0.075	5.23 ± 1.1%	5.14 ± 1.0%	5.33 ± 1.1%
0.08	5.24 ± 1.1%	5.16 ± 1.0%	5.33 ± 1.0%
0.085	5.34 ± 1.0%	5.23 ± 1.1%	5.35 ± 1.0%
0.09	5.46 ± 1.0%	5.32 ± 1.0%	5.36 ± 0.9%
0.095	5.52 ± 1.0%	5.41 ± 1.0%	5.41 ± 0.9%
0.1	5.52 ± 1.0%	5.43 ± 1.0%	5.51 ± 1.0%

Pinky Finger

	Model Order (D)		
Tol	**1**	**2**	**3**
0.005	5.58 ± 4.8%	5.80 ± 5.7%	7.34 ± 14.5%
0.01	5.96 ± 7.1%	6.28 ± 9.7%	6.72 ± 11.9%
0.015	5.69 ± 5.4%	6.51 ± 11.1%	6.25 ± 10.0%
0.02	5.00 ± 2.3%	6.53 ± 11.2%	6.04 ± 7.9%
0.025	4.95 ± 2.2%	4.83 ± 2.1%	5.14 ± 3.1%
0.03	4.84 ± 2.2%	4.75 ± 2.1%	4.80 ± 2.3%
0.035	4.90 ± 2.4%	4.75 ± 2.1%	4.75 ± 2.1%
0.04	4.84 ± 2.3%	4.70 ± 1.9%	4.80 ± 2.1%
0.045	4.86 ± 2.3%	4.75 ± 2.2%	4.80 ± 2.0%
0.05	4.69 ± 2.0%	4.75 ± 2.1%	4.79 ± 2.1%
0.055	4.69 ± 2.0%	4.60 ± 1.8%	4.69 ± 1.9%
0.06	4.71 ± 2.0%	4.62 ± 1.8%	4.63 ± 1.8%
0.065	4.69 ± 2.0%	4.62 ± 1.7%	4.66 ± 1.8%
0.07	4.48 ± 1.5%	4.63 ± 1.7%	4.61 ± 1.6%
0.075	4.50 ± 1.5%	4.54 ± 1.5%	4.58 ± 1.5%
0.08	4.51 ± 1.5%	4.58 ± 1.5%	4.58 ± 1.5%
0.085	4.54 ± 1.5%	4.60 ± 1.4%	4.59 ± 1.5%
0.09	4.55 ± 1.5%	4.64 ± 1.5%	4.63 ± 1.5%
0.095	4.56 ± 1.5%	4.65 ± 1.5%	4.75 ± 1.5%
0.1	4.56 ± 1.5%	4.73 ± 1.5%	4.88 ± 1.6%